Nouveaux copolymères donneur-accepteur : préparation, caractérisation physico-chimique et application des cellules photovoltaïques organiques

Chiara Ottone

UNIVERSITÉ DE GRENOBLE

THÈSE

Pour obtenir le grade de

DOCTEUR DE L'UNIVERSITÉ DE GRENOBLE

Spécialité : **Chimie Physique Moléculaire et Structurale**

Arrêté ministériel : 7 août 2006

Présentée par

Chiara OTTONE

Thèse dirigée par Le **Prof. Saïd Sadki** et par Le **Prof. Adam Pron**

préparée au sein du **Laboratoire d'Électronique Moléculaire, Organique et Hybride (LEMOH) – Structures et Propriétés d'Architectures Moléculaires (SPrAM) – UMR (CNRS, CEA, UJF) 5819, CEA, Grenoble**

dans **l'École Doctorale Chimie et et Sciences du Vivant, de l'Université Joseph Fourier, Grenoble, France**

New donor-acceptor alternating copolymers: preparation, physico-chemical characterization and application to organic photovoltaic

Thèse soutenue publiquement le **26 octobre 2012,**
devant le jury composé de :

Pr. Delphine Felder-Flesch
Laboratoire LEPMI, Institut National Polytechnique de Grenoble
Pr. Guy Louarn
Institut des Matériaux Jean Rouxel, UMR 6502, Université de Nantes
Dr. Valérie Alain Rizzo
Laboratoire PPSM UMR 8531, Ecole Normale Supérieure de Cachan
Dr. Rémi de Bettignies
Institut National Energie Solaire, Chambéry
Pr. Bernard Geffroy
IRAMIS/SPCSI, CEA Saclay
Pr. Saïd Sadki
INAC, UMR5819 – SprAM (CEA – CNRS – UJF), LEMOH, CEA Grenoble
Pr. Adam Pron
INAC, UMR5819 – SprAM (CEA – CNRS – UJF), LEMOH, CEA Grenoble

Université Joseph Fourier / Université Pierre Mendès France / Université Stendhal / Université de Savoie / Grenoble INP

“C'è una forza motrice più forte del vapore, dell'elettricità e dell'energia solare: la volontà.” Albert Einstein

Remerciements

Tout d'abord j'adresse ma reconnaissance à Monsieur Saïd SADKI pour m'avoir accordé sa confiance dans la conduite de ce travail de thèse et pour avoir dirigé mon travail scientifique depuis mon stage jusqu'à' la thèse, avec ses conseils soit humains soit professionnels et son expérience afin de valoriser mon travail.

Egalement je suis totalement reconnaissant à Monsieur Adam PRON qui m'a transmis ses compétences dans le domaine des polymères conducteurs pendant mon cour du M2 et tout au long de ma thèse. Je le remercie pour le temps dédié à m'apprendre à rédiger, pour la patience pendant la rédaction du manuscrit avec les difficultés reliées au « timing » et à la distance.

Entre mes directeurs de thèse je considère aussi Monsieur Mario LECLERC qui m'a accueilli dans son laboratoire au Québec où j'ai eu l'opportunité de synthétiser des nouveaux polymères dans une ambiance très sympathique, avec mes nouveaux collègues et amis québécois! Je n'oublierai jamais les 6 mois dans le loin Canada!

J'adresse mes plus sincères remerciements à Monsieur Guy LOUARN et Delphine FELDER-FLESCH pour avoir accepté d'être rapporteurs de cette thèse, à Monsieur Bernard GEFFROY pour avoir accepté de présider le jury et à Monsieur Remi DE BETTIGNIES et Madame Valérie ALAIN RIZZO pour l'intérêt qu'ils ont porté à mon travail et son examen précis de ma thèse. Je les remercie de m'avoir fait l'honneur de participer à mon jury de thèse, ainsi que pour leurs remarques permettant d'améliorer ce manuscrit.

J'adresse mes plus sincères remerciements à Messieurs Peter REISS, chef de groupe du LEMOH, et Jean-Pierre TRAVERS, directeur du SPrAM (Service et Propriétés des Architectures Moléculaires), pour m'avoir intégré à leurs équipes, ainsi que pour leur sympathie et leur gentillesse.

Merci à tous les membres du LEMOH pour avoir fait de ces 3 années de thèse une expérience très

enrichissante tant du point de vue humain que scientifique.

Grace à leur disponibilité j'ai pu collaborer avec chacun entre eux et recevoir des conseils fondamentaux pour ma thèse, en particulier merci à Fréderic CHANDEZON, Brigitte PEPIN DONAT, Jérôme FAURE VINCENT, Christian LOMBARD et Patrice RANNOU pour m'avoir aidé activement pendant cette thèse et pour m'avoir donné l'opportunité de valoriser mon travail en apportant leurs expériences et compétences. Un grand merci aussi pour les conseils de chimie organique donnés par Yann KERVELLA et Renaud DEMADRILLE…avez-vous eu peur que je puisse faire exploser quelque synthèse, n'est pas? J'adresse aussi ma plus grande reconnaissance à Nicolas BERTON qui m'a « initié » à la chimie organique et à Onintza ROSS pour son aide précieuse dans le développement des cellules solaires.

Enfin les remerciements aux collègues : j'ai une longue liste que je ne voudrais pas oublier personne…premièrement Lucia et Elsa qui sont restées toujours à côté de moi soit dans le travail soit pour partager les histories de nos vies! Merci pour les cafés et apéros pris ensemble !!Merci Antoine, Sudarsan, Axel pas seulement pour leur amitié mais aussi pour les conseils à la fois sur le planning de thèse, sur les conseils d'informatique et sur les philosophies de vie! Merci Aurélie pour ta bonne humeur et disponibilité et bien sûr pour tes nanocristaux! Angela, grazie! Entendre ta voix dans le couloir était comme avoir un peu d'Italie dans le laboratoire! Encore, Anastasia merci pour tes tisanes et gâteux qui accompagnent les discussions les plus variées. Merci Zaireen, pour ta discrétion mais aussi pour ton sourire qu'il ne manquait pas même dans les moments les plus durs !!Merci aussi à Cécile, Dmitry, Nicolas et Fleur, a été un plaisir partager des beaux moments avec vous, soit dans le laboratoire, soit dans le sortie en montagne ou le soir !

En plus, dans mon passage au Canada j'ai eu la chance de connaitre personnes qui je ne pourrais pas oublier facilement. Je tiens à remercier Philippe, Marianne, Pierre-Olivier, Nicolas, Jean Remi, Katéri, Anne Catherine, Ahmed, David, Serge.. Vous étiez capable de me faire apprécier la chimie et aussi le Québec : sans vous les six mois au froid sérient étés beaucoup plus difficiles et beaucoup plus ennuyants.

Je tiens aussi à remercier tous les personnes qui sont restés à côté de moi et qui m'ont soutenu à pendant ma thèse et pendant mon séjour à Grenoble. Je commence toujours par Oussama, Firas et Lara et tous les amis connus à la résidence Ouest…merci au dernier étage du bâtiment B en particulier : Ioana, Fede, Paola, Alfonso, Erwan, Thomas.

Enfin, en dernier mais pas les moins importants, j'adresse un énorme merci à mes parents et ma sœur qui m'ont soutenue malgré la distance et ils ont étés fondamentaux pour me transmettre du courage même quand la fatigue aurait voulu prendre le dessus.

Merci à Fernando, tu as été toujours a' coté de moi (et tu sais qu'est-ce que je veux dire). Cette thèse est un peu la tienne aussi, c'est à toi que je veux la dédier.

Grazie a tutti

Résumé de la thèse

Introduction générale du travail de thèse

L'énergie solaire est la source d'énergie la plus abondante parmi les ressources d'énergies renouvelables de notre Planète. Cependant seulement 0,04% de l'énergie globale utilisée par l'humanité provient directement de l'énergie solaire, car le coût des panneaux photovoltaïques nécessaires à la récupération du rayonnent solaire est beaucoup plus élevé que l'utilisation de la combustion de l'énergie fossile. L'énergie solaire est difficile à récupérer car c'est une énergie diffusée qui nécessite d'être collectée sur des panneaux de grandes surfaces pendant la journée. Les dispositifs classiques à base de silicium ont été inventés pour la première fois au sein des Laboratoires Bells en 1954. Depuis cette époque la technologie photovoltaïque a été fortement optimisée en améliorant l'efficacité de conversion des cellules. Ainsi Schockley- Quiesser ont obtenus pour une jonction p/n, des valeurs supérieures à 25%.

Actuellement la majorité des modules photovoltaïques concerne le silicium poly-cristallin, matériaux capable de fournir un rendement de l'ordre du 10-15% avec un temps de vie supérieur à 50 ans.

Les aides financières des différents gouvernements pour l'installation des panneaux solaires ont permis une augmentation de la production industrielle de plus du 30% par an au cours des dix dernières années. Cependant cette croissance est encore trop faible pour réduire de manière significative la production de gaz à effet serre, vue la demande considérable d'énergie à l'heure actuelle.

Pour atteindre l'objectif de production des cellules solaires à bas coût et flexibles, les matériaux organiques ont attiré l'attention des chercheurs et des industriels à partir des années 1990. Jusqu'à présent ces matériaux ont montré des rendements de conversion en puissance encore relativement faibles. Le rendement maximum de 7% a été obtenu pour an dispositif constitué sur un système à hétérojonction volumique polymère/PCBM (1-[3-(méthoxycarbonyl)propyl]-1-phényle-[6,6]C_{61}). Les facteurs qui limitent l'obtention d'un dispositif performant sont reliés aux matériaux constituant la couche active, les différentes interfaces et les contacts électriques. Pour cette raison, un défi est donné aux chimistes pour trouver un semi-conducteur organique caractérisé par une bonne absorption dans le domaine visible du spectre solaire, un transfert de charges optimal et une mise en œuvre aisée. Parallèlement les physiciens cherchent à améliorer les propriétés électroniques, à optimiser la morphologie et les contacts électriques pour garantir que chaque processus (de la formation des porteurs libres jusqu'à la collecte des électrons) puisse avoir lieu de manière efficace.

Une grande variété de semi-conducteurs organiques a été synthétisée, étudiée et couplée avec des autres matériaux accepteurs d'électrons. Pourtant beaucoup d'étapes technologiques critiques n'ont pas encore trouvé une solution industrielle et pour cette raison, l'OPV n'a pas encore pu être vraiment exploité de manière industrielle.

Une étude récente a montré au moyen d'un modèle de calcul pour une hétérojonction classique basée sur un mélange polymère: PCBM[5] une puissance de conversion maximale de 11,7% pour une cellule simple et

de 14,1% pour les structures de type tandem. Ces valeurs sont très encourageantes et poussent la communauté scientifiques à atteindre ces valeurs théoriques. Par exemple un nouveau record de rendement de 9,2% pour des cellules solaires organiques a été récemment publié.

Cette thèse concerne l'élaboration de nouveaux semi-conducteurs organiques de hautes masses moléculaires et de faible bande interdite. Dans le domaine de l'organique, l'expression "faible bande interdite" renvoie aux matériaux pour lesquels la bande interdite est inferieure à 2 eV, valeur arbitraire, mais qui aide à distinguer ce type de matériaux des autres types de semi-conducteurs organiques.

Grace à leur structure électronique ces polymères conjugués sont spécialement adaptés pour des applications dans les cellules photovoltaïques, mais d'autres applications peuvent être aussi envisagées, par exemple dans le domaine des transistors ambipolaires à effet de champ, des photodiodes etc. Par contre, dans cette étude, l'attention sera focalisée sur les applications pour des cellules solaires à hétérojonction volumique. Ce choix de l'application solaire organique s'explique par le financement de thèse obtenu et des collaborations entre notre groupe de recherche et l'équipe de l'Institut National de l'Energie Solaire (INES) de Chambéry et le Laboratoire des Polymères Electroactifs et Photoactifs de l'Université de Laval de Québec (Canada) spécialisés dans le photovoltaïque organique.

Pour la préparation de nouveaux polymères à faible bande interdite différentes méthodes de synthèse macromoléculaire ont étés menés. Une méthode devenue très populaire dans la dernière décade, et que sera l'approche décrit dans ce travail de thèse, est la synthèse de copolymères alternés constitués par des unités donneuses d'électrons et par des unités acceptrices d'électrons. Ces polymères donneur-accepteur, appelés aussi polymères "*push-pull*", peuvent être préparés en utilisant différent types des réactions de couplage C-C.

L'élaboration de ces nouveaux polymères nécessite une caractérisation physico-chimique approfondie. Cela concerne des études de la microstructure du polymère par spectroscopie (RMN et autres techniques), la détermination des paramètres macromoléculaires comme la masse macromoléculaire et la polymolécularité, au moyen de la chromatographie d'exclusion stérique.

En particulier, les propriétés optiques et électrochimiques des polymères synthétisés sont des paramètres cruciaux pour les applications au photovoltaïque organique. Les propriétés optiques donnent des informations sur l'efficacité de la récolte des photons, les propriétés électrochimiques donnent des informations sur le positionnement des niveaux d'énergie HOMO et LUMO. Ces études ont été menés en utilisant la spectroscopie UV-*Vis*-NIR, la volampérométrie cyclique et aussi la spectroélectrochimie Raman couplée UV- *Vis*-NIR qui fournit des informations complémentaires et permet parfois de déterminer plus précisément les niveaux HOMO et LUMO des polymères.

Les propriétés du transport électrique de polymères semi-conducteurs dépendent fortement de l'organisation supramoléculaire, du degré de cristallinité, ainsi des études de diffraction ont été effectués sur les polymères qui ont démontré des propriétés optiques et redox les plus prometteuses. Les propriétés thermiques des composés synthétisés ont été également déterminées par DSC and ATG. Ces dernières études sont d'une grande importance technologique car un certain nombre d'étapes de fabrication d'une cellule solaire impliquent le traitement thermique de la couche active.

Des calculs basés sur la " Differential Functional Theory" (DFT) et une étude détaillé par Résonance Paramagnétique Electronique (EPR) ont donné des informations complémentaires sur la variation des propriétés optiques et électrochimiques des unités donneuses et acceptrices du polymère π-conjugué. En plus une étude de simulation de spectre RPE "EPR tracing study", permettant d'associer différents signaux à des structures spécifiques, a été utilisé pour mieux comprendre les relations entre les propriétés structuraux et les processus de transfert d'électron. De plus, les effets *push-pull* peuvent être analysés à l'échelle moléculaire.

Dans la dernière partie de la thèse, des prototypes de cellule solaire ont été fabriqués en utilisant les

polymères les plus performants comme composant d'une hétérojonction volumique. Leurs paramètres photovoltaïques ont été évalués.

L'organisation de la thèse est le suivant.

Dans le premier chapitre, l'état de l'art concernant la synthèse, la fonctionnalisation et l'ingénierie des polymères utilisés dans la fabrication des cellules solaires est décrit. Ce chapitre est complété par une description du fonctionnement des cellules solaires organiques et par la discussion de paramères photovoltaïques fondamentales.

Dans le deuxième chapitre, l'élaboration de nouveaux copolymères semi-conducteurs a été détaillée. Cela implique les dérivés du poly(3,6-carbazole) dans une première partie puis dans une seconde partie du chapitre, les dérivés du poly(2,7 carbazole), qui démontrent de meilleures propriétés électroniques et qui sont plus prometteurs pour les applications à l'électronique organique. En particulier la voie synthétique (*via* couplage de Suzuki) consistent à utiliser des dérivés du 2,7-carbazole, comme unité D, et du thienopyrrolodiones, comme unité A, ont été discutés de manière exhaustive. Dans la troisième partie de ce chapitre, la synthèse (*via couplage de* Stille) de copolymères à base de thienopyrroledione, avec une plus forte unité donneuse que le carbazole, le dialkoxybenzodithiophene est décrite.

Dans le troisième chapitre, la caractérisation physico-chimique des composés synthétisés est présentée en utilisant les techniques précédemment citées. Les calculs de DFT ont été réalisés grâce à la collaboration avec C. Morell et A. Grand du CEA/INAC/SCIB, puis d'autres calculs ont été menés avec le Professeur G. Louarn de l'Institut des Matériaux Jean Rouxel (IMN) à l'Université de Nantes (France) permettant de conforter et renforcer les résultats obtenus par Résonance Raman Scattering (RRS) et par Spectroscopie infrarouge-FTIR.

Dans le quatrième chapitre la caractérisation par la technique de Résonance Paramagnétique Electronique (RPE) est décrite. Cette étude a été réalisée en collaboration avec le Dr Brigitte Pepin-Donat et Mr Christian Lombard.

Dans le cinquième et dernier chapitre, des tests en dispositifs photovoltaïques ont été effectués. Cette partie expérimentale a été développée en collaboration avec deux équipes de recherche, à savoir le Laboratoire des Polymères Electroactifs et Photoactifs au Canada et l'institut de l'Energie Solaire de Chambéry.

Résumé de l'état de l'art

Les composés organiques et conjugués de hautes masses macromoléculaires, normalement appelés polymères semi-conducteurs or polymères electroactifs, ont étés considérés pendant longtemps comme des matériaux exotiques. Il a fallu attendre 1977, avec la découverte du polyacetylène par Heeger, MacDiarmid, Shirakawa et al. A cette époque, le polyacetylène conducteur électronique n'a pas trouvé d'applications industrielles. Cependant cette découverte a stimulé une recherche approfondie sur les propriétés électroniques des polymères conjugués [10–12] Plus récemment, la découverte par Sariciftci, Smilovitz, Heeger and Wudl du transfert de charge photoinduit entre un polymère conjugué et le fullerène a permis le développement des cellules solaires en hétérojonction volumique.

Le développement des nouveaux matériaux pour des applications photovoltaïques a pour objectif la substitution des cellules solaire à base de silicium, avec des matériaux bas couts et facile à mettre en œuvre.

En 2011, un record a été réalisé par Mitsubishi Chemical Co avec un rendement du 9%. Un tel succès a motivé la recherche sur les nouveaux matériaux π-fonctionnels avec des nouvelles stratégies de fabrication. Une de stratégie de fabrication est la création des hétérojonctions volumiques à base des polymères Π-conjugués, agissant de donneurs des électrons, et de dérives de fullerène agissant comme accepteurs

d'électrons. Par contre cette stratégie n'est pas encore compétitive avec les autres technologies PV caractérisés par de rendement de l'ordre du 15-20%. Pour atteindre cet objectif, il est nécessaire de synthétiser de nouveaux matériaux mais aussi d'améliorer les contacts et les interfaces dans les dispositifs PV. La synthèse des nouveaux matériaux organiques caractérisés par une faible bande interdite semblerait être le facteur clé pour pouvoir améliorer les performances des cellules solaires en hétérojonction volumique.

Avec une bande interdite appropriée entre 1,4 et 2 eV, un bon recouvrement du spectre solaire est possible pour favoriser l'augmentation des courants de court-circuit. De plus, le positionnement des niveaux HOMO et LUMO devrait permettre un transfert de charge favorable entre donneur et accepteur, aidé par une bonne morphologie de la couche active.

Résumé du Chapitre 2 : Nouveaux copolymères « push-pull »

Ce travail concerne l'élaboration de nouveaux matériaux à faible gap, appelés les copolymères *push-pull* caractérisés par une unité donneuse (*push*) et une acceptrice (*pull*). L'état de l'art sur les unités *push- pull* les plus étudiées a dirigé notre choix de synthèse.

L'attention a été focalisée surtout sur les unités benzothiadiazole et diketopyrroledione et sur les unités carbazole et benzodithiophene, car ce sont les polymères les plus performants. Des efficacités de l'ordre de 6 % ont étés obtenus principalement sur les dérivés du poly (2,7-carbazole) et poly(benzodithiophene). Les unités acceptrices ont étés aussi analysées en présence d'accepteurs à base de dérivés de fullerène et nanocristaux.

Après avoir sélectionné les bonnes unités *push* and *pull*, dans le deuxième chapitre la méthode de synthèse pour l'obtention des polymères désirés sera discutée.

Différents couplages C-C, comme Suzuki et Stille, peuvent être facilement utilisés pour la préparation de ces matériaux. Néanmoins, des recherches ultérieures doivent être conduites pour un meilleur control des paramètres macromoléculaires. Sauf le polymère P1, tous les autres polymères présentent des valeurs discrètes de M_n et nécessitent un fractionnement macromoléculaire pour réduire les indices de polydispersité.

Résumé du Chapitre 3 : Caractérisation physico-chimiques des copolymères *push-pull* synthétisés

Une étude détaillée en utilisant des techniques complémentaires de spectroscopie, d'électrochimie, de diffraction et d'analyses thermiques ont permis de caractériser les propriétés cruciales pour les applications dans le photovoltaïque organique.

Les propriétés électrochimiques et spectroélectrochimiques ont démontré le potentiel de ces matériaux donneurs pour des hétérojonctions volumiques car ils sont caractérisés par des niveaux HOMO et LUMO adaptés et résultats en concordance avec les valeurs théoriques par DFT. En plus le mode vibrationnel développé a permis d'attribuer tous les modes Raman et IR de ces polymères.

Une étudie approfondie en spectroscopie RPE a permis d'étudier tous les mécanismes des réactions et les processus qui sont concernés dans la formation et la disparition des radicales libres. Pour cette raison, on a utilisé cette technique pour observer les transferts inter et intramoléculaires à niveau des polymères « *push-pull »* et entre les polymères et les dérivés de nanocristaux et de fullerènes.

Résumé du Chapitre 4 : Transfert de charge intra- and inter- moléculaire dans les polymères and dans les mélanges avec fullerène ou nanocristaux semi-conducteurs- Résonance Paramagnétique Nucléaire (RPE) et Calcules DFT.

L'étude du transfert entre les polymères (donneurs) et le PCMB ou les nanocrystals (accepteurs) a montré que, si d'un côté le transfert en présence du PCBM est efficace, au contraire, pour les nanocristaux le signal

enregistré est visiblement plus faible.

En plus, les unités *push* and *pull* appartenant aux trois polymères ont pu être attribuées par correspondance avec les signaux RPE et leur validité a été renforcée avec des calculs de DFT sur la densité du spin du radical cation.

Il est aussi envisageable d'effectuer une étude avec une illumination à 600 nm, qui devrait accorder mieux avec le maximum d'absorption des polymères étudiés.

Résumé du Chapitre 5 : Cellules Solaires Organiques

Une étude complète sur les polymères appartenant à la famille du poly(3,6-carbazole) à été effectué en hétérojonction volumiques et a permis de comparer deux polymères à faible bande interdite : le 3,6-PCDTBT et le 3,6-PCDOTBT. Les performances en cellules solaires obtenues présentent des efficacités de 0.35% pour le polymère PCDTBT. Il est possible de supposer que le principal problème pour ces polymères soit relié aux faibles valeurs de masse moléculaire. En plus, l'effet stérique des chaines octyles sur le 3,6-PCDOTBT, influences la conjugaison de la chaine de polymère.

Un deuxième group des composés en contenant le groupement du thienopyrrolodione, le 2,7-carbazole ou dialkoxybenzothiophene, a été testé. Entre ces polymères, le P3 a démontré la valeur plus élevé des polymères conjugues, cependant les études en diffèrent conditions expérimentales ont démontré que les performances du dispositif sont très sensibles aux conditions expérimentales en limitant la reproductibilité.

Abbreviations list

2,7-PoCDTBT	Poly[N-(octyl)-2,7-carbazole-alt-5,5-(4',7'-dí-2(thienyl)-2',1',3'-benzothiadiazole)]
3,6-PCDOTBT	Poly[N-(ethylhexanoate)-3,6-carbazole-alt5,5-(4',7'-di-2-(4-octylthienyl)-2',1',3'-benzothiadiazole)]
3,6-PCDTBT	Poly[N-(ethylhexanoate)-3,6-carbazole-alt-5,5-(4',7'di-2-thienyl-2',1',3'- benzothiadiazole)]
3,6-PCODTBT	Poly[N(ethylhexanoate)-3,6-carbazole-alt-5,5-(4',7'-di-2-(4-octylthienyl)2',1',3'-benzothiadiazole)]
A	Acceptor
AFM	Atomic Force Microscopy
AM	Air Mass
$AsPh_3$	Triphenylarsine
BDT	Benzo[1,2-b;3,4-b]dithiophene
BHJ	Bulk-Heterojunction
BT	2,1,3-benzothiadiazole
BTD	Benzodiathiazole
$C_2O_2Cl_2$	Oxalyl chloride
CB	Carbazole
D	Donor
DFT	Differential Functional Theory
DIO	Di-iodooctane
DMAP	4-Dimethylaminopyridine
DMF	N,N-dimethylformamide
DMSO	Dimethyl sulfoxide
DOPT	Dioctylthieno[3,2-b:2,3-d]pyrrole
DPP	Diketopyrrolepyrrole
DSC	Differential scanning calorimetry
DTBT	4,7-dithien-2-yl-2,1-3-benzothiadiazole
DTP	Dithieno[3,2-b:2,3-d]pyrrole
DTQ	Dithieno[3,2-f:2',3'-h]quinoxaline
EA	Electron Affinity
EQE	External Quantum Efficiency
Et_4NOH	Tetraethilammoniumhydroxide
FF	Fill Factor
HOMO	Highest Occupied Molecular Orbital
HRMS	High-resolution Mass Spectrometry
IC	Indolo[3,2-b]carbazole
IP	Ionization Potential
IPCE	Internal Photons to Current Efficiency
ITO	Indium tin oxide
LSIMS	Liquid Secondary Ion Mass Spectrometry
LUMO	Lowest Occupied Molecular Orbital

MDMO-PPV	Poly[2-methoxy-5-(2'-ethylhexyloxy)¬1,4-phenylenevinylene]
Me_3N	Trimethylamine
M_n	Number average molecular mass
MO	Molecular orbital
M_w	Weight average molecular mass
NBS	N-Bromosuccinimide
NBu_4BF_4	Tetrabutylammoniumtetrafluoroborate
NCs	Nanocrystals
$Ni(dppp)Cl_2$	1,2-Bis(diphenylphosphinoethane)nickel(II) chloride
NMR	Nuclear Magnetic Resonance
OC1C10-PPV	Poly(2-methoxy-5-(3',7'-dimethyl-octyloxy)-p-phenylenevinylene)
ODCB	*o*-dichlorobenzene
$P(oAC)_2$	Palladium(II) acetate
$P(o\text{-}tol)_3$	Tri(o-tolyl)phosphine
$P(t\text{-}Bu)_3$	Tri-tert-butylphosphine
P3FTBT6	Poly(3-fluorene-thiophene-benzo-thiophene-6)
P3HT	Poly(3-hexylthiophene)
P6	Poly[2,6-(4,4-bis-(2-ethylhexyl)-4H-cyclopenta[2,1-b;3,4¬b]-dithiophene)-alt-4,7-(2,1,3-benzodiathiazole)]
PBDTDTffBT	Poly[benzodithiophene-benzodiathia-fluorine-fluorine]benzothiazole
PBDTTPD	Poly(benzodithiophen)-thienopyrroledione
PBDTTT-CF	Poly[4,8-bis-substituted-benzo[1,2-b:4,5-b0]dithiophene-2,6-diyl-alt-4-substituted-thieno[3, 4-b]thiophene-2,6-diyl]-carbonyfluorine
PBnDT-FTAZ	Polybenzodithiophene-fluroine-(2alkylbenzo[d][1,2,3]triazole
PBTTPD	Poly[(bithiophene)-thieno[3,4-c]pyrrole-4,6-dione
PCBM	1-(3-methoxycarbonyl)-propyl-1-phenyl-(6,6)C61
PCDOTBT	Poly[N-9''-hepta-decanyl-2,7-carbazole-alt-5,5-(4',7- di-2- thienyl-2',1',3'-benzothiaziazole) : PC70BM
PCDTBT	Poly[N-9''-hepta-decanyl-2,7-carbazole-alt-5,5-(4',7- di-2- thienyl-2',1',3'-benzothiaziazole) : PC70BM
PCE	Photon Conversion Efficiency
PD	Pyrrolodione
$Pd(dppf)Cl_2$	Bis(diphenylphosphino)ferrocene]dichloropalladium(II)
$Pd(PPh_3)_4$	Tetrakis(triphenylphosphine)palladium(0)
$Pd_2(dba)_3$	Tris(dibenzylideneacetone)dipalladium(0)
PDI	Polidispersity index
PDPPTPT	Poly[{2,5-bis(2-hexyldecyl)-2,3,5,6-tetrahydro-3,6-dioxopyrrolo[3,4-c]pyrrole-1,4-diyl}-alt-{[2,2'-(1,4-phenylene)bisthiophene]-5,5'-diyl}]
PDTSTPD	Poly[dithieno[3,2-b:2',3'-d]silole - thieno[3,4-c]pyrrole-4,6-dione]
PED	Potential Energy Distribution
PEDOT: PSS	Poly(3,4-ethylenedioxithiophene):Poly(styrenesulfonate)
PES	Photoelectron Spectroscopy

PF10TB	Poly[2,7-(9,9-dialkylfluorene-alt-5,5-(4’,7’-di-2-thienyl-2’-1’-3’-benzothiadiazole)
P-Ge	Poly(germole)
PPh	Triphenylphosphine
PPV	Poly(phenylene)vinylene
R	Coefficient for linear regression
r.t.	room temperature
SCLC	Space Charge Limited Current
SEC	Analytical Size-Exclusion Chromatography
SPhos	2-Dicyclohexylphosphino-2',6'-dimethoxybiphenyl
TGA	Thermogravimetric analysis
THF	Tetrahydrofuran
TPD	Thieno[3,4-c]pyrrole-4,6-dione
TPD	N-alkylthieno[3,4-c]pyrrole-4,6-dione
VFF	Valence Force Field

Contents

Introduction

Solar power is the most abundant renewable resource on our planet. In spite of this abundance, only 0.04% of the basic power used by humans comes directly from solar sources because harvesting solar energy, using a photovoltaic (PV) panel, costs more than burning fossil fuels.[1]

Solar energy is difficult to harvest because it is a diffuse energy source that requires collection over large land areas and because the sun only shines during the day. Classical based silicon photovoltaic devices were born to Bell Labs in 1954. Since that time, photovoltaic has been greatly optimized and a power conversion efficiency (PCE), approaching the Schockley–Queisser limit for a single p/n junction, of over 25% has been reported.[2]

Recently the majority of photovoltaic modules concerns silica polycrystalline which presents yields of the order of 10-15% and a lifetime longer than 30 years. Government incentives to install photovoltaic capacity has resulted in growth for the solar industry of over 30% per year for the last decade, but this growth curve is still too low to significantly reduce global greenhouse gas production, due to rising energy demand.[3]

To reach the goal of producing low cost and flexible solar cells, organic materials have played an attractive role since the 1990s , but still now they have shown low yield of power conversion efficiencies reaching the best value of around 7% for a bulk heterojunction system of polymer/PCBM (1-[3-(methoxycarbonyl)propyl]-1-phenyl-[6,6]C_{61}).[4]

Limiting factors to obtain a well performing device are mainly related to active layers materials and their interfaces with electric contacts. As a consequence, a difficult challenge has been given to chemists to find an organic semiconductor characterized by a good absorption on the *UV-Vis* solar, optimum charge-transport stability and processability properties, approaching the problem from several angles. Then, physicists and engineers should be able to investigate electrical properties to optimize morphologies and relationships between active layers and electrical contacts, to guarantee that each process going from free charges formation to electrons collection take place.

A big variety of organic semiconductors has been synthesized, studied and coupled with others different materials, allowing a better understanding of phenomena involved in the process. Nevertheless a lot of challenging steps still have to be solved limiting the OPV exploitation.

A recent and stimulating study carried out a model calculation on the classical bulk-heterojunction device configurations for an active layer of polymer:fullerene.[5] They predicted a maximum power efficiency of 11.7% for single junction cells and 14.1% for tandem structures. This is very encouraging, and the community is steadily approaching these numbers: for example, a new record high efficiency of 9.2% for organic solar cells has been recently reported.[6]

The presented thesis is devoted to the elaboration of new high molecular weight organic semiconductors of low band gap. In organic matter, the term "low band gap" refers to materials whose energy gap is < 2eV – an arbitrary value, which however helps to distinguish them from other types of organic semiconductors. Taking into account their electronic structure, these polymers are especially suitable for applications in photovoltaic cells, but other applications can also be envisioned such as ambipolar field effect transistors, photodiodes and other devices of electronic and electrochemical nature. Here we limit ourselves to applications in bulk heterojunction-type solar cells. This is caused by the available sources of financing the thesis as well as the existing collaboration links between our research group and teams from the INES (Insitut National de l'Energie Solaire) of Chambéry and from the Labortoire des Polymères Electroactifs et Photoactifs de l'Université de Laval of Québec City (Canada), specializing in organic photovoltaics.

There are several methods of preparing polymeric low band gap semiconductors. One of them, which became very popular in the last decade, is the synthesis of alternating copolymers consisting of electron donating and electron accepting units. These donor-acceptor (DA) polymers, alternatively called "*push-pull* polymers", can be prepared from appropriate building blocks using different types of C-C coupling reactions. This approach was also used in the research presented here.

Any application of these polymers requires their detailed physico-chemical characterization. This involves the elucidation of the polymer chain microstructure by spectroscopic means (NMR and other techniques), determination of their macromolecular parameters such as molecular mass and its distribution by size exclusion chromatography. For photovoltaic applications optical and redox properties of the synthesized polymers are of crucial importance. The former gives information about the efficiency of photon harvesting, the latter determines the positions of the HOMO and LUMO levels – crucial for solar cells functioning. Such investigations have been undertaken using UV-*Vis*-NIR spectroscopy and cyclic voltammetry and also by UV-*Vis*-NIR and Raman specroelectrochemistry, which provide complementary information and sometime allow more precise determination of the HOMO and LUMO levels.

Since electrical transport properties of semiconducting polymers strongly depend on their supramolecular organization, degree of crystallinity and orientation of macromolecules, diffraction studies have been carried out for these polymers which showed promising optical and redox properties. Thermal properties of the synthesized compounds have been determined by DSC and TG. Such studies are of technological importance since many procedures of solar cells fabrication involve thermal annealing of the active layer.

The Differential Functional Theory (DFT) calculations and a detailed study by Electron Paramagnetic Resonance (EPR) were carried out to furnish some complementary information about the variations of the optical and electrochemical properties of the donor and the acceptor moieties in the polymer π-conjugated backbone. In addition "EPR tracing study", allowing to ascribe various signals to specific structures, was undertaken with the goal to go further in the insight of the relationships between the structural properties and the electron transfer processes in the investigated composite systems. At the same time, *push-pull* effects could be analyzed at the molecular scale.

In the final step of the research, test devices were fabricated using the most promising polymers as bulk heterojunction components and their parameters evaluated.

The organization of this thesis is as follows.

In the first chapter the present state of the art in the synthesis, functionalization and engineering of polymers used for the fabrication of organic solar cells is outlined. The chapter is completed by the description of organic solar cells functioning and critical discussion of factors influencing the cell principal parameters. In the second chapter the elaboration of new semiconducting copolymers is described in detail. This involves poly(3,6-carbazole) derivatives and then, in the second part of this chapter, poly(2,7 carbazole)

derivatives, which show better electronic properties and seem more promising for organic electronics applications. In particular, synthetic routes (*via* Suzuki coupling) to new copolymers, consisting of 2,7-carbazole derivatives as D units, and thienopyrrolodiones as A units, are critically discussed. In the third part of this chapter the synthesis (*via* Stille coupling) of thienopyrrolodione copolymers with a stronger than carbazole electron donor, namely dialkoxybenzodithiophene is described. In the third chapter a detailed physico-chemical characterization of the synthesized compounds is presented which involves all techniques described above. This chapter will be supported by DFT calculations carried out in collaboration with C. Morell et A. Grand of CEA/INAC/SCIB laboratory, concerning variation of the optical and electrochemical properties of copolymers and with the Professor G. Louarn from the Institut des Matériaux Jean Rouxel (IMN), at the Université de Nantes (France), to support results obtained the by Resonance Raman Scattering (RRS) and the Fourier Transform Infrared absorption (FTIR).

In the fourth chapter the characterization through the EPR technique were made possible through collaboration with Brigitte Pepin-Donat and Christian Lombard. In the fifth (last) chapter the fabrication of test photovoltaic devices is described and the results of preliminary tests are analyzed. This part of research was carried out together with two partners, namely Laboratoire des Polymeres Electroactifs and Photoactifs in Canada and INES of Chambéry.

[1] C. Ruiz, E. M. García-Frutos, G. Hennrich, and B. Gómez-Lor, "Organic Semiconductors toward Electronic Devices: High Mobility and Easy Processability," *The Journal of Physical Chemistry Letters*, vol. 3, pp. 1428–1436, 2012.

[2] W. Shockley and H. J. Queisser, "Detailed Balance Limit of Efficiency of p-n Junction Solar Cells," *Journal of Applied Physics*, vol. 32, no. 3, p. 510, 1961.

[3] A. J. Moulé, "Power from plastic," *Current Opinion in Solid State and Materials Science*, vol. 14, no. 6, pp. 123–130, 2010.

[4] Y. Sun, C. J. Takacs, S. R. Cowan, J. H. Seo, X. Gong, A. Roy, and A. Heeger, "Efficient, Air-Stable Bulk Heterojunction Polymer Solar Cells Using MoO_x as the Anode Interfacial Layer," *Advanced Materials*, vol. 23, , pp. 2226–2, 2011.

[5] W. M. Blom, V. D. Mihailetchi, L. J. Koster, and D. E. Markov, "Device Physics of Polymer:Fullerene Bulk Heterojunction Solar Cells," *Advanced Materials*, vol. 19, no. 12, pp. 1551–1566, 2007.

[6] U. S. Washington, DC, "Service, R.F. Science," vol. 332, no. (6027), p. 293, 2011.

Chapter 1

New materials for organic solar - cells: state of the art

1.1 Introduction

Low and high molecular weight conjugated compounds constitute a special class of organic matter, offering spectroscopic, electrochemical and electronic properties difficult to match by other classes of organic and inorganic substances. Low molecular compounds have been studied for decades, mainly as different types of dyes. More recently, they attracted attention as semiconductors, serving as components of various types of organic electronic devices such as field effect transistors [1], [2] photodiodes and photovoltaic cells.[3–8] They are not subject of the present thesis and will not be discussed here.

High molecular weight conjugated compounds, frequently termed as conjugated polymers, conducting polymers, semiconducting polymers or electroactive polymers, have also been known for decades. However, since they found no technological application, for many years they were treated as exotic materials and drew little scientific attention. This limited interest was also caused by the fact that their electronic properties were not well understood. The breakthrough came in 1977, after the discovery of the highly conductive form of polyacetylene by Heeger, MacDiarmid, Shirakawa and their coworkers.[9] Conductive form of polyacetylene did not found any technological application either, due to its lack of processability and environmental instability, but its discovery stimulated intensive research focused on better understanding of electronic properties of conjugated polymers and on the synthesis of environmentally stable, solution processable compounds.[10–12] As far as polymeric solar cells are concerned, important work of Sariciftci, Smilovitz, Heeger and Wudl on photoinduced charge transfer between a conjugated polymer and fullerene.[13] This paper stimulated research on organic solar cells of so called “bulk heterojunction-type” which started to grow exponentially.

The silicon based PVCs still have advantages over the organic ones in both efficiency and lifetime of the device. A module of conversion efficiency of 20% and operational stabilities of more than 25 years, under outside conditions, has been demonstrated for a monocristal device.[14], [15] However the fabrication of silicon, independent of its form (single crystal, polycrystalline, amorphous), is energetically very consuming since it requires reduction of silica to silicon at very high temperatures.

Fabrication of materials for organic photovoltaics is energetically less consuming, moreover, many of them are solution processable which is a technological advantage. In April 2011, a significant implementation of performances gave a new certified record of 9% recorded by Mitsubishi Chemical Co.[16] These goals motivate the research on new π-functional materials and new strategies of solar cells design and fabrication.

Organic semiconductors are used in three types of solar cells, shown schematically in Figure 1.1.

- dye sensitized solar cells (Gratzel cells): 11.2% of yield.[17]
- hybrids solar cells (conjugated polymer/nanocrystals) - P3HT/CdSe system, 2.9% yield.[18], [19]
- organic solar cells (n-type/p-type materials) - Polymer/$PC_{71}BM$ 9% yield.[16]

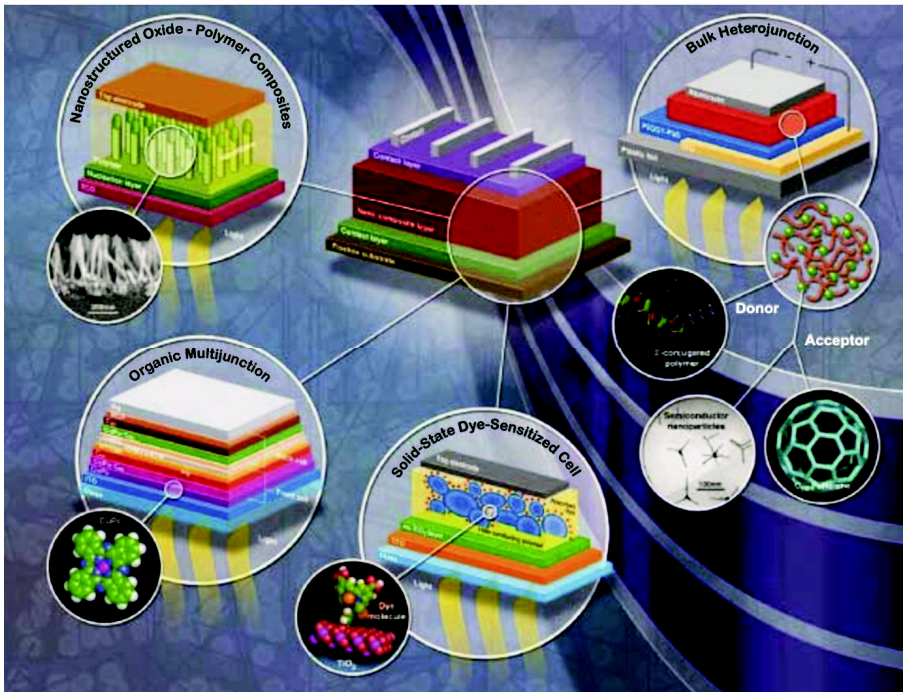

Figure 1.1: Organic Solar cell devices.[3]

Gratzel cells use low molecular dyes as sensitizers and will not be discussed here. Polymeric low band gap semiconductors, which constitute subject of this thesis, are applied in the two other types of cells. In the subsequent text their synthesis as well as their basic properties will be discussed.

1.2 Organic solar cells

1.2.1 Structure of organic solar cells

Organic solar cells are mostly formed by an active layer sandwiched between two electrodes. This active layer usually consists of two semiconducting components, a donor-type and an acceptor-type. One of the electrodes is transparent (ITO, indium tin oxide), serving as an anode, whose work function is *ca.* - 4.7 eV. The other electrode is metallic, made for example of aluminum whose work function is about -4.3 eV. The work functions of the anode and the cathode should match the highest occupied molecular orbital (HOMO) of the used donor semiconductor and the lowest unoccupied molecular orbitals (LUMO) of the acceptor one, respectively. The use of an intermediate layer (PEDOT: PSS, poly(3,4-ethylene-dioxithiophene) doped with polystyrene sulfonic acid) can improve the contact between the active layer and the anode [20] and at the same way, a LiF layer can improve the open circuit voltage (V_{oc}) of the device.[21] So, the active layer should allow the charge separation and a good bipolar transport throughout the volume. At early stages of the research on photovoltaics, a bilayer of a donor and an acceptor was usually used. Since in the working cell the charge separation occurs at the interface of the donor and acceptor phases, small interfacial area of the bilayer configuration limits the charge separation and by consequence the efficiency of the cell.

To overcome this problem, the so called bulk-heterojunction configuration was finally proposed, yielding much larger interface area (see Figure 1.2). This bulk heterojunction model is, in reality, a blend in which two co-continuous phases of the donor and the acceptor are formed.

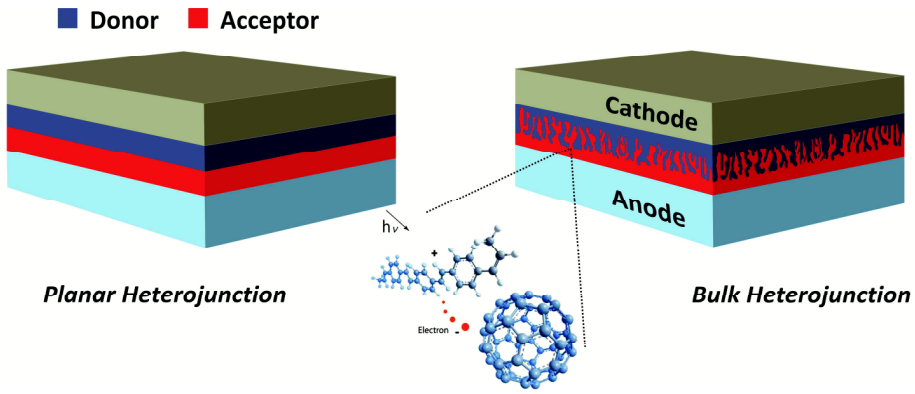

Figure 1.2: Device configuration in planar model and bulk heterojunction model.

1.2.2 Operation mechanism in organic solar cells

The main topic of the thesis is the synthesis of new polymers for BHJ photovoltaic cells, their detailed physico-chemical characterization and their application in test cells. However, for its clarity, it is better to outline the operation mechanisms and to discuss the principal parameters of an organic solar cell before focusing on the design, synthesis and characterization of polymers. Chemical structures of polymers, their macromolecular, as well as supramolecular parameters, strictly affect the physical properties of the device. As a consequence, if the final aim of the work is the fabrication of new performing materials for organic solar cells application, it is important to understand the fundamental parameters regulating the operation mechanism of the device.

The energy conversion process can be described considering four fundamental steps [22], [23]:

1. absorption of light and excitons generation
2. excitons diffusion
3. dissociation of the excitons with generation of charges
4. charge transport and collection.

All these steps are schematically depicted in Figure 1.3.

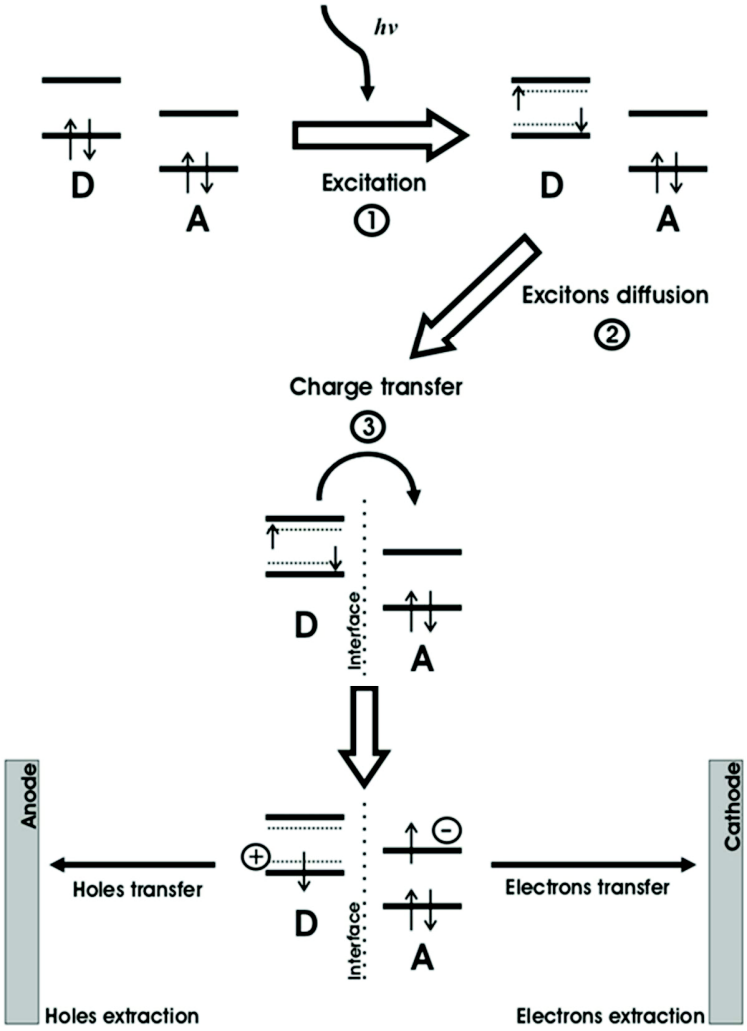

Figure 1.3: Energy conversion process in organic solar cells.[22], [23]

The excitonic character of optical properties is the reason why organic solar cells are often referred to excitonic cells. While optical absorption in a conventional inorganic semiconductor results in the immediate creation of free charge carriers, in an organic semiconductor it leads to the formation of a spatially localized electron-hole pair, a Frenkel-type exciton, which is electrically neutral. Conjugated materials absorption bands are usually intensive, because of the large wave function overlapping between the electronic ground state and the lowest excited state, and broad, because of the significant geometry relaxations taking place in the excited state.

Large molar absorption coefficients of organic semiconductors can lead to a good match, with sizable portion, of the solar spectrum and efficient light harvesting in relatively thin layers films. For this reason, tandem cell geometries started to be used to maximize photons collection.

Due to the fact that optical absorption does not produce directly free holes and electrons, current generation is allowed only by exciton dissociation. To form free carriers, excitons must migrate to the donor-acceptor

interface, before their relaxation and recombination.[24] Because excitons are neutral species, their motion is not influenced by an electrical field and they diffuse randomly. To prevent recombination, the thickness of the organic layer has to be comparable to the exciton diffusion length. In BHJ model it is necessary to find a compromise between the thicknesses of organic layers: thin layers are better for efficient exciton diffusion, but thicker layers more efficiently absorb the sunlight. Once carriers have been separated they move toward the electrodes with an efficiency depending upon their mobility.[25] In crystalline inorganic semiconductors, the three dimensional character and rigidity of the lattice ensure wide valence and conduction bands. To the contrary, in organic semiconductors, the weakness of the electronic couplings, the large exciton vibration coupling and the disorder effects result in lower carriers mobilities. Moreover, these mobilities are additionally influenced by the morphological features of the layer.

1.2.3 Physical parameters of organic solar cells

Power conversion efficiency (PCE,η)

Studying the variation of the current density, related to the applied tension, it is possible to determine main physical parameters of a solar cell. For example in dark conditions, solar cells act as a diode and, under light, a current is produced. The power conversion efficiency corresponds to the ratio between the maximal power, given by the cell, and the power of the incident light. So, the conversion yield is calculated by the formula (Eq.1.1):

$$\eta = \frac{P_{max}}{P_{min}} = \frac{I_{sc} \cdot V_{oc} \cdot FF}{P_{in}} \qquad (Eq.1.1)$$

Where V_{oc} is the open circuit voltage, I_{sc} is the short circuit current and FF is the fill factor. All these parameters are defined in Figure 1.4.

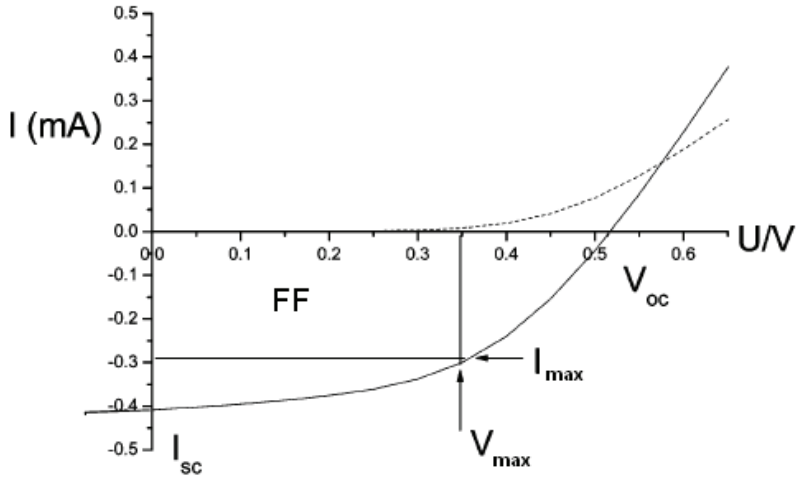

Figure 1.4: I-V Characteristics under light and in the dark (dot line).

The yield of power conversion efficiency is determined under a specific irradiation. The standard irradiation is the AM (Air mass) 1.5 spectrum with a light power of 100 mW·cm^{-2}. AM 1.5 irradiation corresponds to the solar spectrum, at the Earth surface, which passes through the atmosphere with an incident angle of 48.2°.[26]

Open circuit voltage (V_{oc})

The V_{oc} represents the tension at which the current is equal to zero. Normally, in inorganic cells of the metal-semiconductor-metal type, V_{oc} is limited by the energy difference between the work functions at the electrodes. In organic solar cells, it is demonstrated that the work functions do not influence the V_{oc} value to a large extent. On the other hand, this parameter depends on the acceptor LUMO level and on the donor HOMO level. Open circuit voltage decreases linearly with the decrease of the LUMO of the acceptor and it increases linearly with the decreasing of the donor HOMO level (see Figure 1.5).[21], [27]

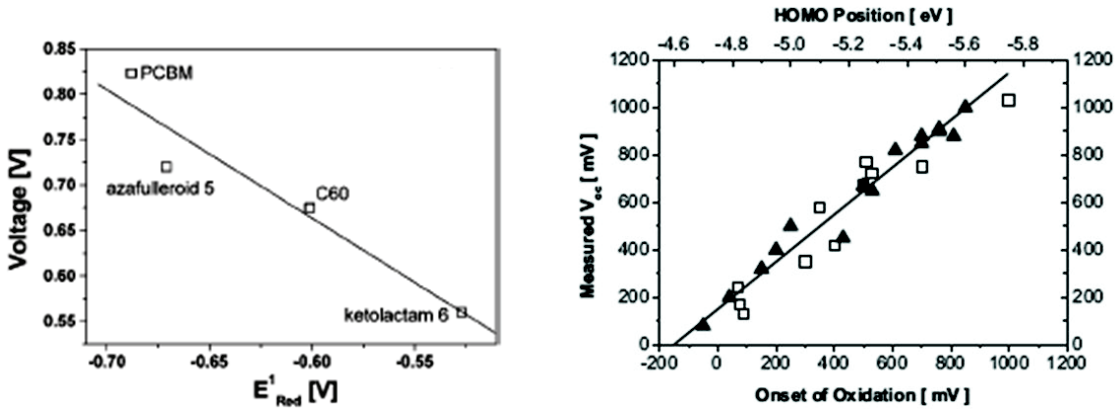

Figure 1.5: a) V_{OC} linear variation depending on the reduction potential of the acceptor material (and as a consequence on its LUMO level) and on b) the oxidation potential of the donor material (and as a consequence on its HOMO). Electrochemical analysis were performed using, as a reference, a Ag/AgCl wire (calibrated with ferrocene) in an electrolytic solution of NBu_4PF_6 (0.1 M) in acetonitrile, v = 200 mV·s^{-1} at room temperature.[27], [28]

As a consequence, it can be stated that an optimal energy gap of 1.5 eV is a good compromise between the above explained contradictory factors. Moreover the HOMO level position for an optimal polymer should be around -5.4 eV. It is therefore possible to explain why the V_{oc} is determined by the difference between the donor HOMO level and the acceptor LUMO level. Considering, in addition, excitons binding energy, Scharber et all. proposed an empiric formula (Eq.1.2), which relates V_{oc} with the HOMO and LUMO levels of the D and A components of the cell [28]:

$$V_{oc} = E_{LUMO}(A) - E_{HOMO}(D) - 0.3\ eV \qquad (Eq.1.2)$$

A minimum energy difference of 0.3 eV between the HOMO level of the polymer and the LUMO level of the acceptor is necessary to facilitate excitons splitting and charge dissociation, so considering a PCBM 1-(3-methoxycarbonyl)-propyl-1-phenyl-(6,6)C_{61} acceptor material (LUMO of -4.2 eV), the lowest possible LUMO level of the donor material, would be of -3.9 eV. On the other hand, a decrease of V_{oc}, increases necessarily the energy gap, lowering the sun light absorption ability of the polymer and, as a consequence, the J_{sc} value. The origin of the open circuit voltage parameter is under debate and it has been demonstrated that it additionally depends on other than the polymer HOMO level factors. It was shown that an important factor affecting the V_{oc} value is the ratio of the donor and the acceptor components. With increasing PCBM to polymer ratio, V_{oc} decreases almost linearly (see Figure 1.6).[29] This variation could be explained by the dielectric permittivity difference between the donor and the acceptor. The relative permittivity of PCBM is usually higher than that of

conjugated polymers which results in a decrease of the free charge carriers energies and to a decrease of V_{oc}.[30]

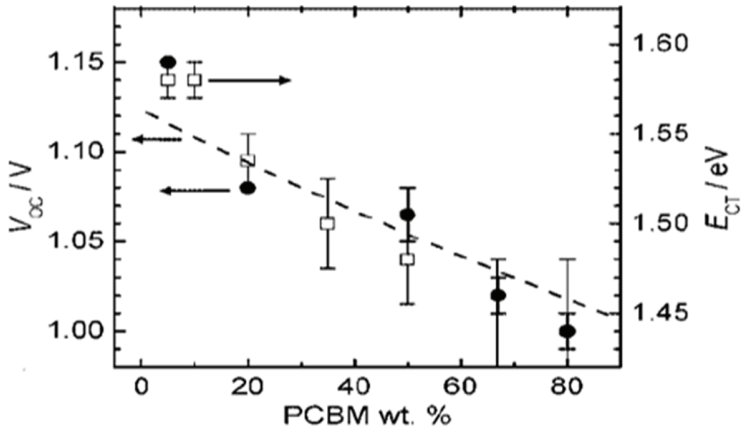

Figure 1.6: V_{oc} variation depending on the acceptor to donor ratio in a BHJ model based on poly[2,7-(9,9-dialkylfluorene-alt-5,5-(4',7'-di-2-thienyl-2'-1'-3'-benzothiadiazole)(PF10TB) and on PCBM.[29]

The V_{oc} can in this case be described by the following formula (Eq.1.3):

$$V_{oc} = \left[E^0\left(\frac{D}{D^+}\right) - E^0\left(\frac{A}{A^+}\right)\right] - \frac{Z}{e}\left(\frac{1}{\varepsilon_{ref}} - \frac{1}{\langle\varepsilon_{ref}\rangle}\right)\left(\frac{1}{r^+} - \frac{1}{r^-}\right) - \Delta \quad (Eq.1.3)$$

Where $E^0\left(\frac{D}{D^+}\right)$ and $E^0\left(\frac{A}{A^+}\right)$ are redox outward potentials of the donor oxidation and of the acceptor reduction, $Z = \frac{e^2}{8\cdot\pi\cdot\varepsilon_0}$ (ε_0 is the dielectric permittivity in the vacuum and e is the elementary charge), ε_{ref} the solvent permittivity in which redox potentials are determined, ε_r the average relative permittivity of the active layer, r^+ the cation radius et r^- anion radius and Δ describes the energetic lost due to recombination and due to problems at interfaces.

Furthermore morphology is involved because of its important influence on the saturation dark current. For example Thompson and coworkers reported the inverse dependence of V_{oc} on the saturation dark current density for small –molecules, for example (tetracene, rubrene):C_{60} BHJ solar cell.[31] Polycrystalline BHJs containing aggregates show lower V_{oc} and higher J_{sc}. The inversed behavior is registered for more amorphous systems. Such correlation was reinforced for polymers by Frisbie and coworkers.[32] These experiments underline the importance of weak ground state interactions between the polymer and PCBM, determining the open circuit voltage value.[33] Consequently, the V_{oc} depends linearly (given the logarithmic dependence of V_{oc} on J_{sc}) on the spectral position of the charge-transfer band.[33], [34] Recently Ohkita and coworkers demonstrated that the V_{oc} decreases at the increase of the saturation current density for P3HT: fullerene BHJ devices.[35]

To conclude, V_{oc} is determined by the donor and acceptor energy levels and it is influenced by the ratio of the acceptor and donor components in the layer because of the changes in dielectric permittivity. In addition to this, considering that photons energy is in inversely proportional to the wavelength length, the higher wavelength absorbance creates free charge carriers at minor energies causing a decrease of V_{oc}.[36] V_{oc} could be limited by the presence, between electrodes of secondary currents and by interfaces and electrodes quality. To improve the V_{oc} it could be useful to interpose a PEDOT:PSS layer between the anode and the active material because its

work function is intermediate between the work function of ITO layer and that of the HOMO of the majority of polymers used for OPV. For the same reason a thin LiF layer should be deposited between the active layer and the cathode to reach a higher V_{oc}.[37]

Short circuit current (I_{sc})

Short circuit current is obtained when the tension applied to the electrodes is equal to zero. It depends on the generated charges density and on their mobility.

Theoretically, the maximal current is a function of the photons number which could be extracted from the device, hence of the donor's gap. High wavelength absorption is necessary to obtain high currents. Since PCBM has poor absorption in the visible and near IR-range, where most of the solar flux is located, the donor polymer has to serve as the main light absorber and, to cover the good absorption range, it should be characterized by an energy gap from 1.4 eV to a maximum of about 2 eV. An inferior gap, even if could increase the amount of light absorbed, causes an increase of the HOMO level and a consequent lowering of the V_{oc}.

In an ideal case, without recombination: $I_{sc} = n \cdot e \cdot \mu \cdot E$, where n is the density of the free photogenerated carriers, e is the elementary charge, μ is the ambipolar mobility and the E is the internal electric field. The short circuit density is given by the ratio between the short circuit current (I_{sc}) and the active surface (A) of the cell $J_{sc} = \frac{I_{sc}}{A}$.

The theoretical values of J_{sc} are higher than the experimental ones, because different loss mechanisms occur during the charge generation, transport and extraction.[23] To minimize these losses, the following parameters must be optimized: molecular weight, charge mobility and the layer morphology.

Fill factor (FF)

The fill factor is given by the ratio between the maximal power generated by the cell and the product of the short circuit current density and the open circuit voltage. (Eq.1.4)

$$FF = \frac{P_{max}}{I_{sc} \cdot V_{oc}} = \frac{I_{max} \cdot V_{max}}{I_{sc} \cdot V_{oc}} \qquad (Eq.1.4)$$

It depends on the number of free charge carriers collected to the electrodes. It is limited by charges recombination. High values of FF could be obtained only with small series resistance (R_s) and large shunt resistance (R_{sh}) which are influenced by the morphology of the blend. Though, mobility depends on the organization of nanostructures of materials and on the contact with electrodes.

External quantum efficiency (EQE)

The External Quantum Efficiency (EQE) or Incident Photon to Current Efficiency (IPCE) represents the ratio between the number of free charge carriers collected to the electrodes and the incident photons' number.

In practice the IPCE spectrum can be obtained by recording the short circuit current for different wavelengths at a defined incident power (P_{in}).

For each wavelength the IPCE is calculated by the formula (Eq.1.5):

$$IPCE = \frac{h \cdot c}{e} \cdot \frac{J_{sc}}{P_{in} \cdot \lambda} = 12400 \cdot \frac{J_{sc}}{P_{in} \cdot \lambda} \qquad (Eq.1.5)$$

Where λ is the wavelength [nm], J_{sc} is the short circuit current density [mA·cm^{-2}] and P_{in} incident power [W·cm^{-2}].

The internal quantum efficiency (IQE)

This parameter is defined as the ratio between the number of electrons collected to the cathode and the number of photons absorbed in the device.[38] (Eq.1.6)

$$IQE(\lambda) = \frac{IPCE(\lambda)}{Abs(\lambda)} \qquad (Eq.1.6)$$

Where *Abs(λ)* is the cell absorbance to an established wavelength.

In a BHJ consisting of PCDTBT (poly[N-9''-hepta-decanyl-2,7-carbazole-alt-5,5-(4',7- di-2- thienyl-2',1',3'-benzothiaziazole) : $PC_{70}BM$[39] an IQE approaching 100% was obtained.[39]

1.2.4 Bulk heterojunction active layer materials

1.2.4.1 Introduction-bulk heterojunction

Solution processed BHJ solar cells offer the possibility of manufacturing the active layer over a large area in one step at room temperature, by different methods of printing or film casting, including those which are used industrially. Selection of materials adapted for this processing technique is very important for general functioning of the device. The power conversion efficiency has improved from below 1% to over 8% in the last past 16 years, playing mainly on the donor material engineering.

Significant results were obtained for the first generation of conjugated donor materials such as poly(phenylene)vinylene (PPV), poly[2-methoxy-5-(2'-ethylhexyloxy)1,4-phenylenevinylene] (MDMO-PPV), resulting in a maximal power conversion efficiency of 3.3 % for a PPV-based BHJ solar cell.[21]

Then, in the second phase, due to a small band gap (about 1.9 eV), cells based on regioregular poly(3-hexylthiophene) (rr-P3HT) showed a higher current density, over 10 mA·cm^{-2} and, after further morphological optimizations, a PCE of 5.5% was achieved.[40] Unfortunately, because of its high HOMO level (-5.1 eV), the V_{oc} corresponding to a BHJ solar cell with $PC_{61}BM$, was restricted to 0.6 V.

Finally in the third phase, a large spectrum of π-conjugated polymers has been studied. In different bulk heterojunction solar cells, some "record" values have been shown (See table 1.1): high V_{oc} over 1 V [41], [42], J_{sc} over 17.3 mA·cm^{-2} [43] and FF over 70%.[44], [45]

Polymer	Polymer:PC_xBM	V_{oc} (V)	J_{sc} ($mA \cdot cm^{-2}$)	FF (%)	η_{max} (%)
P3FTBT6 [41], [42] 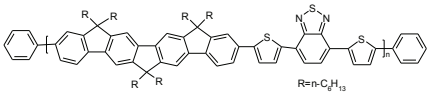	1:4($PC_{71}BM$)	**1.04**	10.3	42	4.50
P2 (*Poly[(4,4-didodecyldithieno[3,2-b:20,30-d]silole)-2,6-diyl-alt-(4,7-bis(2-thienyl)-2,1,3-benzothiadiazole)-5,50-diyl])* [43] 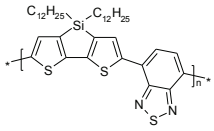	1:1($PC_{71}BM$)-4% chloronaftalene (CN)	0.57	**17.3**	61	5.9
PBnDT-FTAZ [44], [45] 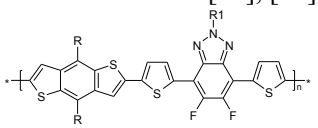	1:2 ($PC_{61}BM$)	0.79	11.83	**72.9**	6.81

Table 1.1: Record values of V_{oc}, J_{sc} and FF reached for three polymers belonging to the third phase of π-conjugated polymer in BHJ with PC_xBM derivatives.

If all these parameters could be obtained for the same BHJ solar cell, it would be possible to obtain a PCE of exceeding 12%. Unfortunately it is difficult to have a rational balance between V_{oc} and J_{sc}.

Developments were directed to increase PCE determining parameters, following the Eq.1.1 and taking into account the mechanisms previous explained (see the *paragraph 1.2.3*).

Among polymers synthesized to date and tested in photovoltaic devices, a dithienyl-benzothiazole – 2,7-carbazole alternating copolymer, namely poly[N-hepta-decanyl-2,7-carbazole-alt-5,5-(dithienyl-benzothiadiazole) (PCDTBT), emerged as a promising material for plastic electronics, since its first synthesis by Leclerc's group in 2001.[46] It showed a PCE of 3.6% with V_{oc} of 0.9 V. After optimization it increased to 6%, and the cell showed an excellent stability.[39], [47]

In the acceptor component, fullerene derivatives with solubilizing groups are usually used.[1]

To summarize, with very few exceptions it is difficult to combine good performance with good stability in one device, therefore search for new polymers for photovoltaics is still needed.

1.2.4.2 Conjugated polymers engineering and new families of low band gap polymers

The most characteristic feature of conjugated polymers is their spatially extended π bonding system. It is instructive to analyze its peculiarities using the simplest polyene – polyacetylene – as an instructive example.

How does it evolve with increasing molecule length? In ethene (ethylene) the π-bonding system is described by one bonding (π) and one antibonding (π^*) orbital. Following the Pauli principle, the π system in the shortest conjugated molecule (1,3-butadiene) must consist of two bonding (π) and two antibonding (π^*) orbitals. In 1,3,5-hexatriene, where three π bonds are in conjugation, three π bonding and three π^* antibonding orbitals can be distinguished (see Figure 1.7). Note that with increasing number of π bonds the energetic spacing between the particular bonding and antibonding orbitals decreases. The energy difference between the highest occupied π orbital (HOMO) and the lowest unoccupied π^* orbital (LUMO) also decreases. For polyenes of high polymerization degree, which is the case of polyacetylene, the discrete energy levels merge into two bands: fully occupied π-band and empty π^*-band, which are separated by an energy gap. The upper edge of the π band corresponds in this case to the HOMO level whereas the lower edge of the π^*-band – to the LUMO level.

The positions of the HOMO and LUMO levels and the band widths determine electronic and redox properties of conjugated polymers.[10], [48], [49]

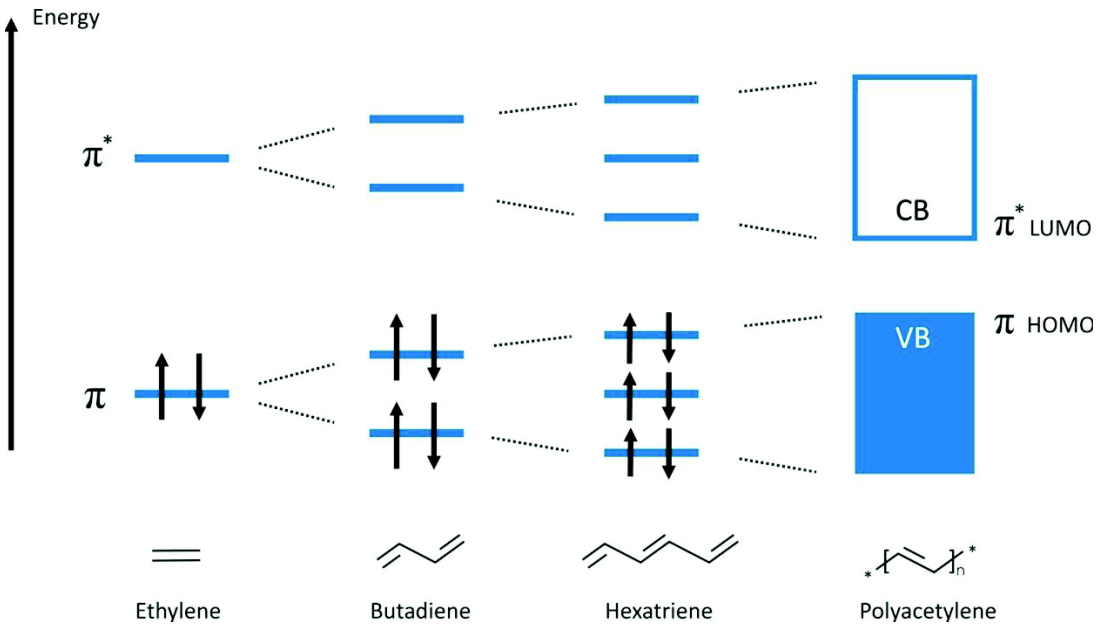

Figure 1.7: Evolution of the electronic structure of polyenes with increasing number of π-π bonds being in conjugation.*

Depending of the chemical constitution of the polymer chain the band gap of conjugated polymers can be varied between 1 and 3 eV.

This thesis is devoted to conjugated polymers in their neutral i.e. semiconducting state. However, another interesting feature of these materials should be briefly pointed out. They can be transformed into organic

conductors or even organic metals (in some cases) through the so called "doping reaction". This doping process is in reality a redox reaction transforming the neutral polymer chains into polycations (oxidative or p-type doping) or polyanions (reductive or n-type doping). In polymers containing acidic sites in their main chain, acid-base type of doping is also possible. Phenomenological manifestation of the doping reaction is an increase of the polymer conductivity by several orders of magnitude.[50] The environmental stability of the doped polymers depends on the position of their HOMO and LUMO levels. For example, polymers with high lying HOMO levels, like polypyrrole or poly(3,4-ethylenedioxythiophene) are more stable in their polycationic (doped) from than in their neutral (undoped) one. Doped conjugated polymers are usually applied as components of modified electrodes, hole transporting layers, antistatic coatings (in blends with conventional polymers) and others.

Generally a π -conjugated polymer could be divided into three components: conjugated backbone, side chains of alkyl or alkoxy-type which facilitate its solution processing and substituents which modify the π electron density in the polymer backbone. The conjugated backbone is the most influencing component and, even if a lot of designs have been reported, it is possible to find empirical strategies to optimize the choice of polymer chains and their components. The principle of molecular design, band gap engineering, structure-properties relationships and device performances can give suggestions of how a conjugated polymer could be optimized for OPV applications.

First of all the magnitude of the band gap and the energy levels positions have to be considered. On one side it is important to narrow the optical band gap to obtain polymers with broader absorption without affecting molar absorption coefficients of polymers. The ideal design of a "low band-gap polymer" should allow absorption light of the wavelength above 600 nm. The band gap modulation is useful to cover a large range of the solar spectrum with most of the intensity centered below 2000 nm.[51]

The sun intensity spectrum is based on data from NREL[1] (see Figure 1.8).

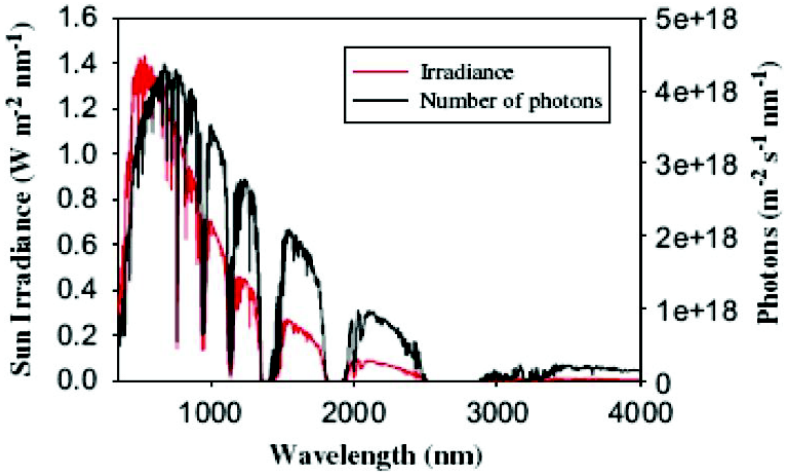

Figure 1.8: Sun irradiance (red) and number of photons (black) as a function of wavelength.[36]

The representation of the solar spectrum in photon flux, as function of wavelength, shows how many photons are available for conversion into electrons. So, from one side, it is better to focus the attention on longer

[1] *http://www.nrel.gov/solar radiation/*

wavelengths but, on the other side, the energy of the charge carriers, at longer wavelengths, is lower and it limits the voltage difference produced by the device. However the absorption should be extended beyond 600 nm. As already described, the way to reduce the band gap is by either raising the HOMO or lowering the LUMO level.

Unfortunately optical properties are not the only one parameter that should be considered in making π-polymers for organic photovoltaic. To obtain high efficiencies from BHJ polymer solar cells, the π-type materials properties have to be taken into account throughout the development process. While a higher V_{oc} could be reached by lowering the donor HOMO level, the reduction of a polymer band gap is only possible lifting up the HOMO level. In this way a loss of V_{oc} inevitably occurs. On the other hand the acceptor LUMO level has to be at least 0.3 eV below the donor LUMO level to allow excitons dissociation and electrons transfer. It is clear that a compromise is necessary.

From the synthetic point of view, designing of such polymers is not a trivial task. Some of the general design strategies to control their energy levels and band gap are described below. They are also summarized in Figure 1.9.

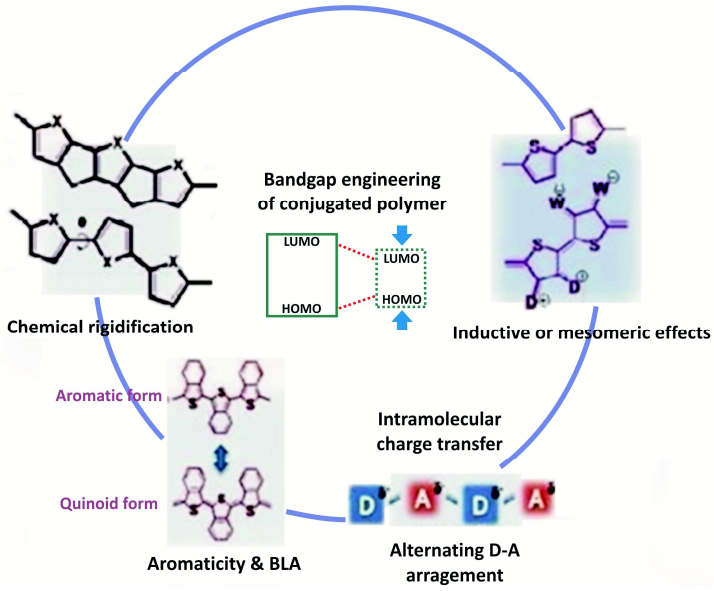

Figure 1.9: Band gap engineering strategies.[52]

Band gap narrowing is in general easier in the case of alternating copolymers than in homopolymers. In the latter case one of the options, usually used in the synthesis of low band gap aromatic or heterocyclic conjugated polymers, is to favor quinoid structures, in which two aromatic units are fused together and the resonance of the first aromatic unit dearomatize the second one which has to adopt a quinoid structure.[53], [54] In this way, the stabilized quinoid form allows a reduction of the energy gap. On the other hand, these polymers are characterized by a high HOMO level producing a low V_{oc} on BHJ solar cells.[55]

Another strategy, very popular in recent years, and also used in this work, is the synthesis of alternating copolymers consisting of electron donating (*push*) and electron accepting (*pull*) units.[2] The intra-chains

transfer processes facilitate double bond formation and the consequent planarization of the polymer chain [54], allowing a more significant delocalization.

Concerning the electron-donating moiety, fluorene, carbazole and thiophene polymeric derivatives are the most frequently used, considering their applications in electronics devices, such as field-effect transistors [56], photovoltaic cells, photodiodes [3] and biosensors.[57], [58]

On the other hand, the variety of electro-accepting units usually includes 2,1,3-benzothiadiazole (BT), 4,7-dithien-2-yl-2,1-3-benzothiadiazole (DTBT) [59], diketopyrrolepyrrole (DPP) [45], thieno[3,4-c]pyrrole-4,6-dione (TPD) [60], dithieno[3,2-f:2',3'-h]quinoxaline (DTQ) [61].

1.3 Strategies to synthesize conjugated polymers

1.3.1 Classical synthesis methods

Synthesis of conjugated polymers lies in the efficient carbon-carbon single bond formation between two unsaturated carbons in the aromatics units. Particular reactions provide a good method to form Csp^2-Csp^2 and Csp-Csp^2: as electrochemical methods [62], chemical oxidative polymerization and transition-metal-catalyzed cross coupling reactions. The latter involves a transition metal-catalyzed cross oxidative addition reaction across the C-X bond of an electrophile. Then a transmetallation step with a main group organometallic nucleophile takes place, followed by a reductive elimination step leading to the carbon -carbon bond formation. At the same time the catalyst is regenerated. The most used transition-metal catalysts are nickel or palladium based complexes. The organometallic nucleophiles can be Grignard reagents [63], stannyl [64], boron reagents (Suzuki Miyaura, see Figure 1.10) [65] or copper.[66]

When the electrophilic and nucleophilic centers of the monomeric substrates are accessible, regioregularity can be achieved. In addition to this, reaction conditions are quite mild and can tolerate different functional groups. The most efficient methods to obtain a conjugated copolymer are Still and Suzuki reactions. Suzuki is used for preparing benzene rings-containing polymers.

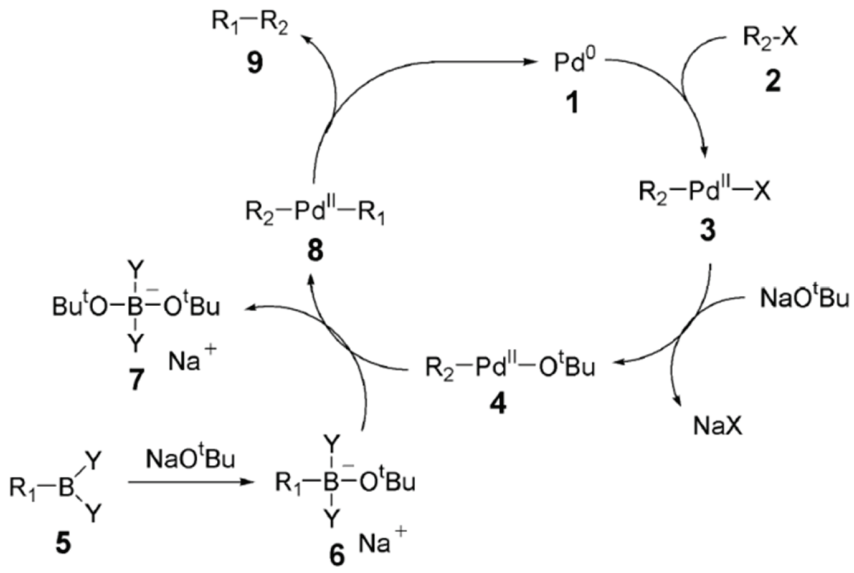

Figure 1.10: Suzuki mechanism with boronic groups on the benzene ring of the monomer.

For the preparation of homopolymers the nickel-mediated Yamamoto dehalogenation coupling reactions are frequently used.[67]

In the last year, a new polymerization method, the so called direct arylation, has been developed and optimized by the Mario Leclerc group.[68] Actually, this method has been found to be well-performing for polycondensation reaction between a thienopyrrole electron accepting sub-unit coupled first with a carbazole electron-donating moiety and, second, very recently, with a new thertiophene electron donating unit.[68] Reactions are usually carried out in a microwave oven. The advantage of using the direct arylation is the possibility to avoid toxic byproducts or the eventual instability of the organometallic intermediates employed for Suzuki and Stille cross coupling.

The development of these reactions, using palladium catalysts, can allow C-C bonds formation between aromatic units with activated hydrogen, without the use of organometallic intermediates. This type of reaction is mostly developed for the synthesis of small molecules, but it is more and more frequently adapted for the synthesis of conjugated polymers.

1.4 *Push-pull* copolymers - The last generation

As we have already explained, adopting the donor-acceptor (DA) approach [69], narrow band gap copolymers containing *push-pull* units have been designed by alternating electron-rich (donating) and electron-deficient (accepting) aromatic or heterocyclic units along the same π-conjugated backbone, affording polymer with red-shifted absorption spectra towards wavelengths of 500-800 nm, where the solar photon flux is most intensive.[1]

Concerning this subject, in the last years, a lot of works were published. The most efficient polymers,

synthesized, in the last few years, are listed in the Table 1.2 and depicted in the Figure 1.11. It should be noted that the majority of them (with the exception of P3HT) belongs to the family of the *push-pull* copolymers.

Polymers	E_g^{opt} (eV)	V_{oc} (eV)	J_{sc} (mA·cm^{-2})	FF	PCE %	Ref. Groups
P-Ge	1.69	0.85	12.6	0.68	7.3	John Reynolds[70]
PDTSTPD	1.73	0.88	12.2	0.68	7.3	Mario Leclerc[60]
PDPPTPT	1.53	0.80	10.3	0.65	5.5	René Janssen[71]
P3HT	1.90	0.84	10.6	0.73	6.7	Yonfang-Li[72]
PBDTDTffBT	1.70	0.91	12.9	0.61	7.2	Wei You[44]
PDTDTBT	1.75	0.92	10.7	0.57	5.7	Yang Yang[73]
PBDTTT-CF	1.60	0.76	15.2	0.67	7.7	Gang Li [74]
IP2	1.37	0.57	17.3	0.61	5.9	Guillermo Bazan[43]
PCDTBT	1.88	0.91	11.9	0.66	7.2	Alan Heeger[75]
PBDDTTPD	1.73	0.85	11.5	0.70	6.8	Jean Marie Fréchet[34]
IP4	1.60	0.75	12.5	0.59	5.5	Ye Tao[76]

Table 1.2: Summary of the most performing copolymers and their respective reference groups. The E_g^{opt} values and the device parameters (V_{oc}, J_{sc}, FF, PCE%) are presented.

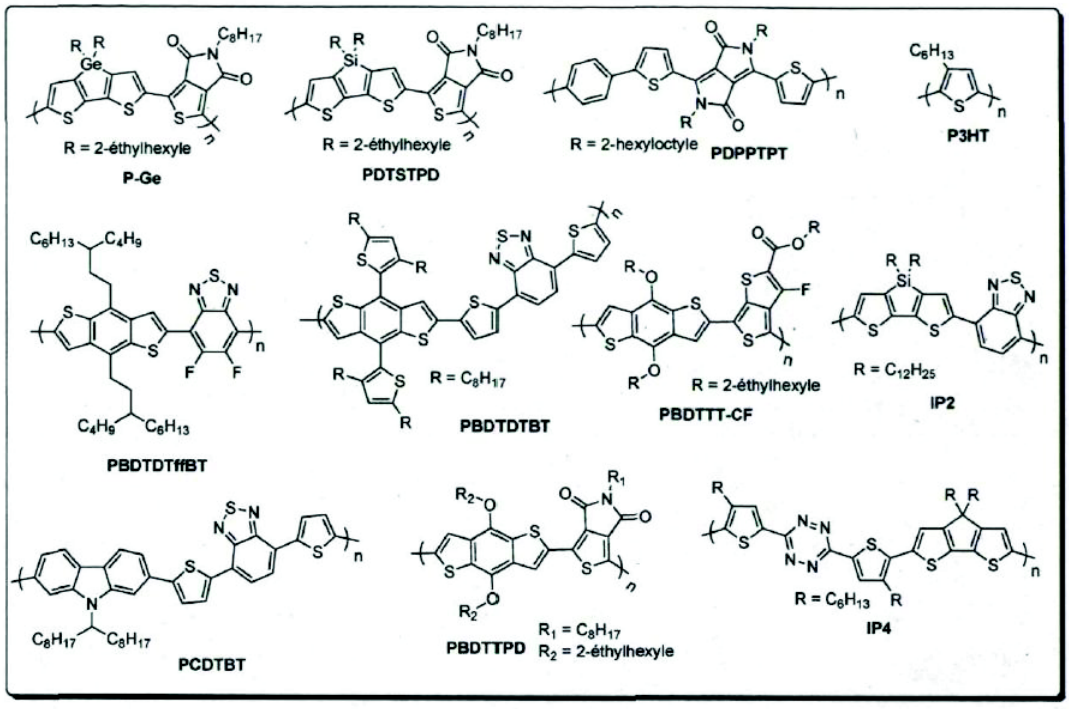

Figure 1.11: Chemical structure of the most performing copolymers in organic photovoltaics.[77]

It becomes difficult to be exhaustive on the state of the art of all existing conjugated polymer families, taking into account the plethora of the newly synthesized systems. Consequently we will focus on these families of conjugated polymers which are subject of the present thesis. This involves polymers with carbazole-, benzodithiophene- and bisthiophene-type donors and benzothiadiazole and thienopyrroledione acceptors. Finally we will discuss some new polymers containing isoindigo groups.

1.4.1 *Push* moieties

1.4.1.1 Carbazole derivatives

In the past, carbazoles were mostly used for OLEDs and OFETs applications. Homopolymers based on 9-alkyl-2,7-carbazole units are popular hole transporting organic semiconductors since they combine good electrical properties with solution processability [78], but they can also be used as building blocks in *push-pull* copolymers.[79]

To understand peculiarities of this family of conjugated polymers it becomes important to outline the chemistry of carbazole and the applied synthesis methods.[80] Because of the electron-donating effects of the nitrogen, polycarbazole chemistry is very different from that of polyfluorenes - a similar family of conjugated polymers.

Favorite sites for the electrophilic attack on fluorene moiety are the 2- and the 7- positions, to the contrary, favorite sites on carbazole are the 3-and 6-positions, followed by the 1- and the 8- positions. As a results, poly(2,7-carbazole)s cannot be synthesized starting from carbazole. Starting from carbazole it is possible to produce poly(3,6-carbazole)s, 3,9-carbazole [81] or 1,8-carbazole [82] units (see Figure 1.12).

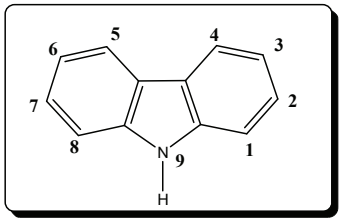

Figure 1.12: Carbazole units with link positions.

The problem with polymers containing these units is the conjugation pathway *via* nitrogen which is less efficient and results in lager band-gap.[83] Nevertheless upon structure modification, those materials can be easily tuned to match the optimal solar spectra emission. For example, copolymers of carbazole and other electron accepting moieties can be synthesized.

The most common and performing polymer of the 2,7-carbazole family was prepared by Suzuki [84], [85] or Yamamoto coupling of dihalo-N-alkylcarbazoles.[86] The Suzuki coupling was carried out between 4-chlorobenzene acid and 4-chloro3-nitrobromobenzene, which occurs selectively at the more reactive bromide site to give 2-nitro-4,4-dichlorobiphenyl. Subsequently the final precursor, the N-octyl-2,7-dichlorocarbazole, was produced by a reductive ring-closure with triethyl phosphite, followed by alkylation.[87] Because of a low reactivity of chlorides in carbazole, it was necessary to pass to the more reactive dibromide substituents in this copolymerization.

To obtain a 2,7-dibromocarbazole in a more efficient way, the commercially available 4,4-dibromobiphenyl was used as a substrate, which after nitration and subsequent reductive ring closure gave the desired product.[88] The critical ring closure step was carried out using triphenylphosphine.[89]

A significant problem related to N-alkylcarbazole-based polymers is their low solubility which yield low molecular masses in soluble and processable fractions. To overcome this problem the addition of branched alkyl side chains is required.[90] Another problem is related to the instability of these polymers under UV light, because of radical cations formation. This point may be overcome by replacing the alkyl groups with aryl substituent. To stabilize 2,7-carbazole it is useful to block 3-and 6-positions because they are favorable sites for oxidation. Substitution on this position induces twisting between adjacent carbazole units in the polymer chain because of the steric effect. Subsequently the gap increases.

The most known group which carries out research on carbazole polymers is the group of Professor Mario Leclerc at the Université de Laval (Québec-Canada). Their research is focused on copolymers for solar cell applications and, among others, they synthesized a copolymer of 2,7-carbazole with heptadecanyl N-substituent and dithienylbenzothiadiazole. A high molecular weight of about 37 kDa with a polidispersity index (PDI) of 2.0 was obtained. The polymer showed the optical bandgap of 1.88 eV with a low-lying HOMO. Optimization of the fabrication of cells based on blends of this polymer led to efficiencies of 6% and the IQE values close to 100%. [39] More recently PCEs of 7.1% were obtained for modified cells exploiting this polymer.[91]

A series of new carbazole copolymers with different acceptor moieties was reported by the same group. Good results pushed Leclerc group to study others different copolymers changing several acceptor moieties.[92], [93]

1.4.1.2 Benzo[1,2-b;3,4-b]dithiophene derivatives

Benzodithiophenes (BDT) constitute another important class of electron donating unit in DA copolymers, suitable for applications in photovoltaic cells.[34], [94], [95] Applications of these new BDT based polymeric materials boost the PCE of polymer solar cells greatly, and recent results indicate that 7.8% PCEs have been achieved by using this class of polymers.[34] (See Figure 1.13)

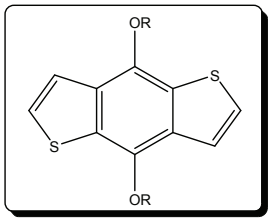

Figure 1.13: Benzodithiophene unit.

In 2008, a BDT-based conjugated polymer was firstly reported for solar cell applications by Hou et al.[55] Band gaps and molecular energy levels of BDT based polymers were successfully tuned by molecular structure design.[55] In the meantime, other groups also exhibited strong interest in this useful conjugated component, and more and more photovoltaic materials with BDT units were developed and reported.

BDT has a symmetric and planar conjugated structure, and hence a regular stacking can be expected for the BDT based conjugated polymers. BDT isomers have a benzo core in the center and two flanking thiophene rings. BTD units offer two advantages: alkylation, to increase solubility of polymers, could be carried out on the central benzene ring. In addition two thiophene units prevent steric hindrance with adjacent acceptor units, leading to a more planar backbone. In comparison with the polymers with other widely used conjugated building blocks, the polymers based on BDT have a relatively better balance between the band gap and the HOMO level

which is closer to the ideal HOMO energy level.

Starting with thiophene-3-carboxylic acid, the BDT monomers can be synthesized. Mostly, three kinds of functional groups, including alkoxy, alkyl and alkylthiophene, were used as side groups on the and 8 positions of the BDT unit to make solution processable polymers. The alkoxy-substituted BDT can be easily synthesized through a one-pot two-step reaction.[55] 4,8-subsituted BDT has two pairs of protons, and the chemical behavior of these protons is similar as to that of protons in a thiophene unit. Protons in 2 and 6 positions exhibit lower pKa value than those in 3 and 7 positions so the 2,6-dilithium salt of BDT can be readily formed by treating the BDT with *n*-butyllithium under room temperature in THF (see Figure 1.14).

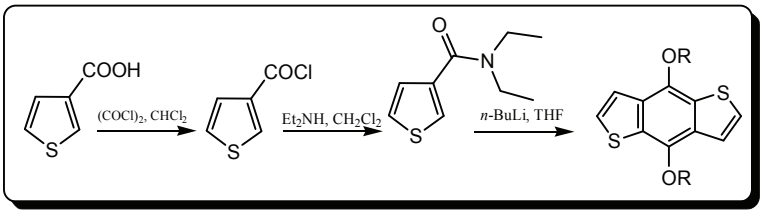

Figure 1.14: Synthesis of BDT core.

Possibility of band gap and the molecular energy levels tuning in BDT-polymers attracted much attention. By co-polymerizing with different conjugated components or by introducing different functional groups, the band gaps and the molecular energy levels of these polymers can be modified in a broad range. In order to minimize the mismatch between the solar irradiation spectrum and the absorbance of a PSC device, the band gap of the polymer should be reduced. To tune the band gap a thiophene unit was first added.[55] The effect of thiophene was not sufficient to significantly decrease the bandgap. The band gap and the HOMO level of the this polymer are 2.59 eV and 5.71 eV respectively.[96] Only after replacing its alkyl groups by alkoxy ones, its band gap can be reduced to 1.83 V but at the same time the V_{oc} of the PSCs is lowered.[55]

Important steps were made by Yang and his group, who was able to obtain a conversion efficiency of 6.6%.[74] The most impressive results were obtained using a *n*-octyl functionalized ketone group and a fluor atom bonded to the main thienothiophene unit. Fluor is important since its presence increases the V_{oc} because of its high electron affinity. The discussed polymer is characterized by a molecular weight of about 20 kDa and an energy gap of 1.6 eV. Its application in solar cells leads to PCE values of 7.7%.[97]

1.4.2 *Pull* moieties

1.4.2.1 Benzothiadiazole derivatives

Benzodiathiazole moiety is actually the most frequently used acceptor.

It is characterized by a strong electron accepting ability and its properties could be optimized, for example, by directly connecting the BTD unit with others monomers (see Figure 1.15).

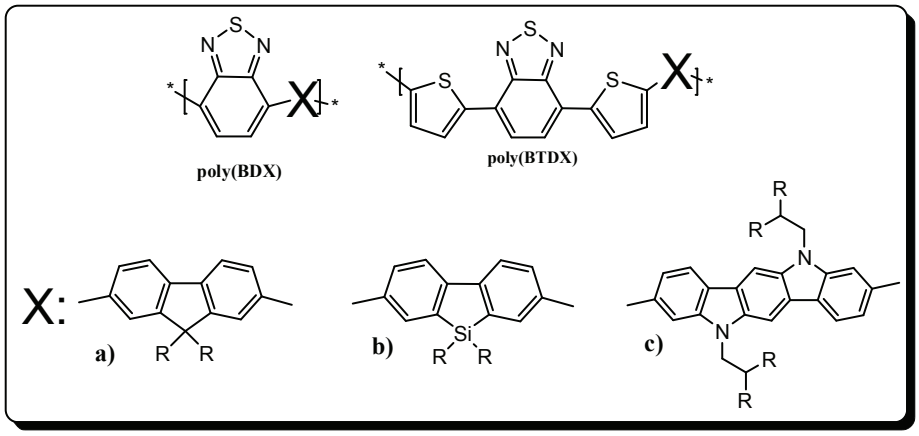

Figure 1.15: BD and BTD units copolymerized with X: a) fluorene, b) silole, c) indolocarbazole.

These polymers are usually obtained by Suzuki or Stille coupling of the corresponding monomers.

Poly[2,6-(4,4-bis-(2-ethylhexyl)-4H-cyclopenta[2,1-b;3,4b]-dithiophene)-alt-4,7-(2,1,3-benzodiathiazole)], abbreviated as **P6**, was one of the first DA polymers containing benzodithiazole units. Initially prepared polymer showed a rather low molecular weight and yielded photovoltaic cells of a PCE of 3.2%.[98], [99] Bazan et al. [100] demonstrated that it was possible to increase the molecular weight using the microwave synthesis. Finally Heeger et al. [101], by optimizing the active layer structure and its morphology, was able to reach a performance of 5.5%, even if V_{oc} was quite low (0.62 V).

Frequently, the benzothiadiazole unit is linked to electron donating units via a conjugated spacer, for example 2,5-thienylene ring as illustrated in Fig. 1.15. The use of these spacers lowers the steric hindrance and improves the conjugation, due to better planarity of the polymer chain [102]. As a consequence, better cell performances are reached. DTBT was copolymerized with several electron donating comonomers such as fluorene, dibenzosilole, germanofluorene, dithieno[3,2-b:2,3-d]pyrrole (DTP) and the indolo[3,2-b]carbazole (IC).

Copolymers with fluorene (see Figure 1.15) suffered from low molecular weight and yielded a rather modest PCE of 2.2% in the devices. However, the V_{oc} value was around 1.0 V and it represented one of the best values ever reported for a BHJ solar cell.[103]

Dibenzosiloles (see Figure 1.15) are more resistant against oxidation, but they are more difficult to synthesize as compared to fluorenes. The best result was reported by Cao et al.[104] For the synthesized alternating copolymer of dibenzosilole and DTBT a PCE of 5.4% in the BHJ configuration was reached.

Copolymers with dithieno[3,2-b:2,3-d]pyrrole (DTP) are also interesting because in BHJ they show a low band gap of 1.46 eV and a reasonable value of PCE (2.2%) despite their low molar weights (1.8 kDa).[74]

Indolo carbazole electron donating units were also copolymerized with DTBT (see Figure 1.11). The main difficulty in this case is poor solubility of the product which limits the molecular weight. Introduction of alkyl solubilizing groups improved the polymer characteristics and allowed to fabricate devices with a PCE value of 1.47%.[105]

1.4.2.2 Thieno[3,4-c]pyrrole-4,6-dione derivatives

Polymers containing thieno[3,4-c]pyrrole-4,6-dione units (see Figure 1.16) as electron acceptors were first reported by Tour and Zhang in the late 90's. [106]

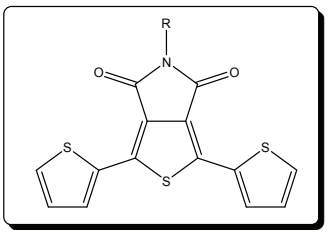

Figure 1.16: Thieno[3,4-c]pyrrole-4,6-dione unit.

Since that time the synthetic procedure was simplified and nowadays the synthesis follows only four steps. In a series of papers Leclerc et al. reported the application of TPD –based copolymers in BHJ-type solar cells.[94] The polymer, poly(benzodithiophen)-thienopyrroledione (PBDTTPD), is characterized by a symmetric and planar structure which improves the electron delocalization, facilitating the chain-chain interactions. The copolymer prepared by Stille coupling showed molecular weight (M_n) of 13 kDa and the band gap of 1.81 eV. The following parameters were obtained for a test device fabricated from this copolymer: PCE = 5.5 %; V_{oc} = 0.85 V; FF = 0.66, J_{sc} = 9.81 mA·cm^{-2}. Independently, Jen et al. [95] synthesized the same copolymer whose molecular weight was however higher (M_n = 33 kDa) but the PCE value in a test device was lower (4.1%). N-alkylthieno[3,4-c]pyrrole-4,6-dione (TPD), exhibits promising properties as a building block in BDT-based polymers. In 2010, four different research groups reported a series of results of PBDTTPDs-based PSCs. In these works, the same conjugated backbone, BDT-alt-TPD, was selected, and different alkyl side groups were employed.[34], [94], [95], [107] These polymers have very similar band gaps and molecular energy levels. The best photovoltaic result, 6.8%, was reported by Frechet et al.[34] It was found that the choice of the alkyl substituents impacts structural order and orientation in the polymer backbones, which critically affects photovoltaic performance of PSCs. A more detailed research of BDT-TPD-based polymers was reported by Leclerc et al.[108] In this work, the relationship among the length of the alkyl chain in the TPD units, the morphology of the copolymers, and the photovoltaic properties of the copolymer based PSCs were fully investigated, providing a good example for the molecular structural optimization of photovoltaic polymers.[108]

Finally Tao and Leclerc et al. [60] obtained a new polymer of this family by copolymerizing DOPT with dithieno[3,2b:2',3'-d]silole, which showed a low band gap of 1.69 eV and reached a PCE of 7.3%, with a V_{oc} of 0.88 V, a FF of 0.68 and a J_{sc} of 12.2 mA·cm^{-2} in test devices.

It is interesting to underline the fact that this family of low band gap copolymers is quite recent (2010) but good cell performances in BHJ configuration have already been reported for several of its members. They can further be improved upon device optimization.

1.4.2.3 Isoindigos

(E)-1H,1'H-[3,3']biindolylidene-2,2'-dione (isoindigo) (see Figure 1.17) - a well-known dye-can be obtained from various natural sources. It has been widely used in the dye industry and can easily be obtained easily from various natural sources. Hence, applications of isoindigo fall into the scope of renewable and sustainable synthetic sources. Unlike blue-colored indigo, isoindigo itself is brown colored and in its solution spectrum (dimethyl sulfoxide solvent) shows two absorption maxima at 365 and 490 nm. Isoindigo also shows better stability than indigo when exposed to light.[109] Isoindigo-based oligomers were first investigated by Reynolds and co-workers [110] and showed promising absorption spectra and favorable electrochemical and photovoltaic (PV) properties.

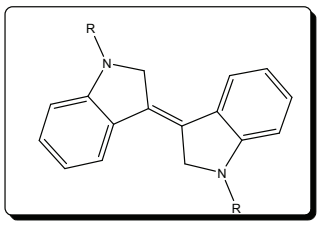

Figure 1.17: Isoindigo unit.

Although the authors also disclosed the photophysical and electrochemical properties of isoindigo-based polymers, their PV performance was not investigated.[111] Very recently, the PV performance of isoindigo-based polymers was independently reported by Zhang et al.[112], [113] and Wang.[114] Only a moderate PV performance was recorded for this particular class of polymers. However, their double indolinone units, which are strongly electron withdrawing, their broad absorption spectra, their high extinction coefficients, and appropriate energy levels inspired others to modify their chemical structures and explore their PV performance further. It was noticed that when different donor units were combined with isoindigo, the resulting polymers exhibited totally different optoelectronics properties. Recently, some successful attempts of the introduction of high performance dyes into conjugated polymers and oligomers have been reported.[115–117] However a relatively low PCE, up to 3% was obtained, with large V_{oc} of 0.9 V, but low J_{sc} of around 5 mA·cm^{-2}.

1.5 Acceptors materials

In BHJ cells the low band gap copolymers, described in *Chapter 2* are used as electron donating components and must accompanied and electron accepting materials. These acceptor materials should satisfy some important requirements to allow functioning of a BHJ solar cell device. As it was mentioned before, the first characteristic should be related to a good matching of the energy gap, mainly promoting the charge transfer from the donor to the acceptor material and allowing good values of V_{oc}. Secondly, it should be characterized by a complementary absorbance to that of the polymer and it should assure a good electrons mobility, at least equal to that of holes in the p-type donor material. Finally, it should have a good solubility, at least 12 mg·mL^{-1} in the processing organic solvents, with good miscibility properties with the donor material to prevent phase segregation. Normally the most frequently used electron acceptors belong to the fullerene's family and they are modified to increase their solubility, as for example in the case of PCBM molecules (see Figure 1.18).

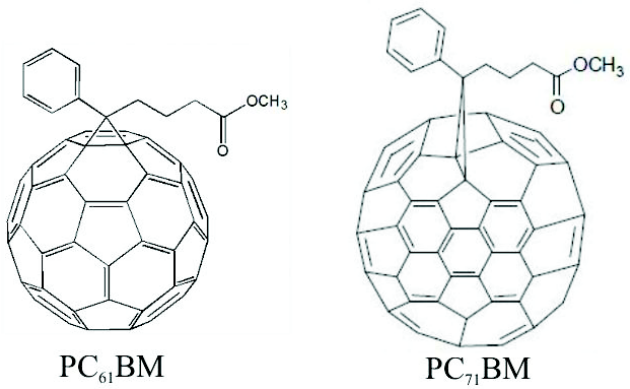

Figure 1.18: The most used electron acceptors in BHJ solar cells: $PC_{61}BM$ and $PC_{71}BM$.

1.5.1 PCBM and Fullerenes

Fullerene derivatives which are the most frequently used in photovoltaic applications are depicted in Figure 1.18. Their application in these devices follows an important discovery reported in 1992 concerning the photoinduced electrons transfer from a conjugated semiconducting polymer to C_{60}.[13], [118], [119] This finding proved that at the fullerene/polymer interface the processes of excitons dissociation and charge separation are very efficient. Fullerenes were quickly replaced by more soluble fullerene derivatives like PCBM.[120] Recently, a derivative of C_{70} namely $PC_{71}BM$ (Figure 1.18) has been increasingly frequently used as a component of BHJ. It is more soluble than $PC_{61}BM$ (respectively 80 $mg \cdot mL^{-1}$ and 50 $mg \cdot mL^{-1}$ in chlorobenzene). Both molecules show very similar LUMO levels but the spectrum of $PC_{71}BM$ covers a wider range of the solar spectrum. Moreover, thin layers nanostructuration is easier with the use of this fullerene derivative. Comparative studies demonstrated that BHJ with $PC_{71}BM$ show better conversion efficiency, mostly due to a short circuit current augmentation. The IPCE measurements confirmed that this enhancement was related to a better quantum yield in the blue region of the spectrum. Better performances are balanced by a quite high cost, which often moves the choice versus the classical PCBM.

In the BHJ configuration many efforts have been undertaken to obtain the maximum energy conversion efficiency controlling the microscopic morphology by thermal annealing.[24], [121], [122]

1.5.2 Nanocrystals

In the past decade inorganic semiconductor nanocrystals have been tested as acceptor phase components of BHJs.[19] One of the significant advantages of the use of nanocrystals is the possibility of precise tuning of their LUMO and HOMO levels due to the so called “quantum confinement effect”.[123], [124] Second, nanocrystals can be controllably prepared in different shapes, for example nanospheres, nanorods, tetrapodes and others (see Figure 1.19). This allows for the modulation of the percolation threshold of the acceptor phase in BHJ, a key parameter for functioning of the cell. Third, their “solubility” or more precisely dispersibility in processing solvents can be tuned by selecting appropriate capping ligands.[19]

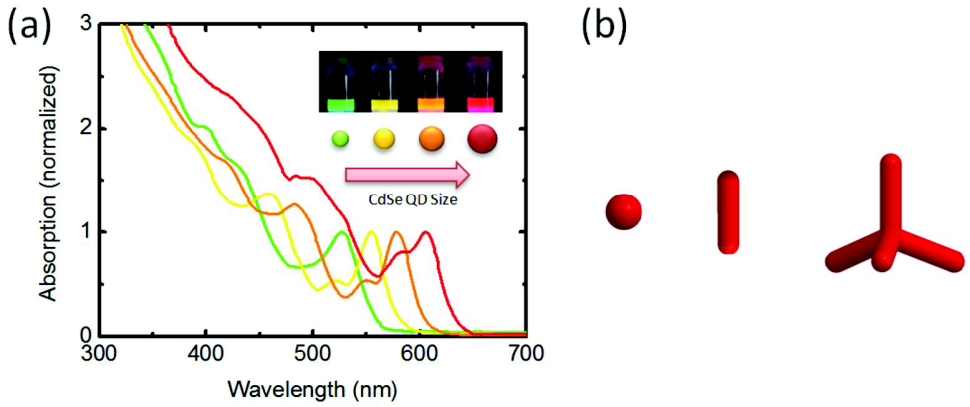

Figure 1.19: (a) Absorption spectrum of CdSe QDs with different sizes. Inset: Photoluminescence (PL) of differently sized QDs (3 nm -6 nm) under UV irradiation. (b) Schematic illustration of different shapes of NCs, from left to right: quantum dot (QD), nanorod (NR), and tetrapod (TP).[125]

However, mixing of semiconducting polymers with inorganic nanocrystals is not a trivial task because both BHJ components have a strong tendency to phase separate. In addition, typical initial capping ligands like TOPO, hexadecylamine, thioles, carboxylic acids, phosphonic acids etc. form an insulating layer on the nanocrystals' surface, impeding to a large extent the charge transfer. Several approaches are used to overcome these obstacles. For example initial insulating ligands can be exchanged for labile ones like pyridine, which are then removed during the solution processing, leaving "naked" nanocrystals in the polymer matrix. Another approach involves the use of conjugated capping ligands [126] or tailor-made ligands able to molecularly recognize appropriately functionalized polymer chain.[127]

The dispersion used for processing usually contains more than 90 vol.% of solvent prior to solvent evaporation. It is assumed that the polymer is fully soluble in the solvent. The (spherical) nanoparticles are assumed to remain dispersed (in a binary nanoparticle-solvent system) until the volume fraction of nanoparticles exceeds a critical value. This value will depend on a number of factors including the nanoparticle geometry, composition and solvent-nanoparticle interaction. Solvent evaporation causes a transition from a one-phase to a two-phases region. These morphologies are thermodynamically unstable and this problem has implications for PCE values and their stability in the time. The nanoparticle material that, so far, has given the highest PCE values in BHJ with conjugated polymers (2.8%) is CdSe.[128] This relatively high value was achieved by using a high boiling point solvent (trichlorobenzene) which promoted formation of a vertical segregated morphology within the photoactive layer.

Two interesting points emerge from the comparison of fullerene derivatives - polymer and inorganic nanoparticles - polymer solar cells PV. These are: (a) the maximum PCE values for the best fullerene -polymer PV cells (i.e., $PC_{71}BM$/PCPDTBT) are approximately twice those for the best inorganic nanoparticle polymer PV cells (i.e., CdSe-OC1C10-PPV) and (b) the best inorganic nanoparticle-polymer photoactive layer in terms of PCE contains CdSe nanoparticles which have comparable energy levels to those of PCBM. A key reason to explain relatively low PCE values for inorganic nanoparticles polymer PV cells is that they exhibit a much lower current density. It is suggested that this is a result of relatively small EQE values responsible for relatively low I_{sc} values and hence PCEs of inorganic nanoparticles/polymer PV cells is their relatively low EQE values. It seems that the relatively low EQE values for those PV cells is due, at least in part, to the greater tendency of the

inorganic nanoparticles to aggregate during solvent evaporation compared to PCBM. In addition, the relatively small diameter of PCBM cf. inorganic nanoparticles gives a larger interfacial area and much smaller polymer domain size. This favors exciton dissociation and an increased PCE.

1.6 Device optimization - Control of the morphology

Control of the morphology, as explained before, is crucial for BHJ functioning. Several factors influence the BHJ morphology which can be classified as intrinsic (cristallinity of materials and the miscibility) and extrinsic (device fabrication, solvent choice, weight ratio of the donor and the acceptor materials, high-boiling-point processing additives, control of the film thickness and thermal annealing).

1.6.1 Solvent nature influence

Shaheen and coworkers [20] have demonstrated that the choice of the solvent could improve FF and J_{sc} keeping V_{oc} constant. The yield of solar cells based on MDMO:PPV:PCBM (1:4) goes from 0.9% to 2.5% using respectively toluene and *o*-dichlorobenzene. This improvement was explained by morphological differences between the films spin-coated from different solvents, the layer deposited from chlorobenzene-layer showing smoother surface. The same phenomenon was reported for PDCTBT:PCBM films.[47]

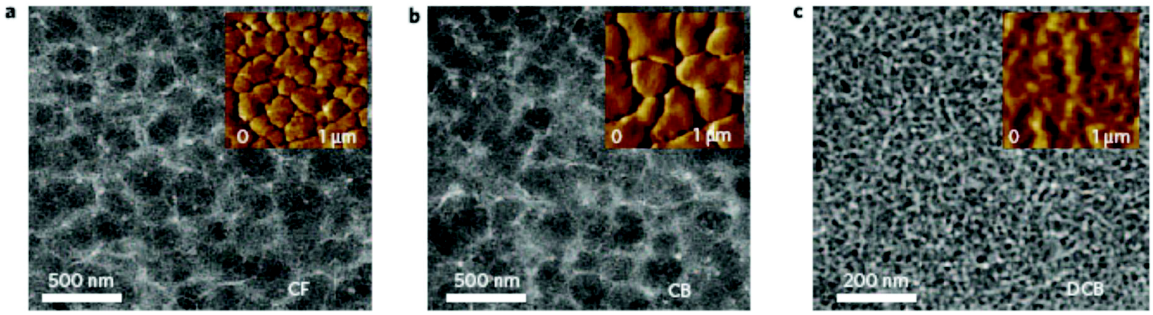

Figure 1.20: TEM images of spin-coated films of PCDTBT:PCBM starting from a chloroform (a), chlorobenzene (b), dichlorobenzene (c) solution.[47]

The influence of the solvent derives from kinetic or/and thermodynamic reasons. For example, the size of active layer domains decreases with the decrease of the solvent evaporation rate. It is therefore possible to obtain more homogenous films (see Figure 1.20). This was observed for example in the case of P3HT:PCBM cells.[25]

1.6.2 Annealing influence

Films annealing could have a significant effect on the morphology improving film cristallinity. However, phase segregation can be favored if the annealing is pursued during long time. In general for all carbazole containing polymers excessive annealing may lead to a decrease in cell efficiency.[25]

1.6.3 Additives influence

Another factor influencing the morphology is the use of low-vapor-pressure small-molecule additives, such as 1,8-octanedithiol and 1,8-diiodooctane (DIO) [129] and 1-chloronaphthalene (CN).[130] The interest of using these small molecules is that the final morphology of the film is essentially determined by the evaporation of these low -vapor-pressure molecules.

Because of the high boiling temperature, additives evaporate slowly. So, in a bulk-heterojunction device, fullerenes stay in solution longer than the polymer and they tend to aggregate, causing an important separation phase. In addition also the chains aggregation of polymer seems to be favored, producing a bathochromic shift of the absorption spectra.[131] The effect of additives on the phase segregation is represented in the Figure 1.21.

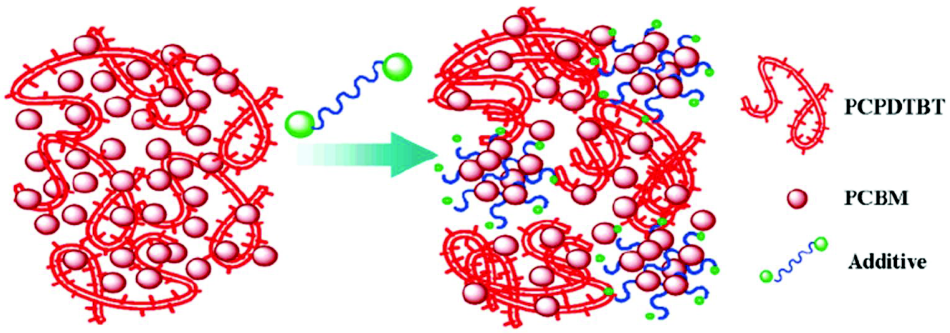

Figure 1.21: Hypothetic role of an additive during a BHJ of PCPDTBT/PCBM formation.

The choice of additives depends on which morphological aspect of film has to be improved. For example, the most used 1,8-diiodooctane promotes polymer aggregation and increase the domain sizes, [129] to the contrary, CN seems to prevent polymer aggregation.[132]

1.7 Conclusion

Bulk-heterojunction solar cells based on π-conjugated polymers, acting as electron donor moieties, and on fullerene derivatives, acting as electron accepting moieties, should be able to compete with other PV technologies, reaching the ideal PCE of 15-20%. This challenge requires a lot of attention on the development of new materials characterized by appropriate intrinsic properties, but also on the understanding of interfacial phenomena occurring, for example, in the interdigited active layer and/or between active layer and electrodes. In addition, a strong-relationship, between chemical and physical parameters, should be taken into account to may reach the final goal.

Tailor-made synthesis of functional polymers, exhibiting low band gaps seems to be a key factor in further improvement of BHJ-based cells. With an appropriate band gap, between 1.4 and 2 eV, a good solar spectrum matching is expected, favoring an increase of short circuit current values. At the same time a good positioning of HOMO an LUMO energy levels, should allow a good charge transfer from the donor to the acceptor material. Optimization of morphology which should form a percolation path, could also favor charges transportation to the electrodes.

In this work the attention is focused on the synthesis of new low-band gap polymers and the adopted chemical strategy aims on developing the so called *push-pull* copolymers, formed by a donor (*push*) and an acceptor (*pull*) electron units in the polymer backbone. In the case of these polymers molecular (chain regularity), macromolecular (molecular weight and its dispersion) and supramolecular parameters have to be controlled.

The state of the art of the most known accepting and donating units motivate the choice of the starting moieties later used for the synthesis of the target polymers. The most known *push* and *pull* units were presented, focusing the attention respectively on benzothiadiazole and diketopyrroledione units and on carbazole and benzodithiophene units. Some of the most performing devices, reaching efficiency of 6% and of 5.5%, were based on poly(2,7-carbazole)bulk heterojunctions and on poly(benzodithiophene) bulk-heterojunction.

Properties of the accepting units were also analyzed, focusing the attention on fullerene derivatives and nanocrystals. Finally the morphological optimization was not neglected, because the distribution of the acceptor phase within the donor phase has also to be taken into account.

[1] P. M. Beaujuge and J. M. J. Fréchet, "Molecular Design and Ordering Effects in π-Functional Materials for Transistor and Solar Cell Applications," *Journal of the American Chemical Society*, vol. 133, no. 50, pp. 20009–29, 2011.

[2] A. Pron, P. Gawrys, M. Zagorska, D. Djurado, and R. Demadrille, "Electroactive materials for organic electronics: preparation strategies, structural aspects and characterization techniques," *Chemical Society Reviews*, vol. 39, no. 7, pp. 20009–29, 2010.

[3] Y. J. Cheng, S. H. Yang, and C. S. Hsu, "Synthesis of Conjugated Polymers for Organic Solar Cell Applications," *Nature Photonics*, vol. 3, no. 12, p. 15, 2009.

[4] R. H. Hadfield, "Single-photon detectors for optical quantum information applications," *Nature Photonics*, vol. 3, no. 12, pp. 696–705, 2009.

[5] Y. Woo and A. J. Heeger, "Semiconducting polymers: the Third Generation," *Chemical Society Reviews*, vol. 39, no. 7, pp. 2354–2371, 2010.

[6] Y. Lin, Y. Li, and X. Zhan, "Small molecule semiconductors for high-efficiency organic photovoltaics," *Chemical Society Reviews*, vol. 41, no. 11, pp. 4245–4272, 2012.

[7] J. E. Anthony, "Small-Molecule, Nonfullerene Acceptors for Polymer Bulk Heterojunction Organic Photovoltaics," *Chemistry of Materials*, vol. 23, no. 3, pp. 583–590, 2011.

[8] F. Zhang, D. Wu, Y. Xu, and X. Feng, "Thiophene-based conjugated oligomers for organic solar cells," *Journal of Materials Chemistry*, vol. 21, no. 44, p. 17590, 2011.

[9] C. K. Chiang, C. R. Fincher, Y . W. Park, A. J. Heeger, H. Shirakawa, E. J. Louis, S. C. Gau, and A. G. MacDiarmid, "Electrical Conductivity in Doped Polyacetylene," *Physical Review Letters*, vol. 39, no. 17, pp. 1098–1101, 1977.

[10] A. J. Heeger, "Semiconducting and Metallic Polymers: The Fourth Generation of Polymeric Materials (Nobel Lecture)," *Angewandte Chemie International Edition*, vol. 40, no. 14, pp. 2591–2611, 2001.

[11] H. Shirakawa, "The Discovery of Polyacetylene Film: The Dawning of an Era of Conducting Polymers (Nobel Lecture)", The Nobel Foundation 2001, *Angewandte Chemie International Edition*, vol. 40, no. 14, pp. 2574–2580, 2001.

[12] A. G. MacDiarmid, "'Synthetic Metals': A Novel Role for Organic Polymers (Nobel lecture) - 'Synthetische Metalle': eine neue Rolle für organische Polymere (Nobel-Vortrag)," *Angewandte Chemie International Edition*, vol. 40, no. 14, pp. 2581–2590, 2001.

[13] N. S. Sariciftci, L. Smilowitz, A. J. Heeger, and F. Wudl, "Photoinduced Electron Transfer from a Conducting Polymer to Buckminsterfullerene," *Science*, vol. 258, no. 5087, pp. 1474–1476, 1992.

[14] D. L. King, S. Igari, W. Warta, and M. Green, "Progress in Photovoltaics, Research and Applications (2005)," pp. 1349–1354, 2005.

[15] R. W. Miles, K. M. Hynes, and I. Forbes, "Photovoltaic solar cells: An overview of state-of-the-art cell development and environmental issues," *Progress in Crystal Growth and Characterization of Materials*, vol. 51, pp. 1–42, 2005.

[16] U. S. Washington, DC, "Service, R.F. Science," vol. 332, no. (6027), p. 293, 2011.

[17] B. O'Regan and M. Grätzel, "A low-cost, high-efficiency solar cell based on dye-sensitized colloidal TiO_2 films," *Nature*, vol. 353, no. 6346, pp. 737–740, 1991.

[18] B. Sun and N. C. Greenham, "Improved efficiency of photovoltaics based on CdSe nanorods and poly(3-hexylthiophene) nanofibers," *Physical Chemistry Chemical Physics*, vol. 8, no. 30, pp. 3557–3560, 2006.

[19] W. U. Huynh, J. J. Dittmer, and A. P. Alivisatos, "Hybrid nanorod-polymer solar cells," *Science*, vol. 295, no. 5564, pp. 2425–7, 2002.

[20] S. E. Shaheen, C. J. Brabec, N. S. Sariciftci, F. Padinger, T. Fromherz, and J. C. Hummelen, "2.5% efficient organic plastic solar cells," *Applied Physics Letters*, vol. 78, no. 6, pp. 841–843, 2001.

[21] C. J. Brabec, S. E. Shaheen, C. Winder, N. S. Sariciftci, and P. Denk, "Effect of LiF/metal electrodes on the performance of plastic solar cells," *Applied Physics Letters*, vol. 80, no. 7, pp. 1288–1290, 2002.

[22] W. M. Blom, V. D. Mihailetchi, L. J. Koster, and D. E. Markov, "Device Physics of Polymer: Fullerene Bulk Heterojunction Solar Cells," *Advanced Materials*, vol. 19, no. 12, pp. 1551–1566, 2007.

[23] N. Moliton, "How to model the behavior of organic photovoltaic cells," *Polymer International*, vol. 55, no. September 2005, pp. 583–600, 2006.

[24] B. C. Thompson and J. M. J. Fréchet, "Polymer-fullerene composite solar cells.," *Angewandte Chemie (International ed. in English)*, vol. 47, no. 1, pp. 58–77, 2008.

[25] G. Li, V. Shrotriya, J. Huang, Y. Yao, T. Moriarty, K. Emery, and Y. Yang, "High-efficiency solution processable polymer photovoltaic cells by self-organization of polymer blends," *Nature Materials*, vol. 4, no. 11, pp. 864–868, Oct. 2005.

[26] J. Rostalski and D. Meissner, "Monochromatic versus solar efficiencies of organic solar cells," *Solar Energy Materials and Solar Cells*, vol. 61, no. 1, pp. 87–95, 2000.

[27] C. J. Brabec, A. Cravino, D. Meissner, N. S. Sariciftci, T. Fromherz, M. T. Rispens, L. Sanchez, and J. C. Hummelen, "Origin of the Open Circuit Voltage of Plastic Solar Cells," *Advanced Functional Materials*, vol. 11, no. 5, pp. 374–380, 2001.

[28] M. C. Scharber, D. Mühlbacher, M. Koppe, P. Denk, C. Waldauf, A. J. Heeger, and C. J. Brabec, "Design Rules for Donors in Bulk-Heterojunction Solar Cells—Towards 10 % Energy-Conversion Efficiency," *Advanced Materials*, vol. 18, no. 6, pp. 789–794, 2006.

[29] D. Veldman, Ö. İpek, S. C. J. Meskers, J. Sweelssen, M. M. Koetse, S. C. Veenstra, J. M. Kroon, S. S. V. Bavel, J. Loos, and R. A. J. Janssen, "Compositional and Electric Field Dependence of the Dissociation of Charge Transfer Excitons in Alternating Polyfluorene Copolymer / Fullerene Blends," *Molecular Materials*, no. d, pp. 7721–7735, 2008.

[30] M. Loi, S. Toffanin, M. Muccini, M. Forster, U. Scherf, M. Scharber, B. Maria, and A. Loi, "Charge Transfer Excitons in Bulk Heterojunctions of a Polyfluorene Copolymer and a Fullerene Derivative," *Advanced Functional Materials*, vol. 17, no. 13, pp. 2111–2116, 2007.

[31] M. D. Perez, C. Borek, S. R. Forrest, and M. E. Thompson, "Molecular and morphological influences on the open circuit voltages of organic photovoltaic devices," *Journal of the American Chemical Society*, vol. 131, no. 26, pp. 9281–9286, 2009.

[32] D. M. Stevens, Y. Qin, M. A. Hillmyer, and C. D. Frisbie, "Enhancement of the morphology and open circuit voltage in bilayer polymer/fullerene solar cells," *Journal of Physical Chemistry C*, vol. 113, pp. 11408–15, 2009.

[33] K. Vandewal, K. Tvingstedt, A. Gadisa, O. Inganas, and J. V. Manca, "On the origin of the open-circuit voltage of polymer-fullerene solar cells," *Nature Materials*, vol. 8, no. 11, pp. 904–909, 2009.

[34] C. Piliego, T. W. Holcombe, J. D. Douglas, C. H. Woo, P. M. Beaujuge, and J. M. J. Fréchet, "Synthetic control of structural order in N-alkylthieno[3,4-c]pyrrole-4,6-dione-based polymers for efficient solar cells" *Journal of the American Chemical Society*, vol. 132, no. 22, pp. 7595–7597, 2010.

[35] S. Yamamoto, A. Orimo, H. Ohkita, H. Benten, and S. Ito, "Molecular Understanding of the Open-Circuit Voltage of Polymer:Fullerene Solar Cells," *Advanced Energy Materials*, vol. 2, no. 2, pp. 229–37, 2011.

[36] E. Bundgaard and F. Krebs, "Low band gap polymers for organic photovoltaics," *Solar Energy Materials and Solar Cells*, vol. 91, no. 11, pp. 954–985, 2007.

[37] S. Alem, R. de Bettignies, J.-M. Nunzi, and M. Cariou, "Efficient polymer-based interpenetrated network photovoltaic cells," *Applied Physics Letters*, vol. 84, no. 12, p. 2178, 2004.

[38] S. A. McDonald, G. Konstantatos, S. Zhang, P. W. Cyr, E. J. D. Klem, L. Levina, and E. H. Sargent, "Solution-processed PbS quantum dot infrared photodetectors and photovoltaics," *Nature Materials*, vol. 4, no. 2, pp. 138–142, 2005.

[39] A. Roy, S. Cho, N. Coates, J. S. Moon, D. Moses, M. Leclerc, K. Lee, A. J. Heeger, S. H. Park, and S. Beaupre, "Bulk heterojunction solar cells with internal quantum efficiency approaching 100%," *Nature Photonics*, vol. 3, no. 5, pp. 279–282, Apr. 2009.

[40] Y. Kim, S. Cook, S. M. Tuladhar, S. A. Choulis, J. Nelson, J. R. Durrant, D. D. C. Bradley, M. Giles, I. McCulloch, C.-S. Ha, and M. Ree, "A strong regioregularity effect in self-organizing conjugated polymer films and high-efficiency polythiophene: fullerene solar cells," *Nature Materials*, vol. 5, no. 3, pp. 197–203, 2006.

[41] Q. Zheng, B. J. Jung, J. Sun, and H. E. Katz, "Ladder-type oligo-p-phenylene-containing copolymers with high open-circuit voltages and ambient photovoltaic activity," *Journal of the American Chemical Society*, vol. 132, no. 15, pp. 5394–5404, 2010.

[42] A. Gadisa, W. Mammo, L. M. Andersson, S. Admassie, F. Zhang, M. R. Andersson, and O. Inganäs, "A New Donor–Acceptor–Donor Polyfluorene Copolymer with Balanced Electron and Hole Mobility," *Advanced Functional Materials*, vol. 17, no. 18, pp. 3836–3842, 2007.

[43] R. C. Coffin, J. Peet, J. Rogers, and G. C. Bazan, "Streamlined microwave-assisted preparation of narrow-bandgap conjugated polymers for high-performance bulk heterojunction solar cells," *Nature chemistry*, vol. 1, no. 8, pp. 657–661, 2009.

[44] S. C. Price, A. C. Stuart, L. Yang, H. Zhou, and W. You, "Fluorine substituted conjugated polymer of medium band gap yields 7% efficiency in polymer-fullerene solar cells," *Journal of the American Chemical Society*, vol. 133, no. 12, pp. 4625–31, 2011.

[45] A. P. Zoombelt, S. G. J. Mathijssen, M. G. R. Turbiez, M. M. Wienk, and R. A. J. Janssen, "Small band gap polymers based on diketopyrrolopyrrole," *Journal of Materials Chemistry*, vol. 20, no. 11, p. 2240, 2010.

[46] J.-F. Morin and M. Leclerc, "Syntheses of Conjugated Polymers Derived from N-Alkyl-2,7-carbazoles," *Macromolecules*, vol. 34, no. 14, pp. 4680–4682, 2001.

[47] S. Cho, J. H. Seo, S. H. Park, S. Beaupré, M. Leclerc, and A. J. Heeger, "A thermally stable semiconducting polymer," *Advanced materials*, vol. 22, no. 11, pp. 1253–1257, 2010.

[48] A. J. Heeger, "Nobel Lecture: Semiconducting and metallic polymers: The fourth generation of polymeric materials," *Reviews of Modern Physics*, vol. 73, no. 3, p. 681, 2001.

[49] A. J. Heeger, S. Kivelson, J. R. Schrieffer, and W. P. Su, "Solitons in conducting polymers," *Reviews of Modern Physics*, vol. 60, no. 3, pp. 781–850, 1988.

[50] A. Pron and P. Rannou, "Processible conjugated polymers: from organic semiconductors to organic metals and superconductors," *Progress in Polymer Science*, vol. 27, no. 1, pp. 135–190, 2002.

[51] C. Winder and N. S. Sariciftci, "Low bandgap polymers for photon harvesting in bulk heterojunction solar cells," *Journal of Materials Chemistry*, vol. 14, no. 7, p. 1077, 2004.

[52] Y.-J. Cheng, S.-H. Yang, and C.-S. Hsu, "Synthesis of conjugated polymers for organic solar cell applications," *Chemical Reviews*, vol. 109, no. 11, pp. 5868–5923, 2009.

[53] J. L. Brédas, "Relationship between band gap and bond length alternation in organic conjugated polymers," *The Journal of Chemical Physics*, vol. 82, no. 8, p. 3808, 1985.

[54] H. Brisset, C. Thobie-Gautier, A. Gorgues, M. Jubault, and J. Roncali, "Novel narrow bandgap polymers from sp^3 carbon-bridged bithienyls: poly(4,4-ethylenedioxy-4H-cyclopenta[2,1-b;3,4-b′]dithiophene)," *Journal of the Chemical Society, Chemical Communications*, vol. 1994, no. 11, pp. 1305–1306, 1994.

[55] J. Hou, M.-H. Park, S. Zhang, Y. Yao, L.-M. Chen, J.-H. Li, and Y. Yang, "Bandgap and Molecular Energy Level Control of Conjugated Polymer Photovoltaic Materials Based on Benzo[1,2- b :4,5-b]dithiophene," *Macromolecules*, vol. 41, no. 16, pp. 6012–6018, 2008.

[56] S. Allard, M. Forster, B. Souharce, H. Thiem, and U. Scherf, "Organic semiconductors for solution-processable field-effect transistors (OFETs)," *Angewandte Chemie International Edition*, vol. 47, no. 22, pp. 4070–4098, 2008.

[57] J. Janata and M. Josowicz, "Conducting polymers in electronic chemical sensors," *Nature Materials*, vol. 2, no. 1, pp. 19–24, 2003.

[58] A. A. Argun, P.-H. Aubert, B. C. Thompson, I. Schwendeman, C. L. Gaupp, J. Hwang, N. J. Pinto, D. B. Tanner, A. G. MacDiarmid, and J. R. Reynolds, "Multicolored Electrochromism in Polymers: Structures and Devices," *Chemistry of Materials*, vol. 16, no. 23, pp. 4401–4412, 2004.

[59] J. Lu, N. Drolet, J. Ding, Y. Tao, and R. Movileanu, "Crystalline low band-gap alternating indolocarbazole and benzothiadiazole-cored oligothiophene copolymer for organic solar cell applications," *Chemical Communications*, no. 42, pp. 5315–5317, 2008.

[60] T.-Y. Chu, J. Lu, S. Beaupré, Y. Zhang, J.-R. Pouliot, S. Wakim, J. Zhou, M. Leclerc, Z. Li, J. Ding, and Y. Tao, "Bulk heterojunction solar cells using thieno[3,4-c]pyrrole-4,6-dione and dithieno[3,2-b:2',3'-d]silole copolymer with a power conversion efficiency of 7.3%," *Journal of the American Chemical Society*, vol. 133, no. 12, pp. 4250–4253, 2011.

[61] C.-H. Chen, C.-H. Hsieh, M. Dubosc, Y.-J. Cheng, and C.-S. Hsu, "Synthesis and Characterization of Bridged Bithiophene-Based Conjugated Polymers for Photovoltaic Applications: Acceptor Strength and Ternary Blends," *Macromolecules*, vol. 43, no. 2, pp. 697–708, 2010.

[62] J. Roncali, "Conjugated poly(thiophenes): synthesis, functionalization, and applications," *Chemical Reviews*, vol. 92, no. 4, pp. 711–738, 1992.

[63] K. Tamao, K. Sumitani, and M. Kumada, "Selective carbon-carbon bond formation by cross-coupling of Grignard reagents with organic halides. Catalysis by nickel-phosphine complexes," *Journal of the American Chemical Society*, vol. 94, no. 12, pp. 4374–4376, 1972.

[64] J. K. Stille, "The Palladium-Catalyzed Cross-Coupling Reactions of Organotin Reagents with Organic Electrophiles[New Synthetic Methods]," *Angewandte Chemie International Edition In English*, vol. 25, no. 6, pp. 508–524, 1986.

[65] N. Miyaura and A. Suzuki, "Palladium-Catalyzed Cross-Coupling Reactions of Organoboron Compounds," *Chemical Reviews*, vol. 95, no. 7, pp. 2457–2483, 1995.

[66] K. Sonogashira, "Development of Pd-Cu catalyzed cross-coupling of terminal acetylenes with sp(2)-carbon halides," *Journal of Organometallic Chemistry*, vol. 653, no. 1–2, pp. 46–49, 2002.

[67] T. Yamamoto, A. Morita, Y. Miyazaki, T. Maruyama, H. Wakayama, Z. H. Zhou, Y. Nakamura, T. Kanbara, S. Sasaki, and K. Kubota, "Preparation of π-conjugated poly(thiophene-2,5-diyl), poly(p-phenylene), and related polymers using zero valent nickel complexes. Linear structure and properties of the π-conjugated polymers," *Macromolecules*, vol. 25, no. 4, pp. 1214–1223, 1992.

[68] P. Berrouard, A. Najari, A. Pron, D. Gendron, P.-O. Morin, J.-R. Pouliot, J. Veilleux, and M. Leclerc, "Synthesis of 5-Alkyl[3,4-c]thienopyrrole-4,6-dione-Based Polymers by Direct Heteroarylation," *Angewandte Chemie International Edition*, vol. 51, no. 9, pp. 2068–71, 2012.

[69] E. E. Havinga, W. Ten Hoeve, and H. Wynberg, "Alternate donor-acceptor small-band-gap semiconducting polymers; Polysquaraines and polycroconaines," *Synthetic Metals*, vol. 55, no. 1, pp. 299–306, 1993.

[70] C. M. Amb, S. Chen, K. R. Graham, J. Subbiah, C. E. Small, F. So, and J. R. Reynolds, "Dithienogermole as a fused electron donor in bulk heterojunction solar cells," *Journal of the American Chemical Society*, vol. 133, no. 26, pp. 10062–5, 2011.

[71] J. C. Bijleveld, V. S. Gevaerts, D. Di Nuzzo, M. Turbiez, S. G. J. Mathijssen, D. M. De Leeuw, M. M. Wienk, and R. A. J. Janssen, "Efficient solar cells based on an easily accessible diketopyrrolopyrrole polymer," *Advanced materials*, vol. 22, no. 35, pp. E242–E246, 2010.

[72] Y. Sun, C. Cui, H. Wang, and Y. Li, "Efficiency Enhancement of Polymer Solar Cells Based on Poly(3-hexylthiophene)/Indene-C_{70} Bisadduct via Methylthiophene Additive," *Advanced Energy Materials*, vol. 1, no. 6, pp. 1058–1061, 2011.

[73] L. Huo, J. Hou, S. Zhang, H.-Y. Chen, and Y. Yang, "A Polybenzo[1,2-b:4,5-b′]dithiophene Derivative with Deep HOMO Level and Its Application in High-Performance Polymer Solar Cells," *Angewandte Chemie International Edition*, vol. 49, no. 8, pp. 1500–1503, 2010.

[74] H. Chen, J. Hou, S. Zhang, Y. Liang, G. Yang, Y. Yang, L. Yu, Y. Wu, and G. Li, "Polymer solar cells with enhanced open-circuit voltage and efficiency," *Nature Photonics*, vol. 3, pp. 649–653, 2009.

[75] Y. Sun, C. J. Takacs, S. R. Cowan, J. H. Seo, X. Gong, A. Roy, and A. Heeger, "Efficient, Air-Stable Bulk Heterojunction Polymer Solar Cells Using MoO_x as the Anode Interfacial Layer," *Advanced Materials*, vol. 23, pp. 2226–2, 2011.

[76] Z. Li, J. Ding, N. Song, X. Du, J. Zhou, J. Lu, and Y. Tao, "Alternating Copolymers of Dithienyl-s-Tetrazine and Cyclopentadithiophene for Organic Photovoltaic Applications," *Chemistry of Materials*, vol. 23, no. 7, pp. 1977–1984, 2011.

[77] D. Gendron, "Synthèse et étude de nouveaux dérivés du 2,7-carbazole et du 1,4- dicétopyrrolopyrrole pour applications en dispositifs photovoltaïques," PhD Thesis, Université Laval, 2011.

[78] T.-Y. Chu, S. Alem, P. G. Verly, S. Wakim, J. Lu, Y. Tao, S. Beaupre, M. Leclerc, F. Belanger, D. Desilets, S. Rodman, D. Waller, and R. Gaudiana, "Highly efficient polycarbazole-based organic photovoltaic devices," *Applied Physics Letters*, vol. 95, no. 6, p. 063304, 2009.

[79] S. Beaupré, M. Belletête, G. Durocher, and M. Leclerc, "Rational Design of Poly (2,7-Carbazole) Derivatives for Photovoltaic Applications," *Macromolecular Theory and Simulations*, vol. 20, no. 1, pp. 13–18, 2011.

[80] S. Wakim, S. Beaupré, N. Blouin, B.-R. Aich, S. Rodman, R. Gaudiana, Y. Tao, and M. Leclerc, "Highly efficient organic solar cells based on a poly(2,7-carbazole) derivative," *Journal of Materials Chemistry*, vol. 19, no. 30, p. 5351, 2009.

[81] J. V. Grazulevicius, P. Strohriegl, J. Pielichowski, and K. Pielichowski, "Carbazole-containing polymers: synthesis, properties and applications," *Progress in Polymer Science*, vol. 28, no. 9, pp. 1297–1353, 2003.

[82] T. Michinobu, H. Osako, and K. Shigehara, "Alkyne-Linked Poly(1,8-carbazole)s: A Novel Class of Conjugated Carbazole Polymers," *Macromolecular Rapid Communications*, vol. 29, no. 2, pp. 111–116, Jan. 2008.

[83] K. Tamura, M. Shiotsuki, N. Kobayashi, T. Masuda, and F. Sanda, "Synthesis of highly conjugated poly(3,9-carbazolyleneethynylenearylene)s emitting variously colored fluorescence," *Polymer*, vol. 50, no. 19, pp. 4479–4487, 2009.

[84] N. T. S. Phan, M. Vandersluys, and C. W. Jones, "On the Nature of the Active Species in Palladium Catalyzed Mizoroki_Heck and Suzuki_Miyaura Couplings_Homogeneous or Heterogeneous Catalysis, A Critical Review," *Advanced Synthesis & Catalysis*, vol. 348, no. 6, pp. 609–679, 2006.

[85] T. Okamoto, Y. Jiang, F. Qu, A. C. Mayer, J. E. Parmer, M. D. McGehee, and Z. Bao, "Synthesis and Characterization of Pentacene - and Anthradithiophene - Fluorene Conjugated Copolymers Synthesized by Suzuki Reactions," *Macromolecules*, vol. 41, no. 19, pp. 6977–6980, 2008.

[86] J.-F. Morin and M. Leclerc, "2,7-Carbazole-Based Conjugated Polymers for Blue, Green, and Red Light Emission," *Macromolecules*, vol. 35, no. 22, pp. 8413–8417, 2002.

[87] J.-F. Morin and M. Leclerc, "Syntheses of Conjugated Polymers Derived from," *Macromolecules*, vol. 34, no. 14, pp. 4680–4682, 2001.

[88] F. Dierschke, A. C. Grimsdale, and K. Müllen, "Efficient Synthesis of 2,7-Dibromocarbazoles as Components for Electroactive Materials," *Synthesis*, no. 16, pp. 2470–2472, 2003.

[89] A. W. Freeman, M. Urvoy, and M. E. Criswell, "Triphenylphosphine-mediated reductive cyclization of 2-nitrobiphenyls: a practical and convenient synthesis of carbazoles," *The Journal of Organic Chemistry*, vol. 70, no. 13, pp. 5014–5019, 2005.

[90] J. Li, F. Dierschke, J. Wu, A. C. Grimsdale, K. Mullen, and K. Mu, "Poly(2,7-carbazole) and perylene tetracarboxydiimide: a promising donor/acceptor pair for polymer solar cells," *Journal of Materials Chemistry*, vol. 16, no. 1, pp. 96–100, 2006.

[91] R. Fucci, N. Bianco, L. Mongibello, A. Parretta, and C. Privato, " Energy yield prediction of amorphous silicon PV modules using full time data" *Solar Energy*, pp. 3248–3254, 2010.

[92] N. Blouin, A. Michaud, D. Gendron, S. Wakim, E. Blair, R. Neagu-Plesu, M. Belletete, G. Durocher, and M. Leclerc, "Toward a Rational Design of Poly(2,7-Carbazole) Derivatives for Solar Cells," *Journal of the American Chemical Society*, vol. 130, no. 130l, p. 732, 2008.

[93] J. Li and A. C. Grimsdale, "Carbazole-based polymers for organic photovoltaic devices," *Chemical Society Reviews*, vol. 39, no. 7, pp. 2399–2410, 2010.

[94] Y. Zou, A. Najari, P. Berrouard, and S. Beaupre, "A Thieno [3 , 4-c] pyrrole-4 , 6-dione-Based Copolymer for Efficient Solar Cells," *Journal of the American Chemical Society*, vol. 132, no. 15, pp. 5330–5331, 2010.

[95] Y. Zhang, S. K. Hau, H.-L. Yip, Y. Sun, O. Acton, and A. K. Y. Jen, "Efficient Polymer Solar Cells Based on the Copolymers of Benzodithiophene and Thienopyrroledione," *Chemistry of Materials*, vol. 22, no. 9, pp. 2696–2698, 2010.

[96] T. H. I. Tuyet, M. A. I. Dang, S. -J. Park, J.-W. Park, D.-S. Chung, C. E. O. N. Park, Y.-H. Kim, and S.-K. Kwon, "Synthesis and Characterization of Poly(Benzodithiophene) Derivative for Organic Thin Film Transistors," *Polymer*, vol. 45, no. 22, pp. 5277–5284, 2007.

[97] Y. Liang, Z. Xu, J. Xia, S.-T. Tsai, Y. Wu, G. Li, C. Ray, and L. Yu, "For the Bright Future-Bulk Heterojunction Polymer Solar Cells with Power Conversion Efficiency of 7.4%," *Advanced Materials*, vol. 22, no. 20, p. E135-E138, 2010.

[98] A. M. Ballantyne, L. Chen, J. Nelson, D. D. C. Bradley, Y. Astuti, A. Maurano, C. G. Shuttle, J. R. Durrant, M. Heeney, W. Duffy, and I. McCulloch, "Studies of Highly Regioregular Poly(3-hexylselenophene) for Photovoltaic Applications," *Advanced Materials*, vol. 19, no. 24, pp. 4544–4547, 2007.

[99] P.-L. T. Boudreault, A. Najari, and M. Leclerc, "Processable Low-Bandgap Polymers for Photovoltaic Applications," *Chemistry of Materials*, vol. 23, no. 3, pp. 456–469.

[100] R. C. Coffin, J. Peet, J. Rogers, and G. C. Bazan, "Streamlined microwave-assisted preparation of narrow-bandgap conjugated polymers for high-performance bulk heterojunction solar cells," *Nature Chemistry*, vol. 1, no. 8,p. 657, 2009.

[101] J. Peet, J. Y. Kim, N. E. Coates, W. L. Ma, D. Moses, A. J. Heeger, and G. C. Bazan, "Efficiency enhancement in low-bandgap polymer solar cells by processing with alkane dithiols," *Nature Materials,* vol. 6, no.7, p. 497, 2007.

[102] P. Herguth, X. Jiang, M. S. Liu, and A. K. Y. Jen, "Highly Efficient Fluorene- and Benzothiadiazole-Based Conjugated Copolymers for Polymer Light-Emitting Diodes," *Macromolecules*, vol. 35, no. 16, pp. 6094–6100, 2002.

[103] M. Svensson, F. Zhang, S. C. Veenstra, W. J. H. Verhees, J. C. Hummelen, J. M. Kroon, O. Inganas, and M. R. Andersson, "High-Performance Polymer Solar Cells of an Alternating Polyfluorene Copolymer and a Fullerene Derivative," *Advanced Materials*, vol. 15, no. 12, pp. 988–991, 2003.

[104] E. Wang, L. Wang, L. Lan, C. Luo, W. Zhuang, J. Peng, and Y. Cao, "High-performance polymer heterojunction solar cells of a polysilafluorene derivative," *Applied Physics Letters*, vol. 92, no. 3, p. 33307, 2008.

[105] E. Zhou, S. Yamakawa, Y. Zhang, K. Tajima, C. Yanga, and H. Hashimoto, "Indolo[3,2-b]carbazole-based alternating donor–acceptor copolymers: synthesis, properties and photovoltaic application," *Journal of Material Chemistry*, vol. 19, pp. 7730–7737, 2009.

[106] Q. T. Zhang, J. M. Tour, and S. Carolina, "Low Optical Bandgap Polythiophenes by an Alternating Donor / Acceptor Repeat Units in Polythiophenes. Intramolecular Charge Transfer for Reducing Band Gaps in Fully Substituted Conjugated Polymers,"*Journal of the American Chemical Socie*ty, vol. 120, no. 22, pp. 5355–5362, 1998.

[107] G. Zhang, Y. Fu, Q. Zhang, and Z. Xie, "Benzo[1,2-b:4,5-b']dithiophene-dioxopyrrolothiophen copolymers for high performance solar cells," *Chemical Communications*, vol. 46, no. 27, pp. 4997–4999, 2010.

[108] A. Najari, S. Beaupré, P. Berrouard, Y. Zou, J.-R. Pouliot, C. Lepage-Pérusse, and M. Leclerc, "Synthesis and Characterization of New Thieno[3,4-c]pyrrole-4,6-dione Derivatives for Photovoltaic Applications," *Advanced Functional Materials*, vol. 21, no. 4, pp. 718–728, 2011.

[109] M. Puchalska, K. Polec_Pawlak, I. Zadrozna, H. Hryszko, and M. Jarosz, "Identification of indigoid dyes in natural organic pigments used in historical art objects by high-performance liquid chromatography coupled to electrospray ionization mass spectrometry," *Journal of mass spectrometry JMS*, vol. 39, no. 12, pp. 1441–1449, 2004.

[110] J. Mei, K. R. Graham, R. Stalder, and J. R. Reynolds, "Synthesis of isoindigo-based oligothiophenes for molecular bulk heterojunction solar cells," *Organic Letters*, vol. 12, no. 4, pp. 660–663, 2010.

[111] R. Stalder, J. Mei, and J. R. Reynolds, "Isoindigo-Based donor and acceptor Conjugated Polymers," *Macromolecules*, vol. 43, no. 20, pp. 8348–8352, 2010.

[112] G. Zhang, Y. Fu, Z. Xie, and Q. Zhang, "Synthesis and Photovoltaic Properties of New Low Bandgap Isoindigo-Based Conjugated Polymers," *Macromolecules*, pp. 1414–1420, 2011.

[113] B. Liu, Y. Zou, B. Peng, B. Zhao, K. Huang, Y. He, and C. Pan, "Low bandgap isoindigo-based copolymers: design, synthesis and photovoltaic applications," *Polymer Chemistry*, vol. 2, no. 5, pp. 1156–1162, 2011.

[114] E. Wang, Z. Ma, Z. Zhang, P. Henriksson, O. Inganas, F. Zhang, and M. Andersson, "An isoindigo-based low band gap polymer for efficient polymer solar cells with high photo-voltage," *Chemical Communications*, vol. 47, no. 17, pp. 4908–4910, 2011.

[115] A. B. Tamayo, M. Tantiwiwat, B. Walker, and T.-Q. Nguyen, "Design, Synthesis, and Self-assembly of Oligothiophene Derivatives with a Diketopyrrolopyrrole Core," *Journal of Physical Chemistry B*, vol. 112, no. 39, pp. 15543–15552, 2008.

[116] L. Bürgi, M. Turbiez, R. Pfeiffer, F. Bienewald, H.-J. Kirner, and C. Winnewisser, "High-Mobility Ambipolar Near-Infrared Light-Emitting Polymer Field-Effect Transistors," *Advanced Materials*, vol. 20, no. 11, pp. 2217–2224, 2008.

[117] M. M. Wienk, M. Turbiez, and J. Gilot, "Narrow-bandgap diketo-pyrrolo-pyrrole polymer solar cells: the effect of processing on the performance," *Advanced*, 2008.

[118] G. Yu and A. J. Heeger, "Charge separation and photovoltaic conversion in polymer composites with internal donor/acceptor heterojunctions," *Journal of Applied Physics*, vol. 78, no. 7, p. 4510, 1995.

[119] J. J. M. Halls, C. A. Walsh, N. C. Greenham, E. A. Marseglia, R. H. Friend, S. C. Moratti, and A. B. Holmes, "Efficient photodiodes from interpenetrating polymer networks," *Nature*, vol. 376, no. 6540, pp. 498–500, 1995.

[120] P. A. Troshin, H. Hoppe, J. Renz, M. Egginger, J. Y. Mayorova, A. E. Goryachev, A. S. Peregudov, R. N. Lyubovskaya, G. Gobsch, N. S. Sariciftci, and V. F. Razumov, "Material Solubility-Photovoltaic Performance Relationship in the Design of Novel Fullerene Derivatives for Bulk Heterojunction Solar Cells," *Advanced Functional Materials*, vol. 19, no. 5, pp. 779–788, 2009.

[121] C. J. Brabec, S. Gowrisanker, J. J. M. Halls, D. Laird, S. Jia, and S. P. Williams, "Polymer-fullerene bulk-heterojunction solar cells," *Advanced materials*, vol. 22, no. 34, pp. 3839–3856, 2010.

[122] H. Hoppe and N. S. Sariciftci, "Morphology of polymer/fullerene bulk heterojunction solar cells," *Journal of Materials Chemistry*, vol. 16, no. 1, p. 45, 2006.

[123] R. Rossetti, S. Nakahara, and L.E. Brus, "Quantum size effects in the redox potentials, resonance Raman spectra, and electronic spectra of CdS crystallites in aqueous solution," *The Journal of Chemical Physics*, vol. 79, no. 2, pp. 1086–1088, 1983.

[124] R. Rossetti and L. Brus, "Electron-hole recombination emission as a probe of surface chemistry in aqueous cadmium sulfide colloids," *Journal of Physical Chemistry*, vol. 86, no. 23, pp. 4470–4472, 1982.

[125] Y. Zhou, M. Eck, and M. Krüger, "Bulk-heterojunction hybrid solar cells based on colloidal nanocrystals and conjugated polymers," *Energy Environmental Science*, vol. 3, no. 12, p. 1851, 2010.

[126] R. Pokrop, K. Pamuła, S. Deja-Drogomirecka, M. Zagorska, P. Reiss, G. Louarn, F. Chandezon, and A. Pron, "Molecular hybrids of CdSe semiconductor nanocrystals with terthiophene carboxylic acid or its polymeric analogue," *Journal of Physical Chemistry C Chem C*, vol. 113, no. 9, pp. 3487–3493, 2009.

[127] J. De Girolamo, P. Reiss, and A. Pron, "Supramolecularly assembled hybrid materials via molecular recognition between diaminopyrimidine-functionalized poly(hexylthiophene) and thymine-capped CdSe nanocrystals," *Journal of Physical Chemistry B*, vol. 111, no. 40, pp. 14681–14688, 2007.

[128] B. Sun, E. Marx, and N. C. Greenham, "Photovoltaic Devices Using Blends of Branched CdSe Nanoparticles and Conjugated Polymers," *Nano Letters*, vol. 3, no. 7, pp. 961–963, 2003.

[129] J. K. Lee, W. L. Ma, C. J. Brabec, J. Yuen, J. S. Moon, J. Y. Kim, K. Lee, G. C. Bazan, and A. J. Heeger, "Processing additives for improved efficiency from bulk heterojunction solar cells," *Journal of the American Chemical Society*, vol. 130, no. 11, pp. 3619–3623, 2010.

[130] J. S. Moon, C. J. Takacs, S. Cho, R. C. Coffin, H. Kim, G. C. Bazan, and A. J. Heeger, "Effect of processing additive on the nanomorphology of a bulk heterojunction material," *Nano Letters*, vol. 10, no. 10, pp. 4005–4008, 2010.

[131] J. Peet, N. S. Cho, S. K. Lee, and G. C. Bazan, "Transition from Solution to the Solid State in Polymer Solar Cells Cast from Mixed Solvents," *Macromolecules*, vol. 41, no. 22, pp. 8655–8659, 2008.

[132] W. Nie, C. M. Macneill, Y. Li, R. E. Noftle, D. L. Carroll, and R. C. Coffin, "A Soluble High Molecular Weight Copolymer of Benzo[1,2-b:4,5-b']dithiophene and Benzoxadiazole for Efficient Organic Photovoltaics.," *Macromolecular Rapid Communications*, vol. 32, no. 15, pp. 1163–1168, 2011.

Chapter 2

New *push-pull* copolymers

2.1 Introduction

It is clear from the literature review presented in the previous chapter that lowering the band gap and controlling the positions of the HOMO and LUMO levels constitute key factors in the development of new conjugated polymers, better suited for application in photovoltaics.[1–3] Among several possible strategies, described in detail in the *Chapter 1 paragraph 1.4*, we have selected the design of alternating donor-acceptor copolymers in which *push-pull* driving forces between the donor and acceptor units, together with the photoinduced intramolecular charge transfer, facilitate electron delocalization and formation of low-bandgap quinoid mesomeric structures over the polymer backbone.[4], [5]

2.2 Donor-acceptor alternating copolymers based on benzodithiazole (BTD) electron accepting units and carbazole (CB) electron donating units: 3,6-carbazoles vs 2,7-carbazoles

2.2.1 Introduction

At the beginning of our study, the research interest was focused on the (poly)carbazole derivatives for light-emitting diodes and transistors devices [6]; subsequently, only in 2006 [7], poly(carbazole) derivatives were reported as donors in BHJ solar cells.[8] Even if the efficiency of these first devices was low, HOMO energy levels for carbazole-based polymers were typically in the good range for an optimal solar spectrum absorption (between -5.2 to -5.8 eV) [9–11] and for their application as donors in polymer/fullerene BHJ cells. The potential of this group of polymers was additionally reinforced when devices reaching power conversion efficiencies of above 6% were reported.[12–16]

At the same time, the corresponding family of 3,6-linked carbazoles seemed to be interesting because they had an advantage of being cheaper and easier to prepare [17] than the 2,7-linked carbazole polymers. Hole-transporting units based on 3,6-substituted carbazole have already enabled fabrication of efficient dye-sensitized solar cells.[18–20] Despite these promising results, only few polymers based on 3,6-linked carbazole derivatives have been studied so far for photovoltaic applications. At the time of the work on 3,6-linked carbazole, presented here, there was only one report on the use of a 3,6-carbazole based copolymer as a component in the donor-acceptor BHJ device.[21]

The copolymers studied in the frame of this thesis are characterized by two moieties acting respectively as acceptor and donor units: benzothiadiazole and carbazole. We should precise that, at the beginning, the *push* moiety (N-(ethylhexanoate)-3,6-carbazole) contained an ester function which was necessary to allow the linking of a PCBM molecule and to form a double cable polymer.[22] On the other hand, concerning benzothiadiazole moieties, two units were synthesized: benzothiadiazole and octyl-benzothiadiazole. In the latter one, octyl chains on external positions of the thiophene ring improve the solubility, as compared to polymers with benzothiadiazole units.[23], [24]

Detailed physicochemical characterization of these copolymers, together with their application in test solar cells (discussed respectively in *Chapter 3 and 5*), prompted us to move our attention to the synthesis of more performing poly(2,7-carbazole) copolymers. It will be demonstrated that the HOMO level of poly(3,6-carbazole)s is usually higher of by ca. 0.15 eV than that of poly(2,7-carbazole)s (*Chapter 3 paragraph 3.1*). This results in a decreasing of the open circuit voltage. Then mobility measurements (see *Chapter 5 paragraph 5.4*) show that poly(3,6-carbazole)s exhibit significantly lower charge carrier mobility as compared to poly(2,7-carbazole)s.[15]

In the studies of new poly(2,7-carbazoles) special attention was paid to the elucidation of the structure-properties relationship. To limit the number of parameters, the electron accepting unit was kept unvaried and the carbazole unit was modified. The synthesis of a 2,7-carbazole monomer involves one more synthesis step than the preparation of 3,6-carbazole. Initial choice of a linear alkyl group as N-substituent was supported by the idea to increase the side-chain chain interdigitation which, together with π-stacking, helps to form ordered supramolecular organization in solution deposited films of conjugated polymers.[24–27] These polymers were synthesized either by classical organic preparative methods or by microwave Suzuki polymerizations. After a preliminary test of polymerization, it was clear that octyl chains could not render the obtained polymer

sufficiently soluble, to assure facile processing. Therefore, in further syntheses branched N-substituents were introduced.

2.2.2 Synthesis of 3,6-poly(carbazole) derivatives: poly[N-(ethylhexanoate)-3,6-carbazole-alt-5,5-(4',7'di-2-thienyl-2',1',3'- benzothiadiazole)] (PCDTBT) and poly[N(ethylhexanoate)-3,6-carbazole-alt-5,5-(4',7'-di-2-(4-octylthienyl)2',1',3'-benzothiadiazole)] (PCDOTBT)

2.2.2.1 Synthesis of the electron accepting (pull) building blocks-dibromo derivatives of dithienyl-benzothiadiazoles: 4,7-bis(5-bromothiophen-2-yl)benzo-2,1,3-thiadiazole and 4,7-bis(4-octylthiophen-2-yl)benzo-2,1,3-thiadiazole

The synthetic route to these building blocks-dibromoderivatives of dithienyl-benzothiadiazoles **(4a)** and **(4b)** is schematically depicted in Figure 2.1. In the first step Suzuki coupling is carried out between commercially available 4,7-dibromobenzo-2,1,3-thiadiazole **(1)** and *n*-thien-2-yl-boronic acid (**(2a)** and **(2b)**) to yield 4,7-bis(*n*-thiophene-2-yl)benzo-2,1,3-thiadiazole (**(3a)** and **(3b)**) which are subsequently dibrominated with N-bromosuccinimide (NBS) to give the desired building blocks **(4a)** and **(4b).**

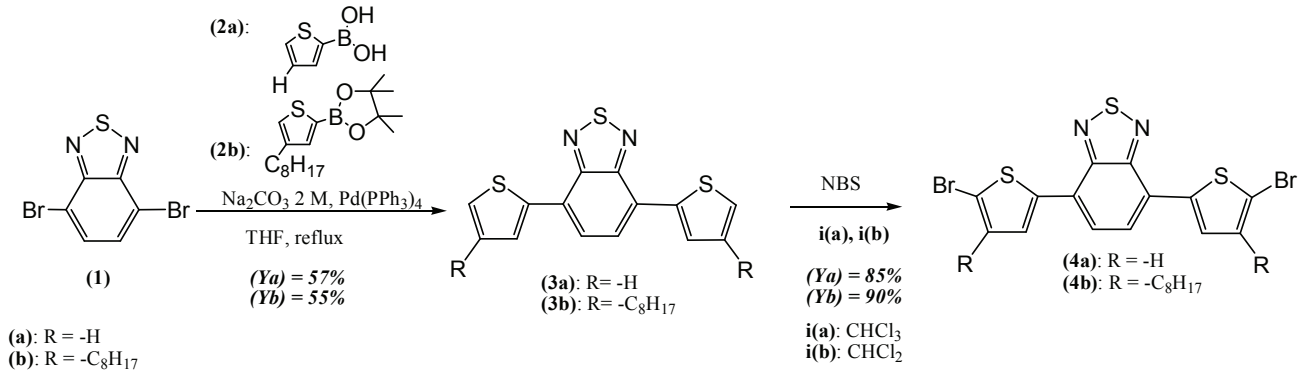

*Figure 2.1: Synthesis of the electron accepting (pull) building blocks-dibromoderivatives of dithienyl-benzothiadiazoles 4,7-Bis(5-bromothiophen-2-yl)benzo-2,1,3-thiadiazole **(4a)** and 4,7-Bis(4-octylthiophen-2-yl)benzo-2,1,3-thiadiazole **(4b)**.*

2.2.2.2 Synthesis of the electron donating (push) builiding block - N-(ethylhexanoate)-3.6-bis(5',5'-tetramethyl-[1',3',2']dioxaborolan-2'-yl)carbazole

To synthesize the boronato derivative of N-(ethylhexanoate)-3,6-bis(thiophene-2-yl)carbazole **(8)** three reaction steps were required (see Figure 2.2).

Protocols, till the compound **(7)**, were optimized by the Dr. Nicolas Berton, during his PhD. At that time, the objective was to develop a N-(ethylhexanoate)-3.6-bis(5',5'-tetramethyl)carbazole **(7)** characterized by an ester group on the 9-N position of 3,6-dibromocarbazole, allowing an eventual link of a fullerene molecule (PCBM) in the so called "double cable" configuration.

Nevertheless, here, the attention was not focused on this kind of "double cable" polymer, but the ethylhexanoate chain on carbazole acted, in this case, as a solubilizing group for the carbazole molecule.

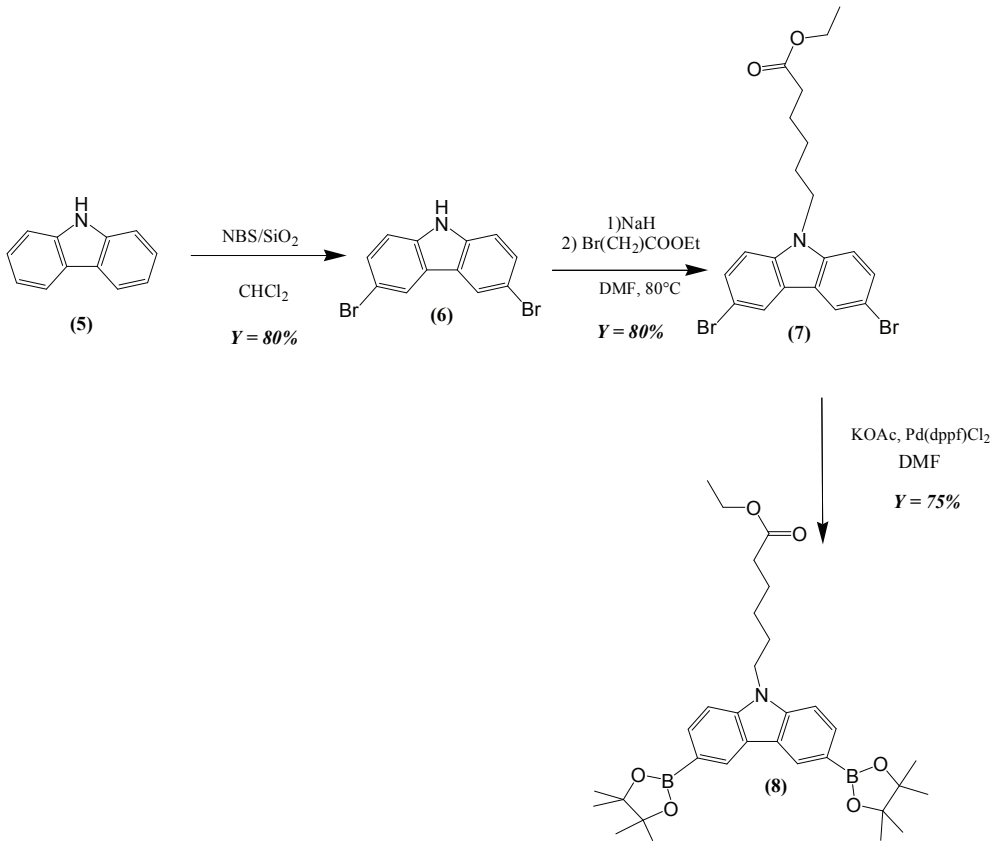

Figure 2.2: Synthesis of the electron donating (push) building block, N-(ethylhexanoate)-3.6-bis(5',5'-tetramethyl-[1',3',2']dioxaborolan-2'-yl) carbazole unit.

Following protocols from the literature [28], [29] carbazole **(5)** was dibrominated to obtain **(6)**, through an electrophilic substitution in 3 and 6 positions with 2 equivalents of N-bromosuccinimide (NBS), in presence of silica. Because of the low solubility of the monomer in dichloromethane, an important amount of solvent was required to carry out the reaction (here 200 mL for gram). 3,6-dibromocarbazole **(6)** was then alkylated in the 9-N position with ethyl-6-bromohexanoate, after deprotonation in presence of sodium hydride (NaH).[30] The reaction was carried out in DMF at 80°C, leading to a yield of 80% for **(7)**. The presence of 9-N-ethylhexanoate, as already mentioned, increases the solubility of the compound in dichloromethane or ethyl acetate, allowing purification through a silica chromatographic column. It was noticed that the purification through the chromatographic column using hexane/dichloromethane as an eluent, caused an important loss of the product in the column. So, hexane/ethyl acetate was preferably used. Finally to obtain **(8),** it was not possible to apply the classical synthesis via *n*-BuLi [31] due to the presence of the ester group which could be reduced. For this reason a less aggressive catalytic reaction, already used for fluorenes boronation [32], was followed using $Pd(dppf)Cl_2$ and potassium acetate. **(8)** was obtained with a yield of 75% preserving the ester function.

2.2.2.3 Preparation of poly[N-(ethylhexanoate)-3,6-carbazole-alt-5,5-(4',7'-di-2-thienyl-2',1',3'-benzothiadiazole)] (PCDTBT) and poly[N-(ethylhexanoate)-3,6-carbazole-alt5,5-(4',7'-di-2-(4-octylthienyl)-2',1',3'-benzothiadiazole)] (PCDOTBT) via Suzuki polycondensation

Palladium catalyzed Suzuki polycondensation proved to be a very convenient way to prepare this type of polymers as reported in several papers published by Leclerc's group [13] and other groups.[33], [34] Thus, both poly[N-(ethylhexanoate)-3,6-carbazole-alt-5,5-(4',7'-di-2-thienyl2',1',3'-benzothiadiazole)](PCDTBT) and poly[N-(ethylhexanoate)-3,6-carbazole-alt-5,5-(4',7'-di-2-(4-octylthienyl)-2',1',3'-benzothiadiazole)] (PCDOTBT) were synthesized using this type of cross-coupling reaction (see Figure 2.3).[13]

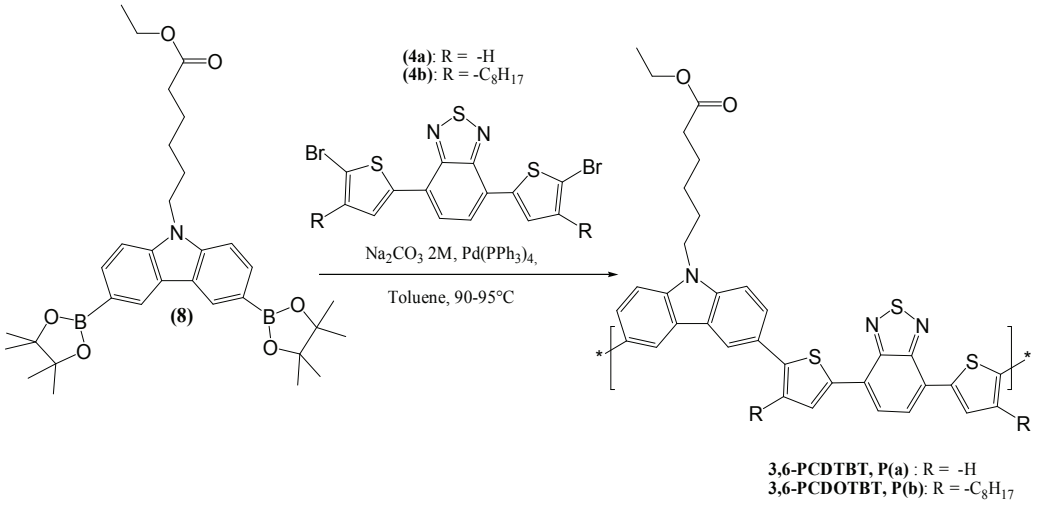

*Figure 2.3: Scheme of the preparation of two low-band gap polymers: the 3,6-PCDTBT(**P(a)**) and the 3,6-PCDOTBT(**P(b)**).*

The applied synthetic procedure in its final step involves precipitation of the product in methanol. Crude polymers, prepared in this manner, usually contain a significant amount of oligomeric fractions whose presence increases their polydispersity indices, as a consequence they have to be removed by sequential extraction with experimentally established set of solvents in a Soxhlet apparatus.[35], [36] After their removal their PDIs are still quite high (see Table 2.1). For both polymers two fractions differing in their molecular mass were collected after sequential extraction with acetone and chloroform, but for 3,6-PCDOTBT the molecular mass was measured only for the chloroform fraction. In the case of 3,6-PCDTBT a residual product remained in the Soxhlet cartridge, after the extraction with chloroform. Fractionation through sequential extraction is effective for 3,6-PCDTBT, as seen from the values of number average molecular mass (M_n) and polydispersity index (PDI) (see Table 2.1).

		M_w (kDa)	**M_n (kDa)**	**PDI**
3,6-PCDTBT	*acetone*	1.7	1.3	1.28
	$CHCl_3$	2.8	1.6	1.78
3,6-PCDOTBT	*acetone*	-	-	-
	$CHCl_3$	6.5	3.0	2.17

Table 2.1: Macromolecular parameters (M_w, M_n and PDI) of acetone and chloroform fractions of the 3,6-PCDTBT and 3,6-PCDOTBT.

It is known that UV-*Vis* spectroscopic properties of conjugated polymers are strongly dependent on the molecular mass. Moreover, this dependence persists to surprisingly high M_n values.[37] For 3,6-PCDTBT and 3,6-PCDOTBT this phenomenon is also clearly demonstrated – the band ascribed to the π-π^* transition is bathochromically shifted for the chloroform fraction as compared to the acetone one, confirming higher M_n of the former (see Figure 2.4).

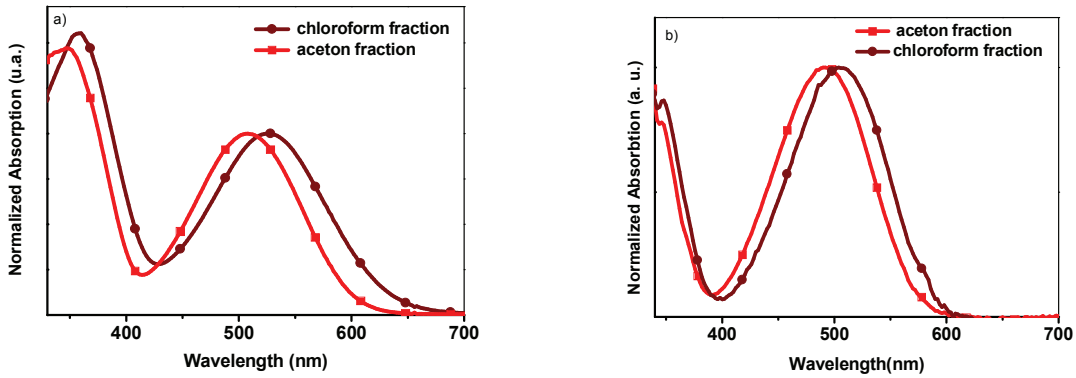

Figure 2.4: UV-Vis absorption spectra of two Soxhlet fractions of (a) 3,6-PCDTBT in acetone and chloroform fractions obtained in chloroform and (b) 3,6-PCDOTBT in acetone and chloroform fractions obtained in chloroform.

Molecular weights remain, however, relatively low, similarly as in the case of other 3,6-linked poly(carbazole) derivatives, previously reported. [38]

2.2.3 Synthesis 2,7-poly(carbazole) derivative: poly[N-(octyl)-2,7-carbazole-alt-5,5-(4',7'-dí-2-(thienyl)-2',1',3'-benzothiadiazole)] (2,7-PoCDTBT)

As already indicated (see *subsections 1.4.1.2* in *Chapter 1* and *2.2.1* in this chapter) physical properties of 2,7 poly(carbazole) derivatives are more adapted for the applications in photovoltaics than those of 3,6 poly(carbazole)–based compounds. For these reasons we have decided to investigate alternating copolymers of 2,7-carbazoles with different electron accepting comonomers. In this subsection the synthesis of such a copolymer - poly[N-(octyl)-2,7-carbazole-alt-5,5-(4',7'-di-2-(thienyl)-2',1',3'-benzothiadiazole)] - will be discussed.

2.2.3.1 Synthesis of the electron donating (push) block: N-(octyl)-2,7-bis (5, 5' -tetramethyl-[1', 3', 2'] dioxaborolan-2'-yl) carbazole

This building block was synthesized in four steps, starting from 4,4'-dibromobiphenyl **(9)** (see Figure 2.5).

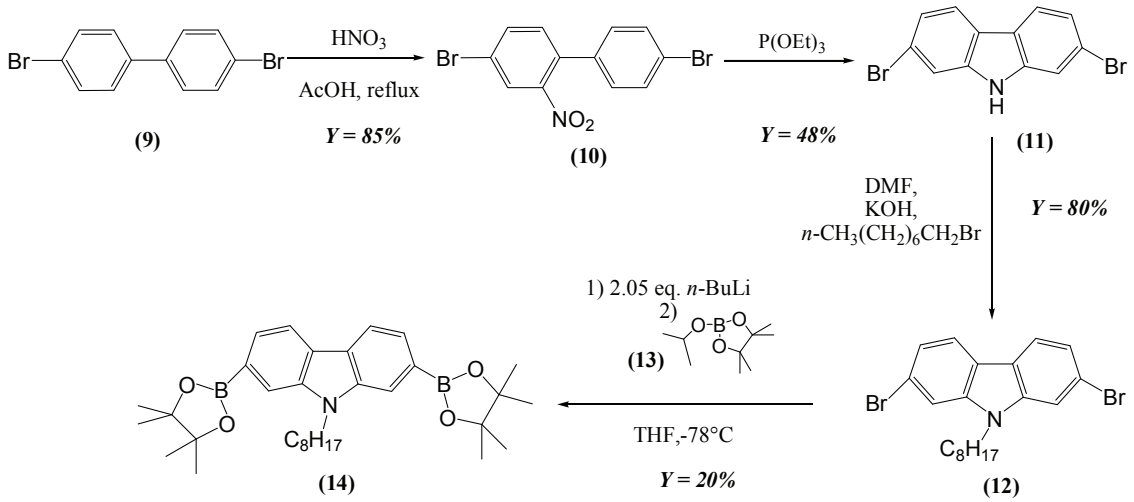

Figure 2.5: Synthesis of 2,7-Bis(4,4,5,5-tetramethyl-1,3,2-dioxaborolan-2-yl)-N-9'-octylcarbazole.

The first step involved nitration of the ring to give **(10)**.[7] Then the ring closure was carried out *via* Cadogan reaction to yield **(11)**. The resulting product was N-alkylated giving **(12),** through the procedure first described by Marzoni.[39] In the final step **(12)** was transformed into boronic diester **(14)**, the desired building block. The overall yield was moderate (20%), moreover the separation of the diester from the monoester by column chromatography was rather difficult.

2.2.4 Preparation of poly([N-(octyl)-2,7-carbazole-alt-5,5-(4',7'-di-2-(thienyl)-2',1',3'-benzothiadiazole]) via Suzuki polycondensation

The polycondensation reaction is schematically depicted in Figure 2.6.

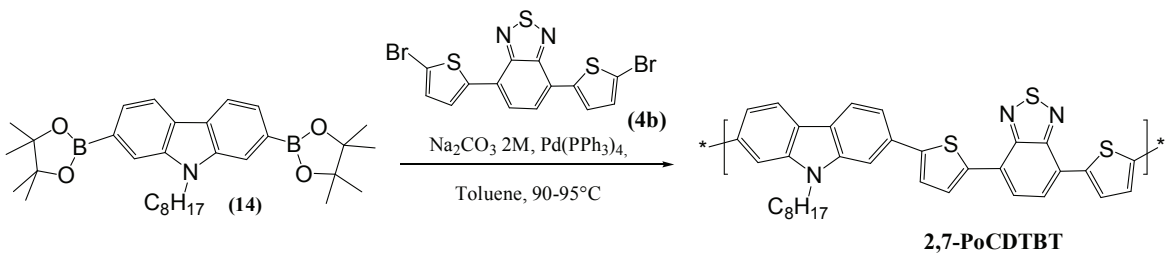

Figure 2.6: Scheme of the preparation of poly([N-(octyl)-2,7-carbazole-alt-5,5-(4',7'-di-2-(thienyl)-2',1',3'-benzothiadiazole]) by Suzuki coupling (2,7-PoCDTBT).

Two procedures for the coupling reaction were applied: microwave assisted and classical one. Synthesis in microwave field have became increasingly popular in recent years, surprisingly this technique remains relatively unexplored in the domain of conjugated polymers preparation.[40] The microwave synthesis offers several advantages since microwave reactors provide homogenous heating of the substrates, prevent side reactions and yield cleaner products in higher yields, which are easier to separate.

In both cases the reaction was carried out in toluene, in the same conditions (solvent and catalyst) as in the case of the preparation of 3,6-(poly)carbazoles (see *paragraph 2.2.2.3*). To increase the reaction rate and the molecular mass of the product an additive was added, Aliquat 336. The crude polymers, obtained by precipitation in methanol, were extracted in a Soxhlet apparatus using the following sequence of solvents: acetone, chloroform and *o*-dichlorobenzene. At this step, after Soxhlet extraction, they showed a poor solubility: an important amount of crude product still remained in the Soxhlet cartridge. It seems that linear octyl chains do not render the polymer sufficiently soluble.

Only macromolecular parameters (molecular masses and PDI) of the chloroform fraction obtained through the classical polymerization were measured: the corresponding weight average molecular mass, M_w, was of 6.3 kDa whereas the number average molecular mass, M_n, was 4.4 kDa, yielding the polydispersity index, PDI, of 1.43. Nevertheless, again, to have an idea about the trend in the conjugation length variation and, as a consequence, about the respective trend in the number average molecular weight, M_n, UV-*Vis* spectra were recorded. A bathochromic shift, passing from the acetone fraction to the o-dichlorobenzene one, appears for polymers obtained by both polymerization methods, indicating an augmentation of the conjugation length for the latter (see Figure 2.7).

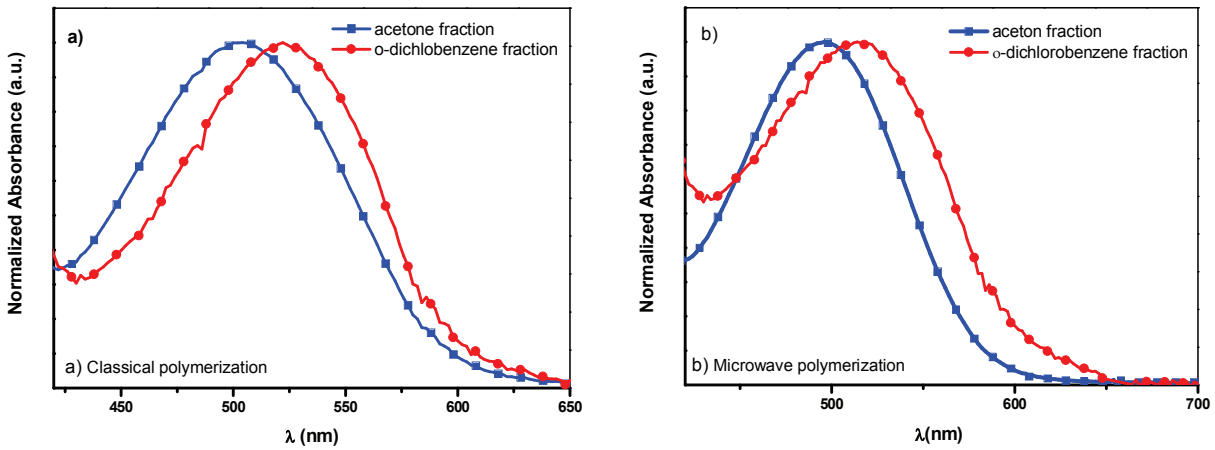

Figure 2.7: Solution UV-Vis spectra absorption of the 2,7-PoCDTBTobtained in chloroform. (a) 2,7-PoCDTBT, prepared through Suzuki polymerization; (b) 2,7-PoCDTBT, prepared through microwave polymerization.

Finally, UV-*Vis* absorption spectra of the chloroform fraction of the polymers obtained by classical Suzuki polymerization and by microwave-assisted copolymerization are compared. No significant differences could be noticed. (See Figure 2.8(a) and (b)).

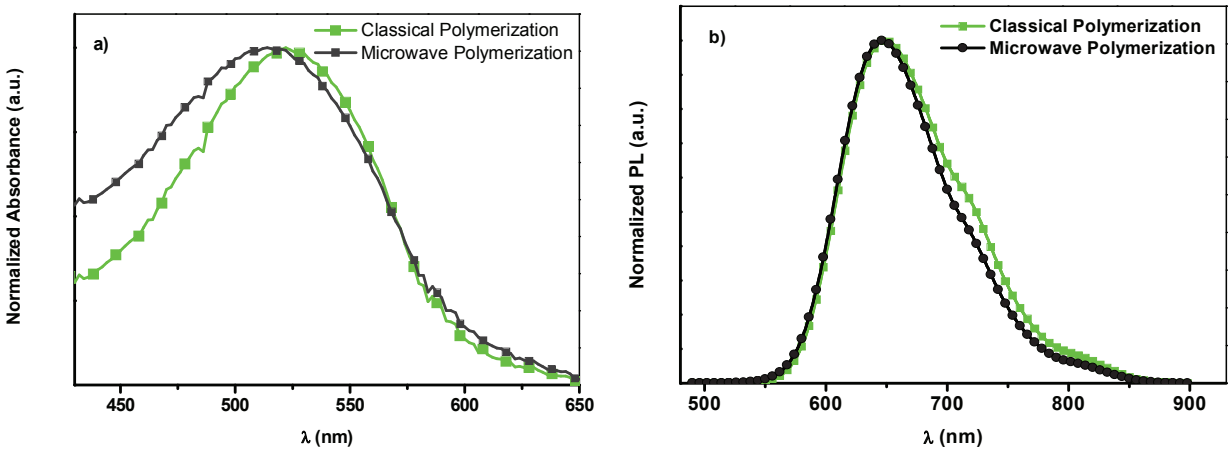

Figure 2.8: UV-Vis spectra absorption of the 2,7-PoCDTBT polymer obtained by classical and microwave Suzuki polymerization. (a)UV-Vis spectra absorption of the 2,7-PoCDTBT in $CHCl_3$ solution. (b) Photoluminescence spectra of the 2,7-PoCDTBT in $CHCl_3$ solution.

To conclude, the poor solubility was a very limiting parameter for processability of the obtained polymers. In addition, according to the literature [14], even if alkyl chains seem to promote a better interdigitation of lateral chains in the solid state, branched alkyl chains are still preferred because they seem to increase the surface contact between the polymer and PCBM. Moreover, they yield polymers which are more soluble and lead to higher molecular weight products in the reaction of copolymerization. For all these reasons, we did not carry out further physico-chemical characterizations of these polymers and the attention was moved to carbazole with branched N-substituents.

2.3 Donor-acceptor alternating copolymers containing a new electron accepting unit: the thienopyrrolodione moiety

During my stay in the "Laboratory of electroactive and photoactive polymers" headed by Prof. Mario Leclerc at the Université de Laval of Québec, I focused my attention on a new class of *push-pull* copolymers containing thienopyrrolodione derivatives as acceptor units (see Figure 2.9). As donor units I selected: N-branched-2,7-carbazole.

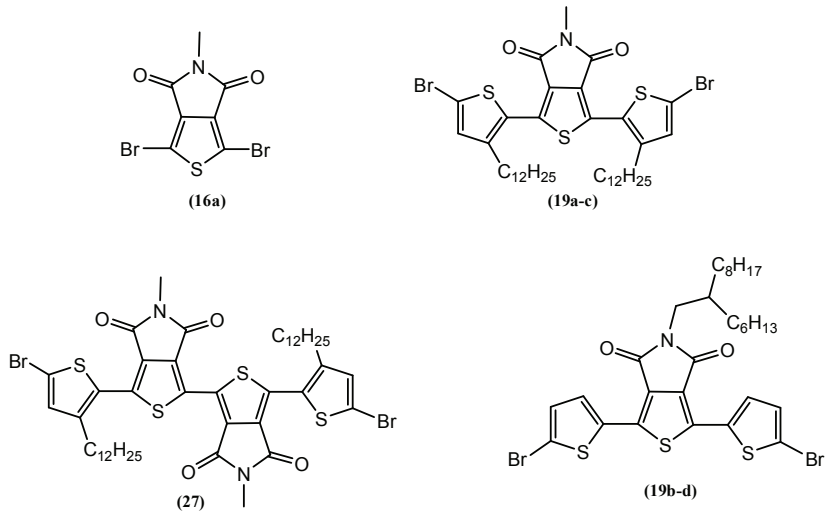

Figure 2.9: Electron accepting units: the thienopyrrolodione moiety.

In this paragraph the attention will be focused on the discussion of four pyrrolodione (PD) building blocks. The first unit (16a) was a kind of reference unit and it was represented by the PD moiety. To this unit, two dodecyl-thiophene monomers were added, forming the bis-thienopyrrolodione unit (TPD) (19a-c) with the goal to increase the conjugation of the acceptor moiety and to improve the solubility of the resulting polymer. In previous works long alkyl N-substituent were usually introduced to the pyrrolodione moiety.[41] We have decided to synthesize derivatives with short (methyl) N-subtituents, assuming that dodecyl groups of the thiophene ring should assure the solubility of the DA copolymer. This step was important for adjusting the band gap of the final polymer. To comparatively study the effect of substituents on the properties of the resulting polymer we have also synthesized (19b-d) in which a branched substituent is attached to pyrrolodione nitrogen. Finally, an acceptor unit containing two pyrrolodione groups in its central part and two terminal dodecylthiophene rings was synthesized (27).

Blocks containing these units were then used to prepare four different alternating copolymers with 2,7-carbazole. Alternating copolymers of bis-TPD with other than carbazole electron donor, namely dialkoxybenzodithiophene and bisthiophene were also synthesized (see Figure 2.10).

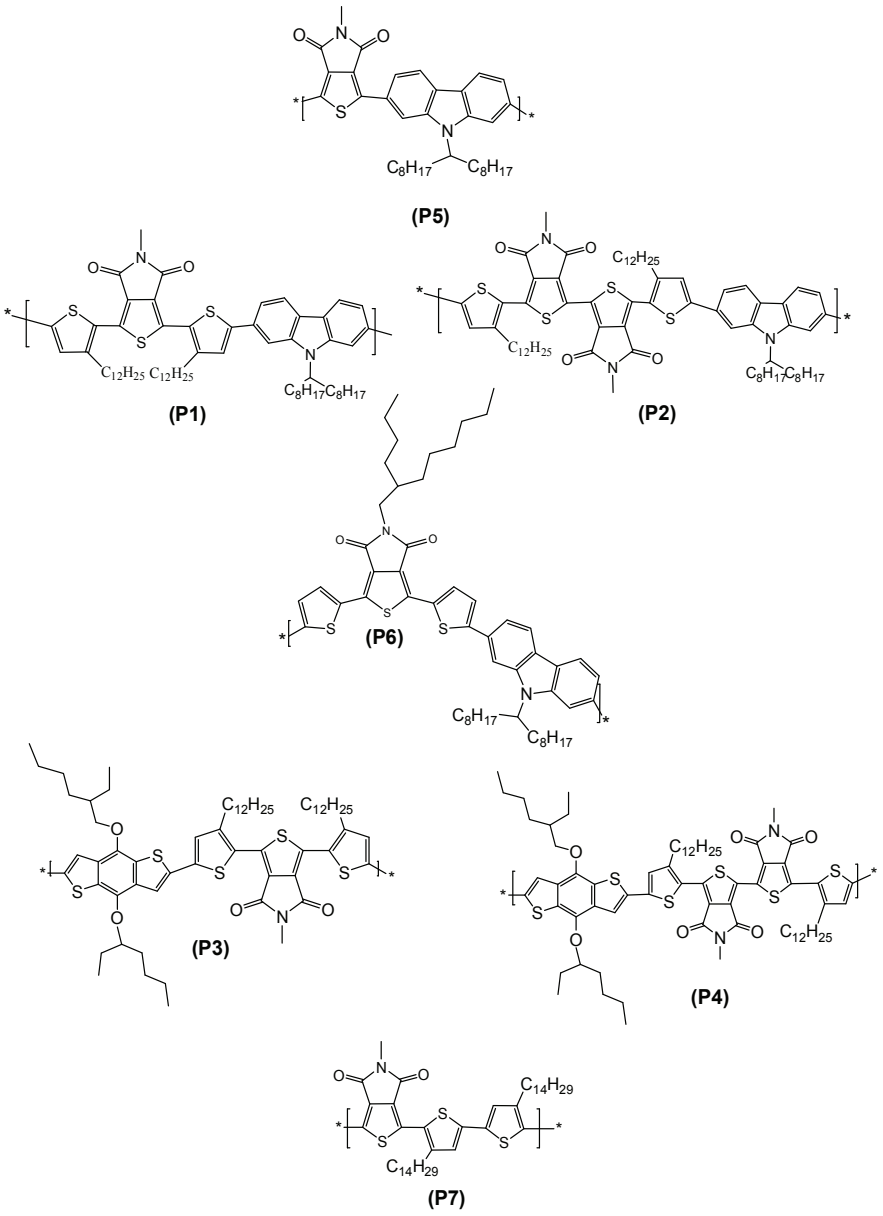

Figure 2.10: Representation of copolymers based on pyrrolodione electron accepting unit coupled with: 2,7-carbazole unit (P1, P2, P5, P6), dialkoxybenzodithiophene (P3 and P4) and bisthiophene (P7). [1]

[1] *Polymers are not presented following a logical increasing numbering to better compare experimental results described in the Chapter 3.*

2.3.1 Synthesis of thienopyrrolodione-based electron accepting (*pull*) building blocks

Four types of *pull* building blocks, containing pyrrolodione or thienopyrrolodione units were synthesized. The corresponding synthetic pathways are schematically depicted in Figures 2.11 and 2.12.

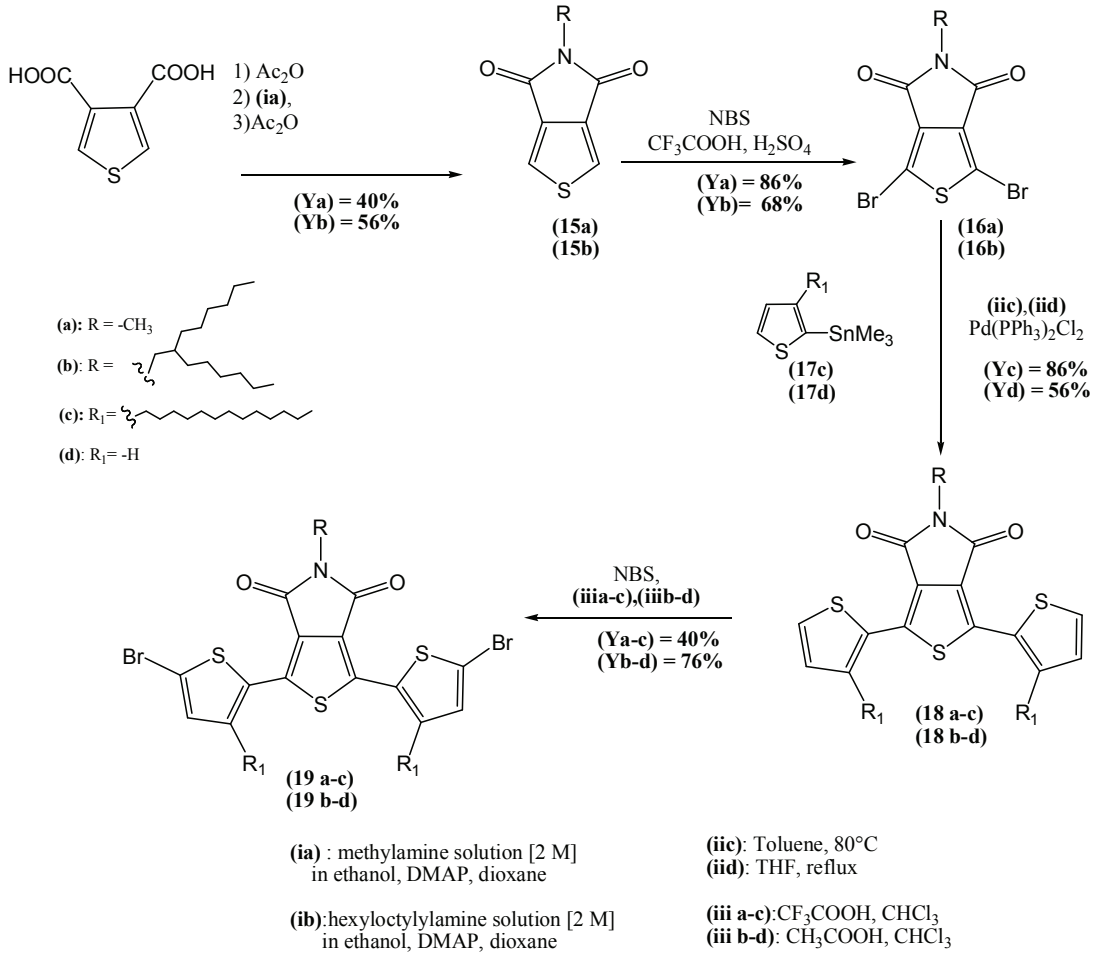

Figure 2.11: Synthesis of thienopyrrolodione-based electron accepting (pull) building blocks, (16a), (19a-c) and (19b-d) to carry out respectively the following polymers: P5, P1 and P6.

Building blocks, **(16a)**, **(19a-c)** and **(19b-d)** can be synthesized considering the following protocol. In the first step, commercially available thiophene-3,4-dicarboxylic acid is transformed into **(15a)** or **(15b)**.[42] Subsequently, **(15a)** or **(15b)** are brominated at 2 and 5 positions to give **(16a)** or **(16b)**. **(16a)** is the first electron acceptor unit which combined with carbazole yields **P5** polymer. For preparing **(19a-c)** or **(19b-d)** – the second and third type of thienopyrrolodione-based building blocks studied in this research - **(16a)** or **(16b)** are reacted with stannyl derivatives of 3-*n*-thiophene (**(17c)**, **(17d)**) to yield **(18a-c)** or **(18b-d)**). Bromination of **(18a-c)** and **(18b-d)** at α carbons leads to the targeted compounds : 1,3-bis(5-bromo-3-dodecyl-2-thienyl)-5-methyl-4H-thieno[3,4-c]pyrrole-4,6(5H)-dione **(19a-c)**, and 1,3-dibromo-5-di(thien-2'-yl)-5-hexyloctyl[3,4-c]pyrrole-4,6-dione **(19b-d)** (see Figure 2.11). **(19b-d)** characterized by a 2-hexyloctyl group attached to pyrrole nitrogen and no substituent on thiophene spacers was synthesized in order to elucidate the effect of the solubilizing substituent position on the physico-chemical properties and solubility of the resulting polymer.

We have also synthesized a *pull* building block containing two thienopyrrolodione units with the goal to increase its electron withdrawing ability. The synthetic pathway to this derivative is schematically depicted in Figure 2.12.

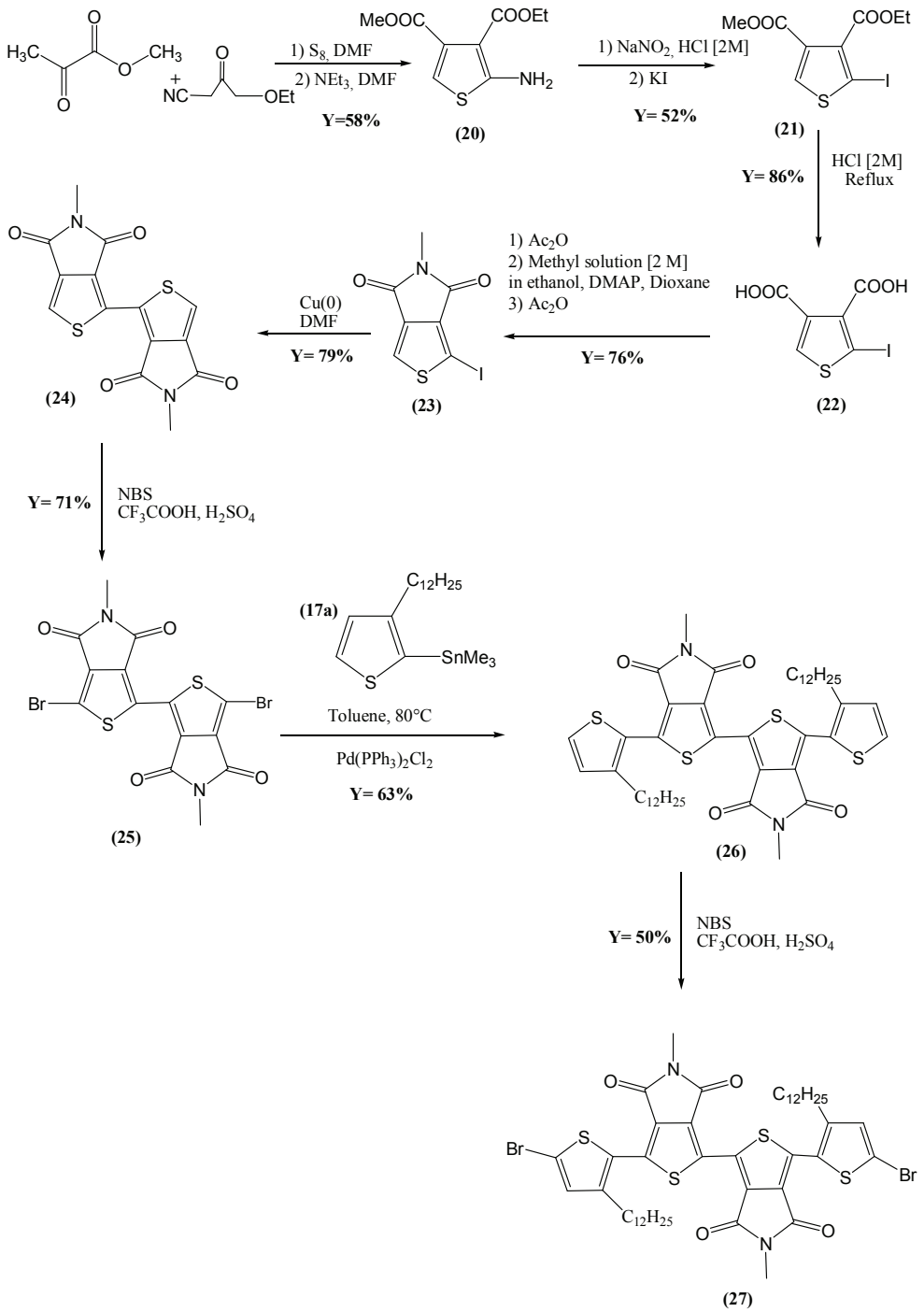

Figure 2.12: Synthesis of the acceptor building block (27) for the P2 copolymer.

(20) i.e. a thiophene derivative containing an amine group at the 2-position and two ester functions at the 3- and 4-positions, is obtained from two commercial products methyloxopropanoate and the ethyl cyanoacetate,

respectively, through a Gewald-type reaction (see Figure 2.12). The substitution of the amine group in **(20)** with I, to give **(21)**, is carried out by a Sandmeyer-type reaction. Subsequently, **(22)** is obtained from **(21)** *via* hydrolysis of the two ester functions. Next, the pyrroledione ring is closed, to yield the key intermediate **(23)**. In the subsequent step, the thienopyrroledione dimer, **(24),** is obtained *via* an Ullmann reaction. Next, **(24)** is brominated at α- carbons to give **(25)**, which is then reacted with the stannyl derivative of 3-*n*-dodecylthiophene, **(17a)**, to yield **(26)**. The final product, 3,3-bis(5-bromo-3-dodecyl-2-thienyl)-5,5'-dimethyl-4H,4'H-1,1'-bithieno[3,4-c]pyrrole-4,4',6,6'(5H, 5'H) -tetraone **(27)**, is prepared by the bromination of α- carbons. This building block is then used for the preparation of copolymers **P2** and **P4**.

2.3.2 Synthesis of electron donating (*push*) building blocks

In this paragraph the synthesis of the electron donating *(push)* building blocks: 2,7-carbazole, dialkoxybenzodithiophene and bisthiophene will be described.

2.3.2.1 N-(octyl)-2,7-bis (5, 5' -tetramethyl-[1', 3', 2'] dioxaborolan-2'-yl) carbazole

The studies described in *Chapter 2 (paragraph 2.2.4)* unequivocally show that linear alkyl N-substituent in the carbazole unit does not assure sufficient solubility of the resulting polymer, even if they are long. Thus, we decided to prepare a new carbazole building block in which a branched substituent is attached to the nitrogen atom. The synthesis of this molecule, 2,7-bis(4,4,5,5-tetramethyl-1,3,2-dioxaborolan-2-yl)-N-9'-heptadecanylcarbazole **(32)**, is schematically depicted in Figure 2.13.

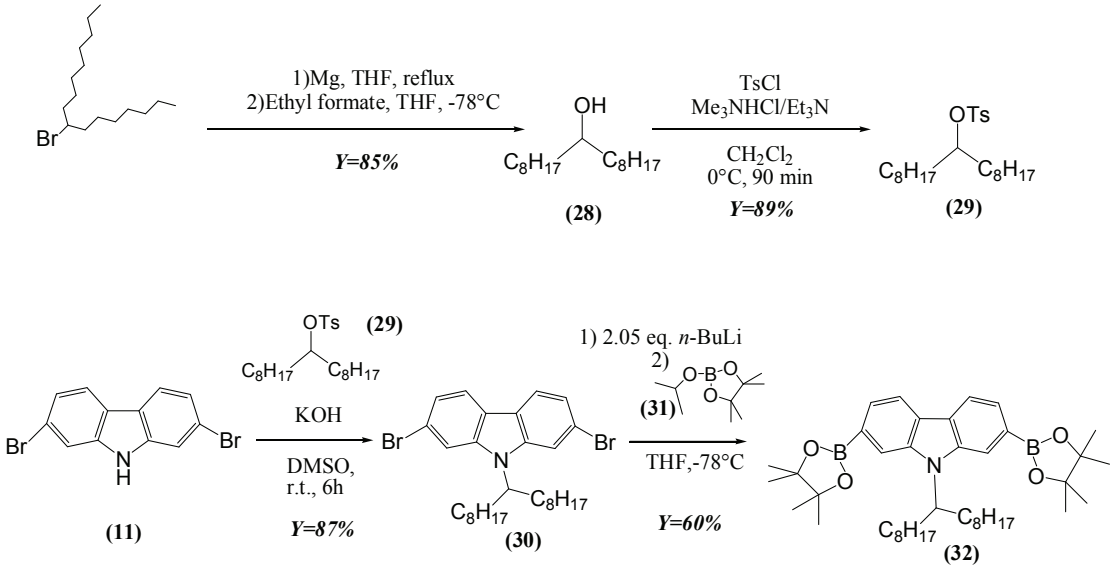

Figure 2.13: Synthesis of 2,7-Bis(4,4,5,5-tetramethyl-1,3,2-dioxaborolan-2-yl)-N-9' heptadecanylcarbazole.

The synthesis of this compound differs from the previous one, namely N-(octyl)-2,7-bis (5, 5' -tetramethyl-[1', 3', 2'] dioxaborolan-2'-yl) **(14)** in the preparation and subsequent linking of the branched N-substituent. Synthesis steps are the following. Heptadecan-9-ol **(28)** was obtained through a two steps Grignard reaction,

with the formation of the Grignard reactive which was added to a solution of ethyl formate in THF. The tosylate derivative **(29)** was reached through Yoshida reaction, starting from **(28)** and the p-toluensulfonyl chloride.[13] Then, a crucial step was the addition of **(29)** to the solution of **(11)** in DMSO in anhydrous conditions, to yield **(30)**. The control of the addition time of **(29)** during the reaction is fundamental because, in this way, secondary reactions were prevented, maximizing the yield of the alkylation reaction. In addition, only at this point the solubility of the polymer to be synthesized could be controlled. Conditions, similar to those proposed by Marzoni et Garbrecht [43], were used. Then, as for the monomer **(12)** (see *paragraph 2.2.3.1*), a transmetallation reaction was carried out between **(30)** and *n*-butyllithium at -78°C [44], followed by 2-isopropoxy-4,4,5,5-tetramethyl-l,3,2-dioxaborolane **(31)** one pot introduction, to give a carbazole donor building block, 2,7-bis(4,4,5,5-tetramethyl-1,3,2-dioxaborolan-2-yl)-N-9'-heptadecanylcarbazole **(32)**.

2.3.2.2 2,6-Bis(trimethyltin)-4,8-di(2-ethylhexyloxyl)benzo[1,2-b:3,4-b']dithiophene

The second *push* unit was the 2-ethylhexyloxydibenzodithiophene moiety (see Figure 2.14) whose electron donating power is stronger than that of carbazole. This building block was synthesized following protocols from the literature [45], [46] and thanks to the collaboration with S. Beaupré from the Laval University.

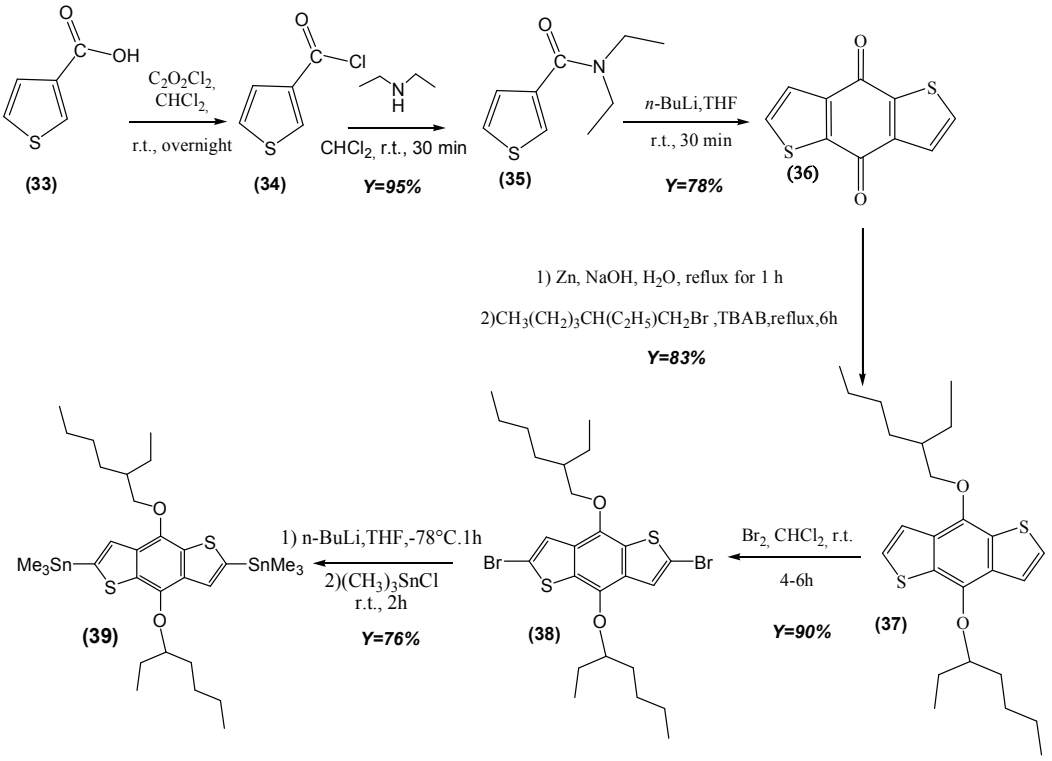

Figure 2.14: Synthesis of 2,6-bis(trimethyltin)-4,8-di(2-ethylhexyloxyl)-benzo[1,2-b:3,4-b]dithiophene.

The synthesis of the stannylated derivative of ethylhexyloxydibenzodithiophene, a building block suitable for

Stille coupling, requires six steps, as depicted in Figure 2.14. After the chlorination of **(33)**, N,N-diethylthiophene-3-carboxamide, compound **(35)**, was prepared from thiophene-3-carbonyl chloride **(34)** and diethylamine. Then, **(35)** was reacted with *n*-butyllithium in THF at 0ºC to produce benzo[1,2-b:4,5-b′]dithiophene-4,8- dione, **(36)**. Subsequently, **(36)** was reduced by zinc dust in aqueous sodium hydroxide solution. When the reduction reaction was complete, 2-ethylhexyl bromide was added with a catalytic amount of tetrabutylammonium bromide. After being refluxed for 12 h, 4,8-bis(ethylhexyloxy)benzo[1,2-b:4,5-b′]dithiophene, **(37)**, was obtained and then it was brominated, giving **(38)**. The final step of stannylation gave 2,6-Bis(trimethyltin)-4,8-di(2-ethylhexyloxyl)benzo[1,2-*b*:3,4-*b'*]dithiophene **(39)**.

2.3.2.3 4,4'-tetradecyl-5,5'-bis(trimethylstannyl)-2,2'-bithiophene

4,4'-bis(n-tetradecyl)-2,2'-bithiophene was the third type of electron donating unit considered in this study. Its synthesis followed the protocol from the literature used for the preparation of 4,4'-bis(n-dodecyl)-2,2'-bithiophene [47] (see Figure 2.15).

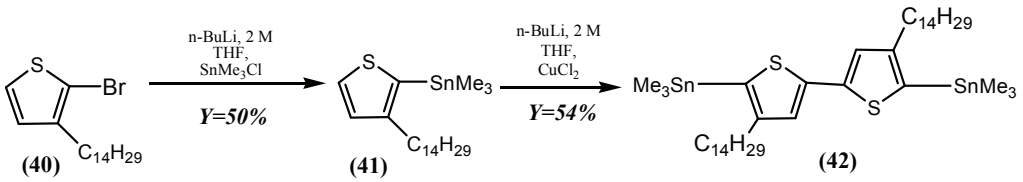

Figure 2.15: Synthesis of stannylated derivative of 4,4'-bis(n-tetradecyl)-2,2'-bithiophene.

Starting from 3-bromothiophene, the monomer **(40)** was obtained through a Grignard reaction and bromination. Then, after the stannylation step of **(40)**, the monomer **(41)** was obtained. Finally **(42)** was afforded through an oxidative coupling.

2.3.3 Preparation of carbazole based copolymers (P1, P2, P5 and P6)

As mentioned in the introduction, the previously described pyrrolodione and thienopyrrolodione-based electron accepting *(pull)* building blocks **(16a)**, **(19a-c)**, **(19b-d)** (see *paragraph 2.3.1*), were copolymerized with the 2,7-carbazole-based building block, 2,7-Bis(4,4,5,5-tetramethyl-1,3,2-dioxaborolan-2-yl)-N-9'-heptadecanylcarbazole **(32)** (see *paragraph 2.3.1.1*). Four copolymers containing 2,7-carbazole units were obtained.

Dibromo derivative of pyrroledione, 1,3-dibromo-5-methyl - 4H -thieno[3,4-c]pyrrole-4, 6(5H)-dione **(16a)**, (see *paragraph 2.3.1*, Figure 2.11), without any thiophene spacer, was directly copolymerized with **(32)**, through a Suzuki polycondensation (polymer **P5**). In parallel preliminary tests of the direct arylation reaction [48], [49], involving the reaction between dibrominated carbazole **(30)** and thienopyrrolodione **(15a)** were carried out in a microwave oven, yielding **P5'** (see Figure 2.16).

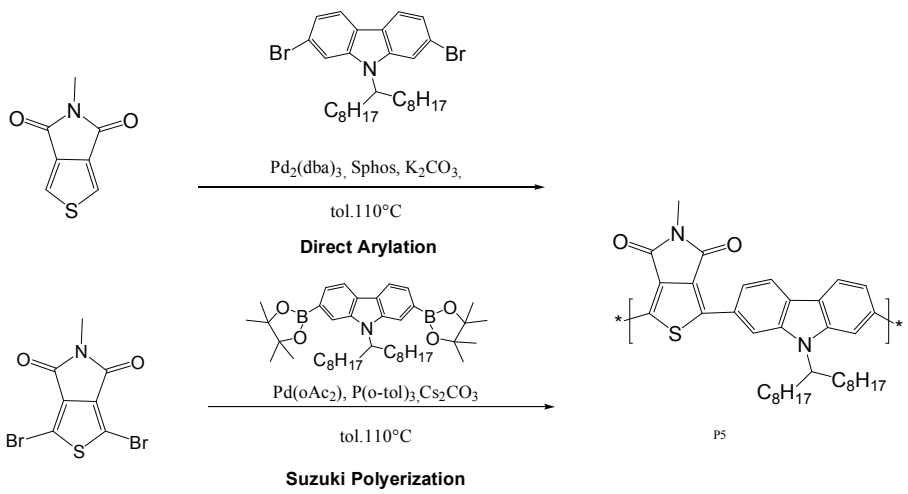

Figure 2.16: Comparison between Suzuki polycondensation and direct arylation protocols.

As already discussed in *Chapter 1 paragraph 1.3.1* the interest in using the direct arylation method, is not only to allow the formation of C-C bonds between aromatic units with activated hydrogen, without the use of organometallic intermediates, but also to prevent, consequently, the formation of toxic by-products.

The obtained polymers were precipitated in methanol and sequential extractions with a Soxhlet apparatus were carried out with: acetone, hexane, chloroform and, in the case of **P5'**, with *o*-dichlorobenzene.

In the case of **P5** two fractions were obtained, for which the macromolecule parameters could be measured: hexane and chloroform ones. For **P5**' polymer it was possible to collect and characterize chloroform and an *o*-dichlorobenzene fractions.

The macromolecular parameters of both polymers' fractions are summarized in the Table 2.2. It should be noticed that after Soxhlet fractionation **P5'** still exhibits a rather large polydispersity index values (PDI), compared to **P5**. Nevertheless, the M_n value measured for the same chloroform fraction is higher in the case of **P5'** as compared to **P5.**

		M_w (kDa)	M_n (kDa)	PDI
P5	*n-Hexane*	5.5	4.1	1.33
	$CHCl_3$	5.2	3.8	1.37
P5'	*$CHCl_3$*	16.9	4.9	3.44
	o-dichlorobenzene	32.3	9.8	3.30

Table 2.2: Macromolecular parameters (M_w, M_n and PDI) of hexane and chloroform fractions for the P5 polymer and of chloroform and o-dichlorobenzene fraction for the P5' copolymer.

This preliminary direct-arylation reaction, complementary with other tests developed at that time in the M. Leclerc group, showed that the direct coupling, of a TP unit with carbazole, could be considered as an alternative and easier process for developing new π-conjugated polymers.[48], [49]

Secondly, to modulate the energy gap and improve the solubility of the previously synthesized polymer (**P5**),

the attention moved towards the thienopyrrolodione derivatives, which contained two *n*-thiophene spacers linked to the pyrrolodione unit. The idea was to couple dibrominated thienopyrrolodione units ((**19a-c), (27)** and **(19b-d)**) with the diboronated 2,7-carbazole **(32)**.

Since the literature data concerning these reactions were nonexistent at the beginning of my thesis I decided to carry out different test polymerizations to identify the conditions leading to the product of the best macromolecular parameters. For these studies I selected 1,3-bis(5-bromo-3-dodecyl-2-thienyl)-5-methyl-4H-thieno[3,4-c]pyrrole-4,6(5H)-dione **(19a-c)** and 2,7-bis(4,4,5,5-tetramethyl-1,3,2-dioxaborolan-2-yl)-N-9'-heptadecanylcarbazole **(32)** which upon Suzuki coupling yield **P1** (see Figure 2.17, **P1**).

Different parameters influencing the molecular weight and its distribution, such as the used catalyst and its load, type of ligands in the catalytic complex, reaction medium, concentration of the reagents and the reaction temperature were tested to optimize the Suzuki coupling. The results of different copolymerization tests are summarized in Table 2.3.

	Catalyst	**Ligand**	**Base or activator**	**Solv.**	**M_w (kDa)**	**M_n (kDa)**	**PDI**
Test 1	$Pd_2(dba)_3$	$P(t\text{-}Bu)_3$	KF	THF	***$CHCl_3$ fraction***		
					3.7	3.2	1.16
Test 2	$Pd_2(dba)_3$	$P(t\text{-}Bu)_3$	KF	THF	***Hexane fraction***		
					2.2	2.0	1.08
Test 3	$Pd_2(dba)_3$	Sphos	K_2CO_3	Tol.	***$CHCl_3$ fraction***		
					23.6	11.2	2.11
Test 4	$Pd_2(dba)_3$	$P(o\text{-}Tyl)_3$	Et_4NOH[1M]	Tol.	No results	No results	No results
Test 5	$Pd_2(dba)_3$	PPh	KF	Tol.	***$CHCl_3$ fraction***		
					3.6	2.9	1.24

Table 2.3: Summary of test Suzuki-type polycondensations carried out for 1,3-bis(5-bromo-3-dodecyl-2-thienyl)-5-methyl-4H-thieno[3,4-c]pyrrole-4,6(5H)-dione (19a-c) and 2,7-Bis(4,4,5,5-tetramethyl-1,3,2-dioxaborolan-2-yl)-N-9'heptadecanylcarbazole (32) to yield P1.

It is clear from these data that **P1** of the highest M_n is obtained in toluene at 110°C with $Pd_2(dba)_3$, SPhos and K_2CO_3. The reaction should be carried out during 3 days. At the end of the reaction end-capping agents have to be added: phenyl boronic acid and bromobenzene.

The same optimized protocol for the palladium-catalyzed Suzuki coupling was also used in the preparation of **P2** and **P6** through the reaction of diboronated 2,7-carbazole **(32)** with 3,3-bis(5-bromo-3-dodecyl-2-thienyl)-5,5'-dimethyl-4H,4'H-1,1'-bithieno[3,4-c]pyrrole-4,4',6,6'(5H, 5'H) -tetraone **(27)** and 3-dibromo-5-di(thien-2'-yl)-5-hexyloctyl[3,4-c]pyrrole-4,6-dione **(19b-d)** (see Scheme 2.17).

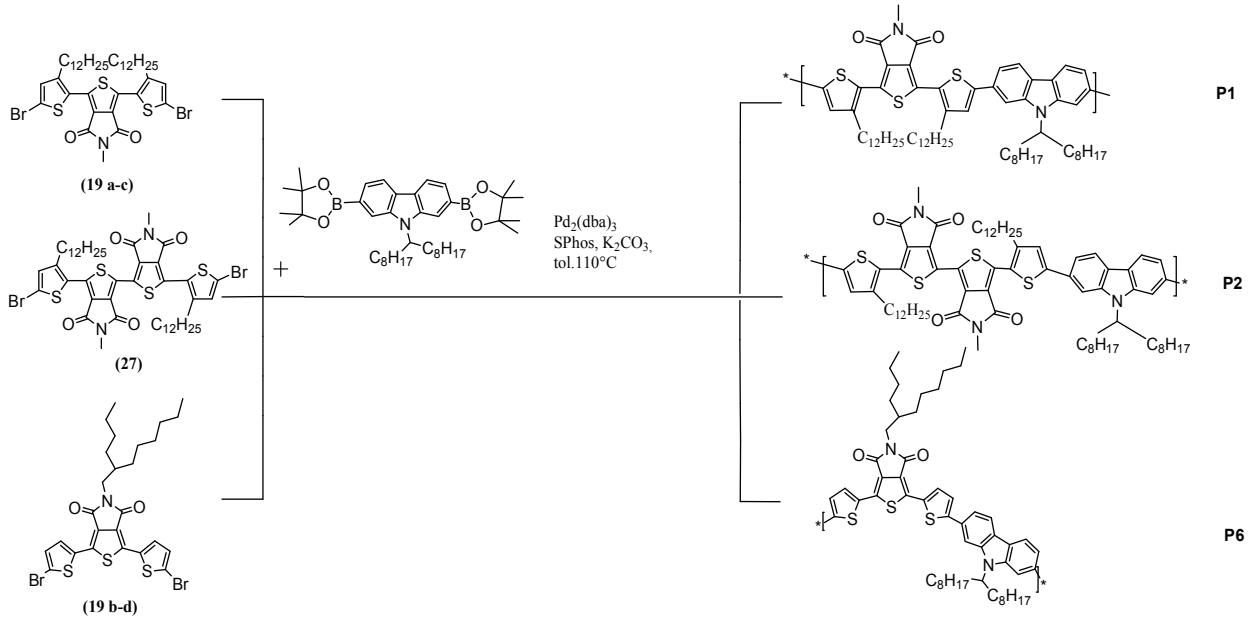

Figure 2.17: Suzuki polycondensation of dibrominated thienopyrrolodione and diboronated 2,7-carbazole.

In all cases, the crude polymers, obtained by precipitation in methanol and still containing some oligomeric fractions, were extracted in a Soxhlet apparatus with hexane and chloroform in the case of **P1,** with chloroform for **P6**.[35], [36] **P2** gave only one fraction, totally soluble in hexane. The results of Size Exclusion Chromatography (SEC) are collected in Table 2.4.

		M_w (kDa)	M_n (kDa)	PDI
P1	*n-Hexane* *$CHCl_3$*	16.1 32.7	11.9 25.4	1.35 1.28
P2	*n-Hexane*	5.2	3.9	1.33
P6	*$CHCl_3$*	10.0	6.0	1.67

Table 2.4: Macromolecular parameters of different fractions of carbazole-thienopyrroledione copolymers.

It is clear that the highest M_n is obtained for **P1**. It is possible that the optimized (with respect to M_n) reaction conditions established for **P1**, may not necessarily be optimal for **P2** and **P6.**

2.3.4 Preparation of dialkoxybenzodithiophene based copolymers (P3 and P4)

Two *push-pull* copolymers containing other than 2,7-carbazole electron donating unit, namely di(2-ethylhexyloxyl) benzo[1,2-b:4,5-b']dithiophene were also synthesized. They were prepared by Stille coupling from the corresponding stannyl derivative **(39)** and either 1,3-bis(5-bromo-3-dodecyl-2-thienyl)-5-methyl-4H-thieno[3,4-c]pyrrole-4,6(5H)-dione **(19 a-c) (P3)** or 3,3-bis(5-bromo-3-dodecyl-2-thienyl)-5,5'-dimethyl-4H,4'H-1,1'-bithieno[3,4-c]pyrrole-4,4',6,6'(5H, 5'H) -tetraone **(27) (P4)** (see Figure 2.18).

The reaction was carried out in degassed, strictly dried toluene using $Pd_2(dba)_3$/$AsPh_3$ catalyst/ligand system.

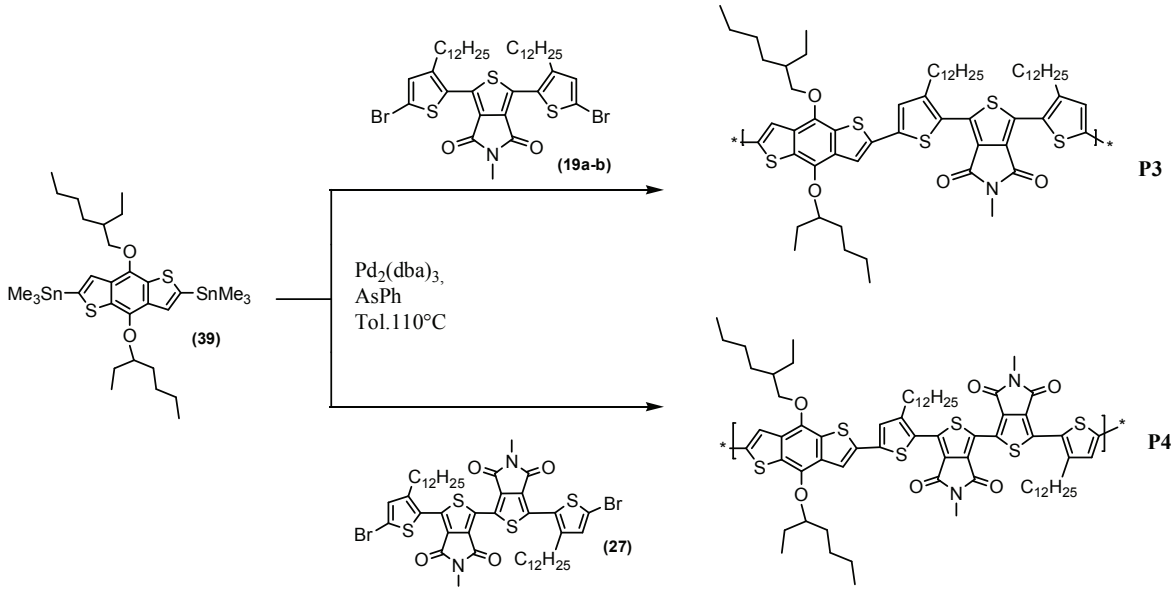

Figure 2.18: Stille polycondensation dibromo derivatives of thienopyrrolodiones and stannyl derivative of dialkoxybezodithiophene.

Similarly as other polymers of the DA series studied in this research, **P3** and **P4** are soluble and can be fractionated using sequential Soxhlet extractions with different solvents. Macromolecular parameters of the obtained fractions are listed im Table 2.5.

		M_w (kDa)	M_n (kDa)	PDI
P3	*$CHCl_3$*	9.6	6.5	~1.47
	o-dichlorobenzene	5.2	3.9	~1.33
P4	*n-Hexane*	6.4	3.0	~2.13

Table 2.5: Macromolecular parameters of different fractions of di(2-ethylhexyloxyl) benzodithiophene-thienopyrroledione copolymers.

2.3.5 Polymerization bithiophene based copolymer

4,4'-dialkyl-2,2'-bithiophene was the third type of an electron donating unit used for the preparation of DA copolymers. Its stannyl derivative **(42)** was used as a building block in Stille polycondensation ($Pd_2(dba)_3$/P(o−tolyl)$_3$) with 1,3-dibromo-5-methyl[3,4-c]pyrrole-4,6-dione **(16a)** leading to (**P7**) (see Figure 2.19). It has been demonstrated that the use of dialkyl bithiophenes as donor units in DA copolymers improves the geometry of the polymer backbone affording a coplanar conformation.[50]

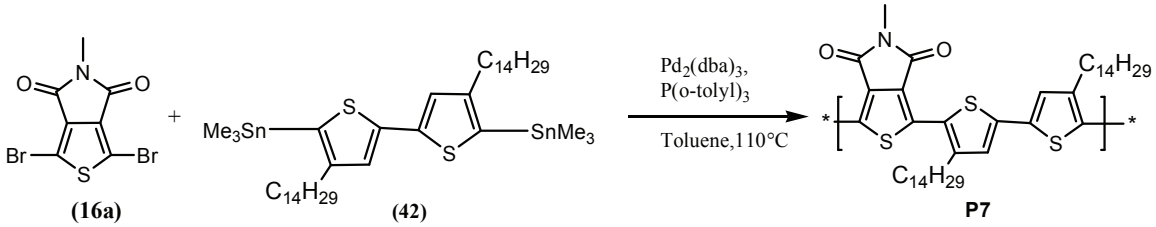

Figure 2.19: Synthesis of the 4,4'-bis(n-tetradecyl)-2,2'-bithiophene donating unit.

The crude copolymer was purple-blue. Two Soxhlet-extracted fractions (hexane and chloroform) were obtained. Their macromolecular parameters are listed in Table 2.6.

		M_w (kDa)	M_n (kDa)	PDI
P7	*n-Hexane*	6.3	4.8	1.31
	$CHCl_3$	6.7	5.1	1.31

Table 2.6: Macromolecular parameters of different fractions of thienopyrroledione- bisthiophene based copolymer.

In a study, carried out in parallel to our research, a very similar polymer containing a long linear tetradecyl N-substituent was reported. It showed a very promising performance in solar cells, reaching the 4.7% of power conversion efficiency.[51] [52]

2.4 Conclusion

The results presented in this chapter clearly indicate that appropriately exploited building block approach can lead to polymers with tunable physical properties. By selecting acceptor (benzothiadiazole or thienopyrrolodione derivatives) and donor (3,6-carbazole, 2,7-carbazole, dialkoxybenzodithiophene) units of different DA strength, it is possible to prepare copolymers which, apart from those containing 3,6-carbazole blocks, seem very promising for photovoltaic applications. Moreover, several C-C coupling methods can be efficiently used for the preparation of these tailor-made copolymers, such as Stille, Suzuki and direct coupling. Some additional research is still needed, directed towards a better control of the macromolecular parameters. With the exception of **P1** all other polymers, synthesized in the frame of this research, show moderate M_n and require fractioning to reduce their polydispersity indices. Improvement is therefore needed in establishing such conditions of the polycondensation which lead to low PDI values without the necessity of *post*-polycondensation fractioning.

[1] Y. J. Cheng, S. H. Yang, and C. S., Hsu, "Synthesis of Conjugated Polymers for Organic Solar Cell Applications," *Nature Photonics*, vol. 3, no. 12, p. 15, 2009.

[2] Y. Liang and L. Yu, "Development of Semiconducting Polymers for Solar Energy Harvesting," *Polymer Reviews*, vol. 50, no. 4, pp. 454–473, 2010.

[3] Y. Liang and L. Yu, "A new class of semiconducting polymers for bulk heterojunction solar cells with exceptionally high performance.," *Accounts of Chemical Research*, vol. 43, no. 9, pp. 1227–1236, 2010.

[4] E. E. Havinga, W. Ten Hoeve, and H. Wynberg, "Alternate donor-acceptor small-band-gap semiconducting polymers; Polysquaraines and polycroconaines," *Synthetic Metals*, vol. 55, no. 1, pp. 299–306, 1993.

[5] Q. T. Zhang, J. M. Tour, and S. Carolina, "Low optical bandgap polythiophenes by an alternating donor / acceptor repeat units in polythiophenes. Intramolecular charge transfer for reducing band gaps in fully substituted conjugated polymers," *Journal of the Americal Chemical Society*, vol. 120, no. 2, pp. 5355–5362, 1998.

[6] V. Rani and K. S. V. Santhanam, "Polycarbazole-based electrochemical transistor," *Journal of Solid State Electrochemistry*, vol. 2, no. 2, pp. 99–101, 1998.

[7] F. Dierschke, A. C. Grimsdale, and K. Müllen, "Efficient Synthesis of 2,7-Dibromocarbazoles as Components for Electroactive Materials," *Synthesis*, no. 16, pp. 2470–2472, 2003.

[8] J. Li, F. Dierschke, J. Wu, A. C. Grimsdale, K. Mullen, and K. Mu, "Poly(2,7-carbazole) and perylene tetracarboxydiimide: a promising donor/acceptor pair for polymer solar cells," *Journal of Materials Chemistry*, vol. 16, no. 1, pp. 96–100, 2006.

[9] L. J. A. Koster, V. D. Mihailetchi, and P. W. M. Blom, "Ultimate efficiency of polymer/fullerene bulk heterojunction solar cells," *Applied Physics Letters*, vol. 88, no. 9, p. 093511, 2006.

[10] D. Deleeuw, M. Simenon, A. Brown, and R. Einerhand, "Stability of n-type doped conducting polymers and consequences for polymeric microelectronic devices," *Synthetic Metals*, vol. 87, no. 1, pp. 53–59, 1997.

[11] B. C. Thompson, Y.-G. Kim, and J. R. Reynolds, "Spectral Broadening in MEH-PPV:PCBM-Based Photovoltaic Devices via Blending with a Narrow Band Gap Cyanovinylene−Dioxythiophene Polymer," *Macromolecules*, vol. 38, no. 13, pp. 5359–5362, 2005.

[12] S. H. Park, A. Roy, S. Beaupré, S. Cho, N. Coates, J. S. Moon, D. Moses, M. Leclerc, K. Lee, A. J. Heeger, S. H. Park, and S. Beaupre, "Bulk heterojunction solar cells with internal quantum efficiency approaching 100%," *Nature Photonics*, vol. 3, no. 5, pp. 279–282, Apr. 2009.

[13] N. Blouin, A. Michaud, and M. Leclerc, "A Low-Bandgap Poly(2,7-Carbazole) Derivative for Use in High-Performance Solar Cells," *Advanced Materials*, vol. 19, no. 17, pp. 2295–2300, 2007.

[14] S. Wakim, S. Beaupré, N. Blouin, B.-R. Aich, S. Rodman, R. Gaudiana, Y. Tao, and M. Leclerc, "Highly efficient organic solar cells based on a poly(2,7-carbazole) derivative," *Journal of Materials Chemistry*, vol. 19, no. 30, p. 5351, 2009.

[15] N. Blouin, A. Michaud, D. Gendron, S. Wakim, E. Blair, R. Neagu-Plesu, M. Belletête, G. Durocher, Y. Tao, and M. Leclerc, "Toward a rational design of poly(2,7-carbazole) derivatives for solar cells," *Journal of the American Chemical Society*, vol. 130, no. 2, pp. 732–742, 2008.

[16] P. M. Beaujuge and J. M. J. Fréchet, "Molecular Design and Ordering Effects in n-Functional Materials for Transistor and Solar Cell Applications," *Journal of the American Chemical Society*, vol. 133, no. 50, pp. 20009–29, 2011.

[17] J.-F. Morin and M. Leclerc, "2,7-Carbazole-Based Conjugated Polymers for Blue, Green, and Red Light Emission," *Macromolecules*, vol. 35, no. 22, pp. 8413–8417, 2002.

[18] N. Koumura, Z.-S. Wang, S. Mori, M. Miyashita, E. Suzuki, and K. Hara, "Alkyl-functionalized organic dyes for efficient molecular photovoltaics," *Journal of the American Chemical Society*, vol. 128, no. 44, pp. 14256–7, 2006.

[19] X. Li, J. Gui, H. Yang, W. Wu, F. Li, H. Tian, and C. Huang, "A new carbazole-based phenanthrenyl ruthenium complex as sensitizer for a dye-sensitized solar cell," *Inorganica Chimica Acta*, vol. 361, no. 9–10, pp. 2835–2840, 2008.

[20] M. Miyashita, K. Sunahara, T. Nishikawa, Y. Uemura, N. Koumura, K. Hara, A. Mori, T. Abe, E. Suzuki, and S. Mori, "Interfacial electron-transfer kinetics in metal-free organic dye-sensitized solar cells: combined effects of molecular structure of dyes and electrolytes," *Journal of the American Chemical Society*, vol. 130, no. 52, pp. 17874–17881, 2008.

[21] S. Boudreault, P.-L. T. Beaupré, and M. Leclerc, "Solar-Energy Production and Energy-Efficient Lighting: Photovoltaic Devices and White-Light-Emitting Diodes Using Poly(2,7-fluorene), Poly(2,7-carbazole), and Poly(2,7-dibenzosilole) Derivatives," *Advanced Energy Materials*, vol. 22, no. 8, pp. E6–E27, 2010.

[22] N. Berton, "PhD Thesis: Synthesis and characterization of thiophene- and carbazole-based π-conjugated copolymers functionalize with fullerene derivatives for organic photovoltaics," University Joseph Fourier, 2009.

[23] N. Berton, C. Ottone, V. Labet, R. De Bettignies, S. Bailly, A. Grand, C. Morell, S. Sadki, and F. Chandezon, "New Alternating Copolymers of 3,6-Carbazoles and Dithienylbenzothiadiazoles: Synthesis, Characterization, and Application in Photovoltaics," *Macromolecular Chemistry and Physics*, vol. 212, pp. 2127–2141, 2010.

[24] L. Yang, H. Zhou, and W. You, "Quantitatively Analyzing the Influence of Side Chains on Photovoltaic Properties of Polymer-Fullerene Solar Cells," *Journal of Physical Chemistry*, vol. 114, no. 39, pp. 16793–16800, 2010.

[25] Y. Li and Y. Zou, "Conjugated Polymer Photovoltaic Materials with Broad Absorption Band and High Charge Carrier Mobility," *Advanced Materials*, vol. 20, no. 15, pp. 2952–2958, 2008.

[26] Y. Liang, D. Feng, Y. Wu, S.-T. Tsai, G. Li, C. Ray, and L. Yu, "Highly efficient solar cell polymers developed via fine-tuning of structural and electronic properties," *Journal of the American Chemical Society*, vol. 131, no. 22, pp. 7792–7799, 2009.

[27] J. M. Szarko, J. Guo, Y. Liang, B. Lee, B. S. Rolczynski, J. Strzalka, T. Xu, S. Loser, T. J. Marks, L. Yu, and L. X. Chen, "When function follows form: Effects of donor copolymer side chains on film morphology and BHJ solar cell performance," *Advanced materials*, vol. 22, no. 48, pp. 5468–5472, 2010.

[28] I. Fabre-Francke, M. Zagorska, G. Louarn, P. Hapiot, A. Pron, and S. Sadki, "Synthesis, electrochemical and spectroscopic investigations of New N-BEDOT derivatives containing anil substituted carbazole subunits.," *Electrochimica Acta*, vol. 53, , pp. 6469–6476, 2008.

[29] J. Auerbach, S. A. Weissman, T. J. Blacklock, M. R. Angeles, and K. Hoogsteen, "n-bromosuccinimide dibromodimethylhydantoin in aqueous base - a practical method for the bromination of activated benzoic-acids," *Tetrahedron Letters*, vol. 34, no. 6, pp. 931–934, 1993.

[30] Z. B. Zhang, M. Motonaga, M. Fujiki, and C. E. McKenna, "The First Optically Active Polycarbazoles," *Macromolecules*, vol. 36, pp. 6956–6958, 2003.

[31] J. E. Gautrot, P. Hodge, D. Cupertino, and M. Helliwell, "2,6-Diaryl-9,10-anthraquinones as models for electron-accepting polymers," *New Journal of Chemistry*, vol. 31, pp. 1585–1593, 2007.

[32] J. Jo, C. Chi, S. Höger, G. Wegner, and D. Y. Yoon, "Synthesis and characterization of monodisperse oligofluorenes," *Chemistry (Weinheim an der Bergstrasse, Germany)*, vol. 10, no. 11, pp. 2681–2688, 2004.

[33] A. Iraqi and I. Wataru, "Preparation and Properties of 2,7-Linked N -Alkyl-9 H -carbazole Main-Chain Polymers," *Chemistry of Materials*, vol. 16, no. 3, pp. 442–448, 2004.

[34] J. Li and A. C. Grimsdale, "Carbazole-based polymers for organic photovoltaic devices," *Chemical Society Reviews*, vol. 39, no. 7, pp. 2399–2410, 2010.

[35] J. Liu, R. S. Loewe, and R. D. Mccullough, "Employing MALDI-MS on Poly(alkylthiophenes): Analysis of Molecular Weights, Molecular Weight Distributions, End-Group Structures, and End-Group Modifications," *Macromolecules*, vol. 32, no. 18, pp. 5777–5785, 1999.

[36] M. Trznadel, A. Pron, M. Zagorska, R. Chrzaszcz, and J. Pielichowski, "Effect of Molecular Weight on Spectroscopic and Spectroelectrochemical Properties of Regioregular Poly(3-hexylthiophene)," *Macromolecules*, vol. 31, no. 15, pp. 5051–8, 1998.

[37] J.-M. Verilhac, G. LeBlevennec, D. Djurado, F. Rieutord, M. Chouiki, J.-P. Travers, and A. Pron, "Effect of macromolecular parameters and processing conditions on supramolecular organisation, morphology and electrical transport properties in thin layers of regioregular poly(3-hexylthiophene)," *Synthetic Metals*, vol. 156, no. 11–13, pp. 815–823, 2006.

[38] N. Moliton, "How to model the behaviour of organic photovoltaic cells," *Polymer International*, vol. 55, pp. 583–600, 2006.

[39] V. Kren, P. Olsovsky, V. Havlicek, P. Sedmera, M. Witvrouw, and E. De Clercq, "N1-Alkylation of Dihydrolysergic Acid," *Tetrahedron*, vol. 53, no. 12, pp. 4503–4510, 1997.

[40] F. Wiesbrock, R. Hoogenboom, and U. S. Schubert, "Microwave-Assisted Polymer Synthesis: State-of-the-Art and Future Perspectives," *Macromolecular Rapid Communications*, vol. 25, no. 20, pp. 1739–1764, Oct. 2004.

[41] A. Najari, S. Beaupré, P. Berrouard, Y. Zou, J.-R. Pouliot, C. Lepage-Pérusse, and M. Leclerc, "Synthesis and Characterization of New Thieno[3,4-c]pyrrole-4,6-dione Derivatives for Photovoltaic Applications," *Advanced Functional Materials*, vol. 21, no. 4, pp. 718–728, Feb. 2011.

[42] D. Cornelis, H. Peeters, S. Zrig, B. Andrioletti, E. Rose, T. Verbiest, and G. Koeckelberghs, "A Chiroptical Study of Chiral Λ- and X- Type Oligothiophenes Toward Modelling the Interchain Interactions of Chiral Conjugated Polymers," *Chemistry of Materials*, vol. 20, no. 6, pp. 2133–2143, 2008.

[43] C. Marzoni and W. L. Garbrecht, "N-Alkylation of Dihydrolysergic Acid ," *Synthesis* , vol. 7, pp. 651–653, 1987.

[44] M. Ranger, D. Rondeau, and M. Leclerc, "New Well-Defined Poly(2,7-fluorene) Derivatives: Photoluminescence and Base Doping," *Macromolecules*, vol. 30, no. 25, pp. 7686–7691, 1997.

[45] J. Hou, M.-H. Park, S. Zhang, Y. Yao, L.-M. Chen, J.-H. Li, and Y. Yang, "Bandgap and Molecular Energy Level Control of Conjugated Polymer Photovoltaic Materials Based on Benzo[1,2- b :4,5-b]dithiophene," *Macromolecules*, vol. 41, no. 16, pp. 6012–6018, 2008.

[46] P. Beimling and G. Koßmehl, "Synthesis of benzo[1,2-b′:4,5-b′]dithiophene and its 4,8-Dimethoxy and 4,8-dimethyl derivatives," *European Journal of Organic Chemsitry*, vol. 119, no. 10, pp. 3198–3203, 1986.

[47] X. Guo, R. P. Ortiz, Y. Zheng, Y. Hu, Y.-Y. Noh, K.-J. Baeg, A. Facchetti, and T. J. Marks, "Bithiophene-imide-based polymeric semiconductors for field-effect transistors: synthesis, structure-property correlations, charge carrier polarity, and device stability," *Journal of the American Chemical Society*, vol. 133, no. 5, pp. 1405–18, 2011.

[48] P. Berrouard, A. Najari, A. Pron, D. Gendron, P.-O. Morin, J.-R. Pouliot, J. Veilleux, and M. Leclerc, "Synthesis of 5-Alkyl[3,4-c]thienopyrrole-4,6-dione-Based Polymers by Direct Heteroarylation," *Angewandte Chemie International Edition*, vol. 51, no. 9, pp. 2068–71, 2012.

[49] C. Ottone, P. Berrouard, G. Louarn, S. Beaupré, D. Gendron, M. Zagorska, P. Rannou, A. Najari, S. Sadki, M. Leclerc, and A. Pron, "Donor-acceptor alternating copolymers containing thienopyrroledione electron accepting units: Preparation, redox behaviour, and application to photovoltaic cells," *Polymer Chemistry*, vol. 3, pp. 2355, 2012.

[50] X. Guo, R. P. Ortiz, Y. Zheng, M. G. Kim, S. Zhang, Y. Hu, G. Lu, A. Facchetti, and T. J. Marks, "Thieno[3,4-c]pyrrole-4,6-dione-based polymer semiconductors: toward high-performance, air-stable organic thin-film transistors," *Journal American Chemical Society*, vol. 133, no. 34, pp. 13685–97, 2011.

[51] M.-C. Yuan, M.-Y. Chiu, S.-P. Liu, C.-M. Chen, and K.-H. Wei, "A Thieno[3,4- c]pyrrole-4,6-dione-Based Donor−Acceptor Polymer Exhibiting High Crystallinity for Photovoltaic Applications," *Macromolecules*, vol. 43, no. 17, pp. 6936–6938, 2010.

[52] Y. Zhang, S. K. Hau, H.-L. Yip, Y. Sun, O. Acton, and A. K. Y. Jen, "Efficient Polymer Solar Cells Based on the Copolymers of Benzodithiophene and Thienopyrroledione," *Chemistry of Materials*, vol. 22, no. 9, pp. 2696–2698, 2010.

Chapter 3

Physico-chemical characterization of synthesized *push-pull* polymers

3.1 Introduction

Polymers, whose synthesis was described in *Chapter 2* were characterized by a set of complementary techniques involving spectroscopic, electrochemical, spectroelectrochemical, diffraction and thermal ones. In the first subsection characteristic features of *push-pull* copolymers containing the same *pull* unit benzodithiazole (BTD) and two different *push* units, namely 2,7-carbazole and 3,6-carbazole are comparatively discussed.

In the next subsection detailed characterization of copolymers with the thienopyrrolodione *pull* unit and the 2,7-carbazole or dialkoxybenzodithiophene *push* units will be presented with special emphasis on the properties which are exploited in photovoltaics.

3.2 Comparison of spectroscopic and electrochemical properties of copolymers containing carbazole and benzodithiazole (BTD) units: 3,6-carbazole vs 2,7-carbazole electron donating units

The main spectroscopic feature of conjugated polymers, including *push-pull* ones, is an intensive absorption band with a maximum in the visible or near IR part of the spectrum. This band is usually ascribed to the π-π* transition in the conjugated backbone and is used for the calculation of the so called "optical band gap". The width of this band gap is mainly influenced by electron donating/accepting properties of the segments constituting the polymer repeating unit and by steric factors.[1], [2] It is also strongly dependent on the molecular mass and its polydispersity.[3] Therefore any comparison between different polymers should be carried out for samples of similar M_n and similar PDI. This applies not only to the UV-*Vis*-NIR absorption spectroscopy but also to photoluminescence.

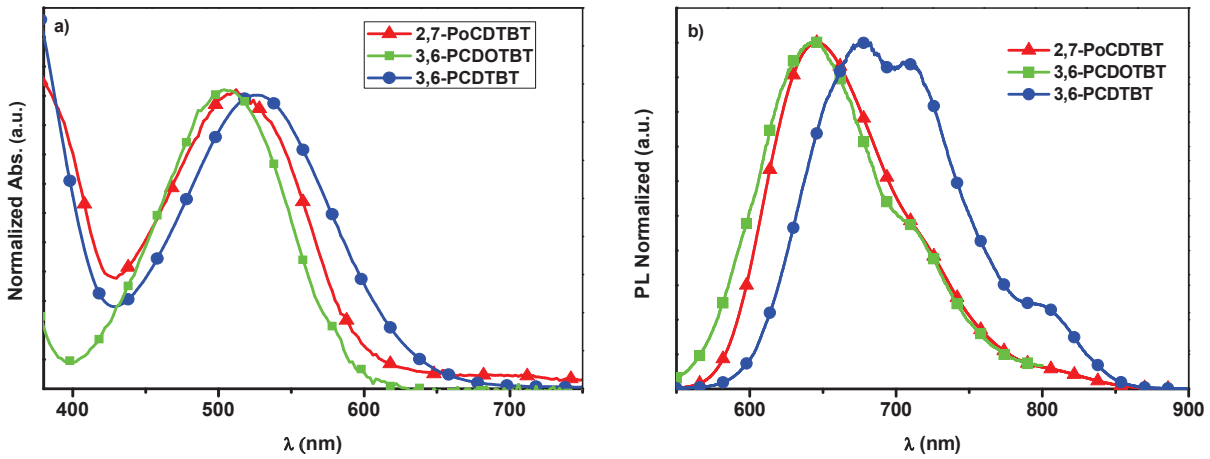

Figure 3.1: Solution (a) UV-Vis absorption spectra and (b) photoluminescence (PL) of 2,7-PoCDTBT (M_n = 4.4 kDa, PDI = 1.43), 3,6-PCDTBT (M_n = 1.6 kDa, PDI = 1.78) and 3,6-PCDOTBT (M_n = 3 kDa, PDI = 2.17) chloroform fractions in chloroform solutions.

In Figure 3.1 absorption and photoluminescence spectra of 3,6-PCDTBT, 3,6-PCDOTBT and 2,7-PoCDTBT are shown. First, by comparing the spectra of 3,6-PCDTBT and 3,6-PCDOTBT we observe a significant hypsochromic shift induced by the addition of two lateral octyl groups to the dithienylbenzothiadiazole unit of the latter. λ_{max} are at 528 nm and 506 nm respectively. Similar trend is observed in the photoluminescence spectra. This shift can be a consequence of electron donating properties of the alkyl groups which, although being rather weak electron donors, may however diminish the electron accepting power of the *pull* unit and rise the LUMO level of the polymer. Alternative explanation involves the steric hindrance caused by the presence of substituents which renders the polymer chain out of planarity. In this case the HOMO level should be lowered.

The UV- *Vis* -NIR and photoluminescence spectra of 2,7-PoCDTBT, *i.e.* the polymer containing 2,7-carbazole units are very similar to those of 3,6-PCDOTBT, implying almost the same optical band gap. However, similar value of the optical band gap indicates only that the energetic difference between the HOMO and LUMO levels in both polymers is close, but provides no information about the relative positions of these levels. To resolve these two, above outlined problems we have used electrochemical methods, and more precisely cyclic voltammetry.

The position of the HOMO level, which is related to the ionization potential (IP) of a given polymer,

can be directly determined by photoelectron spectroscopy (PES).[4], [5] Alternatively, in an indirect manner it can be derived from cyclic voltammetry data, assuming that the onset of the first anodic peak corresponds to the removal of an electron from the HOMO level. Usually the correlation between the IP values determined from PES and electrochemical ones is very good.[6] Similarly, by assuming that the onset of the first reduction potential in the cyclic voltammogram of the studied polymer corresponds to the addition of an electron to the LUMO level, we can determine its position. It should be repeated again here that the HOMO and LUMO levels are not observables, but originate from quantum chemical approximations and by electrochemical methods, we measure IP and electron affinity (EA) values which, however, are related to the HOMO and LUMO levels. Their difference gives the so called "electrochemical band gap".

For the calculations of the HOMO and LUMO levels (approximated by IP and EA) the potentials of the oxidation and reduction peaks onsets must be expressed on the absolute potential scale.[7], [8] If the potentials are given with respect to the ferrocene couple, the following equations can be used:

$$E_{HOMO} = -e(E_{ox\ onset} + 4.8)\ eV \qquad (Eq.\ 3.1)$$

$$E_{LUMO} = -e(E_{red\ onset} + 4.8)\ eV \qquad (Eq.\ 3.2)$$

where -4.8 eV is the potential of ferrocene couple with respect to the vacuum level.[7], [8][1]

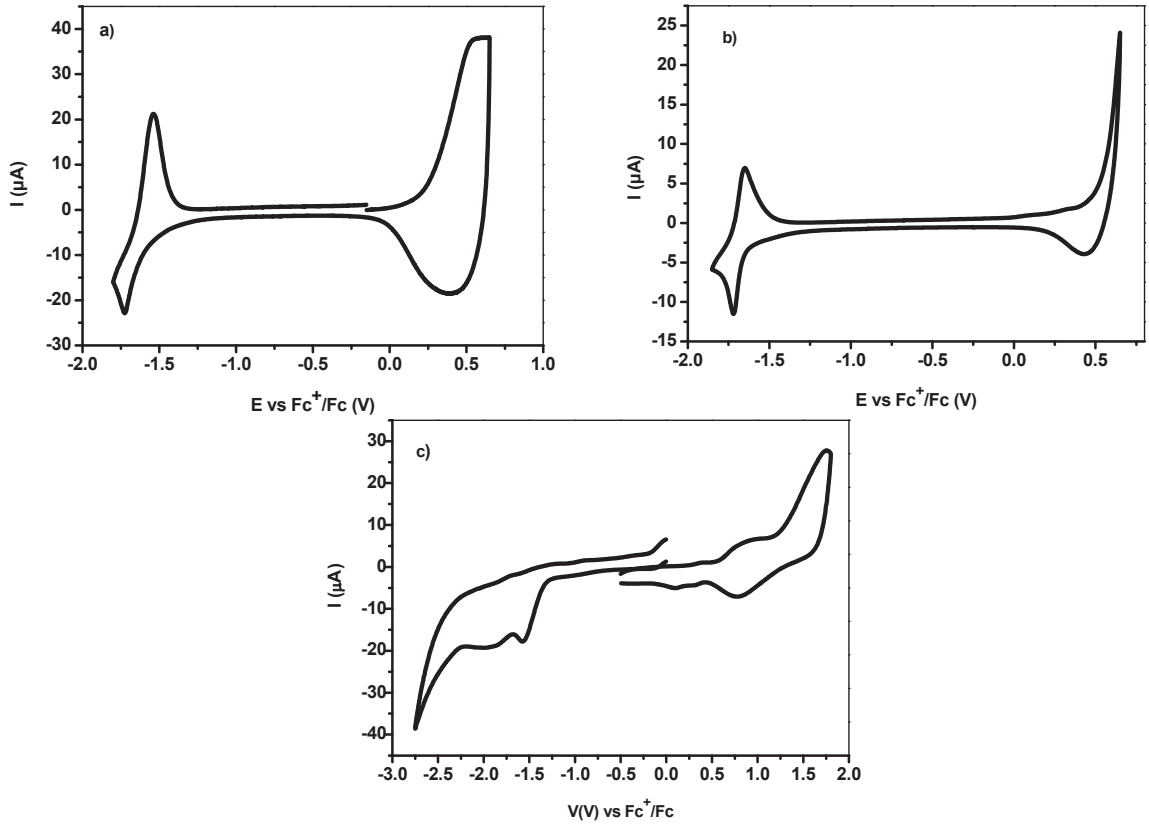

Figure 3.2: Cyclic voltammograms of 3,6-PCDTBT (a), 3,6-PCDOTBT(b) and 2,7- PoCDTBT (c). Potentials vs. Fc^+/Fc; electrolyte: 0.1 M NBu_4ClO_4 in acetonitrile; scan rate 100 $mV \cdot sec^{-1}$.

[1] *The calibration of the Fc^+/Fc couple and subsequently of $E_{ox\ onset}$ and $E_{red\ onset}$ with respect to the vacuum level is still under debate. Values of the formal potential of the Fc^+/Fc couple are considered at -4.8 eV, or at -5.1 eV.*[7] *For the calculations presented in this thesis the value -4.8 was used, actually the most popular in the literature. This estimation is based on the following calculation: the potential of NHE is -4.6 eV with respect to the vacuum level. Then, a value of 0.2 V vs NHE is added for Fc^+/Fc in 0.1 M NBu_4PF_6 in acetonitrile.*

Representative cyclic voltammograms of 3,6-PCDTBT, 3,6-PCDOTBT and 2,7- PoCDTBT are shown in Figure 3.2. First we notice that the redox couple at negative potentials, which is associated with the reduction of the polymer to a polyanion and subsequent reoxidation of this polyanion to the polymer neutral form, is located at approximately the same potential for 3,6-PCDTBT and 3,6-PCDOTBT. This means that their LUMO levels are close. To the contrary, the redox couple at positive potentials, ascribed to the oxidation of the neutral polymer to a polycation and its subsequent reduction back to the neutral state, is shifted to much higher potentials for 3,6-PCDOTBT as compared to 3,6-PCDTBT. In fact, in the former the anodic peak overlaps with an overoxidation peak, occurring at higher potentials, which renders the polymer electrochemically inactive.[9] Thus, the electrochemical data clearly demonstrate that the increase of the band gap in 3,6-PCDOTBT is caused by lowering of its HOMO level. This finding favors the hypothesis that the discussed phenomenon is caused by steric factors (*vide supra*).

The optical band gap of 2,7- PoCDTBT is very similar to that of 3,6-PCDOTBT (see Figure 3.1). However, electrochemical data clearly indicate that its HOMO and LUMO levels are shifted towards higher potentials as compared to the same levels in 3,6-PCDOTBT.

The results of the cyclic voltammetry studies are collected in Table 3.1 together with the calculated HOMO and LUMO levels as well as band gaps. A very good agreement between the electrochemical and optical band gaps should be underlined. In all three cases the determined energy levels and band gaps are in the good range for the use of the synthesized polymers in BHJ in conjunction with PCMB (E_{HOMO} level between -4.9 and - 5.5 eV).[10], [11], [12]

	$E_{OX\ onset}$ (V)	$E_{REDonset}$ (V)	E_{HOMO} (eV)	E_{LUMO} (eV)	$E_{gap\ el}$ (eV)	$E_{gap\ opt}$ (eV)
3,6-PCDTBT	0.25	-1.60	-5.05	-3.20	1.85	1.91
3,6-PCDOTBT	0.45	-1.65	-5.25	-3.15	2.10	2.11
2,7-PoCDTBT	0.53	-1.34	-5.33	-3.46	1.87	2.03

Table 3.1: Optical and Electrochemical Energy Gap of 3,6-PCDTBT, 3,6-PCDOTBT and 2,7-PoCDTBT.

At the end it should be noted that the spectroscopic and electrochemical results obtained for 2,7-carbazole-based polymer are in good agreement with those determined for the well known PCDTBT synthesized in M. Leclerc's group.[13]

3.3 Spectroscopic and electrochemical characterization of pyrrolodione (PD) based copolymers - comparison with DFT calculations for model compounds

3.3.1 Spectroscopic properties

Exploiting the building block approach, described in detail in *Chapter 2*, we were able to tune the UV-*Vis*-NIR spectra of the synthesized DA polymers in a wide spectroscopic range, covering its visible part and the onset of the near infrared one. In all cases a more or less pronounced bathochromic shift of the π–π* band is observed when going from solution (chloroform) spectra to those recorded for thin solid films (see Figure 3.3).

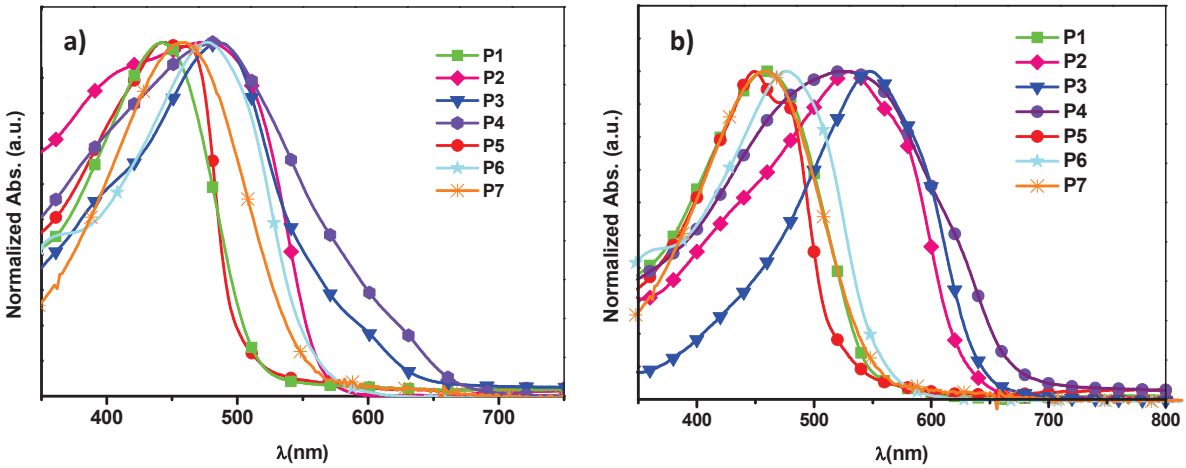

Figure 3.3: Solution UV-Vis absorption spectra of P1, P2, P3, P4, P5, P6 and P7 a) in chloroform solution and b) in the solid state.

For polymers of a given *pull*-unit the position of the π − π* band is strongly influenced by the electron-donating properties of the *push*-segment. Therefore, both λ_{max} and the peak onset (λ_{onset}) which in **P3** are located at 547 nm and 637 nm, respectively, are bathochromatically shifted by ca. 88 nm and 101 nm as compared to the case of **P1**. This is caused by the fact that dialkoxybenzodithiophene is a stronger electron donor than carbazole. Similar effect, resulting in a bathochromic shift of the π − π* band and the band gap narrowing, is also observed for an increased ratio of *pull* to *push* segments. This is clearly evidenced by comparing the spectra of **P1** and **P2**, in which the ratio of thienopyrroledione groups to carbazole ones is 1:1 and 2:1, respectively. For stronger electron donors like dialkoxybenzodithiophene, this effect is much weaker, as it is clear from the data collected from the in Table 3.2 pag. 83, where the values of optical gaps are added (compare couples **P1** vs. **P2** and **P3** vs. **P4**).

Contrary to the expectations, the band gap of **P4** is slightly wider than that of **P3**. It is possible to rationalize this fact by a two-fold difference in the number average molecular mass, M_n, of both studied polymer fractions: (M_n(P3-$CHCl_3$ fr.) = 6.5 kDa and PDI(P3-$CHCl_3$ fr.) = 1.47 and M_n(P4- hex fr.) = 3 kDa and PDI(P4- hex. fr.) = 2.13).

It is also instructive to compare the spectra of **P1** and **P6**. Having the same conjugated backbone, these polymers differ only in the number and positions of the solubility inducing alkyl groups in the *pull* unit. Hypsochromic shift of the π-π* band in **P1** with respect to the analogous band in **P6** has probably its origin

in steric factors. Evidently, in **P1** two bulky alkyl groups in the *pull* segment together with one branched alkyl substituent in the *push* one make the conjugated backbone less planar. This explanation is consistent with the electrochemical results which indicate lowering of the HOMO level in **P1** (*vide infra*).

Finally, for the polymers of the same M_n, the spectra are independent on the preparation methods. In the case of **P5** essentially the same spectra were obtained for polymers prepared by Suzuki coupling and by direct C-C coupling.

3.3.2 Electrochemical properties and DFT calculations

Different combinations of the *push–pull* units not only lead to fine tuning of the optical band gap but also influence the redox properties of the synthesized polymers and by consequence the position of their HOMO and LUMO levels. For this reason the spectroscopic data need electrochemical support.

Figure 3.4 shows representative voltammograms of thin layers of **P1**, **P2**, **P3** and **P4**. They are separated into two parts: the oxidative mode and the reductive one.

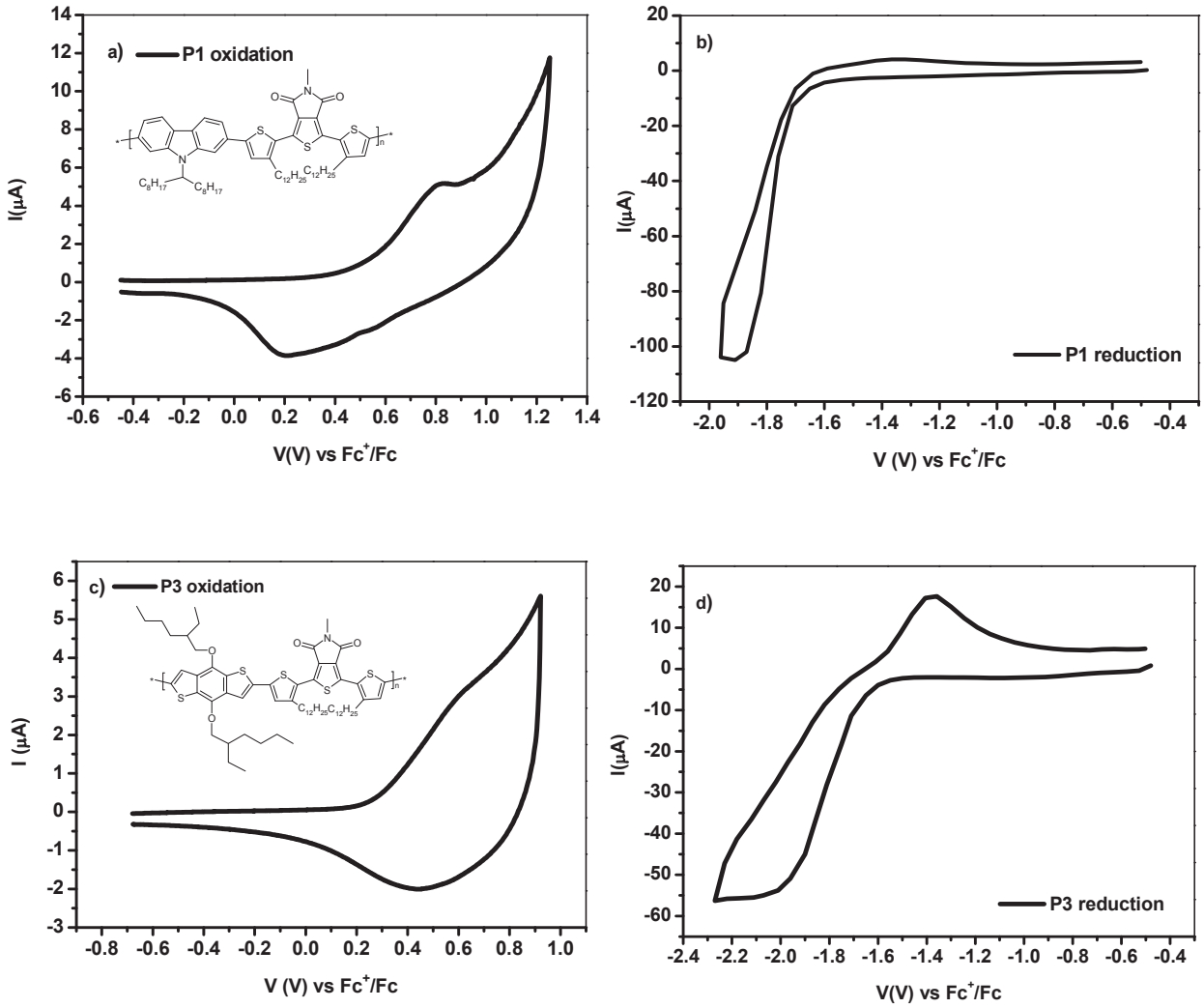

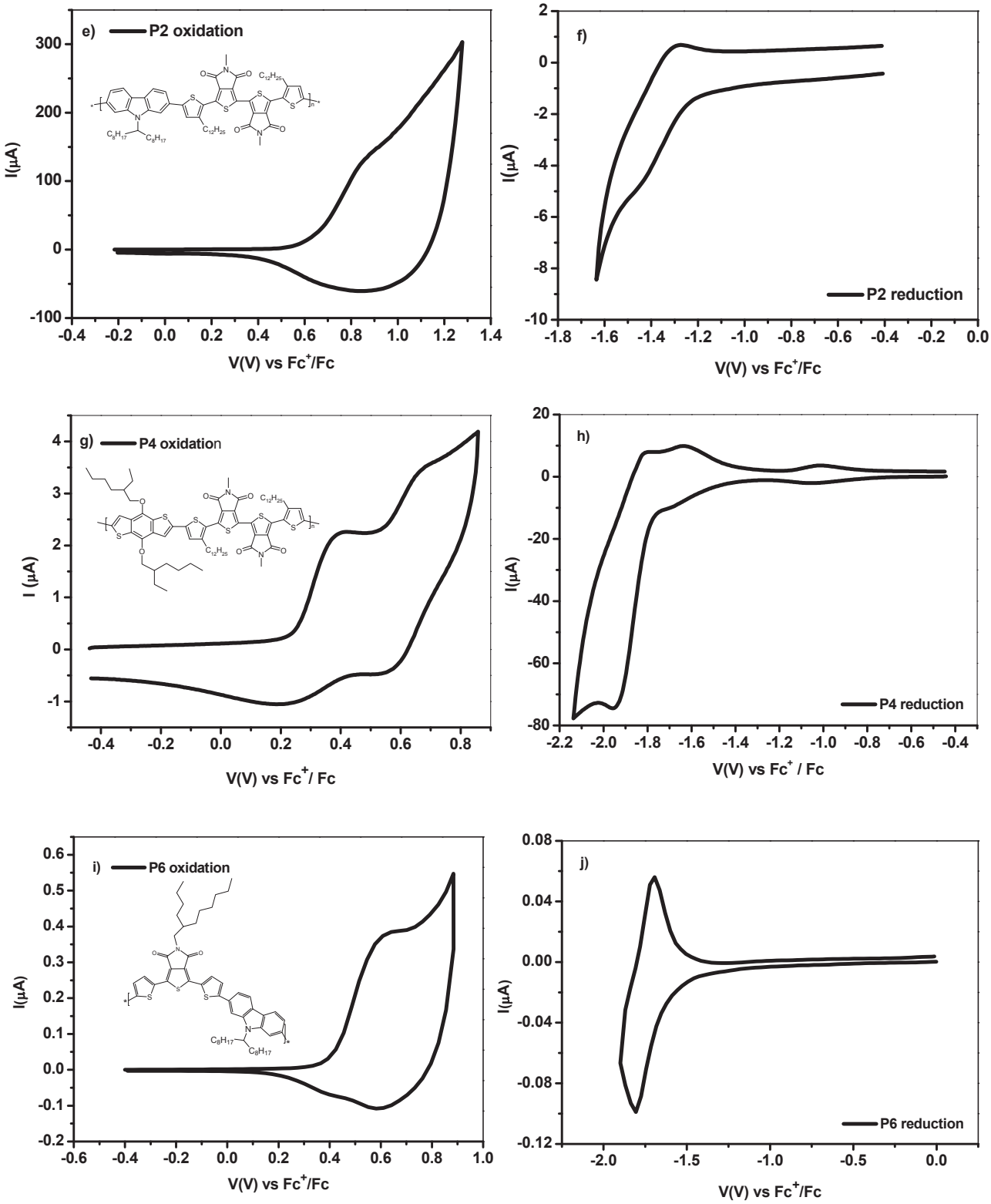

Figure 3.4: Cyclic voltammograms of P1, P2, P3 and P4. Potentials vs. Fc^+/Fc; electrolyte: 0.1 M NBu_4BF_4 in acetonitrile; scan rate 50 $mV \cdot sec^{-1}$. (a) P1 oxidative mode, (b) P1 reductive mode, (c) P3 oxidative mode. (d) P3 reductive mode. (e) P2 oxidative mode, (f) P2 reductive mode, (g) P4 oxidative mode. (h) P4 reductive mode (i) P6, oxidative mode (j), P6 reductive mode.

In the case of **P1**, **P3** and **P2** the anodic peak (see Figure 3.4 a, 3.4 c and 3.4 e), ascribed to the oxidation of the neutral polymer chains to polycations (so called "oxidative or p-doping process"), overlaps with the onset of the irreversible "overoxidation" peak.[9] As a consequence, the oxidative doping is of limited reversibility. On the other hand, for **P4** the first and the second oxidation peaks demonstrate quasi-reversible behavior (see Figure 3.4 g). This is caused by the fact that **P4** is being oxidatively doped at the lowest potential of all polymers studied and by consequence the contribution of the irreversible overoxidation to the voltammogram is negligible.

The reduction of neutral macromolecules of **P1** to radical polyanions (polarons) is totally irreversible, while for **P3**, **P2** and **P4** a partial reversibility is observed (compare Figure 3.4 b and 3.4 d, f, h). As in the voltammogram registered in the oxidative mode, **P4** also presents a second reduction peak, probably corresponding to the transformation of radical anions (negative polarons) into dianions (negative bipolarons).

Push-pull units have an influence on energetic level positions of π-conjugated alternating copolymers and the presence of the electron accepting groups lowers both the LUMO and the HOMO levels whereas the electron donating groups have the opposite effect. This effect can be illustrated by comparing the electrochemical behavior of **P1** and **P3**. A relatively high potential of the onset of the oxidative doping peak of **P1** ($\mathbf{E_{ox.onset}}$**= 0.53 V** *vs* Fc^+/Fc) is shifted in **P3** by 250 mV to lower potentials, as a result of stronger electron-donating properties of the dialkoxybenzodithiophene donor units, as compared to the carbazole ones, which better compensate the electron withdrawing effect of thienopyrroledione. The effect of the acceptor to donor ratio is also clearly evident by comparing the electrochemical properties of **P1** and **P2** (see Figure 3.4 a, b, e, f). Its two-fold increase in **P2** results in a shift of both $E_{ox.onset}$ and $E_{red.onset}$ to higher values, however for $E_{red.onset}$ the effect is more pronounced because the *pull* unit has a stronger influence on the LUMO level than on the HOMO level. This leads to a decrease of the band gap of **P2**, compared to **P1**.

The effect of an increase of the acceptor to donor ratio is much less pronounced if the *push* unit contains a stronger donor, for example dialkoxybenzodithiophene instead of carbazole. **P3** (1:1 D/A ratio) shows only slightly lower $\mathbf{E_{red.onset}}$ **(-1.64 V *vs* Fc^+/Fc)** than **P4** (1:2 D/A ratio) **(-1.54 V *vs* Fc^+/Fc)**. Thus, $\mathbf{E_{ox.onset}}$ are almost unaffected by the change in the D/A ratio (see Table 3.2).

To the contrary, keeping the D/A ratio constant (1:2) and replacing a weaker (carbazole) donor by a stronger (dialkoxybenzodithiophene) one results in profound changes in the redox properties of the polymer. This is demonstrated by comparison of **P2** and **P4**. In the case of **P4** the presence of dialkoxybenzodithiophene in the *push* unit better compensates the electron accepting properties of pyrrolodione and shifts $E_{ox.onset}$ and $E_{red.onset}$ towards lower values (see Table 3.2).

Finally, it is worthwhile to discuss redox properties of **P6**. Its cyclic voltammograms in the oxidative and reductive modes are shown in Figure 3.4 i and j. **P6** is similar in its chemical structure to **P1**. As already indicated both polymers have the same conjugated backbone but differ in the number and positions of the alkyl solubilizing groups. Spectroscopic data seem to indicate that slightly larger gap in **P1** is caused by steric factors associated with a larger number of alkyl groups in the repeat unit. Significant increase of $\mathbf{E_{ox.onset}}$ in **P1** as compared to **P6** by 130 mV leads in consequence to lowering of the HOMO level to -5.33 eV with respect to the vacuum level. This effect seems to confirm lower planarity of the **P1** chain, as a consequence of steric hindrance. $\mathbf{E_{red.onset}}$ is less affected, although it is raised by 70 mV in **P1** as compared to **P6,** probably due to the fact that that **P1** contains a larger number of weakly electron donating alkyl groups. Thus both discussed factors cause an increase of the band gap of **P1** with respect to that of **P6**.

Sample	$E^*_{ox\ onset}$ (V)	$E^*_{red\ onset}$ (V)	E^{**}_{HOMO} (eV)	E^{**}_{LUMO} (eV)	Electrochemical Gap(eV)	Optical Gap (eV)
P1	0.53	-1.67	-5.33	-3.13	2.20	2.26
P2	0.62	-1.27	-5.42	-3.53	1.89	1.97
P3	0.28	-1.64	-5.08	-3.16	1.92	1.91
P4	0.25	-1.54	-5.04	-3.26	1.78	1.86
P6	0.40	-1.60	-5.20	-3.20	2.00	2.22

Table 3.2: Summary of energetic values for P1, P2, P3, P4 and P6 polymers. Oxidation reduction onset potentials (E^{ox}_{onset} and E^{red}_{onset}), HOMO and LUMO energy levels and electrochemical and optical gap are presented. Potentials vs Fc^+/Fc.

P5 and **P7** constitute a separate class of polymers in which the *pull* unit consists of thienopyrroledione moiety only, with no thienyl groups surrounding it. **P7** is very difficult to oxidize and shows the lowest lying HOMO level of all polymers studied in this research (see Figure 3.5 and Table 3.3). This is in part caused by strong *pull* effect of the "naked" thienopyrroledione, but steric factors must also contribute to the lowering of HOMO since the LUMO level of **P5** is even slightly higher than the corresponding levels in the **P1-P4** series. If the electron accepting properties of the *pull* unit were dominating, the LUMO level of **P5** should be much lower. **P7** has much higher lying HOMO level. We believe that this is caused by much less pronounced steric hindrance in **P7** as compared to **P5** since the LUMO levels of both polymers are comparable (see Table 3.3). If electron donating properties of the bithiophene *push* unit were dominating, the LUMO level should be raised. This hypothesis is additionally corroborated by the comparison of the electrochemical properties of **P7** and PBTTPD – a DA polymer known from literature.[14]

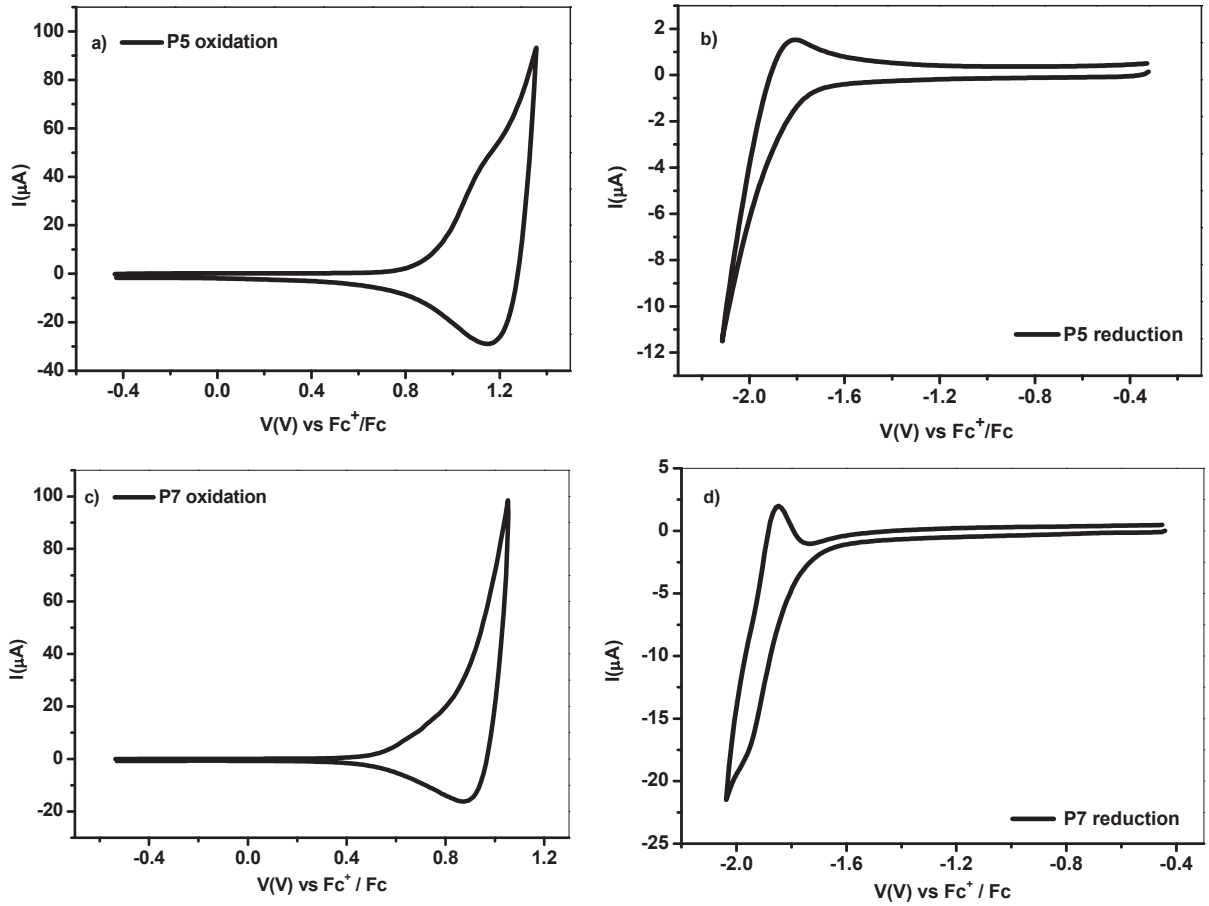

Figure 3.5: Cyclic voltammograms of P5 and P7. Potentials vs. Fc^+/Fc; electrolyte: 0.1 M NBu_4BF_4 in acetonitrile; scan rate 50 $mV \cdot sec^{-1}$. (a) P5 oxidative mode, (b) P5 reductive mode, (c) P7 oxidative mode, (d) P7 reductive mode.

Sample	$E^*_{ox\ onset}$ (V)	$E^*_{red\ onset}$ (V)	E^{**}_{HOMO} (eV)	E^{**}_{LUMO} (eV)	Electrochemical Gap (eV)	Optical Gap (eV)
P5	0.81	-1.79	-5.61	-3.01	2.60	2.43
P7	0.54	-1.74	-5.34	-3.06	2.28	2.25

Table 3.3: Summary of energetic values for P5 and P7 polymers. Oxidation reduction onset potentials (E^{ox}_{onset} and E^{red}_{onset}), HOMO and LUMO energy levels and electrochemical and optical gap are presented.

Introducing a bulky branched alkyl group as N-substituent in PBTTPD significantly increases steric hindrance which leads to a decrease of the conjugated chain planarity and to lowering of the HOMO level from -5.34 eV in **P7** to -5.56 eV in PBTTPD whereas the position of the LUMO level remains approximatetly the same -3.06 eV in **P7** and -3.10 in PBTTPD (see Figure 3.6).

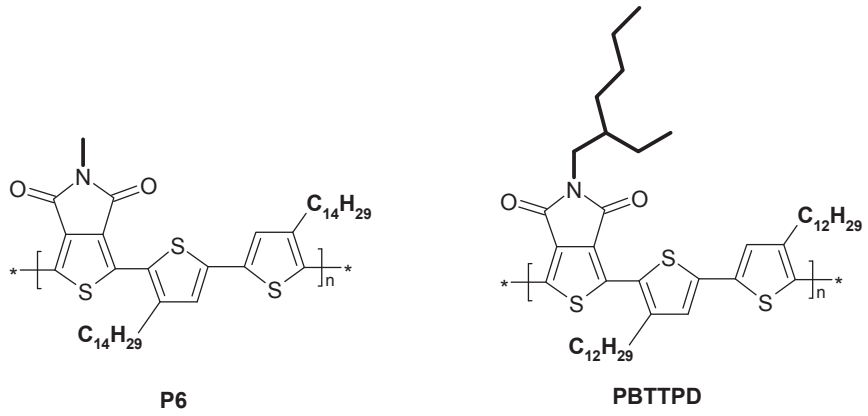

Figure 3.6: Structures of the P7 and PBTTPD – a copolymer known in the literature.[15]

The redox potential values can be obtained with accuracy when the voltammetric responses are reversible. Since in the studied polymers the redox processes were irreversible or partially reversible, the presented values of the HOMO and LUMO levels, determined on the basis of the redox process onset, can be treated only as the first estimation. A good agreement between the optically and electrochemically determined band gaps should be pointed out.

3.4 UV- *Vis* spectroelectrochemistry

The determination of the electrochemical oxidative (reductive) doping onset from the electrochemical studies may be somehow arbitrary due to a broad nature of the CV peaks and their rather complex shape. In addition temporal effects can occur upon variation of the scan rate. As a consequence, for conjugated polymers spectroelectrochemistry can be of help in more precise determination of the HOMO and LUMO levels, since their UV-*Vis*-NIR spectra are extremely sensitive to the doping and undoping processes. We have carried out such studies for **P1**.

In an experiment devoted to the HOMO (LUMO) level determination, the UV-*Vis*-NIR spectroelectrochemical measurements should be carried out in a quasi-static mode, in which the working electrode potential is being raised in small increments and the spectrum is registered when the equilibrium is reached, indicated by no (or negligible) current in the electrochemical cell. By this method the onset of the doping process can be established with the precision below 10 mV. Oxidative or reductive doping of π-conjugated polymers give rise to a bleaching of the π - π* transition band with correlated growth of two bands at higher wavelengths, characteristic of the doped state. Such evolution is clearly seen in the spectra of **P1** registered for increasing working electrode potentials (see Figure 3.7).

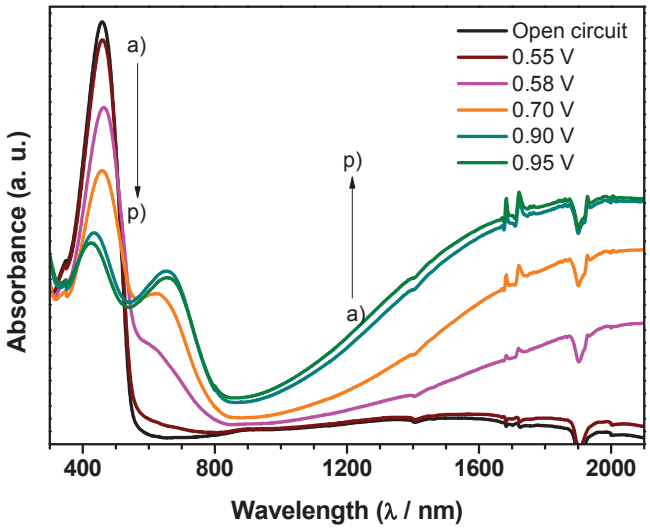

Figure 3.7: UV-Vis-NIR spectra of a thin film of P1 registered for increasing working electrode potential. Electrolyte: 0.1 M NBu_4BF_4 in acetonitrile; potential vs. Fc^+/Fc.

Bleaching of the band at 460 nm is accompanied by an appearance and consecutive growth of two doping-inducted bands with maxima at 651 nm and at 1960 nm. Oxidative doping of conjugated polymers follows in general the two states model involving the formation of radical cations (polarons) in the first step and spinless dications (bipolarons) in the second one.[16], [17] In polymers showing a rather limited conjugation length and by consequence high oxidative doping potential, only the first oxidation process takes place which, then, is followed by the overoxidation. This seems to be the case for **P1** since even at potential approaching the onset of the overoxidation, the $\pi - \pi^*$ transition is not completely bleached out and further spectral evolution becomes minimal. The spectrum registered at E = 0.95 V resembles those characteristic of partially doped conjugated polymers or spectra of polymers in which host-guest interactions impede the doping process.[18] From the point of view of the HOMO level determination the potential of the onset of the doping induced spectral changes is of crucial importance. In **P1** these changes start to appear at E = 0.48 V and up to E = 0.70 V they are very pronounced. The spectroelectrochemically measured onset of the oxidative doping is lower by 50 mV as compared to that determined from cyclic voltammetry. As a result, the HOMO level determined from the spectroelectrochemical investigations is slightly higher than the one obtained using cyclic voltammetry data (-5.28 eV vs -5.33 eV). We tend to believe that the value obtained by spectroelectrochemistry is more precise since it was measured in the quasi-static mode, using a technique extremely sensitive to the oxidative doping.

3.4.1 DFT

Complementary informations about the HOMO and LUMO levels could be given by theoretical calculations, more precisly by the Density Funcitonal Theory (DFT). It was recently demonstrated that DFT calculations can provide deeper information concerning variation of the optical and electrochemical properties of donor and acceptor moieties beloging to the π-polymer backbone.[19–22] Before starting with the results presentation a general overview on the Density Functional Theory will be given.

3.4.1.1 *Density Functional Theory (DFT) – Theory*

To go back up to the geometry of polymers it is necessary to dispose of calculation tools allowing the detailed description of systems composed of a large number of nucleus and electrons. The issue of the quantum numerical calculation methods is to solve the Schrödinger equation for the biggest number of atoms, in a reasonable delay.

$\hat{H}\|\Psi\rangle = E\|\Psi\rangle$	*(Eq. 3.1)*
$\hat{H} = \hat{T}_n + \hat{T}_e + \hat{V}_{e-e} + \hat{V}_{n-n} + \hat{V}_{e-n}$ $= -\sum_A \frac{\hbar^2}{2M_A}\nabla^2\left(\vec{R}_A\right) - \sum_\alpha \frac{\hbar^2}{2m_\alpha}\nabla^2\left(\vec{R}_\alpha\right)$ $+ \frac{1}{2}\sum_\alpha \sum_{\beta\neq\alpha} \frac{e^2}{4\pi\varepsilon_0\left\|\vec{R}_\alpha - \vec{R}_\beta\right\|} + \frac{1}{2}\sum_A \sum_{B\neq A} \frac{Z_A Z_B e^2}{4\pi\varepsilon_0\left\|\vec{R}_A - \vec{R}_B\right\|}$ $- \sum_A \sum_\alpha \frac{Z_A e^2}{4\pi\varepsilon_0\left\|\vec{R}_A - \vec{R}_\alpha\right\|}$	*(Eq. 3.2)*

The equation 3.1 constitutes the time independent Schrödinger equation. $\hat{H}$, the total hamiltonian of the system, integrates the kinetic energy operators of each nucleus and of each electron $\hat{T}_e$ as well as electron-electron $\hat{V}_{e-e}$, nucleus-nucleus $\hat{V}_{n-n}$ and electron nucleus $\hat{V}_{e-n}$ interaction energies (Eq. 3.2). Analytical solutions of Schrödinger equations exist only for the simplest cases, for example, for the hydrogen atom. A certain number of approximations allow dealing with the most complicated systems. The first approximation consists in the separation of the nucleus movements from electrons movements. In this approximation (Born-Oppenheimer approximation), nucleus (characterized by higher masses than electrons) are considered as stationary and electrons move in a nucleus potential. In this way, the Hamiltonian of the system is reduced at its electronic part (Eq. 3.2):

$\hat{H} = \hat{T}_e + \hat{V}_{e-e} + \hat{V}_{e-n}$	*(Eq.3.3)*

The Born-Oppenheimer approximation simplifies the Schrödinger equation, but calculations are still complexes because inter-electron interactions are difficult to express. Electron movements are governed by their mutual electrostatic repulsion and by the Pauli exclusion principe. The Density Functional Theory (DFT) allows taking into account the inter-electron interactions. The theory formalism was developed during the 60s by P. Hohenberg, W. Kohn et L. Sham.[23] Compared to others methods, as the Hartree-Fock theory, the DFT enable to considerably reduce the number of variables. Indeed, while th Hartree-Fock refers to a multielectron wave function depending of 4N variables (3N coordinates of N electrons and N spins), the DFT uses the charges density distribution, reducing the problem to only 3 variables. The resolution of the Kohn and Sham equations allows going back up to orbitals and rebuilding the electron density distribution. Starting from an electron density arbitrary value, an electron density interactive

calculation of the effective potential and the electron wave functions enable the determination of the electronic density corresponding to the minimum of the total energy system.

3.4.1.2 *DFT calculations of HOMO and LUMO energy levels and of the corresponding orbitals for copolymer basic building blocks and copolymers*

We were tempted to verify whether the HOMO and LUMO levels, determined electrochemically or spectroelectrochemically for the polymers studied, correlate with the corresponding values obtained by DFT calculations. These calculations have been carried out for model compounds whose chemical constitutions mimic the repeating units of **P1**, **P2**, **P3** and **P4**.

This part of the presented research has been carried out in collaboration with Dr Chirstophe Morell and Professor André Grand of the CEA/INAC/SCIB Laboratory.

In each case, the geometry of the molecule has been optimized in vacuum at the B3LYP/6-31G_level of theory, [24–27] using the Gaussian 03 package.[28] The calculations were additionally simplified by replacing dodecyl chains in the thienopyrrolodione (TPD) unit and the branched substituents in the benzodithiophene (BTD) unit by ethyl groups; octyl branched substituents of the carbazole moiety were reduced to branched tert-butyl groups. Vibrational frequency calculations were performed at the same level of theory to check the stability of the conformations obtained. Molecular orbital (MO) energy levels were then evaluated for these vacuum-optimized structures.

The shapes of frontier orbitals together with computed HOMO and LUMO energy levels are reported in Figure 3.8 (a) and (b) with the corresponding energy gap for the different repeating units of the *push-pull* copolymers.

Model compound	Units	Representation (a)		E_{gap}
		HOMO	LUMO	
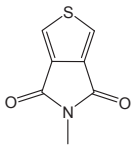	A1	-7.29 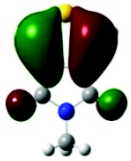	-1.78 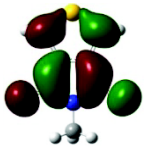	5.51
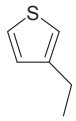	A2	-6.17 	-0.1 	6.07
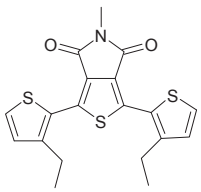	A3	-5.36 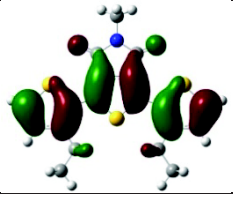	-1.92 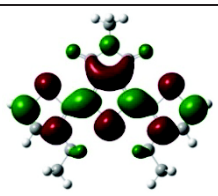	3.44
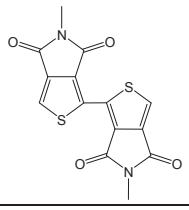	A4	-6.54 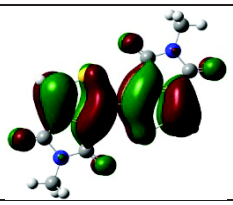	-2.72 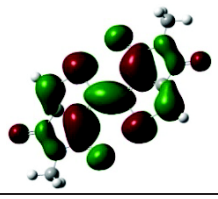	3.82
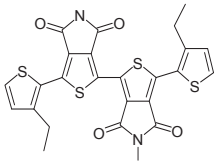	A5	-5.43	-2.5	2.93
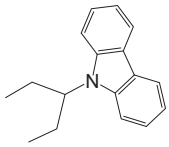	D1	-5.25 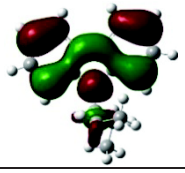	-0.58 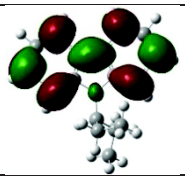	4.67
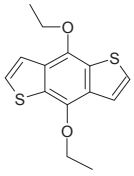	D2	-5.23 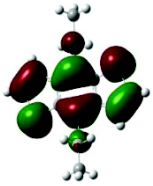	-1.01 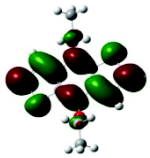	4.23

Model Compound	Representation (b)	
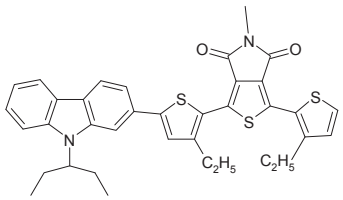 P1	LUMO = -1.96eV 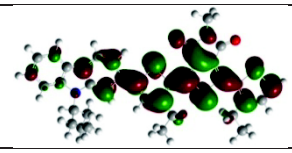 HOMO = -5.08 eV 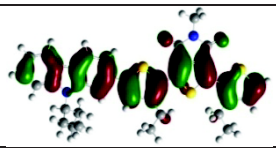	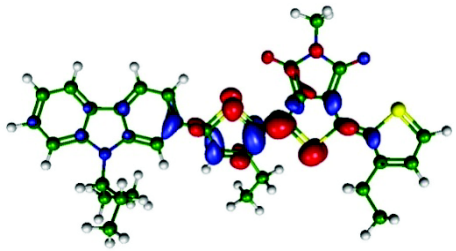 E_{gap} = 3.12 eV
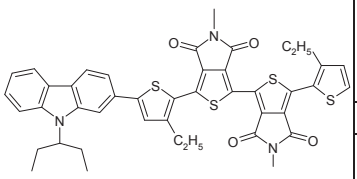 P2	LUMO =-2.44 eV 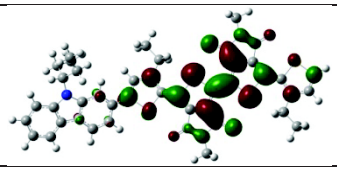 HOMO =-5.14 eV 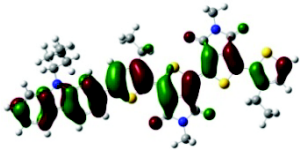	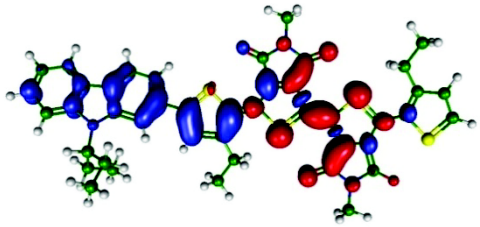 E_{gap} = 2.70 eV
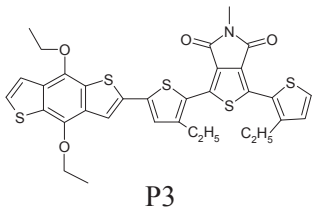 P3	LUMO =-2.24 eV 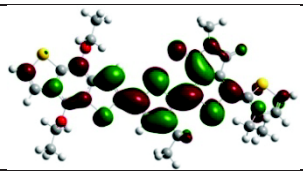 HOMO =-5.09 eV 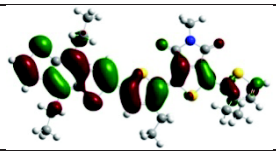	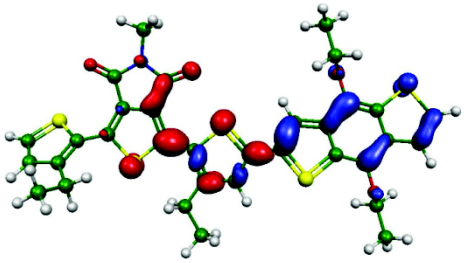 E_{gap} = 2.85 eV
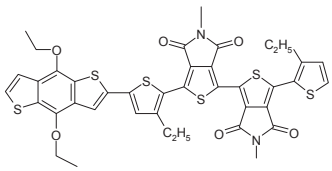 P4	LUMO = -2.56 eV 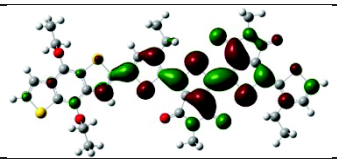 HOMO =-5.11 eV 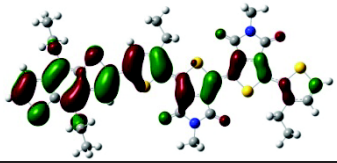	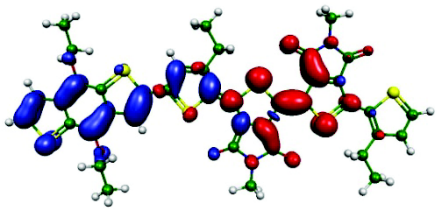 E_{gap} = 2.55 eV

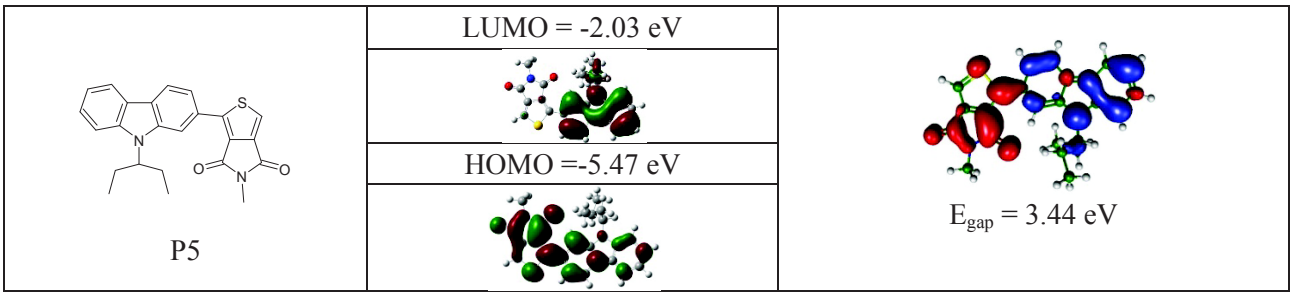

Figure 3.8: Summary of calculated energy levels and frontier orbitals shape of model compounds mimicking the repeating units of the alternating copolymers as determined by DFT calculations (Representation (a) and (b)).

Some characteristic trends in the positions of the HOMO and LUMO levels for the model compounds, corresponding to **P1-P5**, can be pointed out on the basis of the quantum chemical calculations results. First, we observe that logically, the largest band gap corresponds to the case in which no delocalizing effect of the thiophene spacers, present in other model compounds and polymers, could contribute to its narrowing. An excellent linear correlation can be found between the calculated band gaps of the model compounds and the electrochemically determined ones for the corresponding polymers (correlation coefficient for linear regression, R, is equal to 0.98). Good correlation is also found for the calculated and optical gaps (R = 0.97) (see Figure 3.9).

Apart from **P5**, the theoretically calculated HOMO energy levels are rather similar. Thus the resulting differences in the gap are mostly affected by the LUMO levels in agreement with the experimental findings. In **P1-P4** the electron density of the LUMO is mainly localized in the acceptor unit, while the electron donor density is distributed over the entire conjugated backbone. This effect is evident in particular for copolymers **P2** and **P4**, characterized by two TPD units. Again, **P5** can be considered as an exeption in this respect.

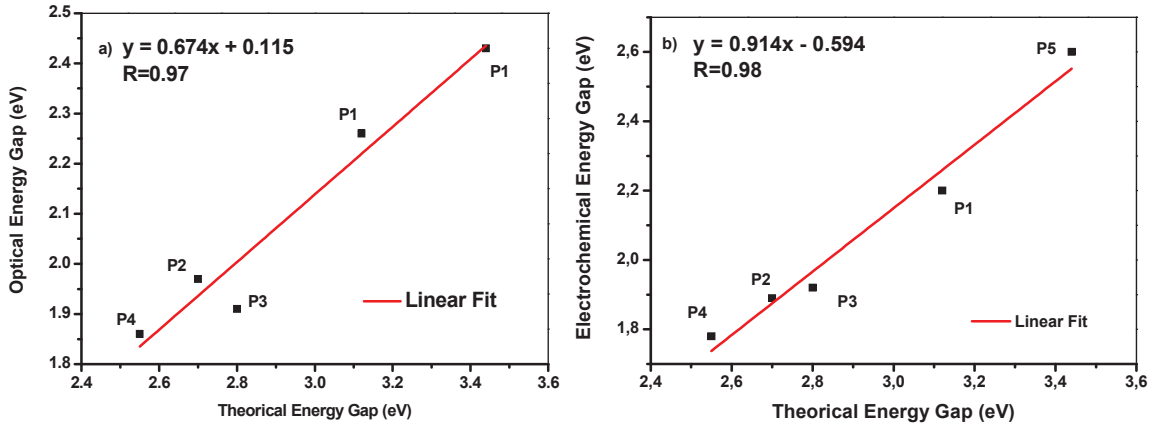

Figure 3.9: Correlation between theoretical energy gap values found for model compounds and optical (a) and electrochemical (b) energy gap values of the corresponding polymers.

By exploiting the DFT calculations it is also possible to show how the *push-pull* effect is manifested in each case (see Figure 3.8 – Representation b).

In **P1**, the *push* effect of the carbazole moiety is slightly more pronounced if compared to the *pull* effect of the TPD moiety; in addition, suprisingly, TPD seems to play both the role of the donating and the

accepting unit. For the other carbazole derivatives, only in the case of **P5**, a good "balance" between the donor effect of carbazole and the acceptor effect of the TPD is respected. In the case of **P2** the bridging thiophene, in the bis-TPD unit, plays, again surprisingly, a *push* role. In this polymer, some donating "spots" are present also in the bis-TPD-moiety although less pronounced than in **P1**.

Passing then through the BTD derivatives, it should be noticed that the effect of thiophene bridge, both in the single TPD moiety (even if less evident) and in the bis-TPD moiety is reproductible.

Finally, a comparison of the calculation results carried out for **P1** and **P3**, confirms the conclusion based on the spctroscopic and electrochemical data that BTD is a stronger electron donor than carbazole. On the other hand, a kind of "role mixing" is manifested in polymers with increased (2:1) ratio of the acceptor to donor units.

3.5 Raman spectroscopy and spectroelectrochemistry

In addition to UV-*Vis*-NIR spectroelectrochemistry of **P1** we have additionally performed Raman spectroelectrochemical investigations of this polymer. This part of the research was carried out in collaboration with Professor G. Louarn from the Institut des Matériaux Jean Rouxel (IMN) in Nantes. We have also jointly elaborated the vibrational models for polymers **P1-P5** with the goal to compare experimental Raman and IR data with the calculated ones.

3.5.1 Raman spectroelectrochemistry

Before describing Raman spectroelectrochemical behavior of **P1** it is instructive to discuss the Raman bands attribution of three of the copolymers containing carbazole sub-units. In Figure 3.10 spectra of **P1** and **P2** are compared with that of **P5** which can be considered as a model compound.

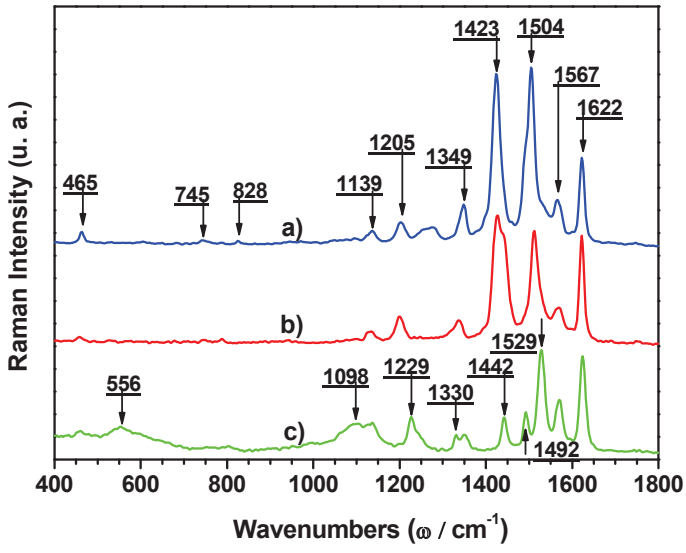

Figure 3.10: Raman spectra (λ_{exc}=1064 nm): a) P2, b) P1,c) P5 in their neutral (undoped) form.

Four bands, at 1139, 1349, 1567 and 1622 cm^{-1}, are common for these three studied polymers and they can be assigned to the alkylcarbazole group, as the CH deformation and three different C-C stretching vibration modes of the benzenoid rings. The strong band located at 1512 cm^{-1} for **P1**, at 1504 cm^{-1} for **P2**,

and at 1529 cm^{-1} for **P5** is absent for carbazole based homopolymers.[7], [18], [29], [30] It can therefore be unambiguously assigned to the C=C stretching vibration of the thienopyrroledione group. Similarly, the bands pointed at 1442 cm^{-1} and 1492 cm^{-1}, present in **P1** and **P2** as shoulders, are assigned to the ring deformation of the thienopyrroledione group.

Alternatively these bands could be assigned to the CH_2/CH_3 deformation of the alkyl groups, but the Raman intensities of these vibration modes, especially in resonance conditions of the π-conjugated backbone, are usually very weak. Finally, the strong band observed at 1427 cm^{-1} and 1423 cm^{-1} for **P1** and **P2**, respectively, is assigned without any ambiguity to the C=C deformation mode to the alkylthiophene monomers.[31] Bands appearing in the 1000-1350 cm^{-1} region are usually assigned to the CH deformation and to the stretching vibration of the C-C inter-ring bonds. By comparison, the bands located at 1205, 1229, and 1262 cm^{-1} rise from the alkythiophenealkylcarbazole, thienopyrroledione-alkylcarbazole, and thienopyrroledione-thienopyrroledione C-C inter-ring bonds. Bands around 1100 cm^{-1} are probably due to the CH in-plane deformation of carbazole and thiophene rings, and bands appearing at wavenumbers lower than 1000 cm^{-1} result from the out-of-plane deformations of the aromatic rings.

Having in mind these rather unambiguous attributions, we could analyze the spectroelectrochemical response of **P1** associated with its doping. Significant changes are expected in the Raman spectra of the electrochemically doped polymer because this process involves lowering of the overall bond order as a consequence of an electron removal from the HOMO level (oxidative doping) or an electron addition to the LUMO level (reductive doping). This alters, in turn, the force constants of some bonds and leads to a shift of selected bands in the spectra of doped polymers. Moreover, doping frequently induces the changes in the bond sequence (for example quinoid vs. benzenoid) as well as in the conformation of the macromolecule. Thus, some Raman bands may disappear and new bands may appear because, upon doping, they may become symmetry forbidden or symmetry-allowed. In Figure 3.11, Raman spectra of **P1**, registered below and above the potential of the oxidative doping onset, are collected. From the open circuit potential (E_{oc} = −0.15 vs Fc^+/Fc) up to E = +0.55 V, no doping-induced changes are seen and all spectra remain essentially the same and characteristic of the neutral state of **P1**. Above this potential the intensity of the spectrum abruptly decreases and two bands originating from the terthiophene-pyrroledione sub-unit of **P1** at 1512 cm^{-1} and 1427 cm^{-1} are shifted to 1450 cm^{-1} and 1409 cm^{-1}, respectively (see the spectrum registered at E = 0.61 V). Such behavior is typical of the electrochemical oxidation of poly(thiophene) derivatives and manifests the doping induced bond order lowering in the terthiophene-pyrroledione sub-unit of the polymer.[31], [32] The shift of these bands is accompanied by a quick disappearance of the band at 1620 cm^{-1} which is diagnostic of the neutral (undoped) carbazole unit. The carbazole band reappears at 1598 cm^{-1} in the spectrum of the degraded polymer (E = 0.92 V). Transformation of the Raman spectrum of doped P1 into the one typical of a degraded polymer, occurring over a very narrow potential range, additionally shows that the potentials of the doping and the overoxidation strongly overlap in this case, consistent with the cyclic voltammetry data.

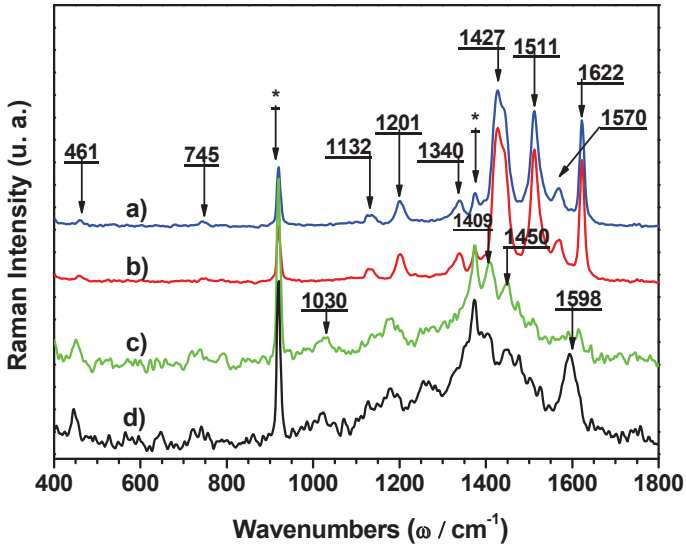

Figure 3.11: Raman spectra of a thin film of P1 registered for increasing working electrode potential (a) -0.15 V, (b) 0.55 V; (c) 0.61 V, and (d) 0.92 V. Electrolyte: 0.1M NBu_4BF_4 in acetonitrile; potential vs. Fc^+/Fc; $\lambda_{exc} = 1064$ nm. (acetonitrile bands).*

3.5.2 Vibrational model of the polymers studied

The attribution of the bands in the Raman spectrum of **P1** in its undoped and doped states was proposed on the basis of the known literature data as well as by comparison with **P5**, which can be considered as a model compound. We were tempted, however, to develop vibrational models for all polymers of the **P1-P5** series with the goal to confront the experimental data with theoretical predictions. This part of the research was also carried out in collaboration with Professor Guy Louarn.

The analysis was based on a theoretical model of geometries (in 2 dimensions). For the geometries determination, computational modes were based on the Density Functional Theory (DFT) (See *paragraph 3.2.3.1*) and the interpretation was complete by the formalism based on the valence force field (electronic structure, geometry, vibration modes).

The Hyperchem 7.5 software was used in this work. To limit the calculation time, the long aliphatic transverse chains were not taken into account for the copolymers calculations.

3.5.2.1 *Geometry*

The geometrical parameters of the studied copolymers were determined by DFT calculations and they are presented in Figure 3.12 and 3.13. The set of angles and bond lengths are determined and reported in calculations of vibrational modes of the repeating unit. To shorten the calculation time alkyl substituent were not simulated.

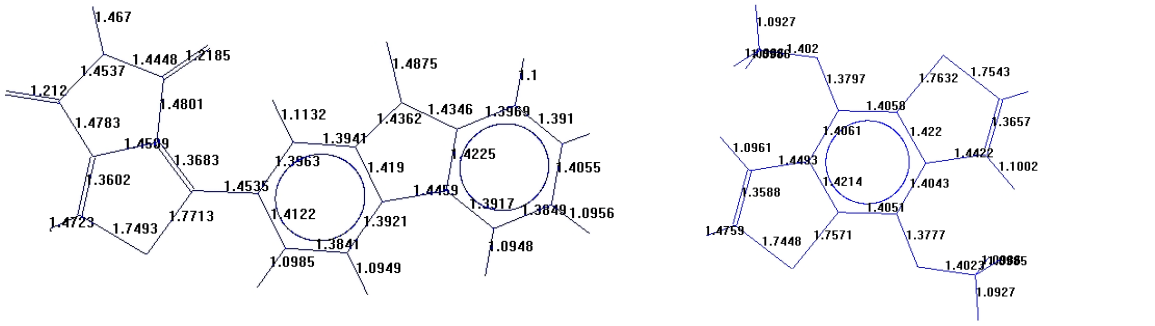

Figure 3.12: Bond lengths determined for carbazole, thienopyrroledione and dialkoxybenzodithiophene subunits in the P1-P5 series of push-pull copolymers.

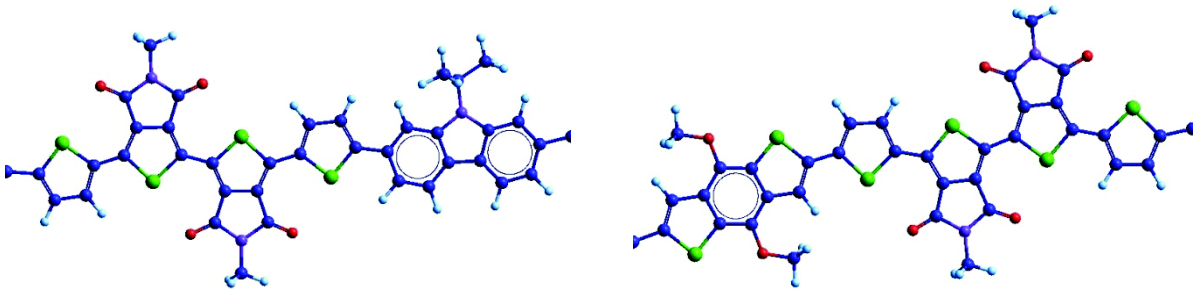

Figure 3.13: Presentation of the repetitive unit geometry of the copolymers P2 and P4 as examples of the studied series (blue: carbon atoms, green: sulphur; red: oxygen, violet: nitrogen).

3.5.2.2 *Vibrational Analyses – Formalism*

In order to interpret Raman and IR spectra a Valence Force Field (VFF) model was developed. The dynamic matrix, calculated on the base of cartesian shifts, was expressed using internal coordinates and built from an interplay of force constants. Theoretical frequency was obtained through the matrix diagonalization where each frequency corresponds to an associated vibrational mode. In this work the valence force field was chosen to better represent the covalent chemical bond. The force constants were defined, simply form the internal coordinates to which they are related (valence stretching, angular deformation, bond-bond interactions,…). At this point, the attribution of experimental mode guides all the calculations.

In Table 3.4 the main force constants used in the modeling are listed. These constants exit directly from the dynamic matrix, expressed in terms of the internal coordinates. The molecule symmetries should be considered, because they allow the expression of the symmetrical matrix diagonalized in different blocs. This shortens calculation time and facilitates the classification of modes, based on their symmetries.

Symbol	Force Constant Value mdyn./Å	Symbol	Force Constant Value mdyn./Å
Thienopyrroledione and alkylthiophene rings			
$F_{C_1\text{-}C_2}$	7.12	$F_{C_2\text{-}C_3}$	6.36
$F_{C_3\text{-}C_4}$	7.25	$F_{C_3\text{-}C_{Alkyl}}$	4.81
$F_{C_1\text{-}S}$	4.99	$F_{C_4\text{-}C_5}$	5.24
$F_{C_5\text{-}C_6}$	6.88	$F_{C_6\text{-}C_7}$	6.29
$F_{C_7\text{-}C_8}$	6.88	$F_{C=O}$	10.12
$F_{C\text{-}N}$	5.14		
Alkylcarbazoles rings			
$F_{C_{14}\text{-}C_{15}}$	6.24	$F_{C_{15}\text{-}C_{16}}$	6.39
$F_{C_{16}\text{-}C_{17}}$	6.41	$F_{C_{17}\text{-}C_{18}}$	4.52
$F_{C_{16}\text{-}N}$	5.15	$F_{C\text{-}H}$	5.01
Benzodithiophene (BDT) rings			
$F_{C_9\text{-}C_{10}}$	7.12	$F_{C_{10}\text{-}C_{11}}$	6.24
$F_{C_{11}\text{-}C_{12}}$	6.31	$F_{C_{11}\text{-}C_{13}}$	6.42
$F_{C\text{-}S}$	4.99	$F_{C\text{-}H}$	5.08

Table 3.4: Main force constant values used in the vibrational mode modeling.

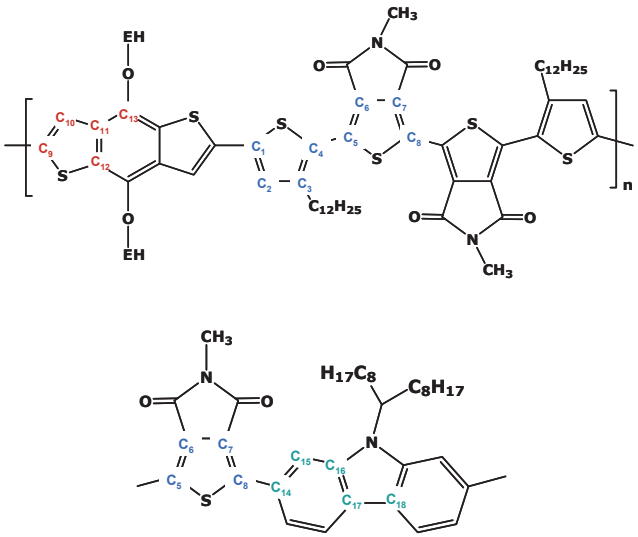

Figure 3.15: Carbon atoms digitization used in the force constants definition, presented in the previous table.

The set of results (vibrational modes) are summarized in Tables 3.5 and 3.6 which list the attribution of Raman and IR active modes, respectively and compare the theoretically calculated modes with experimental ones.

Experimental signals (cm^{-1})					Calc. modes	Assignements*
P1	P2	P3	P4	P5	ν / cm^{-1}	
1623	1623			1624	1623	C-C stretch (alkylcarbazole group)
–	–	1584	1584	–	–	C-C stretch + aromatic ring deformation of the BDT group
–	–	1554	1558	–	–	C-C stretch + aromatic ring deformation of the BDT group
1570	1565	–	–	1570	1576	C-C stretch + alkylcarbazole rings def.
1513	1504	1513	1508	1529	1509	C=C stretch (thienopyrroledione ring)
-	1493	–	–	1493	1483	C-H def + alkylcarbazole ring def.
1440	–	–	–	1442	1444	C=C ring thiophene stretch of the thienopyrroledione group
1427	1423	1419	1420	–	1405	C=C strech of the alkylthiophene ring
–	–	1378	1381	–	–	rings deformation of the BDT group
1341	1348	–	1342	1352	1359	C-C stretch (alkylthiophene and thienopyrroledione rings)
–	1278	1313	1317	1331	–	Heterocycle Def. + CN stretch
–	1259	1254	1253	1248	1245	C-C inter-ring (inter thiophene)
1200	1202	1190	1195	1227	1201	C-C inter-ring (thiophene-benzene)
1130	1136	1136	1135	1138	1139	C-H def (alkylcarbazole and thiophene ring)

1098	1096	–	1099	1096	1110	Ring deform + CH ip def (thienopyrroledione)
–	–	–	986	996	988	Ring thienopyrroledione def
789	825	–	827	805	–	
748	743	–	–	746	747	ring deform + CH ip def (alkylcarbazole)
560	–	–	550	553	–	
460	462	–	466	460	–	

** Stretch : valence stretching ; bend : angular deformation, i.p : in-plan vibration, oop : out-of-plan vibration ; sym : symetrical vibration ; asym : asymetrical vibration.*

Table 3.5: Experimental and calculated Raman bands for copolymers from P1 to P5. An approximate description was determined from the Potential Energy Distribution (PED) calculations.

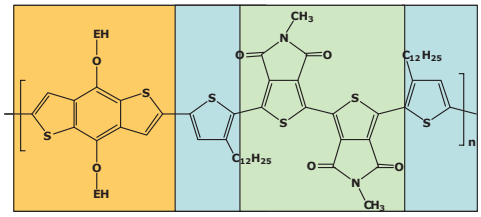

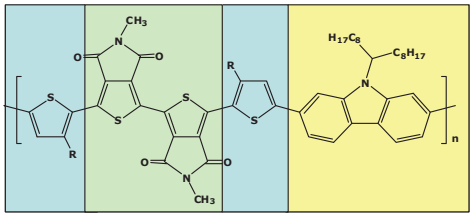

Experimental signals (cm^{-1})					Calc. modes	Assignements*
P1	P2	P3	P4	P5	ν/ cm^{-1}	
–	–	3083	3083	–		C–H stretch (alkylthiophene ring)
3062	–	–	–	3074	3050	C_{aro}–H stretch (alkylcarbazole group)
2957	2957	2957	2957	2957	2955	CH_3 valence stretching (sym.)
2921	2921	2921	2921	2921	2918	CH_2 sym. stretch
2851	2851	2851	2851	2851	2848	CH_2 sym. stretch
1753	1748	1744	1744	1740	1748	C=O asym stretch (thienopyrroledione)
1702	1700	1695	1697	1702	1706	C=O sym stretch (thienopyrroledione)
–	–	1654	1652	–	–	C–C stretch + ring aromatic deformation (BDT group)
1620	1625	–	–	1625	1642	C–C stretch (alkylcarbazole)
1600	1598	–	–	1598	1594	C–C stretch (alkylcarbazole)
–	1540	–	–	1566	1578	C–H ip def + def ring (alkylcarbazole)
–	–	1543	1538	–	–	C–C stretch (BDT ring)
1511	1500	1508	1503	1524	1515	C=C stretch (conjugueted thiophene rings)
1457	1456	1458	1457	1457	–	CH_2 / CH_3 bend

1420	1418	1422	1423	1423	1437	C=C stretch (alkylthiophene)
1372	1372	1367	1367	1372	–	CH_3 deformation
1338	1338	–	–	1338	1323	C–H i.p. def. + def. of ring + N-H def
1250	1253	1257	1257	1249	1245	C-C inter-ring
1191	1194	–	–	1196	1204	N-H i.p. angular deformation
–	–	1167	1166	–	–	C–C stretch +C–H bend
1071	1071	1056	1058	1059	1045	C-H bend
1127	1127	1039	1039	1031	1031	aromatic rings def
993	993	1000	996	998	999	aromatic rings def
845	830	-	-	849	835	C-H o.o.p. bend
797	796	812	814	795	–	
741	740	747	741	751	723	C–S–C deformation
718	720	723	725	724	–	CH_2 rocking

* *Stretch : valence stretching ; bend : angular deformation, i.p : in-plan vibration, oop : out-of-plan vibration ; sym : symetrical vibration ; asym : asymetrical vibration.*

Table 3.6: Experimental and calculated IR bands for copolymers from P1 to P5. An approximate description of the modes (assignments) was determined from the Potential Energy Distribution (PED) calculations.

The experimentally recorded spectra are presented in Figure 3.16. The mode attributed to C=C stretchings in the thiophene ring deserves a special attention. This band is very sensitive to the extent of conjugation and is being shifted to lower wavelengths with increasing conjugation.[33] In **P5** it is located at 1442 cm^{-1}, similar as in **P1** where it is present as a shoulder. For **P2**, **P3** and **P4** it is downshifted to *ca.* 1420 cm^{-1} indicating a better conjugation. This is fully consistent with the UV-*Vis* spectra of these compounds which follow the same trend (compare Figures 3.3 and 3.16).

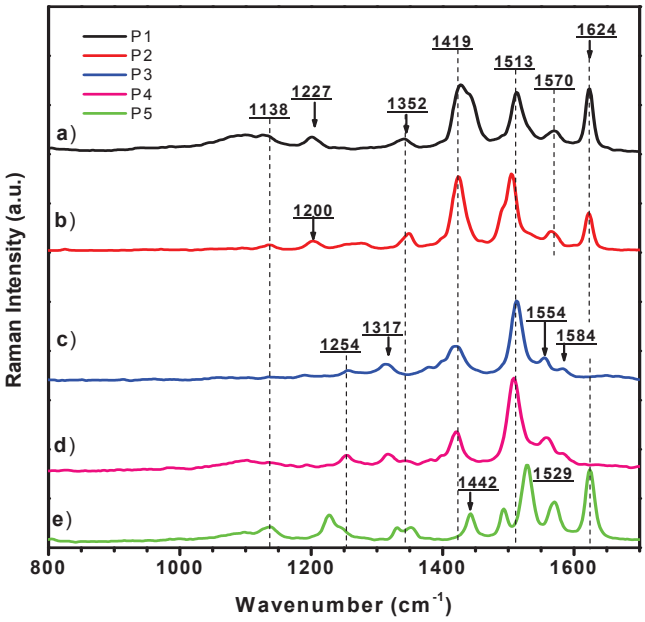

Figure 3.16: Raman spectra of P1, P2, P3, P4 and P5 copolymers (λ_{exc} = 1064 nm).

In the spectral region of 2600 – 3200 cm^{-1} the IR spectra of the polymers studied are dominated by the modes attributed to C-H stretching in aliphatic substituents (see Figure 3.17). A very weak band corresponding to C-H aromatic stretchings is conjugation-dependent and occurs at higher wavenumbers for **P1** and **P5** as compared to the case of **P2**, **P3** and **P4**. This is, again consistent with the trend observed in UV-*Vis* and Raman spectroscopy.

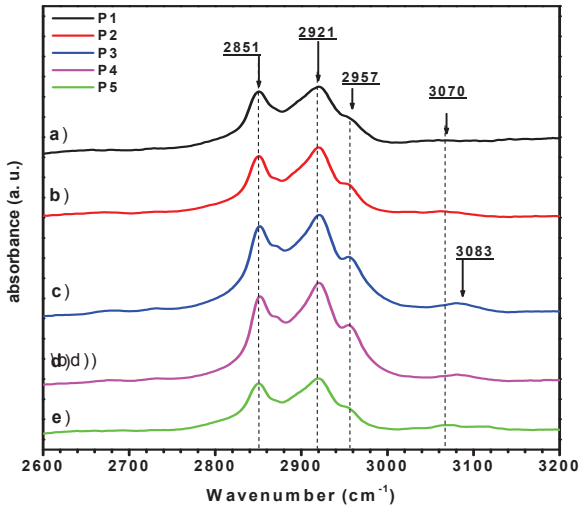

Figure 3.17: Infrared absorption spectra (ATR configuration) of copolymers P1, P2, P3, P4 and P5 recorded at room temperature.

In the range of 600 -1800 cm^{-1} the IR spectra are very rich, which reflects a large variety of IR active modes in the polymers' repeating modes giving rise to IR bands in this region (see Figure 3.18). As already mentioned their exact attribution is given in Table 3.6.

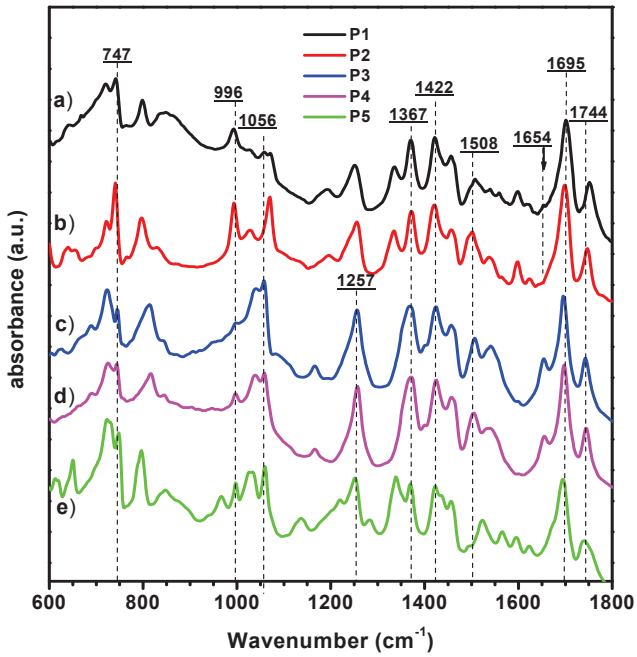

Figure 3.18: Infrared absorption spectra (ATR configuration) of P1, P2, P3, P4 and P5 copolymers recorded at room temperature.

3.6 Supramolecular organization

Taking into account the complexity of their repeating unit and a large variety of lateral substituent of different type **P2**, **P3**, and **P4** show a remarkably ordered structural organization of a similar type. X-ray diffractograms recorded for these four copolymers are displayed Figure 3.19.

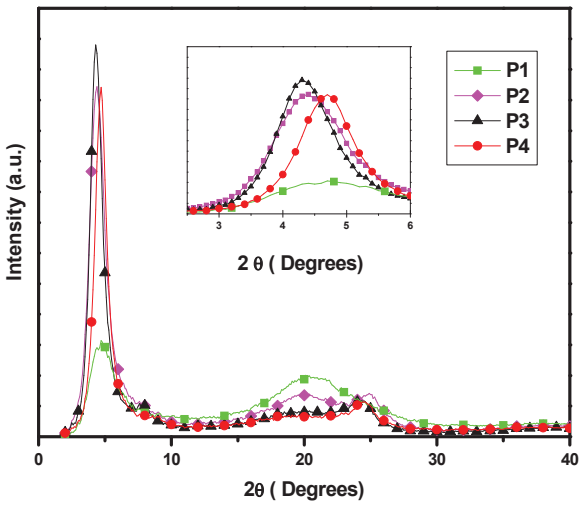

Figure 3.19: X-ray diffraction profiles of P1-P4. The inset shows the maxima of the lowest angle Bragg reflection.

The obtained X-ray patterns strikingly resemble typical diffractograms of poly(alkylthiophene)s with

long *n*-alkyl substituents.[34] For example the diffractogram of **P2** is characterized by a sharp reflection at lower angles (2θ = 4.40°, corresponding to a distance d = 20.06 A). A second less intensive refection can be noticed at 2θ = 24.90° (d = 3.46 A), which is superimposed on a broader halo, peaking at 2θ = 19.95° (d = 4.46 A). The first refection is attributed to a distance between the π-stacks of the polymer chains separated by lateral groups (see scheme presented in Figure 3.20).

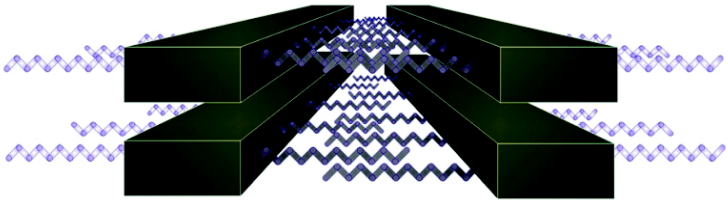

Figure 3.20: Schematic representation of the supramolecular organization of all four copolymers P1-P4.

This distance is imposed by the longest lateral substituent and for this reason is very similar for all polymers studied since all of them are functionalized with the same n-dodecyl side-chains (see inset of Fig. 3.19). It is also shorter than twice the length of the n-dodecyl group. This implies that the lateral alkyl groups are interdigitated. The second refection (d = 3.46 A) corresponds to the interchain distance in the chains π-stacking direction (see Figure. 3.19). The fact that this diffraction peak clearly appears in the diffractogram proves that ordered π-stacks are formed in **P2**, despite certain heterogeneity of its π-conjugated backbone. Finally, the broader halo, whose maximum corresponds to d = 4.45 A, originates from the alkyl interchain correlation distance. **P3** and **P4** exhibit a similar structural organization to **P2**. This strongly indicates that in all three copolymers, the supramolecular structure is governed by two principal effects: π-stacking of the π-conjugated chains and interdigitation of the lateral alkyl groups. **P1** is obviously less ordered as its refection at lower angles arising from the distance between π − π stacks is much less pronounced and no peak corresponding to the interchain distance in the π − π stacking direction is present in its diffractogram.

3.7 Thermogravimetric studies

In view of possible application of the synthesized polymers as components of BHJ in photovoltaic devices, their thermal properties are of crucial importance, for at least two reasons. First, preparation of such devices frequently requires thermal annealing. Second, exposure to high flux of solar radiation may locally heat the BHJ layer.

Thermogravimetric curves of **P1-P4** are presented in Figure 3.21. Comparing **P1** and **P2** (carbazole copolymers) and **P3** and **P4** (benzodithiophene copolymers) it can be concluded that adding of an additional TPD unit and replacing carbazole by dialkoxybenzodithiophene cause a decrease of the degradation temperature (T_d) threshold. The mass loss starts at 430°C for **P1** and at 350°C for **P2**. **P3** and **P4** start to degrade as slightly lower temperature. One should also note a small mass loss of **P1** at temperatures below 100°C, probably associated with desorption of water. These results underline the importance of polymers drying before their use in the fabrication of devices.

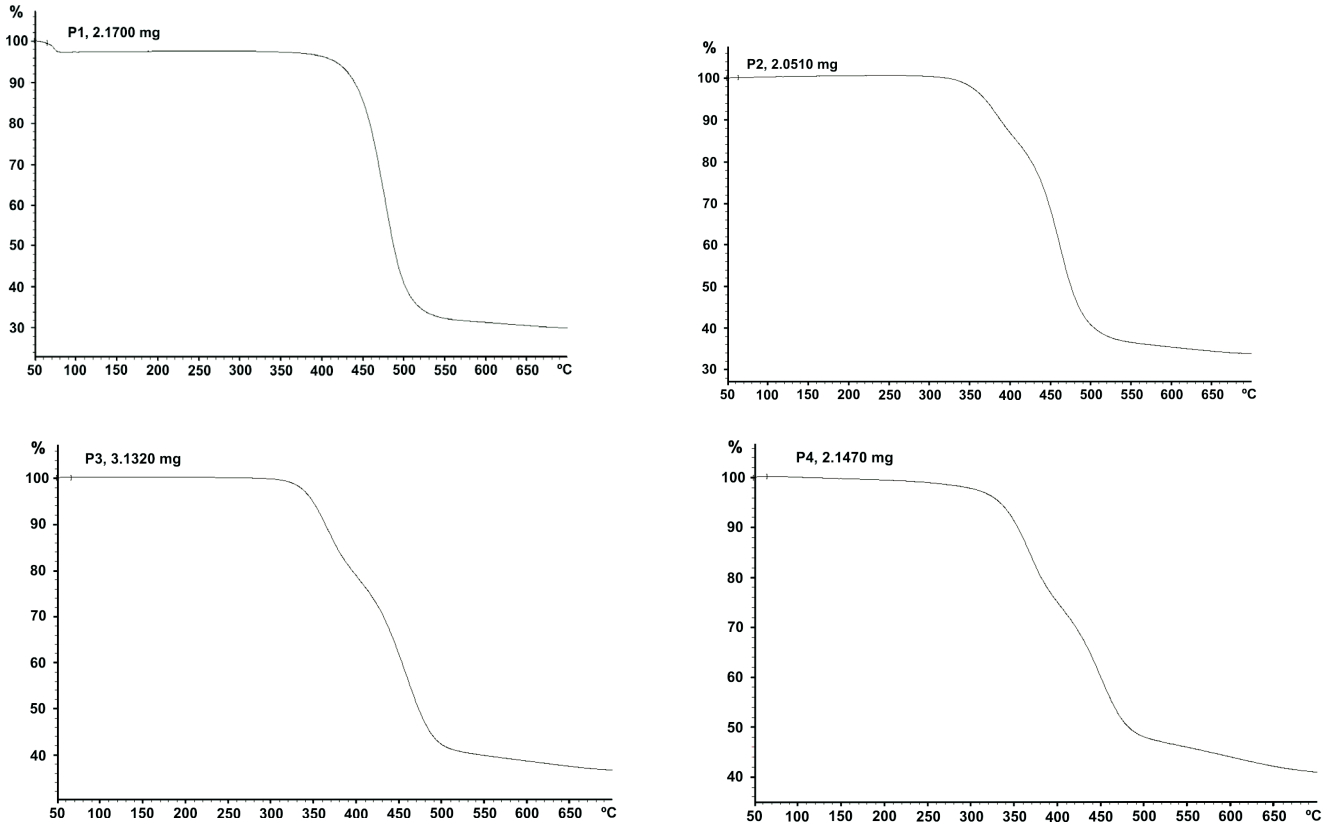

Figure 3.21: Thermogravimetric curves recorded for P1, P2, P3 and P4.

3.8 Polymer fractionation by SEC

Crude conjugated copolymers obtained by Suzuki or Stille couplings usually exhibit a large polydispersity coefficients because, after precipitation in methanol, they still contain oligomeric fractions. These oligomers can be removed by sequential fractionation in a Soxhlet apparatus, however the PDI value, although reduced as compared to crude copolymer, is still significant.

For **P1** and **P3** two fractions were obtained while **P2** and **P4** could not be fractionated in this manner because they were totally soluble in hexane (see Table 3.7 for the macromolecular parameters).

Sample	Fraction	Mn (kDa eq. PS)	Mw (kDa eq. PS)	PDI
P1	n-Hexane	11.9	16.1	1.35
	Chloroform	25.4	32.7	1.29
P2	*n*-Hexane	3.9	5.2	1.33
P3	Chloroform	6.5	9.6	1.48
	o -Dichlorobenzene	3.9	5.2	1.33
P4	*n*-Hexane	3.0	6.4	~ 1.6

Table 3.7: SEC results obtained for carbazole -thienopyrroledione and dialkoxybenzodithiophene-thienopyrroledione copolymers.

For **P1** and **P6** copolymers, detailed studies of the chloroform fraction were carried out. Using analytical size exclusion chromatography (SEC), it was possible to fractionate them into nine sharp fractions showing PDI values ranging from 1.10 down to 1.05 for **P1** and from 1.13 to 1.06 for **P6**. (see Figures 3.22, 3.23 and Tables 3.8 and 3.9).

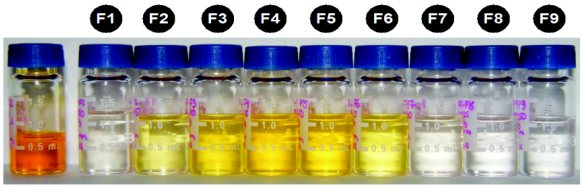

Figure 3.22: Photographic image of $CHCl_3$ solutions of P1 soluble fraction in n-hexane after its initial purifcation by soxhlet extraction vs. its molecular weight-calibrated and low polymolecularity index value's P1/F1-F9 subfractions obtained after 5 consecutive analytical SEC fractionation rings.

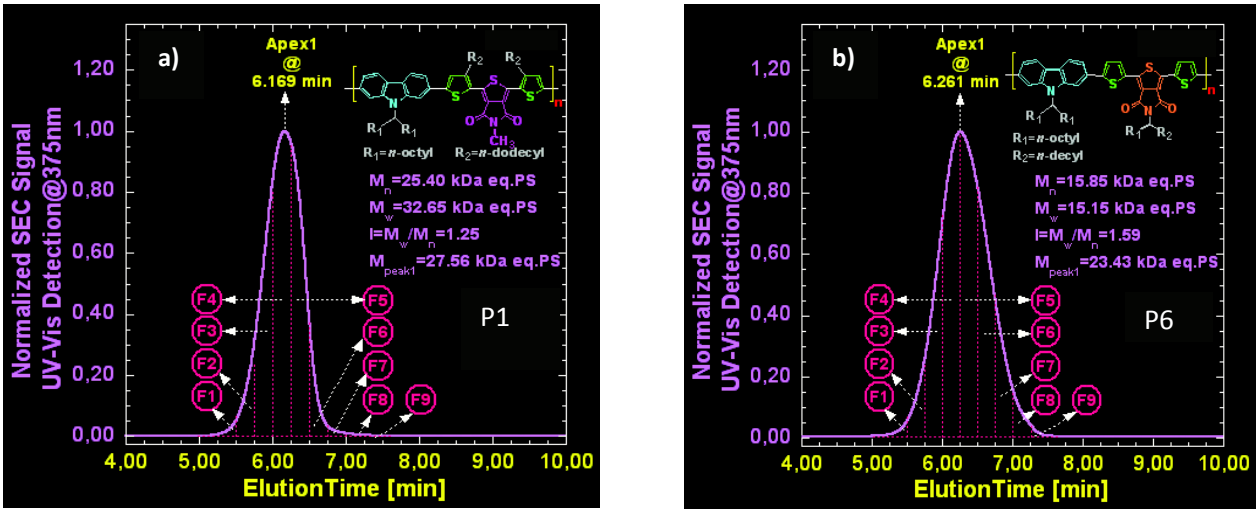

Figure 3.23: SEC elugram, macromolecular parameters M_n, M_w, $I = M_w/M_n$ and M_{peak} (mass at apex of the elugram) and fractionation scheme into its nine P1/F1-F9 fractions (a) and P6/F1-F9 fractions (b) of the soluble fraction in n-hexane of P1 and P6 after their initial purification by soxhlet extraction. Inset: chemical structure of the repeating unit of the D/A low band gap alternating copolymer P1.

P1	M_n (kDa eq. PS)	M_w (kDa eq. PS)	PDI=M_w/M_n
1-Batch	25.4	32.7	~ 1.25
F1	73.1	80.8	~ 1.10
F2	57.7	60.5	~ 1.05
F3	39.8	41.6	~ 1.05
F4	26.9	28.2	~ 1.05
F5	17.8	18.9	~ 1.06
F6	13.2	14.2	~ 1.07
F7	6.91	7.47	~ 1.08
F8	3.75	4.05	~ 1.08
F9	2.17	2.34	~ 1.07

Table 3.8: Fractionation of P1 using analytical size exclusion chromatography.

P6	M_n (kDa eq. PS)	M_w (kDa eq. PS)	PDI=M_w /M_n
1-Batch	15.9	15.2	~ 1.59
F1	122.1	138.0	~ 1.13
F2	75.1	80.4	~ 1.07
F3	48.0	50.9	~ 1.06
F4	31.8	47.7	~ 1.05
F5	20.1	21.3	~ 1.06
F6	12.8	13.7	~ 1.07
F7	7.53	8.13	~ 1.08
F8	4.27	4.57	~ 1.07
F9	2.79	2.96	~ 1.06

Table 3.9: Fractionation of P1 using analytical size exclusion chromatography.

Solution UV-*Vis* spectra of these fractions show an interesting behavior. For the low molecular fractions (from F9 to F5), the maximum of the $\pi - \pi^*$ transition band is being gradually bathochromically shifted from 436 nm to 444 nm for **P1** and from 465 to 478 nm for **P6**. For F4 and fractions of higher mass (F3-F1), its position saturates. The apparent degree of polymerization (DP_n) in F4 is 18 which corresponds to ca. 90 aromatic rings in the polymer backbone. In the case of P6, the DP_n is about 31 and it corresponds to 200 rings. It must be however noted that the use of polystyrene standards leads to an overestimation of the mass of π-conjugated polymers as it is known, for example, from the comparison of the MALDI-TOF and SEC results obtained for regioregular head-to-tail, coupled (HT-HT) poly(3-hexylthiophene-2,5-diyl).[35] It is therefore highly probable that the SEC determined DP_n values for P1, P6 and their fractions are overestimated. Although the reported degrees of polymerization are apparent, the fractionation of the polymer into fractions of very low PDI values enabled us to precisely determine the saturation of the conjugation length, as evidenced by the saturation of the $\pi - \pi^*$ band position. If fractions of higher polydispersity index value are used, for example as in the case of already mentioned regioregular HT-HT poly(3-hexylthiophene-2,5-diyl), no saturation of the λ_{max} position of the $\pi - \pi^*$ band is observed even for samples of very high M_n values. This is due to the presence of low molecular mass fractions in these samples, whose contribution diminishes with increasing molecular mass, but never becomes negligible.

3.9 Conclusion

Detailed physico-chemical studies using complementary spectroscopic, electrochemical, diffraction and thermal techniques enabled us to precisely determine these properties of the synthesized push-pull copolymers which are crucial for their application in photovoltaics.

Electrochemical and spectroelectrochemical investigations clearly showed that the redox properties of all synthesized polymers make them suitable candidates for applications as donor components of the BHJ layers with PCBM as the acceptor component. The positions of the HOMO and LUMO levels derived from these studies turned out to be in a very good agreement with the ones obtained by DFT calculations. Moreover the developed vibrational model enabled us to precisely attribute all Raman and IR modes of the synthesized polymers. Although all synthesized polymers show appropriate redox properties for BHJ applications **P2**, **P3** and **P4** seem superior in this respect because of better matching of their UV-*Vis*-NIR spectra with solar spectrum.

[1] N. Berton, C. Ottone, V. Labet, R. De Bettignies, S. Bailly, A. Grand, C. Morell, S. Sadki, and F. Chandezon, "New Alternating Copolymers of 3,6-Carbazoles and Dithienylbenzothiadiazoles: Synthesis, Characterization, and Application in Photovoltaics," *Macromolecular Chemistry and Physics*, vol. 212, pp. 2127–2141, 2010.

[2] H. Zhou, L. Yang, S. Xiao, S. Liu, and W. You, "Donor−Acceptor Polymers Incorporating Alkylated Dithienylbenzothiadiazole for Bulk Heterojunction Solar Cells: Pronounced Effect of Positioning Alkyl Chains," *Macromolecules*, vol. 43, no. 2, pp. 811–820, 2010.

[3] M. Trznadel, A. Pron, M. Zagorska, R. Chrzaszcz, and J. Pielichowski, "Effect of Molecular Weight on Spectroscopic and Spectroelectrochemical Properties of Regioregular Poly(3-hexylthiophene)," *Macromolecules*, vol. 31, no. 15, pp. 5051–8, 1998.

[4] W R Salaneck, "Photoelectron spectroscopy of polyconjugated polymer surfaces and interfaces," *Reports on Progress in Physics*, vol. 54, p. 1215, 1991.

[5] J. Hwang, E. G. Kim, J. Liu, J. L. Bredas, A. Duggal, and A. Kahn, "Photoelectron Spectroscopic Study of the Electronic Band Structure of Polyfluorene and Fluorene-Arylamine Copolymers at Interfaces," *Journal of Physical Chemistry B*, vol. 111, no. 3, pp. 1378–1384, 2007.

[6] M.P. de Jong, J. Greczynski, W. Osikowicz, R. Friedlein, X. Crispin, M. Fahlman, and W.R.Salaneck, "Photoelectron Spectroscopy of Conjugated Polymers," in *Conjugated Polymers*, Third Edition, T. A. Skotheim and J. Reynolds, Eds. Gainesville, Florida: CRC Press, 2006.

[7] S. Trasatti, "The absolute electrode potential: an explanatory note (IUPAC Recommendations 1986)," *Pure Applied Chemistry*, vol. 58, pp. 955–966, 1986.

[8] C. Cardona, W. Li, A. E. Kaifer, D. Stockdale, and G. C. Bazan, "Electrochemical considerations for determining absolute frontier orbital energy levels of conjugated polymers for solar cell applications," *Advanced Materials*, vol. 23, no. 20, pp. 2367–2371, 2011.

[9] B. Krische and M. Zagorska, "Overoxidation in conducting polymers," *Synthetic Metals*, vol. 28, no. 1–2, pp. 257–263, 1989.

[10] G. Li, V. Shrotriya, J. Huang, Y. Yao, T. Moriarty, K. Emery, and Y. Yang, "High-efficiency solution processable polymer photovoltaic cells by self-organization of polymer blends," *Nature Materials*, vol. 4, no. 11, pp. 864–868, 2005.

[11] W. Ma, C. Yang, X. Gong, K. Lee, and A. J. Heeger, "Thermally Stable, Efficient Polymer Solar Cells with Nanoscale Control of the Interpenetrating Network Morphology," *Advanced Functional Materials*, vol. 15, no. 10, pp. 1617–1622, 2005.

[12] J. Y. Kim, K. Lee, N. E. Coates, D. Moses, T.-Q. Nguyen, M. Dante, and A. J. Heeger, "Efficient tandem polymer solar cells fabricated by all-solution processing," *Science (New York, N.Y.)*, vol. 317, no. 5835, pp. 222–5, Jul. 2007.

[13] N. Blouin, A. Michaud, and M. Leclerc, "A Low-Bandgap Poly(2,7-Carbazole) Derivative for Use in High-Performance Solar Cells," *Advanced Materials*, vol. 19, no. 17, pp. 2295–2300, 2007.

[14] M. T. Guo X, Ortiz RP, Zheng Y, Kim MG, Zhang S, Hu Y, Lu G, Facchetti A, "Thieno[3,4-c]pyrrole-4,6-dione-based polymer semiconductors: toward high-performance, air-stable organic thin-film transistors," *Journal of American Chemical Society*, vol. 133, no. 34, pp. 13685–97, 2011.

[15] Y. Zou, A. Najari, P. Berrouard, and S. Beaupre, "A Thieno [3 , 4-c] pyrrole-4 , 6-dione-Based Copolymer for Efficient Solar Cells," *Journal of the American Chemical Society*, vol. 132, no. 15, pp. 5330–5331, 2010.

[16] Y. Kim, S. Cook, S. M. Tuladhar, S. A. Choulis, J. Nelson, J. R. Durrant, D. D. C. Bradley, M. Giles, I. McCulloch, C.-S. Ha, and M. Ree, "A strong regioregularity effect in self-organizing conjugated polymer films and high-efficiency polythiophene:fullerene solar cells," *Nature Materials*, vol. 5, no. 3, pp. 197–203, 2006.

[17] M. Tsionsky, A. J. Bard, D. Dini, F. Decker, and D. Chimica, "Polymer Films on Electrodes . 28 . Scanning Electrochemical Microscopy Study of Electron Transfer at Poly (alkylterthiophene) Films," *Society*, vol. 2, no. 5, pp. 2120–2126, 1998.

[18] D. Aldakov, T. Jiu, M. Zagorska, R. De Bettignies, P.-H. Jouneau, A. Pron, and F. Chandezon, "Hybrid nanocomposites of CdSe nanocrystals distributed in complexing thiophene-based copolymers," *Physical Chemistry Chemical Physics*, vol. 12, no. 27, pp. 7497–7505, 2010.

[19] N. Blouin, A. Michaud, D. Gendron, S. Wakim, E. Blair, R. Neagu-Plesu, M. Belletête, G. Durocher, Y. Tao, and M. Leclerc, "Toward a rational design of poly(2,7-carbazole) derivatives for solar cells," *Journal of the American Chemical Society*, vol. 130, no. 2, pp. 732–742, 2008.

[20] R. Qin, W. Li, C. Li, C. Du, C. Veit, H. -f. Schleiermacher, M. Andersson, Z. Bo, Z. Liu, O. Inganas, U. Wuerfel, and F. Zhang, "A Planar Copolymer for High Efficiency Polymer Solar Cells," *Journal of the American Chemical Society*, vol. 131, no. 41, pp. 14612–14613, 2009.

[21] S. Wakim, S. Beaupré, N. Blouin, B.-R. Aich, S. Rodman, R. Gaudiana, Y. Tao, and M. Leclerc, "Highly efficient organic solar cells based on a poly(2,7-carbazole) derivative," *Journal of Materials Chemistry*, vol. 19, no. 30, p. 5351, 2009.

[22] N. Leclerc, A. Michaud, K. Sirois, J. F. Morin, and M. Leclerc, "Synthesis of 2,7-Carbazolenevinylene-Based Copolymers and Characterization of Their Photovoltaic Properties," *Advanced Functional Materials*, vol. 16, p. 1694, 2006.

[23] W. Kohn and L. J. Sham, "Self-Consistent Equations Including Exchange and Correlation Effects," *Physical Review*, vol. 140, no. 4A, pp. A1133–A1138, 1965.

[24] K. Raghavachari, "Perspective on 'Density functional thermochemistry. III. The role of exact exchange'," *Theoretical Chemistry Accounts Theory Computation and Modeling Theoretica Chimica Acta*, vol. 103, no. 3–4, pp. 361–363, 2000.

[25] C. Lee, W. Yang, and R. Parr, "Development of the Colle-Salvetti correlation-energy formula into a functional of the electron density," *Physical Review B*, vol. 37, no. 2, pp. 785–789, 1988.

[26] M. M. Francl, W. J. Pietro, W. J. Hehre, J. S. Binkley, M. S. Gordon, D. J. DeFrees, and J. A. Pople, "Self-consistent molecular orbital methods. XXIII. A polarization-type basis set for second-row elements," *The Journal of Chemical Physics*, vol. 77, no. 7, pp. 3654–3665, 1982.

[27] W. J. Hehre, R. Ditchfield, and J. A. Pople, "Self—Consistent Molecular Orbital Methods. XII. Further Extensions of Gaussian—Type Basis Sets for Use in Molecular Orbital Studies of Organic Molecules," *The Journal of Chemical Physics*, vol. 56, no. 5, p. 2257, 1972.

[28] M. J. Frisch, G. Trucks, S. Scuseria, G. E. Robb, M. A. Cheeseman, J. R.Montgomery, Jr. M.Vreven, T. Kudin, K. Burant, S. Iyengar, J. Tomasi, V, Barone, B. Menucci, M. Cossi, G. Scalmani, N. Rega, G. A. Petersson, H. Nakatsuji, M. Hada, M. Ehara, K. Toyota, R., Fukuda, J. Hasegawa, M. Ishida, T. Nakajima, Y. Honda, O. Kitao, H. Nakai, M. Klene, X. Li, J. E. Knox, H. P. Hratchian, J. B. Cross, V. Bakken, C. Adamo, J. Jaramillo, R. Gomperts, R. E. Stratmann, O.Yazyev, J. Austin, R. Cammi, C. Pomelli, J. W. Ochterski, P. Y. Ayala, K. Morokuma, G. A. Voth, P. Salvador, J. J. Dannenberg, V. G. Zakrzewski, S. Dapprich, A.D. Daniels, M. C. Strain, O. Farkas, D. K. Malick, A. D. Rabuck, K. Raghavachari, J. B., Foresman, J. V. Ortiz, Q. Cui, A. G. Baboul, S. Clifford, J. Cioslowski, B. B. Stefanov, G. Liu, A. Liashenko, P. Piskorz, I. Komaromi, R. L. Martin, D. J. Fox, T. Keith, M. A. Al-Laham, C.Y. Peng, A. Nanayakkara, M. Challacombe, P. M. W. Gill, B. Johnson, W. Chen ,M. W. Wong, C.Gonzalez, J. A. Pople, "Gaussian 03, Revision C.02 2004, Gaussian, Inc., Wallingford CT," *ReVision*, p. 2004, 2004.

[29] T. Johansson, W. Mammo, M. Svensson, R. Andersson, and O. Ingana, "Electrochemical bandgaps of substituted polythiophenes," *Journal of Materials Chemistry*, vol. 13, no. 6, p. 1316, 2003.

[30] D. Dini, F. Decker, G. Zotti, G. Schiavon, S. Zecchin, F. Andreani, and E. Salatelli, "A comparative study of isomeric polydialkylterthiophenes with regular regiochemistry of substitution. Electrochemical synthesis," *9th European Conference on eGovernment*, vol. 41, no. 12, pp. 3484–3489, 2000.

[31] R. Anandhi and S. Umapathy, "Resonance Raman spectroscopic studies on the Conducting State of Polyvinylcarbazole and its Model Compounds," *Journal of Raman Spectroscopy*, vol. 29, no. 4, pp. 901–906, 1998.

[32] Z. X. Li, Y. C. Huang, L. B. Mo, and Y. J. Pei, "A study of poly(N-vinylcarbazole) adsorbed on silver surface by SERS," *Vibrational Spectroscopy* , vol. 21, pp. 39–43, 1999.

[33] H. E. Schaffer, R. R. Chance, R. J. Silbey, K. Knoll, and R. R. Schrock, "Conjugation length dependence of Raman scattering in a series of linear polyenes: Implications for polyacetylene," *The Journal of Chemical Physics*, vol. 94, no. 6, pp. 4161–4170, 1991.

[34] A. Pron, P. Gawrys, M. Zagorska, D. Djurado, and R. Demadrille, "Electroactive materials for organic electronics: preparation strategies, structural aspects and characterization techniques," *Chemical Society Reviews*, vol. 39, no. 7, pp. 20009–29, 2010.

[35] J. Liu, R. S. Loewe, and R. D. Mccullough, "Employing MALDI-MS on Poly(alkylthiophenes): Analysis of Molecular Weights, Molecular Weight Distributions, End-Group Structures, and End-Group Modifications," *Macromolecules*, vol. 32, no. 18, pp. 5777–5785, 1999.

Chapter 4

Intra- and inter- molecular charge transfer in conjugated polymers and their composites with fullerenes or semiconductor nanocrystals - Electron Paramagnetic Resonance (EPR) studies and DFT Calculations

4.1 EPR investigations

4.1.1 Introduction

EPR spectroscopy is a precious tool to study mechanisms of reactions and processes involving formation and disappearance of free radicals. For this reason in the present research, we have used this technique to observe both intramolecular (so called '*push-pull*') electron transfers in the polymer matrix as well as intermolecular electron transfers in composites of conjugated polymers and nanocrystals or fullerene derivatives.

4.1.1.1 Generalities and aim of the study

The principal difference between an inorganic and organic semiconductor is the extent of the excited states localization. Excitons, in silicon crystals, are characterized by a lower binding energy that allows charge separation at room temperature. To the contrary, in organic low and high molecular weight semiconductors, which show low dielectric permittivity, the dissociation of excitons becomes difficult, since their Coulomb binding energy is high compared to k_BT.[1–4] As a result, in photovoltaic cells based on organic semiconductors, recombination processes may occur, lowering the device performance. Considering the field of organic photovoltaics nanoscale mixing of an electron acceptor material with an electron donor one could solve this problem by promoting charge transfer *via* different mechanisms. Finally, as already mentioned in the *Chapter 1 paragraph 1.6* the active layer should form a percolation path to well connect the bulk to electrodes. Considering the bulk-heterojunction concept, excitons, formed on polymer chain (D, donor), could cover the acceptor (A, acceptor) globe, forming a more extended exciton in the bulk.[5]

$$D^* + A \rightarrow (D-A)^*$$

Due to the structural relaxation$(D-A)^* \rightarrow \left(D^{\delta+} - A^{\delta-}\right)^*$, donor-acceptor complexes collapse into radical pairs$\left(D^{\delta+} - A^{\delta-}\right)^* \rightarrow (D^{+\cdot} - A^{-\cdot})$, after charge transfer initiation. For the high hole mobility, radical pairs are easily separated into two independent charge carriers.[6], [7]

$$(D^{+\cdot} - A^{-\cdot}) \rightarrow D^{+\cdot} - A^{-\cdot}$$

The donor and acceptor system could relax back to the ground state releasing energy to the lattice as heat or as emitted light. Because of the fact that in organic solar cell, fullerene radical anion is also characterized by a spin $S = {}^1/_2$ and it pseudorotates between polymer chains, many relaxation and dynamic properties could be identified by using a direct light-induced electron paramagnetic resonance spectroscopy (EPR). As excitons dissociate into radicals ions, polarons move from the fullerene anions to the conjugated backbone faster than 10^{-9} s. Polarons mobility is lower than the free electrons mobility and it is the reason why spins, in radical pairs, can be considered as non-interacting, showing as a consequence separate EPR spectra.

The aim of this EPR study was to understand molecular and intramolecular "donor –acceptor interactions" to predict the relationship between the molecular structure and the charge transfer mechanisms affecting photovoltaic devices performances. The described studies were focused on the most promising polymers of the synthesized series in which intramolecular "donor-acceptor" interactions occur as a consequence of their chemical constitution. The EPR investigations were carried out in close collaboration with the Dr. Brigitte Pepin Donat and Christian Lombard. Aurélie Lefrançois was also closely involved, providing semiconductor nanocrystals, suitable for the fabrication of composites with electroactive polymers.

Finally, the density functional theory calculations of the electronic density of the radical cation (final state after the charge transfer process) are presented, which constitute a theoretical support of the EPR results. Calculations were carried in collaboration with Doctor C. Morell and Professor A. Grand au CEA/INAC/SCIB.

4.1.2 EPR theory

Electron Paramagnetic Resonance (EPR) [8–12] is a spectroscopic technique, similar to the Nuclear Magnetic Resonance (NMR) better known in the organic chemistry field, applied to electron spins instead of nucleus spins. EPR allows studying systems containing at least one unpaired electron (paramagnetic systems). During an EPR experiment, the investigated paramagnetic sample is subjected to an external magnetic field H that varies linearly upon time during recording. The interaction with *H*, called the electronic Zeeman interaction for a free radical species with a single unpaired electron, results in the generation of two separated energy levels that are otherwise (i.e with no magnetic field) degenerated. The separation between the two Zeeman levels matches the *hν* quantum energy, where ν is the fixed frequency of an electromagnetic radiation deriving from the applied magnetic field. This is the resonance phenomenon characterized by the relationship $h\nu = g\,\beta_e H_0$ where h is the Planck's constant, β_e, the Bohr magneton and H_0, the magnitude of the magnetic field H at the resonance. The Landé g-factor is specific to the investigated free radical species and is determined from the independent measurements of $h\nu$ and H_0. For our polymers g –factors are close to the Landé g_e-factor of the free electron (g_e = 2.0023) and typically lie between 2.0023 and 2.005. For

PCBM the *g-factor* value is close to 1.9999. Nanocrystals used in this study are blind. EPR allows probing 3D structure, dynamics and reactivity of organic systems by observing their effect on the EPR parameters of free radicals trapped on them. EPR spectrum of free radicals trapped on complex organic systems generally consists of a single first derivative absorption line (recording the derivative of the absorption line is simply a consequence of the technique used for signal detection) characterized by its g-Landé factor (g), its line shape (Lorentzian (100%L) or Gaussian (0%L) or a linear combination of both with the same g- factor (%L)) and its peak-to-trough line peak width ΔH_{pp} (expressed in Gauss)). In this work we apply the concept of EPR tracing recently developed in our laboratory. [13] It consists of ascribing an EPR fingerprint to each sample. This fingerprint is simply formed by the set of lines necessary to simulate the EPR spectrum. These fingerprints are used to follow the fate of substructures, present in a sample, as a function of various parameters without relaying to their absolute structure. In our case since the studied structures are relatively simple, we will try, by comparing the data from various studies, to ascribe most of the lines to specific structures.

4.1.3 Materials and films preparation

A comparative EPR study was carried out for **P1, P2** and **P3** (Figure 4.1 reminds their chemical structures already shown in *Chapter 2*). In the case of **P1** and **P3**, we studied neat polymer and its blends with PCBM or $CuInS_2$ nanocrystals, while for P2 only neat polymer and its blend with PCBM were studied.

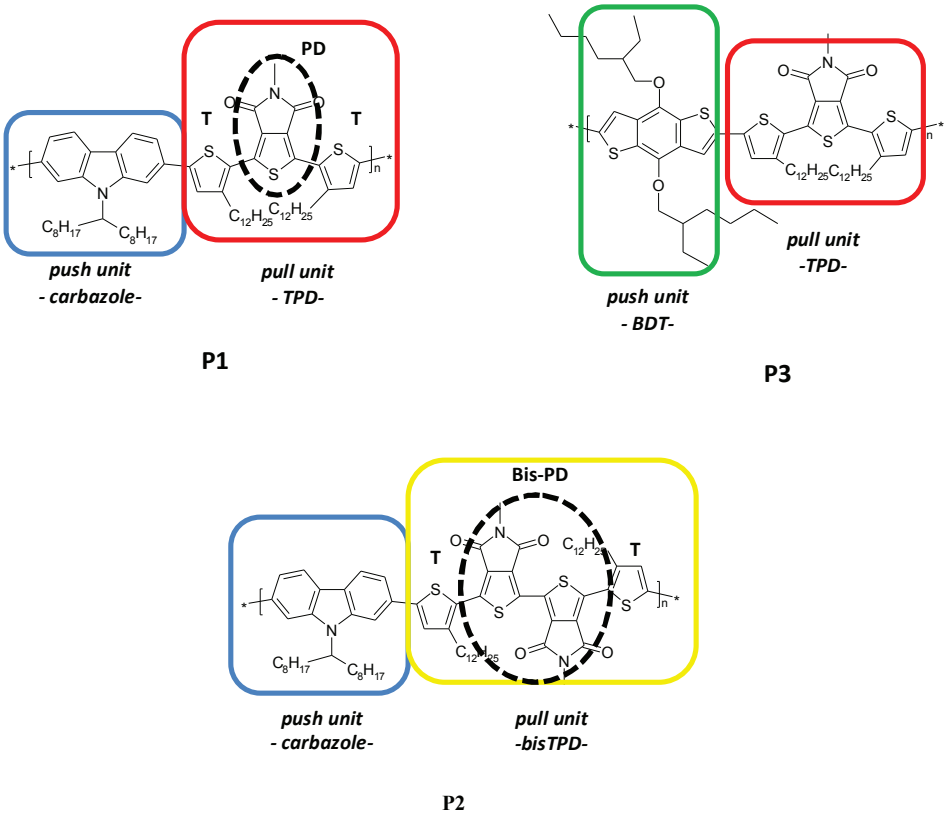

Figure 4.1: Structures of studied polymers (respresented following the order of study.)

The procedure for sample preparation was as follows: i) films of neat **P1** and **P3** polymers were cast from

their solutions in *o*-dichlorobenzene (ODCB) (5 mg/mL); ii) blends of **P1** and **P3** with PCBM were prepared by solution processing from the same solutions to which PCBM was added in the **P1** (or **P3)**/ PCBM ratio (1:3) ; iii) in the analogous way blends of **P1** and **P3** with $CuInS_2$ nanocrystals were prepared with the **P1** (or **P3**)/nanocrystals ratio (1:3); iv) blends of **P2** with PCBM ratio (1:3) were also prepared by solution processing from ODCB. Blends in a form of films were obtained by drop casting on a flexible substrate of PET/ITO. They were finally annealed at 110°C for 3 hours and introduced, once cut, to the EPR tube.

4.1.4 EPR analysis

Analyses were made in a specific order to evaluate the behavior of neat polymers and of polymers blended with two types of electron acceptor materials: PCBM and $CuInS_2$ nanocrystals. To obtain a clearly detectable fullerene signal, spectra were registered at 20 K.[14] Concerning the microwave power and the number of scan acquisitions, if it is not otherwise specified, EPR signals were acquired at 10 dB and 1 NA.

The experimental sequence aimed at detecting the molecular response of the sample, started from a preliminary scan without light to observe the neutral state of the materials. Subsequently samples were illuminated with a laser light at $\lambda = 473$ nm to register the eventual signal related to the formation of a radical and, as a consequence, to follow the charge transfer through the *push-pull* copolymer or between the polymer and PCBM or $CuInS_2$ nanocrystals. The final scan was registered in the dark without light at 20K to observe the relaxation of the process and to observe the eventual residual EPR fingerprint due to the laser enlightening. The spectra are simulated as a sum of 'pure' lines by a simulation software developed in our laboratory by C. Lombard and B. Pépin-Donat. Each 'pure' line ('either Lorentzian or Gaussian or both *g*-centered) is characterized by its *g*-factor, its peak-to-peak linewidth H_{pp} and its lineshape (here, the lineshapes are all 100% Lorentzian) (see Figure 4.2). In this work, since interpretation of EPR data was made by a return study (a kind of masterwmind!) and the sample were not systematically observed in a "logical" order, lines are not ascribed to specific structures according to their numbering (for example, line 13 is the first one to be determined).

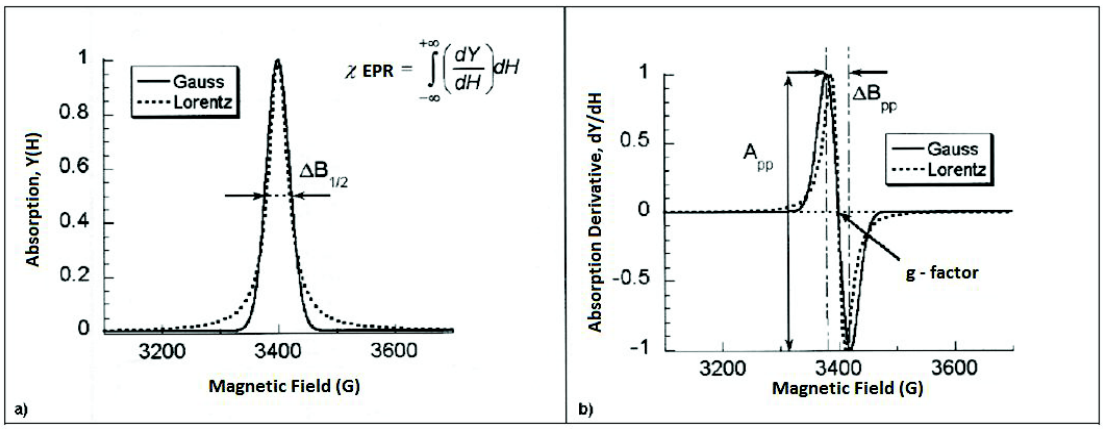

Figure 4.2: EPR spectra and measured parameters.

4.1.5 Experimental results, lines attribution

4.1.5.1 Case of neat P1

In initial experiments neat polymers were considered as reference materials. Spectral response of **P1**, was recorded at room temperature (RT), in the dark and, then, under illumination (λ = 473 nm). It was not possible to detect a clear effect of the light by simply looking at the spectrum (See Figure 4.3).

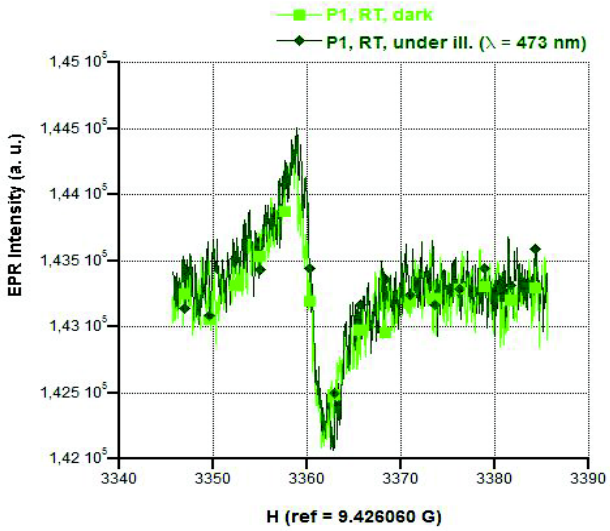

Figure 4.3: EPR spectra of P1 registerd at RT in the dark and under illumination (λ = 473 nm).

At 20 K a clear effect of the light was directly observed in the EPR spectrum, but it could originate from a possible residual EPR fingerprint, created during the sample illumination at RT (see Figure 4.4).

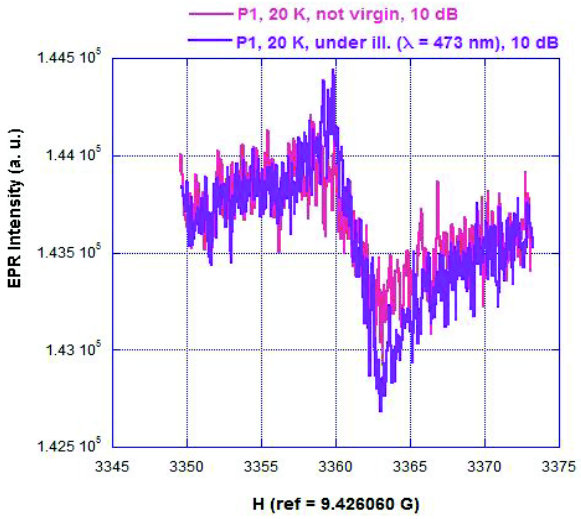

Figure 4.4: EPR spectra of P1 under illumination (λ = 473 nm) at RT and at 20 K.

Nevertheless, by simulating these two spectra obtained at RT without and under illumination (λ = 473 nm) we could observe a small but clear effect of the illumination:

- ***in the case of neat P1 at RT, without illumination***, the spectrum was simulated with only one *line 13* of *g*-factor = 2.00361037 and H_{pp} = 3.443 G (100% Lorentzian) (see Fig. 4.5 and Table 4.1), while

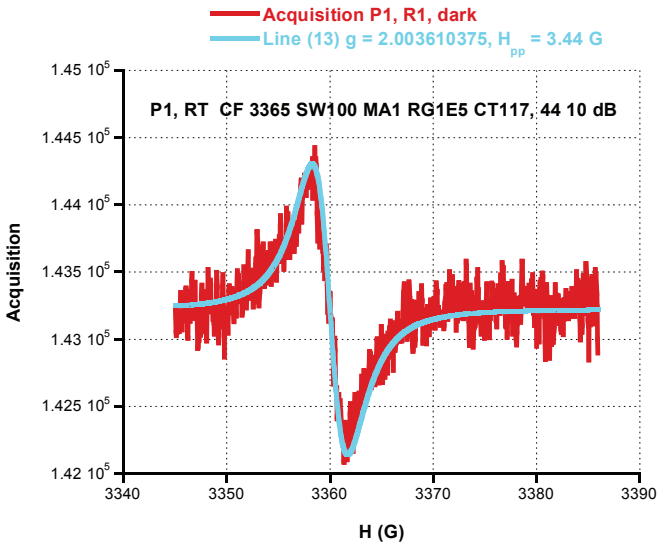

Figure 4.5: EPR spectrum of P1 acquired at RT in the dark, together with its simulation.

	H_{pp} (G)	*g*-factor	% intensity	Structure at the origin of the line
Line 1	1.161	2.00344941	0.00000	
Line 2	1.041	2.00294285	0.00000	
Line 3	1281	2.0024961	0.00000	
Line 4	1.01	2.00207931	0.00000	
Line 5	3.523	2.00279391	0.00000	
Line 6	0.801	2.00012866	0.00000	
Line 7	1.481	2.00012866	0.00000	
Line 8	2.162	1.99992074	0.00000	
Line 9	1.401	2.00175195	0.00000	
Line 10	40.92	1.98916957	0.00000	
Line 11	3.44	2.00277218	0.00000	
Line 12	5.25	2.00465073	0.00000	
Line 13	**3.443**	**2.00361037**	**100.00000**	**Intrinsic default of P1**

Table 4.1: EPR parameters of neat P1, annealed at 110°C. EPR experiments carried out at RT, in the dark.

- ***in the case of neat P1 at RT under illumination*** (λ = 473 nm), the simulation reveals the presence of

three supplementary lines: *line 1* of g = 2.003449414, H_{PP} = 1.66 G; *line 3* of g = 2.002496099, H_{PP} = 1.281 G and *line 4* of g = 2.00207931, H_{PP} = 1.01 G, in addition to *line 13* of g-factor = 2.00361037, H_{PP} = 3.443 G (100% Lorentzian), detected in **P1** without illumination (see Figure 4.6 and Table 4.2).

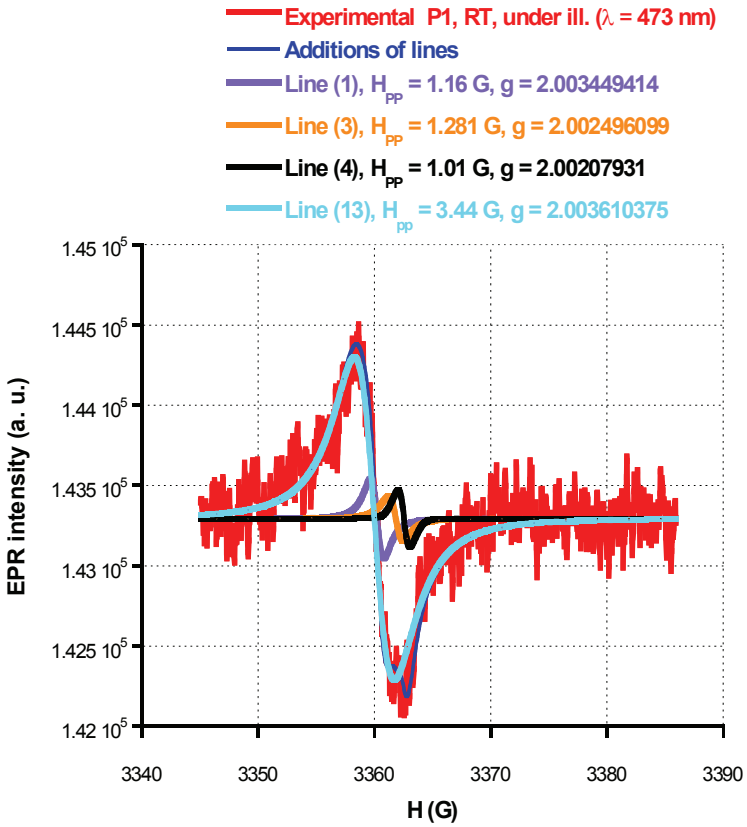

Figure 4.6: EPR spectrum of neat P1 registered at RT under illumination (λ = 473 nm), together with its simulation.

	H_{pp} (G)	*g*-factor	% intensity	Structure at the origin of the line
Line 1	**1.161**	**2.00344941**	**2.64551**	**Paramagnetic species of P1 induced by illumination at 473 nm**
Line 2	1.041	2.00294285	0.00000	
Line 3	**1281**	**2.0024961**	**1.76423**	**Paramagnetic species of P1 induced by illumination at 473 nm**
Line 4	**1.01**	**2.00207931**	**0.83919**	**Not attributed (n.a.)**
Line 5	3.523	2.00279391	0.00000	
Line 6	0.801	2.00012866	0.00000	
Line 7	1.481	2.00012866	0.00000	
Line 8	2.162	1.99992074	0.00000	
Line 9	1.401	2.00175195	0.00000	
Line 10	40.92	1.98916957	0.00000	
Line 11	3.44	2.00277218	0.00000	
Line 12	5.25	2.00465073	0.00000	
Line 13	**3.443**	**2.00361037**	**94.71366**	**Intrinsic default of P1**

Table 4.2: EPR parameters of neat P1 annealed at 110°C. EPR experiment carried out at RT, under illumination (λ = 473 nm).

At this point of the research it was not worthwhile to interpret and attribute each line to specific species before simulating other spectra which brought more information.

Nevertheless, an important point is that we were able to observe the EPR fingerprint of the *push-pull* process, which had occurred during the illumination, despite the very short lifetime of the resulting free radical species. This fingerprint likely result from the trapping of some of free radical species on the polymer backbone during the process.[13]

4.1.6 P1/PCBM (1:3) blend

At RT and at 20 K, in the dark, the studied blend gives rise to a small EPR signal of similar shape. Figure 4.7 shows a representative spectrum registered at RT. This signal can easily be simulated with only one line (*line 4*) which exists also in neat **P1**. This *line 4* is likely not due to the polymer **P1** because of its low *g*-factor ($g < g_{\text{free electron}}$). Surprisingly, *line 13* is not present and the signal is of lower intensity than the intrinsic signal (*line 13*) in neat **P1** (compare Figures 4.5 and 4.7). It is possible that the lack of *line 13* is due to the lower quantity of **P1** in the P1/PCBM (1:3) blend.

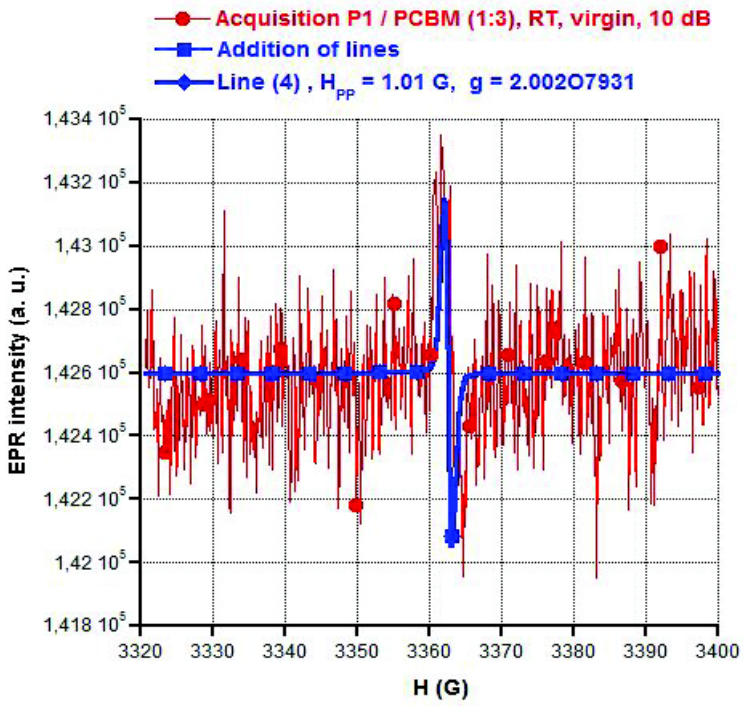

Figure 4.7: EPR spectra of P1/PCBM (1:3) blend registered at RT in the dark, together with its simulation.

	H_{pp} (G)	*g*-factor	% intensity	Structure at the origin of the line
Line 1	1.161	2.00344941	0.00000	
Line 2	1.041	2.00294285	0.00000	
Line 3	1281	2.0024961	0.00000	
Line 4	**1.01**	**2.00207931**	**0.83919**	**n.a.**
Line 5	3.523	2.00279391	0.00000	
Line 6	0.801	2.00012866	0.00000	
Line 7	1.481	2.00012866	0.00000	
Line 8	2.162	1.99992074	0.00000	
Line 9	1.401	2.00175195	0.00000	
Line 10	40.92	1.98916957	0.00000	
Line 11	3.44	2.00277218	0.00000	
Line 12	5.25	2.00465073	0.00000	
Line 13	3.443	2.00361037	0.00000	

*Table 4.3: EPR parameters of **P1/PCBM** (1:3) blend, annealed at 110°C. EPR experiment carried out at RT conditions in the dark.*

Upon illumination of the P1/PCBM (1:3) blend at 20 K with the laser radiation of λ = 473 nm, one line of low *g*- factor (located at higher magnetic field, than the line observed without illumination), clearly appears.

We interpret it in terms of a charge transfer between the polymer (electron donor) and PCBM (electron acceptor). Consequently, the *line 8* is ascribed to the fullerene; its EPR parameters (*g*-factor of 1.999920737 and H_{PP} of 1.401 G) are in full agreement with those reported in the literature [9] for the PCBM radical anion. (see Figure 4.8).

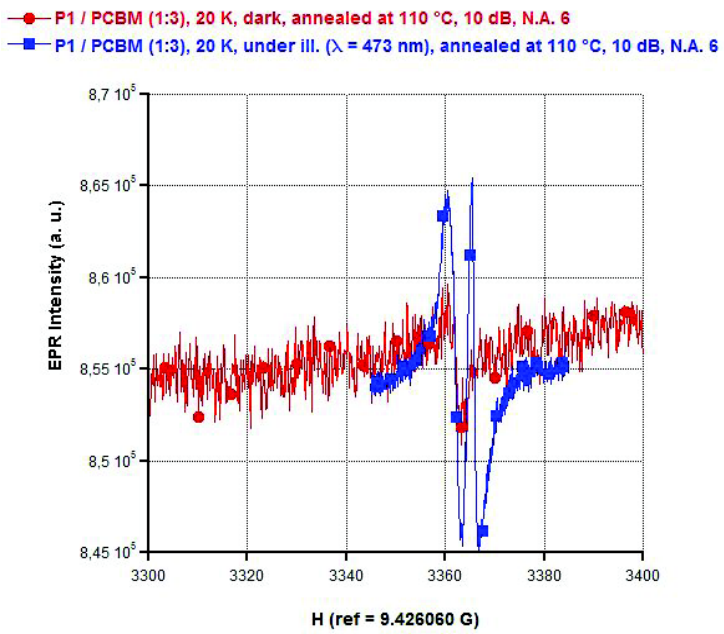

Figure 4.8: EPR Spectra of P1/PCBM (1:3) film registered at 20K with and without illumination.

Spectra recorded after 5, 10 and 30 minutes of relaxation show a quasi-reversible behavior. We suppose that this relaxation is related either to recombination processes or to other reactions of the created free radical species.

Further illumination leads to a subsequent increase in the intensity of both lines, which is reversible in nature.

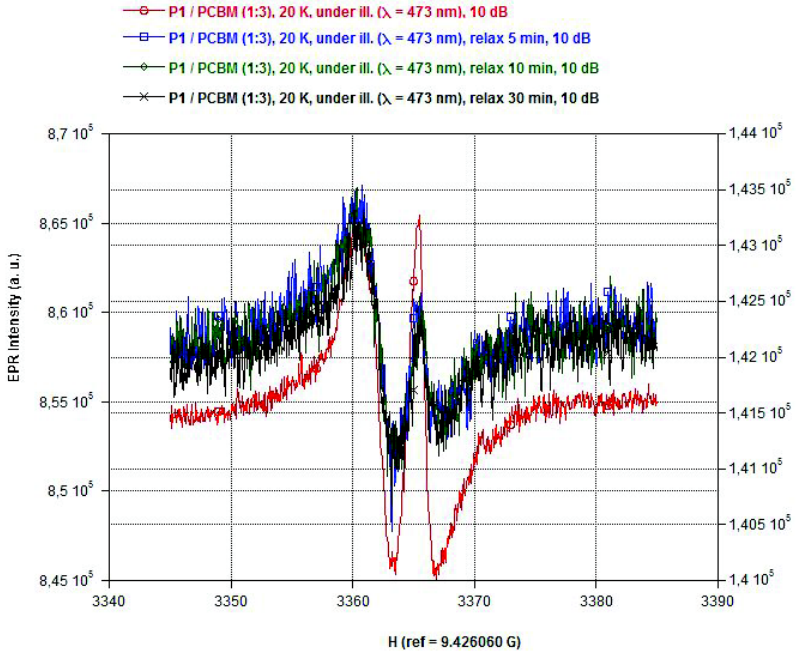

Fig. 4.9: EPR spectra of P1/PCBM polymer at (1:3) ratio, registered at 20 K after 5, 10 and 30 minutes of relaxation. The observed changes are quasi reversible.

Figure 4.10 shows the simulation of the spectrum of the P1/PCBM (1:3) blend, acquired at 20 K under laser light illumination (λ = 473 nm).

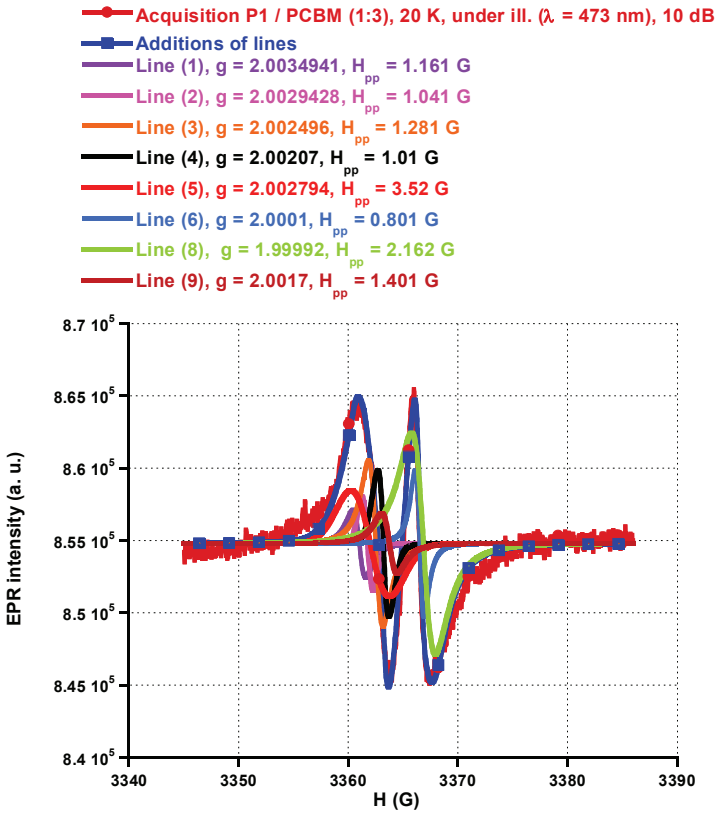

Figure 4.10: EPR spectrum of P1/PCBM (1:3) blend annealed at 110°C, registered at 20 K, under illumination (λ = 473 nm), together with its simulation.

	H_{pp} (G)	*g*-factor	% intensity	Structure at the origin of the line
Line 1	1.161	2.003449414	4.00096	Paramagnetic species of P1 induced by illumination at 473 nm
Line 2	1.041	2.002942852	1.38374	Paramagnetic species of P1 induced by illumination at 473 nm
Line 3	1.281	2.002496099	13.10259	Paramagnetic species of P1 induced by illumination at 473 nm
Line 4	1.01	2.00207931	4.10828	n.a.
Line 5	3.523	2.002793913	18.69609	
Line 6	0.801	2.000128661	4.48706	n.a.
Line 7	1.481	2.000128661	0.00000	
Line 8	2.162	1.999920737	48.60983	PCBM (according to literature data)
Line 9	1.401	2.001751954	5.61144	n.a.
Line 10	40.92	1.989169574	0.00000	

Line 11	3.44	2.002772181	0.00000	
Line 12	5.25	2.004650731	0.00000	

Table 4.4: EPR parameters of P1/PCBM (1:3) blend annealed at 110°C. EPR experiment carried out at 20 K, under illumination (λ = 473 nm).

The registered experimental spectrum was of complex shape and the following lines had to be used for its simulation: *line 1*, $g = 2.0034941$, $H_{pp} = 1.161$ G; *line 2*, $g = 2.0029428$, $H_{pp} = 1.041$ G; *line 3*, $g = 2.002496$, $H_{pp} = 1.281$ G; *line 4*, $g = 2.00207$, $H_{pp} = 1{:}01$ G; *line 5*, $g = 2.002794$, $H_{pp} = 3.52$ G; *line 6*, $g = 2.0001$, $H_{pp} = 0.801$ G; *line 8*, $g = 2.0017$, $H_{pp} = 1.401$ G. At present only few lines can be attributed to specific structures. Actually it is necessary to continue the study of the **P1** and **P3** polymers in order to better understand the relationship between the EPR fingerprints and their structural properties.

4.1.7 EPR saturation studies

In order to better discriminate EPR signals of different paramagnetic species, we recorded the EPR spectrum of P1/PCBM (1:3), at 20 K under illumination for different values of the microwave power (from 0 dB, 10 dB, 20 dB and 30 dB to 40 dB). Unfortunately it was not possible to better resolve the global signal by the saturation processes (see Figure 4.11).

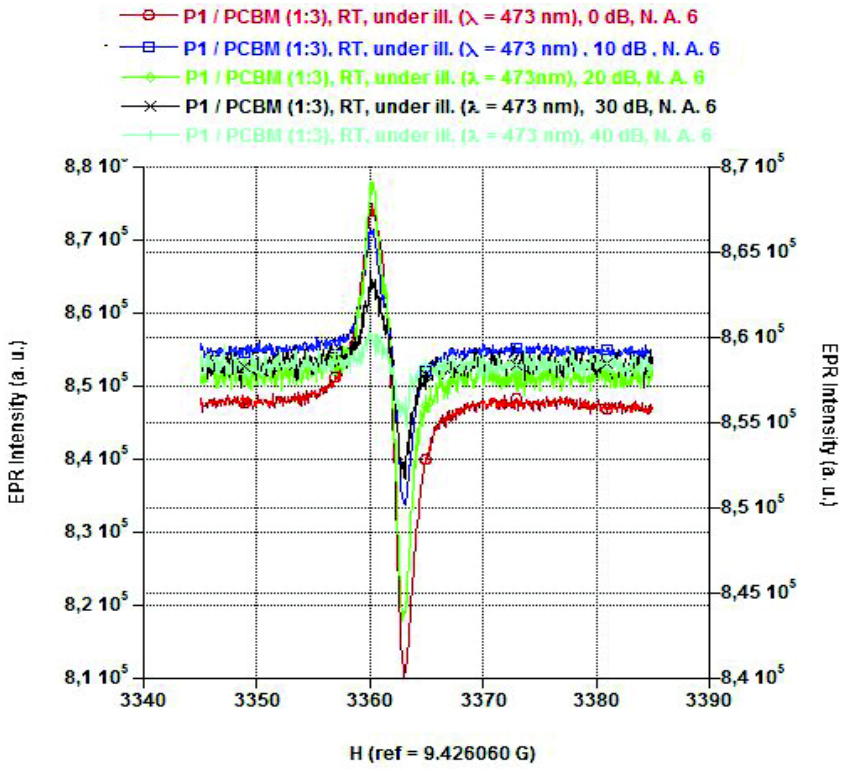

Figure 4.11: Evolution of the EPR spectra of P1:PCBM (1:3) blend with increasing power from 0 dB to 40 dB.

Nevertheless, a slight difference both in the relative intensities of the line shoulders and the changes in the linewidths, clearly seen in the signal attributed to **P1**, demonstrates the presence of at least two different

paramagnetic species in the polymer.

4.1.8 P2/PCBM (1:3) blend

P2 is similar to **P1** except the double TPD unit in the electron accepting moiety, which should strengthen the "acceptor" power of the *pull* block.

A series of experiments were performed for a blend of P2/PCBM of 1:3 weight ratio. In the dark, both at RT and at 20 K, a clear signal was detected. Once the sample was illuminated, the EPR signal became comparable to that registered for **P1** meaning that, the additional electron accepting unit does not influence significantly the electron transfer mechanisms intra polymer and versus the PCBM acceptor.

The signal was satisfactorily simulated, with the same lines as that of P1/PCBM 20 K 473 nm, except that *line 1* and *line 2*, lacking in **P2,** and that *line 5* is now replaced by *line 5'*of same *g* – factor, but of a narrower linewidth. The same *g*-factor reveals similar chemical structure while a decrease in the linewidth can be ascribed to a larger delocalization of the free electron. This leads us to ascribe *line 5* and *line 5'* respectively to the PD and bis-PD structures (see Table 4.5).

	H_{pp} (G)	*g*-factor	% intensity	Structure at the origin of the line
Line 1	1.161	2.003449414	0.00000	
Line 2	1.041	2.002942852	0.00000	
Line 3	**1.281**	**2.002496099**	**4.05809**	**Paramagnetic species of P1 induced by illumination at 473 nm**
Line 4	**1.01**	**2.00207931**	**0.60519**	**n.a.**
Line 5'	**2.643**	**2.002793913**	**27.21119**	**2 PD**
Line 6	**0.801**	**2.000128661**	**27.21119**	**n.a.**
Line 7	1.481	2.000128661	0.00000	
Line 8	**2.162**	**1.999920737**	**40.91335**	**Fullerene**
Line 9	1.401	2.001751954	0.00000	
Line 10	40.92	1.989169574	0.00000	
Line 11	3.44	2.002772181	0.00000	
Line 12	5.25	2.004650731	0.00000	

Table 4.5: EPR parameters of P2/PCBM (1:3)blend, annealed at 110°C. EPR experiment carried out at 20K, under illumination (λ = 473 nm).

Based on the results obtained so far we can give a partial conclusion, concerning the attribution of the various lines to specific structures. Clearly, *line 8* is attributed to the fullerene radical anion; *lines 5* and *5'* are clearly attributed to the PD and two PD moieties. We observe that *line 3* is present both in **P1** and **P2**, but keeps the same H_{pp} and *g*-factor. This result leads us to ascribe this *line 3* either to carbazole or to bridge thiophene group (the latter considered, till now, as belonging to the TPD *pull* unit).

The absence of *lines 1* and *2* in **P2** cannot be explained at the moment. Nevertheless, values of their *g* factors lead us to assume that they should be ascribed to **P1**.

These preliminary line attributions are listed in Table 4.6.

Lines	Species
Line 1	**P1**
Line 2	**P1**
Line 3	**Carbazole or "bridge thiophene"**
Line 5	PD
Line 5'	PD-PD
Line 8	Fullerene radical anion

Table 4.6: Proposed attribution of the simulation lines.

In this case we face a problem because the intensity of *line 5'*, representing the bis-PD, is much lower than that of PCBM *(line 8)* and we can wonder if *line 6* does not correspond to species also interacting with PCBM. Deeper studies have to be carried out to clarify this point.

We can notice that the transfer from **P2** to PCBM is mostly due to the bis-PD unit and we will give an interpretation of this result in *paragraph 4.2* dedicated to the mechanisms.

4.1.9 Case of neat P3

For neat **P3** the same set of experiments was performed as in the case of neat **P1**. Figure 4.12 shows the EPR spectra registered at RT in dark and under illumination. No effect of illumination could be observed. Two alternative interpretation of this effect can be proposed: either the *push-pull* process does not occur or no radical species coming from the *push-pull* effect is able to give a fingerprint which can be trapped during the process. Nevertheless, results obtained for **P1** and later on for **P3** support the first assumption.

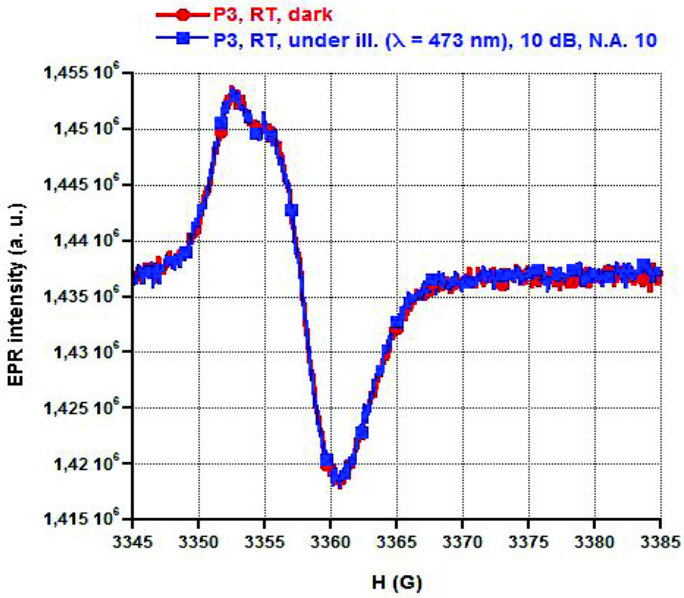

*Figure 4.12: EPR spectra of **P3** registered at RT in the dark and under illumination with laser light (λ = 473 nm).*

The lowering of the temperature to 20 K results in an increase of the EPR line intensity. The simulation of the spectra in "dark conditions" is presented in Figure 4.13 and Table 4.7.

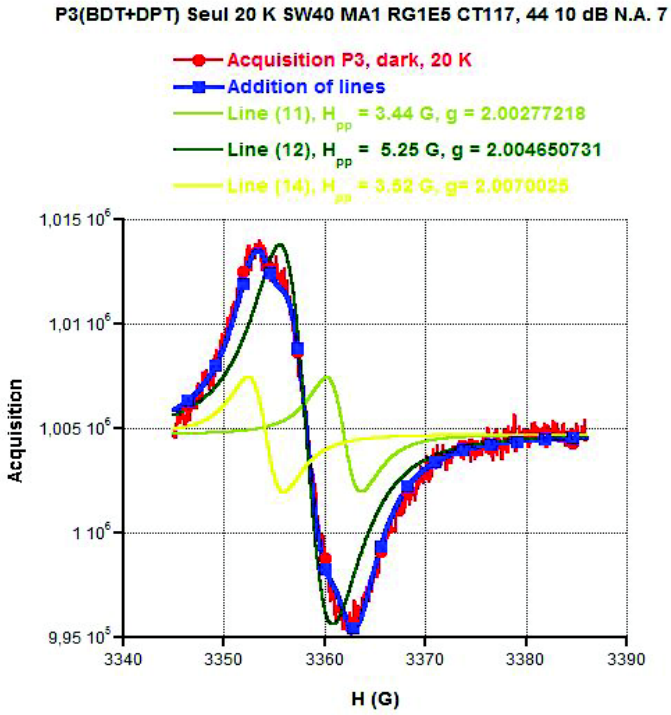

Figure 4.13: EPR spectrum of P3 registered at 20 K in the dark, together with its simulation.

	H_{pp} (G)	*g*-factor	% intensity	Structure at the origin of the line
Line 1	1.161	2.003449414	0.00000	
Line 2	1.041	2.002942852	0.00000	
Line 3	1281	2.002496099	0.00000	
Line 4	1.01	2.00207931	0.00000	
Line 5	3.523	2.002793913	0.00000	
Line 6	0.801	2.000128661	0.00000	
Line 7	1.481	2.000128661	0.00000	
Line 8	2.162	1.999920737	0.00000	
Line 9	1.401	2.001751954	0.00000	
Line 10	40.92	1.989169574	0.00000	
Line 11	**3.44**	**2.002772181**	**10.17391**	**Paramagnetic species of P3**
Line 12	**5.25**	**2.004650731**	**79.10696**	**Paramagnetic species of P3**
Line 13	3.44	2.00361037	0.00000	
Line 14	**3.52**	**2.007002529**	**10.78174**	**Paramagnetic species of P3**
Line 15	2.322	2.006458257	0.00000	
Line 16	3.523	1.000575396	0.00000	

Line 17	13.7	2.004108419	0.00000	
Line 18	1.96	2.002201	0.00000	

Table 4.7: EPR parameters of neat P3 annealed at 110°C. EPR experiment carried out at 20K, in the dark.

The simulation of the spectrum of neat **P3** recorded at 20 K in the dark shows the presence of three lines of *g*-factor in the range of that expected for the polymer. For this reason, at this step of the study we ascribed *line 11, 12* and *14* to **P3**. We observe that *line 11* is very similar to *line 5* observed in **P1** and previously ascribed to PD group. This leads us to attribute *line 11* to the same PD group. H_{pp} and g-factor of *line 12* are very different from that observed for the line attributed in **P1** and **P2** to carbazole or bridge thiophene, we assume that this line corresponds to BDT. We can now complete the table 4.6 presented before (see table 4.7).

Lines	Species
Line 1	**P1**
Line 2	**P1**
Line 3	**Carbazole or "bridge thiophene"**
Line 5	PD
Line 5'	PD-PD
Line 8	Fullerene radical anion
Line 11	PD
Line 12	BDT
Line 14	P3

Table 4.7: Proposed attribution of simulation lines.

We could expect to see a kind of transfer between the *push-pull* units in the polymer **P3**. The simulation was also performed for the spectrum of **P3**, registered at 20 K under light. The same three lines appeared at different ratios, which may reflect that the *push- pull* process has occurred.

4.1.10 P3/PCBM (1:3) blend

The blend of **P3** was analyzed at the same conditions as the analogous blend of **P1**. At RT and at 20 K, the EPR spectrum of P3/PCBM (1:3) blend is characterized by a low intensity "dark" EPR signal, due to localized paramagnetic defects. Under illumination a significant evolution of the spectrum occurs (see Figure 4.14).

From the simulation of the spectra it was possible, as expected, to reveal the presence of *line 8*, previously assigned to the PCBM radical anion (see Figure 4.14 and Table 4.8).

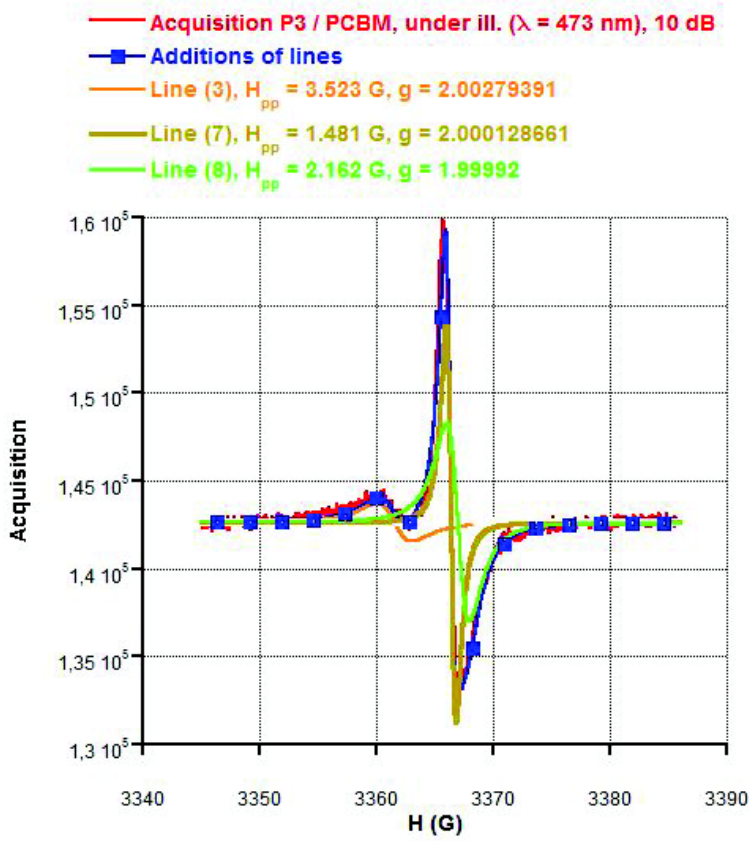

Figure 4.14 : EPR spectrum of P3/PCBM (1:3) blend, registered at 20 K under illumination.

	H_{pp} (G)	*g*-factor	% intensity	Structure at the origin of the line
Line 1	1.161	2.003449414	0.00000	
Line 2	1.041	2.002942852	0.00000	
Line 3	1281	2.002496099	0.00000	
Line 4	1.01	2.00207931	0.00000	
Line 5	**3.523**	**2.002793913**	**23.99162**	**PD**
Line 6	0.801	2.000128661	0.00000	
Line 7	**1.481**	**2.000128661**	**20.25140**	**n.a.**
Line 8	**2.162**	**1.999920737**	**55.02863**	**fullerene**
Line 9	1.401	2.001751954	0.00000	
Line 10	40.92	1.989169574	0.00000	
Line 11	3.44	2.002772181	0.00000	
Line 12	5.25	2.004650731	0.00000	
Line 13	3.443	2.003610375	0.00000	
Line 14	3.52	2.007002529	0.00000	
Line 15	2.322	2.006458257	0.00000	
Line 16	3.523	1.000575396	0.00000	

Line 17	13.7	2.004108419	0.00000	
Line 18	1.96	2.002201	0.00000	

Table 4.8: EPR parameters of P3/PCBM (1:3) blend annealed at 110°C. EPR experiment carried out at 20K, under illumination (λ = 473nm).

In this case, like for P2, we face a problem because the intensity of *line 5*, representing PD, is much lower than that of PCBM *(line 8)* and we can wonder if *line 7* does not correspond to species also interacting with PCBM. Deeper studies have to be carried out concerning this problem.

Relaxations during 4 and 10 min did not lead to a complete disappearance of the illumination-induced EPR fingerprints.

Finally, it is tempting to compare the behavior of **P1** and **P3** blends with PCBM under illumination. The obtained EPR spectra are set together in Figure 4.15.

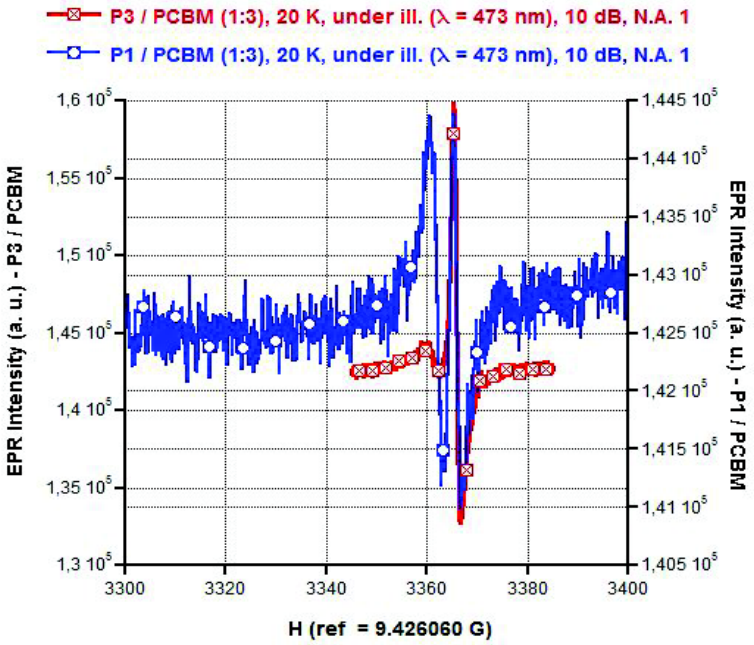

Figure 4.15: Comparison of the EPR spectra of P1/PCBM (1:3) and P3/PCBM(1:3) registered at 20 K under illumination(λ = 473nm).

They show interesting but distinctly different features. These differences could be explained considering different types of radicals formation mechanisms: for **P1** some intrachain transfer phenomena seem to occur, in contrast to **P3**, where direct charge transfer from the polymer to the acceptor seems to prevail.

4.1.11 Photoluminescence studies of P1 (or P3)/$CuInS_2$ nanocrystals blends

P1 and **P3** were also tested with another type of electron acceptor, namely nanocrystals of copper indium disulfide ($CuInS_2$). Studies on the photoluminescence quenching in organic/inorganic hybrid materials demonstrate a significant quenching *via* charge and/or energy transfer in accordance with the relative energy level alignment. [13]. In our case the quenching of photoluminescence was efficient: 42% and 38% for **P1** and **P3**, respectively, at the maximum of the weight % of NCs in the blend (see Figure 4.16).

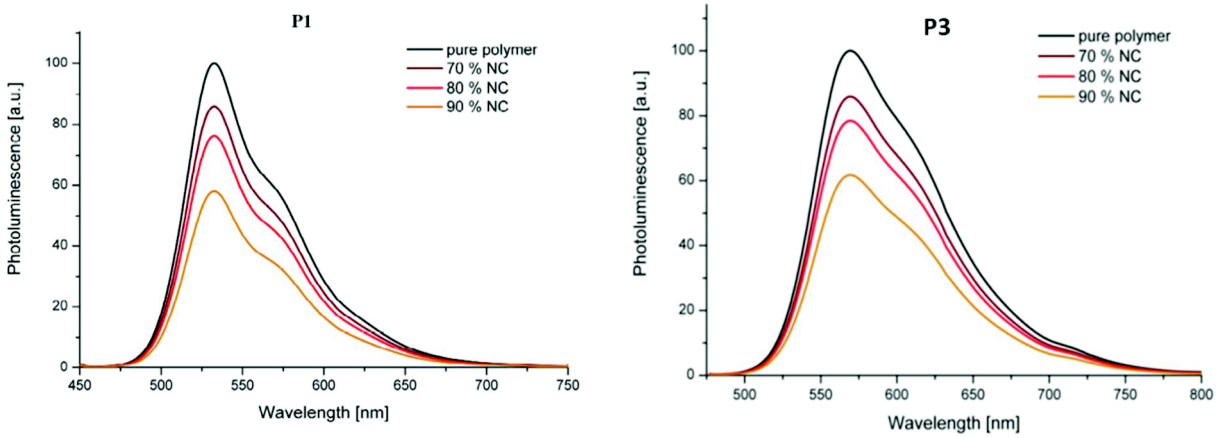

Figure 4.16: Photoluminescence spectra of P1/$CuInS_2$ nanocrystals (1:3) and P3/$CuInS_2$ nanocrystals (1:3) blends registered for increasing content of NCs.

Although photoluminescence experiments are widely used, they do not give information concerning the mechanism of the energy and charge transfer between the components of the blend.

On the other hand, EPR allows to differentiate between these processes and to determine which type of free charge carriers arises from the light induced excitation.

4.1.12 EPR studies of P1 (or P3)/$CuInS_2$ nanocrystals (1:3) blends

It is known that similarly as PCBM, inorganic semiconductor nanocrystals can promote the charge transfer between both components of the blend. Figure 4.17 shows the EPR spectrum of **P1** blended with NCs of $CuInS_2$ (1:3) recorded at 20 K under illumination and after relaxation (10 minutes) in the dark. A clear decrease of the spectrum intensity was observed during the relaxation, showing a slight but clear, at least partially reversible, illumination effect (see Figure 4.17). The results of the spectra simulations are shown in Figure 4.18 and Table 4.9.

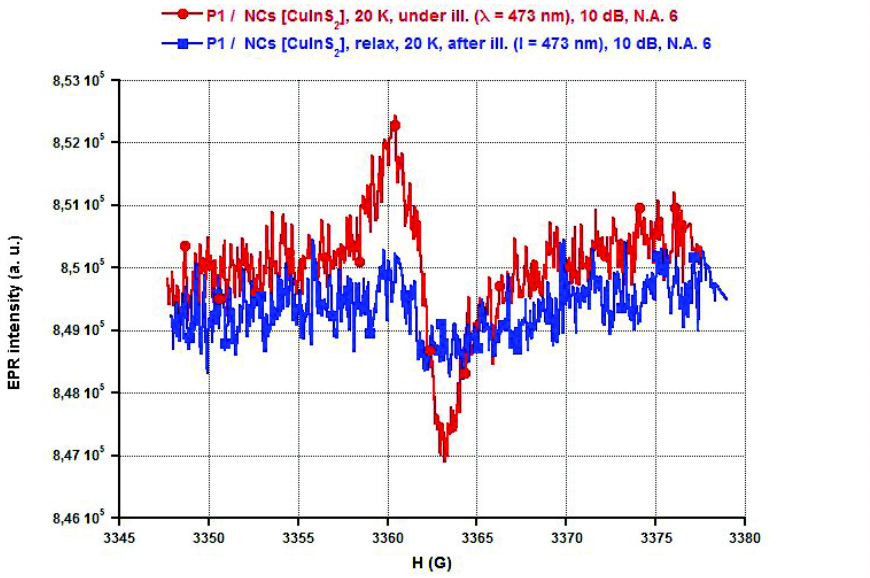

Figure 4.17: EPR spectra of P1/ $CuInS_2$ nanocrystals (1:3) blend, registered at 20K and under illumination (λ = 473 nm) and after relaxation in dark conditions.

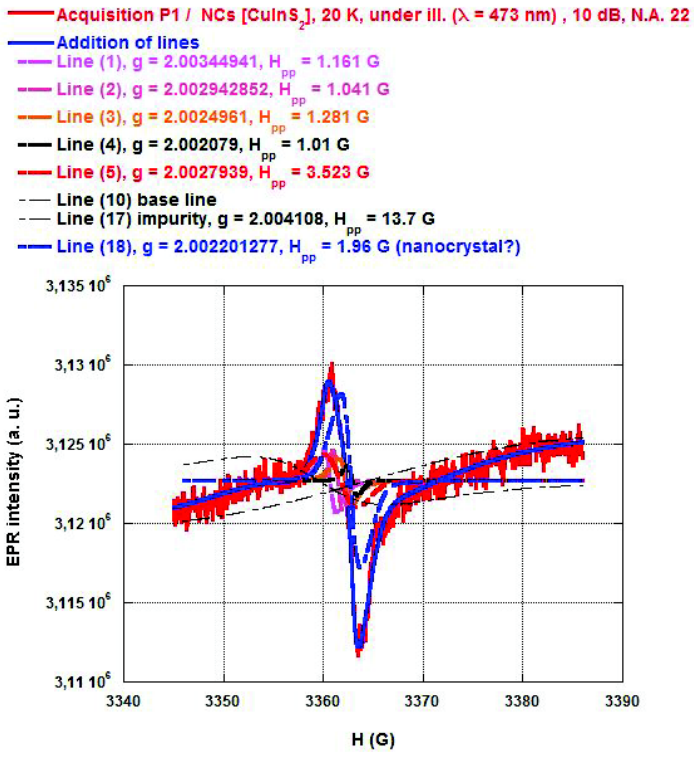

Figure 4.18: EPR spectrum of P1/ $CuInS_2$ nanocrystals (1:3) blend, registered at 20K under illumination (λ = 473 nm), together with its simulation.

	H_{pp} (G)	*g*-factor	% intensity	Structure at the origin of the line
Line 1	**1.161**	**2.0034494**	**10.29821**	**P1**
Line 2	**1.041**	**2.0029429**	**2.45212**	**P1**
Line 3	**1281**	**2.0024961**	**10.29821**	**Carbazole or "bridge thiophene"**
Line 4	1.01	2.0020793	2.23259	**n.a.**
Line 5	**3.523**	**2.0027939**	**23.38170**	**PD**
Line 6	0.801	2.000128661	0.00000	
Line 7	1.481	2.000128661	0.00000	
Line 8	2.162	1.999920737	0.00000	
Line 9	1.401	2.001751954	0.00000	
Line 10	40.92	1.989169574	0.00000	
Line 11	3.44	2.002772181	0.00000	
Line 12	5.25	2.004650731	0.00000	
Line 13	3.44	2.003610375	0.00000	
Line 14	3.52	2.007002529	0.00000	
Line 15	2.322	2.006458257	0.00000	
Line 16	3.523	1.000575396	0.00000	
Line 17	**3.52**	**2.007002529**	**1116.07143**	
Line 18	**1.96**	**2.0022013**	**51.33929**	

Table 4.9: EPR parameters of P1/ $CuInS_2$ nanocrystals (1:3) blend. EPR experiment carried out at 20K under illumination (λ = 473nm).

Recorded spectra corresponding respectively to **P1** with PCBM and **P1** with NCs are compared (see Figure 4.19): the effect observed for the blend of P1/PCBM (1:3) is much stronger than for the blend of P1/NCs (1:3). Two interpretations can be given: i) the active interface promoting charge transfer is smaller in the P1/NCs blend than in P1/PCBM one due to the bigger dimension (7-8 nm) of NCs as compared to PCBM; ii) the transfer from the polymer to NCs is less efficient than the transfer from the polymer to PCBM.

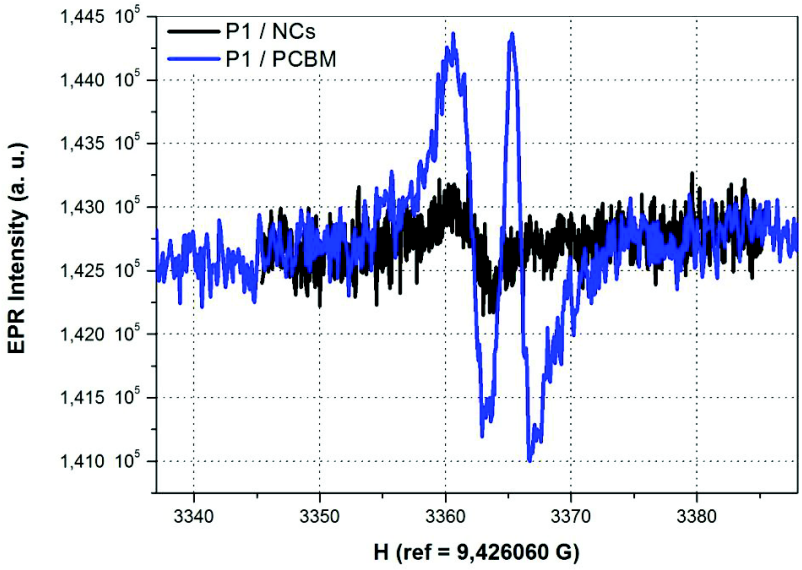

Figure 4.19: EPR spectra P1 blended with NCs and PCBM registered at 20K under illumination (λ = 473nm).

The P3/$CuInS_2$ nanocrystals (1:3) blend was studied by EPR spectroscopy in the same manner as the previously discussed P1/$CuInS_2$ nanocrystals (1:3) blend. Figure 4.20 shows its spectrum registered at 20 K under illumination (λ = 473nm). The registered signal is very weak and obscured by a high signal to noise ratio. Nevertheless, a large accumulation of scans allows detecting a line of the same parameters as those found for the radical formed in **P3** upon illumination of P3/PCBM (1:3) blend. This can be treated as a spectroscopic sign of a transfer from **P3** to the nanocrystal. In Table 4.10 the results of the spectrum simulation are presented.

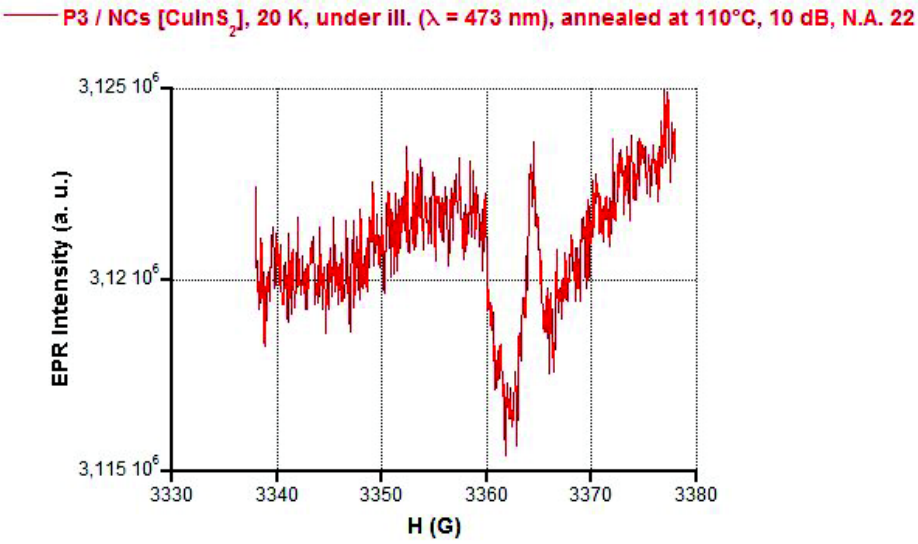

Figure 4.20: EPR spectrum of P3/ $CuInS_2$ nanocrystals (1:3) blend, registered at 20K under illumination (λ = 473 nm).

	H_{pp} (G)	*g*-factor	% intensity	Structure at the origin of the line
Line 1	1.161	2.003449414	0.00000	
Line 2	1.041	2.002942852	0.00000	
Line 3	1281	2.002496099	0.00000	
Line 4	1.01	2.00207931	0.00000	
Line 5	3.523	2.002793913	0.00000	
Line 6	0.801	2.000128661	0.00000	
Line 7	**1.481**	**2.000128661**	**6.03675**	**n.a.**
Line 8	2.162	1.999920737	0.00000	
Line 9	1.401	2.001751954	0.00000	
Line 10	40.92	1.989169574	0.00000	
Line 11	**3.443**	**2.002772181**	**28.34646**	**PD**
Line 12	**5.285**	**2.004650731**	**65.61680**	**BDT**
Line 13	3.443	2.003610375	0.00000	
Line 14	3.52	2.007002529	0.00000	
Line 15	2.322	2.006458257	0.00000	
Line 16	3.523	1.000575396	0.00000	
Line 17	13.7	2.004108419	0.00000	
Line 18	1.96	2.002201	0.00000	

Table 4.10: EPR parameters of P3/ $CuInS_2$ nanocrystals (1:3) blend EPR experiment carried out at 20K under illumination (λ = 473nm).

Also for P3, as shown in figure 4.21, the effect observed for the blend of P3/PCBM (1:3) is much stronger than for the blend of P3/NCs (1:3). The same two interpretations can be given: i) the active interface promoting charge transfer is smaller in the P3/NC blend than in P3/PCBM one due to the bigger dimension (7-8 nm) of NCs as compared to PCBM; ii) the transfer from polymer to NCs is less efficient than the transfer from polymer to PCBM.

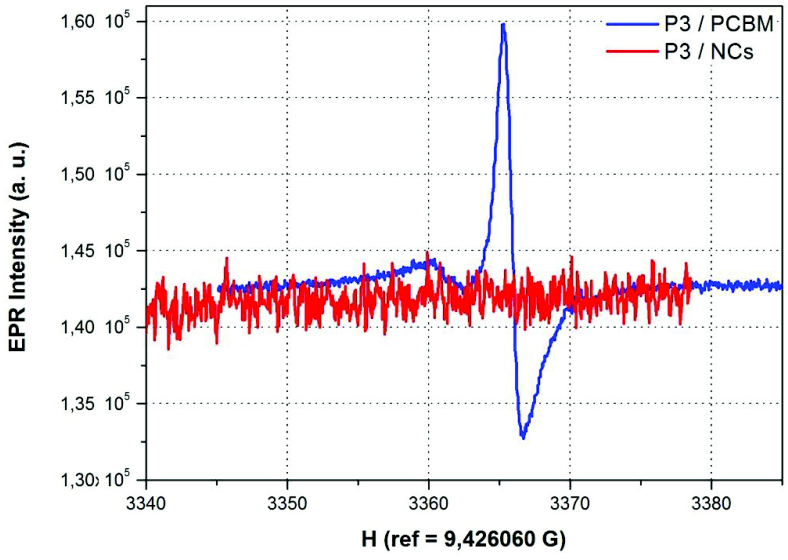

Figure 4.21: Spectra of P1/PCBM (1:3) and P1/NCs (1: 3) after one scan of acquisition at 10 dB. Remark: N.A. of P3/NCs is 6 and N.A. of P3/PCBM is 1.

To summarize, we have succeeded in attribution of the majority of the lines whose superposition yields the experimental spectra. These attributions are helpful in elucidating the electronic transfer mechanisms.

4.2 Electronic transfer mechanisms in neat polymers and in their blends with PCBM and inorganic semiconductor nanocrystals

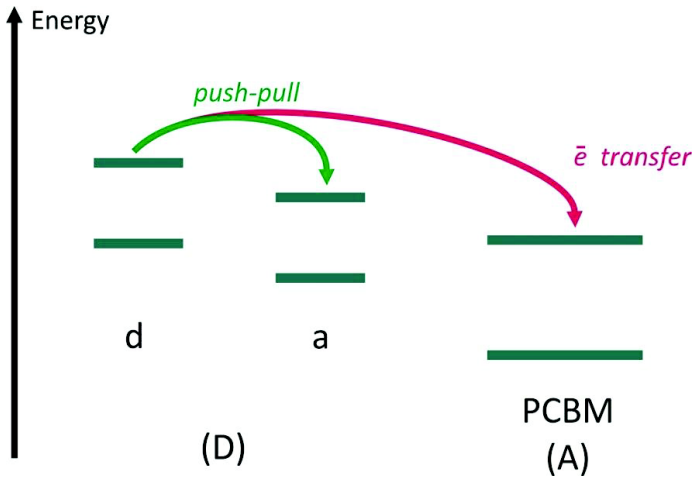

Figure 4.22: Representation of intra-molecular (push-pull) and inter-molecular (electron transfer) mechanisms in a bulk-heterojunction configuration.

First of all, we stress that EPR does not only allow characterizing the final state of an electronic transfer mechanism, but also the trace transient transfers when free radicals are trapped during the process. The obtained EPR results allow us to present following pictures of the various charge transfers in the systems studied.

a) Push-pull effect

- **In P1**: the comparison of the signal of neat P1 in the dark and under illumination clearly demonstrates that an intramolecular *push-pull* process takes place in this polymer. Actually, neat P1 under illumination shows a peak formed by lines attributed to carbazole, which does not appear in the dark conditions. This EPR signal, only present under illumination, is a clear fingerprint of a *push-pull* mechanism. Theoretically, a signal corresponding to the TPD group or to a part of it (for example PD, revealed before by EPR) should be observed simultaneously with the carbazole signal. The non detection of this signal may be explained by the difference in the linewidth between the carbazole and the PD EPR signals: the linewidth (H_{pp}) of PD is of 3.56 G while that of carbazole is equal to 1G, since the intensity of the signal is (for signal of the same lineshape) proportional to $(H_{pp})^2 * I_{pp}$, the height (I_{pp}) of the PD signal is expected to be 12.7 times lower than that of the carbazole line, so it appears hidden in the noise.

- **In P2:** the difference in relative intensities between carbazole or bridging thiophene and bis-PD show that a kind of *push-pull* effect has also occurred.
- **In P3:** We do not observe any EPR evidence of the push-pull effect. Nevertheless it is not possible to affirm that this process does not occur.

Electronic transfer between polymers and PCBM or nanocrystals

- **For the P1/ PCBM blend:** under illumination at 20 K conditions, lines, arising from carbazole, TPD units and fullerene are observed. If carbazole units were the only ones to be excited and able to transfer an electron to TPD in a *push-pull* process, TPD should not show an EPR signal after the transfer to the fullerene. Nevertheless, the *push-pull* process exists as discussed above. We interpret the presence of the EPR signal of PD by the fact that both carbazole and PD are involved in the excitation process. An incomplete charge transfer from the TPD (or PD) acceptor units and the PCBM is unlikely because intramolecular *push-pull* relaxation times should have been too short to be observed by an EPR.

- **For P1/$CuInS_2$ nanocrystals blend**: it seems that charge transfer between **P1** and NCs occurs, as it is the case between P1 and PCBM. Nevertheless the charge transfer appears less intensive or less efficient.

- **For P2/PCBM blend**: the increase in delocalization from PD and bis-PD may explain the fact that the bis-PD unit becomes the principal actor in the charge transfer versus PCBM, which still occurs. To confirm this inversed tendency, some DFT calculations were carried out to obtain the electronic density of the radical cation, *i.e*. the final state of the charge transfer. (see Figure 4.23)

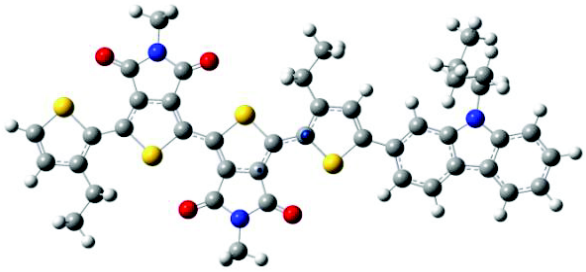

Fig.4.23 . Radical cation localization at the final transfer state for P2.

Theoretical calculations, showing that the spin density of the radical cation (blue points) is localized on the 2-TPD unit, are in full agreement with EPR results.

This behavior has also been predicted from previous DFT calculations (see Chapter 3) even if they do not represent the final conditions after the charge transfer, but they correspond to the difference in the LUMO and HOMO electronic density. It could be noticed that a strong *push* behavior is visible on the thiophene bridge of the bis-TPD groups which most probably explains the absence of a real and well defined *push-pull* effect. Reciprocally, these calculations suggest that *line 3* can be ascribed to the bridging thiophene.

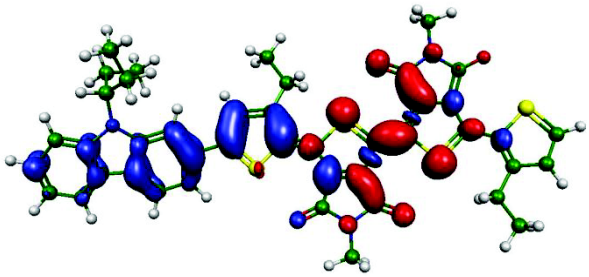

Fig.4.24 . Radical cation localization at the final transfer state for P2.

- **For P3/PCBM blend:** we observe both lines attributed to the dialkoxybenzodithiophene(BTD) moiety (considered as the *push* unit) and the PD moiety (considered as the *pull* unit). As already concluded for P1, the *push-pull* effect cannot be excluded and the presence of PD and BTD units means that both are involved in the exciton formation.

In this case, again, DFT calculations of the spin density of the radical cation are in good agreement with EPR results (see Figure 4.25).

Fig. 4.25: Radical cation localization at the final transfer state for P3.

- **For P3/NCs blend**: EPR signal is of very low intensity and difficult to detect. In this case, from simulations, both *push* and *pull* moieties are involved in the transfer to the nanocrystal.

Taking into account all these conclusions, we can complete the table summarizing attributions of the EPR lines to the various substructures of the studied polymers (see Table 4.11) and summarizing the transfer mechanisms detected by EPR measurements (see Table 4.12).

Lines	Species
Line 1	**P1**
Line 2	**P1**
Line 3	**~~Carbazole~~ or "bridge thiophene"**
Line 5	PD
Line 5'	PD-PD
Line 8	Fullerene radical anion
Line 11	PD
Line 12	BDT
Line 14	P3

Table 4.11: Proposed attribution of the simulation lines.

Polymer	*Push-Pull* effect	Exciton formation	Transfer to PCBM	Transfer to NCs
P1 (*push-pull*)	Yes	***push-pull***	Yes	Yes (small effect)
P2 (*push-pull)*	Yes	***push-pull***	Yes	Not measured
P3(*push-pull)*	Yes	***push-pull***	Yes	Yes (small effect)

Table 4.12: Summary of the transfer mechanisms detected by EPR measurements.

4.3 Conclusion

First of all combining EPR under illumination and EPR tracing we have succeeded in characterizing the various electronic transfers in particularly designed *push-pull* copolymers blended with two types of electron acceptor materials: PCBM and $CuInS_2$ nanocrystals.

Using EPR under illumination experiments, we have evidenced intra-molecular electronic transfers, so called *push-pull* effect, in three studied polymers, by attributing a specific EPR fingerprint (EPR tracing) to each *push* and *pull* species present in polymer backbone.

Then, we have addressed the problem of electronic transfer between polymers (donors) and PCMB or nanocrystals (acceptors). It was demonstrated for all considered polymers that an evident charge transfer appears from the macromolecule to PCBM.

On the other hand for polymers blended with NCs only a very weak signal, ascribed to the charge transfer, appears. In this case, knowing that the NCs EPR signal could not be detected, the demonstration of the phenomenon is given by the fingerprint of the polymer appearing only under illumination.

DFT calculation of the spin density of the radical cation for **P2** and **P3** are in agreement with the EPR signals.

For the future research, a similar study with an illumination at 600 nm, fitting better with the maximum of the absorption band of the studied polymers should give complementary information.

[1] V. I. Arkhipov and H. Bässler, "Exciton dissociation and charge photogeneration in pristine and doped conjugated polymers," *Physica Status Solidi A*, vol. 201, no. 6, pp. 1152–1187, 2004.

[2] B. Rand, D. Burk, and S. R. Forrest, "Offset energies at organic semiconductor heterojunctions and their influence on the open-circuit voltage of thin-film solar cells," *Physical Review B*, vol. 75, no. 11, pp. 1–11, 2007.

[3] M. C. Scharber, D. Mühlbacher, M. Koppe, P. Denk, C. Waldauf, A. J. Heeger, and C. J. Brabec, "Design Rules for Donors in Bulk-Heterojunction Solar Cells—Towards 10 % Energy-Conversion Efficiency," *Advanced Materials*, vol. 18, no. 6, pp. 789–794, 2006.

[4] Y. Astuti, W. Duffy, S. Tierney, W. Zhang, M. Heeney, I. McCulloch, J. Nelson, D. D. C. Bradley, and J. R. Durrant, "Charge carrier formation in polythiophene/fullerene blend films studied by transient absorption spectroscopy," *Journal of the American Chemical Society*, vol. 130, no. 10, pp. 3030–3042, 2008.

[5] I. W. Hwang, C. Soci, D. Moses, Z. Zhu, D. Waller, R. Gaudiana, C. J. Brabec, and A. J. Heeger, "Ultrafast Electron Transfer and Decay Dynamics in a Small Band Gap Bulk Heterojunction Material," *Advanced Materials*, vol. 19, no. 17, pp. 2307–2312, 2007.

[6] C. Brabec, V. Dyakonov, J. Parisi, and N. S. Sariciftci, *Organic Photovoltaic: Concepts and Realization*. Berlin: Springer, 2003.

[7] S. Sensfuss, "Characterization of potential donor acceptor pairs for polymer solar cells by ESR, optical, and electrochemical investigations," *Proceedings of SPIE*, vol. 5215, no. 1, pp. 129–140, 2004.

[8] A. Carrington and McLaclan A.D., *In introduction to magnetic Resonance with applications to Chemistry and Chemical physics*. New York: Harper and Row, 1967.

[9] V. I. Krinichnyi, *LEPR spectroscopy of charge carriers photoinduced in polymer/fullerene composites*, 2009th ed. Hauppauge, New York,: In Encyclopedia of Polymer Composites, pp. 417–446.

[10] R. S. Alger, "Electron Paramagnetic Resonance, Techniques and Applications," *American Journal of Physics*, vol. 37, no. 8, p. 847, 1968.

[11] J. Poole and P. Charles, "Electron Spin Resonance: A comprehensive Treatrise on Experimental Techniques"*, 2 nd ed.* New York: John Wiley and Sons, 1983.

[12] J. A. Weil, J. R. Bolton, and J. E. Wertz, *Electron Paramagnetic Resonance: Elementary Theory and Practical Applications*. New York: John Wiley and Sons, 1994.

[13] B. Pépin-Donat, et al., "EPR tracing method," *E.S.T. under considerations*, 2012.

[14] V. I. Krinichnyi and E. I. Yudanova, "Light-induced EPR spectroscopy of charge carriers photoinduced in polymer/fullerene bulk heterojunctions," *Journal of Renewable and Sustainable Energy*, vol. 1, no. 4, p. 043110, 2009.

Chapter 5

Organic solar cells devices

5.1 Introduction

This chapter, devoted to the description of photovoltaic properties of the polymers synthesized in the frame of this research, is divided into three parts. In the first part polymers containing 3,6-coupled carbazole donor units and BTD acceptor units are discussed.

The second part is focused on photovoltaic properties of P3 and P6, which seemed more promising than those based on 3,6-carbazole electron donating units.

In the third part of this chapter mains problems related to the device fabrications are discussed, as well as some preliminary studies of P1, P5 and P7 aimed at their potential use in photovoltaics.

5.2 Bulk heterojunction of 3,6-PCDTBT blended with PCBM

Judging from its optical (1.96 eV) and electrochemical gap (1.85 eV) as well as the HOMO and LUMO levels, 3,6-PCDTBT turned out to be a promising candidate for the application in photovoltaics. For tests in photovoltaic cells the polymer was blended with fullerene derivative at different 3,6-PCDTBT to PCBM weight ratio:1:1; 1:3 and 1:5. UV-*Vis* spectra of these blends are shown in Figure 5.1 a. They can be treated as a superposition of the PCBM spectrum at that of the polymer. In particular, the peak around 330 nm originates from the presence of PCBM whereas, a broad band above 500 nm can be attributed to the π-π* absorption band of the polymer. Relative intensities of these bands reflect the composition of the blend. Test devices fabricated from these blends were investigated under AM 1.5 illumination at 100 mW·cm^{-2}.

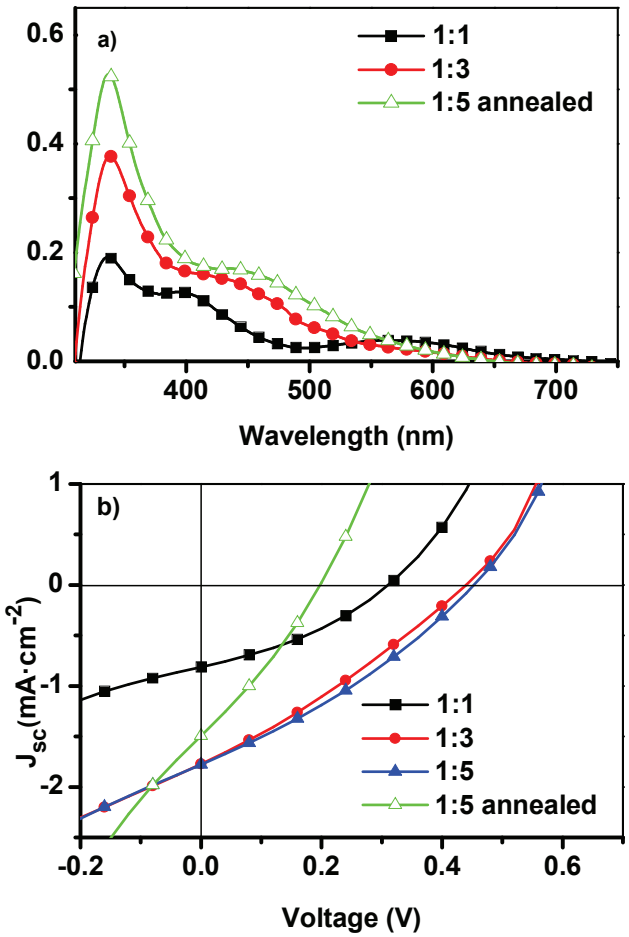

Figure 5.1: a) Current density versus voltage for photovoltaic devices fabricated from blends at different ratios under simulated solar illumination (AM 1.5, 100 mW·cm^{-2}). The device at 1:5 PCDTBT:PCBM blend ratio was annealed in a glove box at 90°C during 5 min. b) Corresponding UV-Vis absorption spectra of 3,6-PCDTBT:PCBM films for 1:3, 1:4 et 1:5 weight ratios normalized versus the principal absorbance PCBM peak.

Effectively, as predicted from the absorption spectra, the best cell, obtained for the PCDTBT: PCBM 1:3 ratio, reaches a J_{sc} of 2.11 mA·cm^{-2}, a V_{oc} of 0.41 V, a FF of 0.32 and a PCE of 0.35%.

As already indicated in *Chapter 1*, *paragraph 1.2.3* the V_{oc} is related to the difference between the donor

HOMO level and the acceptor LUMO level according to the equation 1.2.[1]

The measured V_{oc} of 0.53 V is lower than the value of 0.74 V, predicted by equation 1.2 and more close to the difference between the ITO and aluminum work functions (ca. 0.4 eV).
The relatively low values of V_{oc} and FF seem to indicate an important charge recombination, either in the bulk active layer or at the interfaces with electrodes. Another result that points out to the problem of the interface contacts is the fact that at -1.0 V negative bias, twice more photocurrent density, J, if compared with the short circuit current, J_{sc}, can be extracted from the PCDTBT:PCBM device. In particular, this behavior becomes evident considering the most performing weight ratio of 1:3 of polymer:PCBM. In this case the photocurrent could reach values of about -5 mA·cm^{-2}, which means exactly 2.5 times higher than in the J_{sc} conditions. The system is able to generate more charges than those which could be extracted for positive voltage (see Figure 5.2).

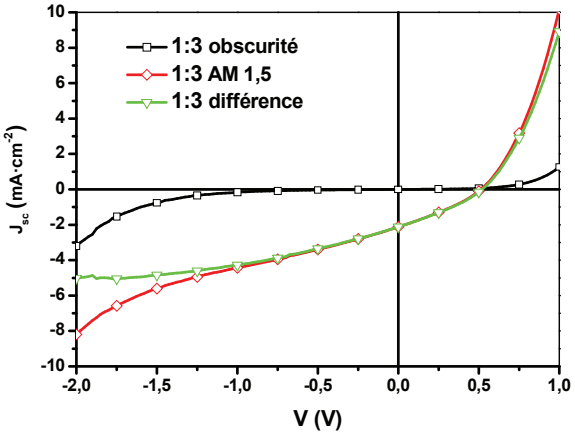

Figure 5.2: J-V characteristics of a solar cell of 3,6-PCDTBT:PCBM in the dark and under simulated solar illumination (AM 1.5, 100 mW·cm^{-2}).

These results underline that the amount of photogenerated charges is higher than the number of charges extracted from the device, under short circuit conditions. As a consequence, improving contacts at the interfaces and/or the nanostructure of the active layer it should be possible to improve the open circuit voltage V_{oc}, the short circuit current density J_{sc} and therefore the PCE of the device. In addition to this, the annealing of the devices at 90°C during 5 min. causes a decrease of the V_{oc}. Again, this indicates that contacts at the electrodes might be an important limitation for the present devices.

[1] $V_{OC} = E_{LUMO}(A) - E_{HOMO}(D) - 0.3eV$ $(Eq. 1.2)$, *where 0.3 V is an empirical factor.*[17]

5.3 Bulk heterojunction of 3,6-PCDOTBT blended with PCBM

The optical and electrochemical band gaps of 3,6-PCDOTBT (both = 2.11 eV) are larger than the corresponding gaps in PCDTBT. Nevertheless this polymer can still be considered as worth testing in photovoltaic devices.

In this case, in the bulk heterojunction tested, the 1:3 ratio of 3,6-PCDOTBT to PCBM was used. The current density - voltage characteristics of BHJs non annealed and annealed at two different temperatures are shown in Figure 5.3.

A yield of 0.21% was reached for films PCDOTBT:PCBM (not annealed), lower than the yield obtained for the PCDTBT: PCBM BHJ of the same weight ratio (1:3). An obvious reduction of J_{sc} to the value of -1.44 mA·cm^{-2} was observed together with a 10% decrease of FF.

Contrary to the expectations, the measured V_{oc} value is not increased in line with a decrease of the HOMO level by 0.2 eV. An explanation could derive from morphological reasons (see *paragraph 5.3*) or from non-optimized electrical contacts to the interface. Annealing treatment at 110°C of the polymers after cathode deposition doesn't improve the yield of the cell. Nevertheless, the J-V characteristics were modified: an increase of J_{sc} and FF compensates a decrease of the V_{oc}, comparing parameters with the device not annealed. Annealing treatments of the materials, at temperatures higher than 110°C, produced lower J-V characteristics.

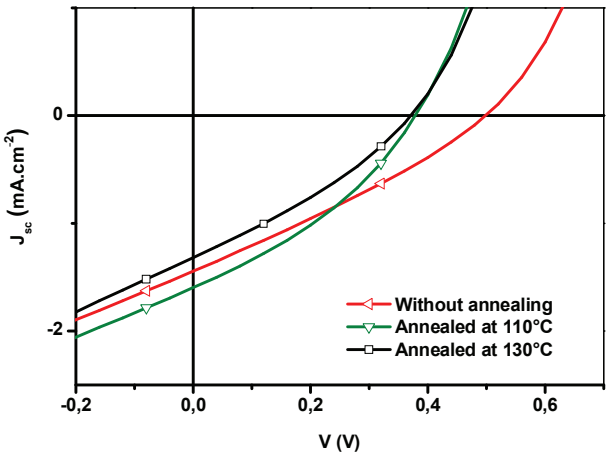

Figure 5.3: Current density versus voltage for photovoltaic devices built from blends of 3,6-PCDOTBT:PCBM at 1:3 ratio under simulated solar illumination (AM 1.5, 100 mW·cm^{-2}).

5.4 Morphologies of polymer/PCBM blends

Further insights can be gained by studying the morphology of the polymer: PCBM layers in test cells. They were studied by AFM. AFM pictures of PCDTBT:PCBM films show a rather high surface roughness of ca. 8 nm (1:1 PCDTBT: PCBM blend), 2.5 nm (1:3) and 3.1 nm (1:5). In addition to this, the presence of large holes with diameters up to 200-300 nm and a depth of several tens of nanometers can be observed (Figure 5.4) which might contribute to the low V_{oc} obtained for these blends. The surface of the 3,6-PCDOTBT:PCBM film is even more irregular as compared to the PCDTBT:PCBM film. The microscopic image is characterized by circular holes and craters of diameters exceeding 1 µm (Figure 5.5). The absences of bumps on the image seem to indicate that the polymer is well solubilized in ortho-dichlorobenzene, thanks to the presence of alkyl chains that should increase solubility of the polymer.

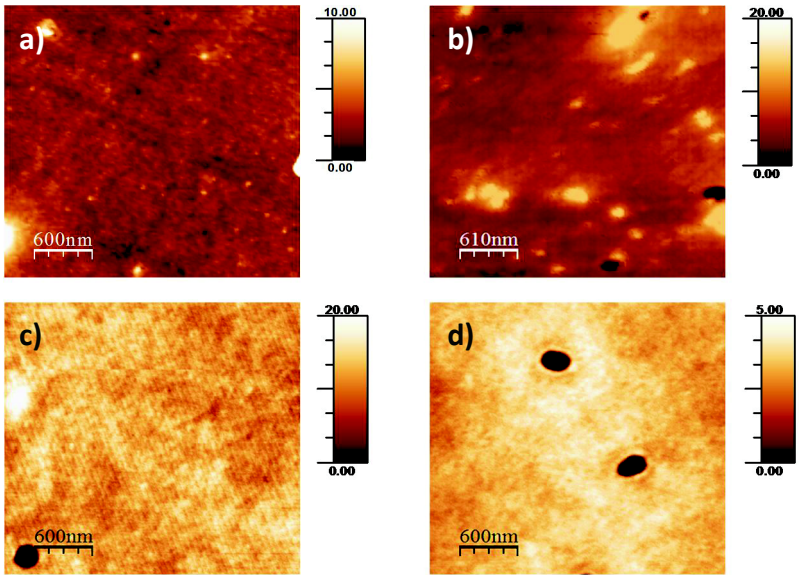

Figure 5.4: AFM images (3 µm x 3 µm) of the films surface morphology (non-contact tapping mode) of the 3,6-PCDTBT (a) and of 3,6-PCDTBT:PCBM 1:3 (b), 1:4 (c) and 1:5 (d).

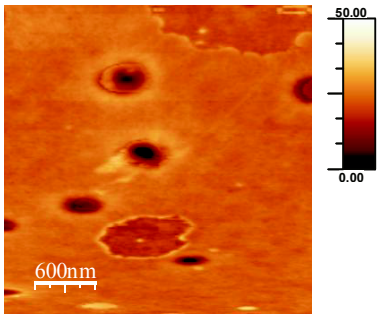

Figure 5.5: AFM image (3 µm x 3 µm) of the film surface morphology (non-contact tapping mode) of the 3,6-PCDOTBT:PCBM (1:3) deposed by spin-coating on PEDOT:PSS.

5.5 Hole carrier mobility

The measurements of the charge carriers mobility in BHJs may also contribute to better understanding the factors limiting the performance of BHJs fabricated from PCDTBT. The mobility was measured by space-charge limited current (SCLC) (see Figure 5.6) in hole only devices of the following architecture: cathode/PEDOT:PSS/active layer(polymer/PCBM blends)/PEDOT:PSS/Al; where the PEDOT:PSS is the electrons stopping layer.

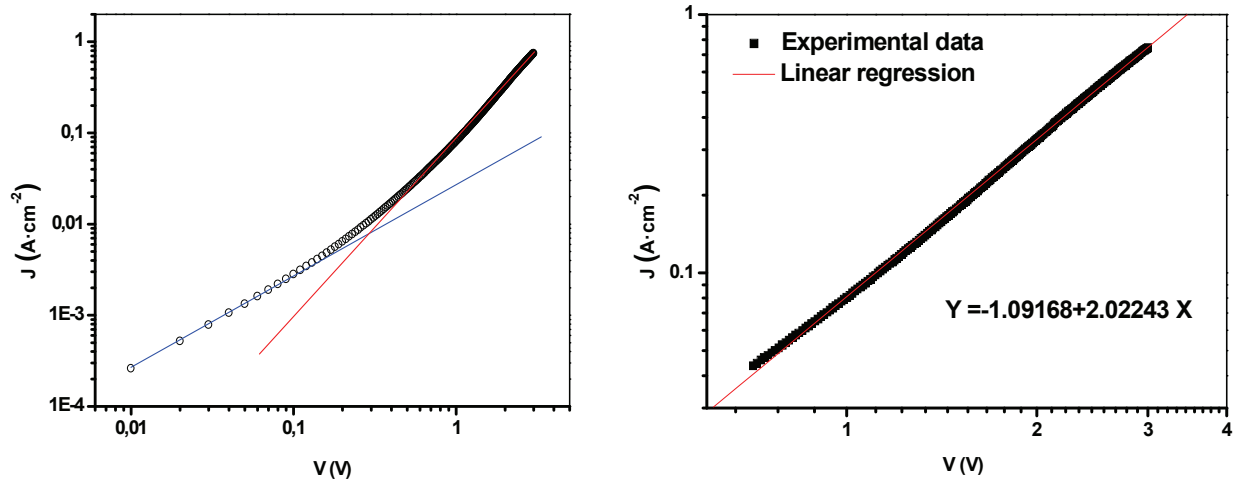

Figure 5.6: Hole carrier mobility (a-b) through the SCLC method for a 3,6-PCDTBT:PCBM 1:3 film.

For high tensions, the current density follows the Mott- Gurney low [1]:

$$J = \frac{9}{8} \cdot \varepsilon_0 \cdot \varepsilon_r \cdot \mu \cdot \frac{V^2}{d^3}$$

where μ is the mobility, ε_0 is the electric permittivity in the vacuum, ε_r the relative permittivity and d the thickness of the film. As a consequence the mobility, through the SCLC method, could be estimated thanks to a linear regression, considering $\varepsilon_r = 3$, typical of these systems.[2]

The measured hole mobility of 3,6-PCDTBT ($1.4 \cdot 10^{-7} cm^2 \cdot V^{-1} \cdot s^{-1}$) is comparable with that reported for not annealed regioregular P3HT: PCBM (3.10^{-8} $cm^2 \cdot V^{-1} \cdot s^{-1}$), but it remains much lower than hole mobility of 2,7-linked polycarbazole derivatives in blends with PCBM (up to 4.10^{-4} $cm^2 \cdot V^{-1} \cdot s^{-1}$).[3] This value can be related to a low-molecular-weight (M_w = 2.8 kDa and M_n = 1.61 kDa) of the studied polymer, since the hole mobility of π-conjugated polymers is known to increase over several orders of magnitude, with the molecular weight, as was measured for different alkyl derivatives of polythiophene.[4]

5.6 Bulk heterojunction TPD *push-pull* derivative copolymers blended with PCBM

Two polymers deriving both from the BTD family (**P3**) and from the carbazole family (**P6**) were chosen to be tested in preliminary photovoltaic measurements in the *Laboratory of Electractive and Photoactive Polymers at the Laval University (Québec - Canada).*

P3 was selected because it displayed a quasi-reversible cyclic voltammogramm during electrochemical reduction (see Figure 3.4 c and d), a low optical gap and the broadest spectrum facilitating the most effective photons harvesting among the TPD polymers studied. In addition BTD derivatives and in particular TPD-BTD polymers showed interesting performances reaching a PCE of 6.8%. For this reason the study of this family seemed to be interesting in view of the development of new performing derivative materials.

Concerning the carbazole polymers, the choice was addressed on **P6** because it was the only one with a good compromise between the molecular weight, stability and processability. In addition, its HOMO and LUMO positions appropriately match those of the PCBM acceptor.

5.6.1 Blends of P3 and P6 with PCBM

The bulk-heterojunction was fabricated by blending **P3** and **P6** with [6,6]-phenyl-C61-butyric acid methyl ester ([60]PCBM) in o-dichlorobenzene (ODCB) at 1:2 ratio. (See preparation details in the *Experimental Part*).

J-V characteristics obtained for the **P3/PCBM** blend are encouraging, showing good V_{oc} and an interesting power conversion efficiency of about 1.63% for a preliminary test (see Figure 5.7).[5]

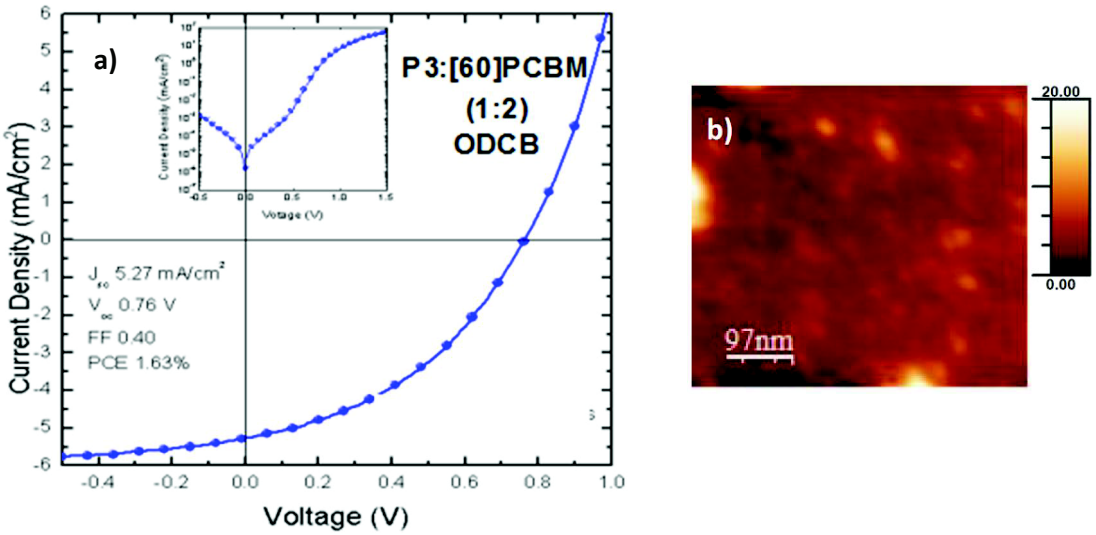

Figure 5.7: a) J-V characteristics under simulated solar illumination (AM 1.5, 100 mW·cm^{-2}) of a solar cell P3:PCBM 1:2 deposited on ITO glass covered by a spin-coated layer of PEDOT:PSS starting from a solution of 5 mg·mL^{-1} polymer concentration in ortho-dichlorobenzene. b) AFM image (3 µm x 3 µm) of the film surface morphology (non-contact tapping mode) of the P3:PCBM 1:3 (e), in ortho-dichlorobenzene, deposed by spin-coating on PEDOT:PSS.

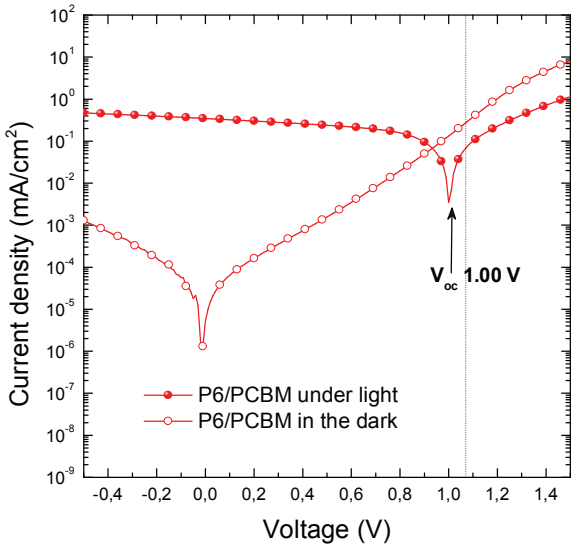

Fig.5.8: J-V characteristics under simulated solar illumination (AM 1.5, 100 mW·cm^{-2}) of solar cells P6:PCBM 1:2 deposited on ITO glass covered by a spin-coated layer of PEDOT:PSS starting from a solution of 10 mg·mL^{-1} polymer concentration in ortho-dichlorobenzene.

The results obtained for a 90 nm thick film of **P6** were as follows: a J_{sc} of about - 0.35 mA·cm^{-2}, a high value of V_{oc} (1.00 V), a FF of 0.39, a low PCE of 0.13% and a J_0 of 4.4 × 10^{-17} mA·cm^{-2}. The V_{oc} value is really interesting because it seems a typical characteristic of TPD-carbazole polymers, reaching V_{oc} values of 1.07 V.[6]

We tend to rationalize that low efficiencies obtained for the P6/PCBM blend could be attributed not only to the need of further optimization, but they can already find an explanation in the results of morphological studies. AFM images show (see Figure 5.9) the presence of holes in the bulk heterojunction active layer which could disturb or limit the transport of charges to the electrodes.

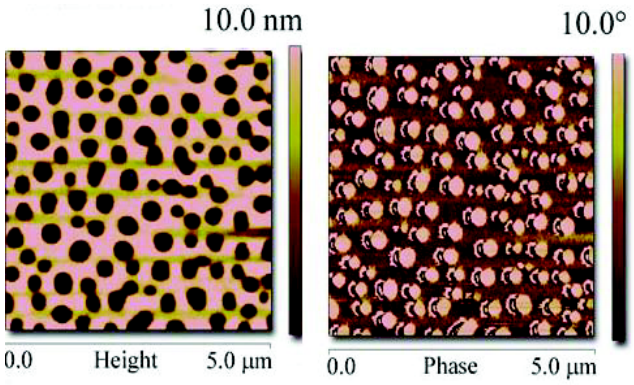

Figure 5.9: AFM images acquired by tapping mode (height and phase images are shown for P6/[60]PCBM blends).

5.7 Preliminary photovoltaic tests on synthesized materials - From polymers to devices

5.7.1 Problem Description

The research presented in this chapter was carried out in close collaboration with Doctor Jerome Faure-Vincent who's developed the BHJs fabrication and testing procedure in SPrAM as well as with his Master 2 student Onintza Ross. The developed procedures, which constituted a new direction in the SPrAM research were verified by optimizing and testing well known BHJs based on P3HT and the 2,7-PCDTBT. PCE of 0.63% for the P3HT:PCBM [7] and of 1.45% for the PCDTBT:PCBM [8] obtained for BHJs processed in open air are encouraging but still not sufficient to assure the process validation.

5.7.2 Solar Cell Preparation

ITO substrates (from the PGO Company) were patterned with a mixture of HCl: HNO_3 (3:1). The etched substrates were then cleaned in an ultrasonic bath with acetone and ethanol for 10 min each, being followed by an UV ozone treatment during 20 min. A layer of PEDOT: PSS was spin-coated (40 nm) over the substrate (40 s at 1500 rpm then 40 s at 2000 rpm) and dried under vacuum for 1h at 120°C. For active layer deposition, polymers were dissolved with [6,6]-phenyl-C-methylbutanoate ($PC_{60}BM$ and $PC_{71}BM$) in ortho-dichlorobenzene (ODCB) and maintained under permanent stirring overnight.

In some cases, addition of 2.5% diiodooctane (DIO) was also done. A concentration between 5 and 20 mg/ml was used depending on polymers. Solutions were then filtered (0.45µm) and spin coated over the PEDOT: PSS layer. The thicknesses of the active layers varied between 80 and 120 nm. Substrates were dried under secondary vacuum (10-8 mbar) during 2h and transferred to an evaporator for the aluminum or silver electrode (100 nm) deposition. Ti/Au contacts (15/40 nm) were used for charge collection and sample annealing was done after the electrode deposition in a glove-box. Note that the whole procedure except the electrical measurements was done in open air and the deposition of the intermediate LiF layer (facilitating the injection of electrons) was not possible in the laboratory.

5.7.3 Electrode materials selection - aluminum vs silver

To verify the validity of the newly developed procedure, commercially available 2,7-poly(carbazole) of known photovoltaic properties was first tested. Protocols coming from the literature [9] were considered and, consequently, aluminum contacts were used. At the beginning PCE values exceeding 1% could not be reached. Moreover the electrical characteristics showed "S-shape" which indicated a possible charge extraction problem. This kind of problem could be overcome improving contacts between the electrodes and the active layer, yielding a decrease in the series resistance and, by consequence, improving of the *J-V* curves and increasing the photogenerated current.

It could be possible that, due to the open air process, active layer materials, involved on the device fabrication, were oxidized causing a variation of HOMO and LUMO levels and an ineffective charge transfer between the donor, the acceptor and the electrode materials.

In addition to this, oxygen could also affect the aluminum cathode by creating a thin layer of alumina (Al_2O_3), a passivation, insulating layer which prevented charge transfer from the active layer to the electrodes. In addition, a tendency of Al to migrate into the polymer film should not have been be neglected. These migrations can not only destroy the polymer film but also create some kind of interface between the

active layer and the electrode avoiding any charge extraction.[10]

For these reasons, some preliminary tests were done, replacing the aluminum electrode by a silver electrode, characterized by a lower Fermi level (*EF = -4.6 eV*) which should provide a better matching of the orbital energy levels and an easier electron extraction. The decision was supported a the simulation [10] demonstrating a negative impact of a bad energy level alignment between the active materials and the aluminum electrodes on the collection of electrons (Figure 5.10 b).

As seen from the *J-V* curve corresponding to the reference blend of 2,7-PCDTBT/PCBM, the V_{oc} value decreased because the of the smaller difference between the work functions of both electrodes *i.e.* ITO and Ag. On the other hand, a short circuit current of -7.06 mA·cm^{-2} was reached, demonstrating a better energy level matching in the case of the Ag electrode.

This change in the device fabrication allowed to obtain a PCDTBT based device showing a power conversion efficiency of 1.45%, significantly higher than the efficiency measured for the device with the Al electrode (1%) (see Figure 5.10 a).

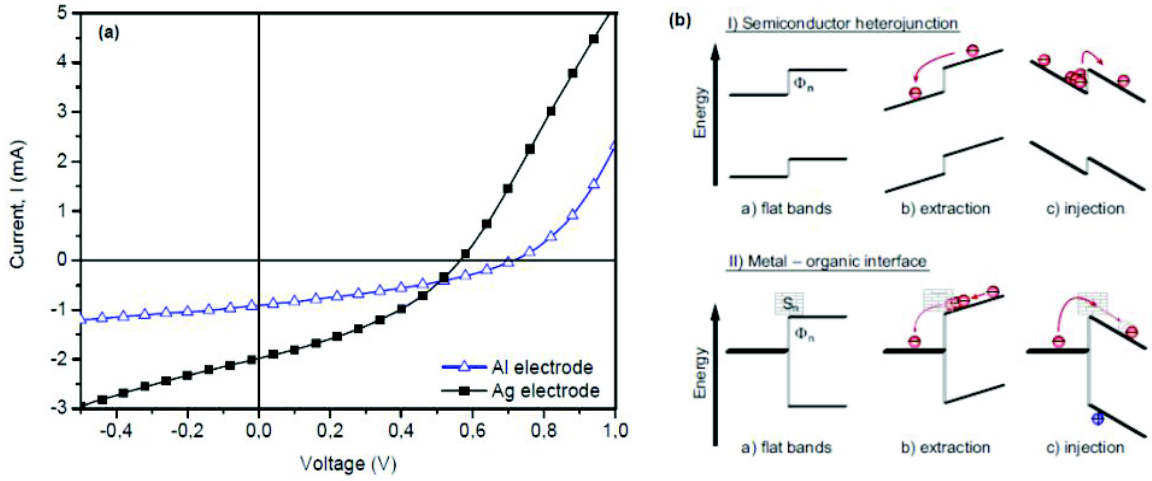

Figure 5.10: a) Comparison of the I-V curves of the reference blend of 2,7-PCDTBT/PCBM for aluminum and silver electrode devices.b) Negative impact of on the electron collection of a bad energy level alignment between active materials and aluminum electrodes.

For this reason, the use of the Al and Ag electrode should be reexamined. Unfortunately because of some evaporation problems the choice of the Ag electrode was the only possibility in my PhD research.

5.7.4 Preparation and characterization of bulk heterojunctions from copolymers containing 2,7-carbazole subunits (cases of P1, P2 and P5)

P1, **P2** and **P5**, in a form of 10 mg·mL^{-1} solutions in *o*-dichlorobenzene were blended with PCBM or $PC_{70}BM$ in a weight ratio of 1:4 (respectively for polymer and PCBM) following conditions generally used for the processing of 2,7-PCDTBT.[11] The obtained films were yellow-orange in appearance, showing high transparency.

Non-filtered and filtered solutions were tested. In the case of **P1**/$PC_{60}BM$ blends filtration through a 0.45 µm PTFE filter resulted in the loss of *ca.*10% of the polymer initial mass. This is manifested in the UV-*Vis* spectrum by a decrease in the intensity of the polymer π-π* band as compared to the PCBM band (see Figure

5.11). Further depositions were carried out without the solution filtration as not to change the ratio of the blend components.

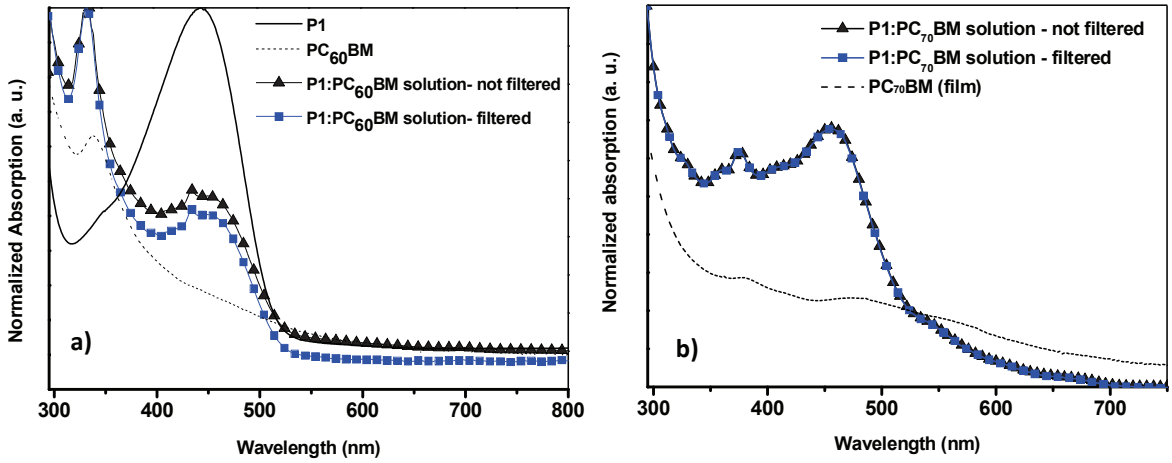

Figure 5.11: a) Comparison of UV-Vis absorption spectra of solutions of P1, $PC_{60}BM$, P1:$PC_{60}BM$ (not filtered) and P1/$PC_{60}BM$ filtered in o-dichlorobenzene. b) Comparison of UV-Vis absorption spectra of $PC_{70}BM$, P1:$PC_{70}BM$ (not filtered) and P1/$PC_{70}BM$ filtered in o-dichlorobenzene.

No change in the polymer concentration was found upon filtration of the solution of **P1** and $PC_{70}BM$.

Some problems appeared in the deposition of **P1** and **P2** films. They formed non-uniform films with a large area of uncovered surface in the center of the substrate: we tend to rationalize it by increased hydrophobic character of these polymers, arising from long dodecyl substituents, which are less compatible with the hydrophilic PEDOT:PSS layer on which they were deposited.

The phenomenon is more relevant for solutions based on $PC_{70}BM$ than for solutions based on $PC_{60}BM$. Relations concerning temperature gradients between the spin-coater apparatus and the substrate should be verified. In Figure 5.11 optical microscopy images present the difference between the surface of a P1/PCBM substrate and the surface of a P1/$PC_{70}BM$ substrate.

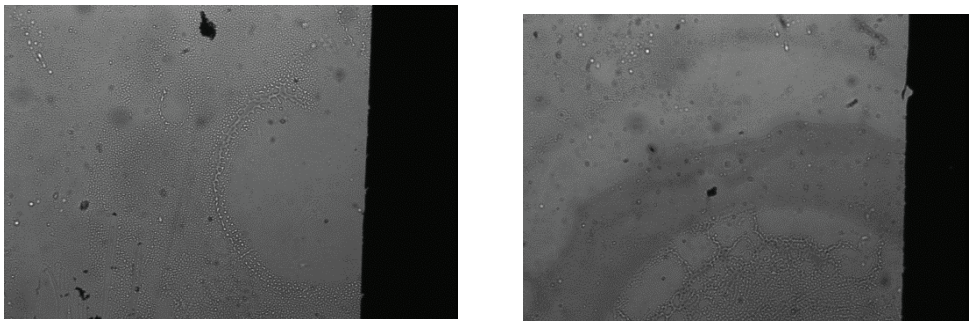

Figure 5.11: Optical Microscopy qualitative images of two substrates deposed with a) P1/PCBM solution and b) P1/$PC_{70}BM$.

In **P5** this effect tends to disappear, confirming that probably the dodecyl substituents play the decisive role in the film deposition. The observed inhomogeneity of the films is, in my opinion the principal cause of the measured low PCE values.

5.7.4.1 *Effect of additives and thermal annealing of the layer on I-V curves*

Some preliminary studies were performed on blends **P1**, **P2** and **P5** with PCBM derivatives.

Films of P1/$PC_{60}BM$, with Ag electrodes, did not give any *J-V* response. Only by changing the electrodes from Ag to Al, a photovoltaic effect of very low PCE (0.014%) was obtained.

Independently of the type of electrodes used, no photovoltaic effect was observed for P1/$PC_{70}BM$, whose microscopic images showed a strong nonuniformity of the layer. In the next step, additives and thermal annealing were used as means of improving the PCE.

A mixture of 2.5% of di-iodooctane to the solution of P1/$PC_{60}BM$ resulted in a weak but measurable photovoltaic effect (see Figure 5.12). Additives generally improve the solubility of fullerene derivatives and the polymer, but their instability in air can affect the performance of the cells.[12]

The effect of thermal annealing was also studied. Two thermal annealing steps, each 10 minutes, during 30 minutes, were applied at 80°C and 100°C inducing relatively important changes in the shape of the *J-V* curves were observed. It is known that the thermal annealing can induce either an improved ordering of the polymer chains within the blend and/or an aggregation of PCBM molecules and thus change the extent of separation of the donor and acceptor phases leading to a bad percolation and charge recombination. The efficiency increase due to the first phenomenon is related to the degree of the crystallinity of the polymer phase. An improvement in PCE values are observed upon annealing of the active layer, they however still remain very low (Table 5.1).

Generally, in amorphous materials such as the poly(carbazole) derivative the PCDTBT (Tg ~ 30ºC) [13] the aggregation of PCBM is the dominant process. Amorphous polymers do not normally improve their morphology upon annealing. Semi-crystalline materials such as P3HT (Tg ~ 67ºC) or (P3OT, Tg ~ -9ºC) [14] can show a favorable higher crystallinity upon thermal annealing. However, the efficiency of an annealing step can change from one system to another; so that; thermal annealing must be studied separately for each system.

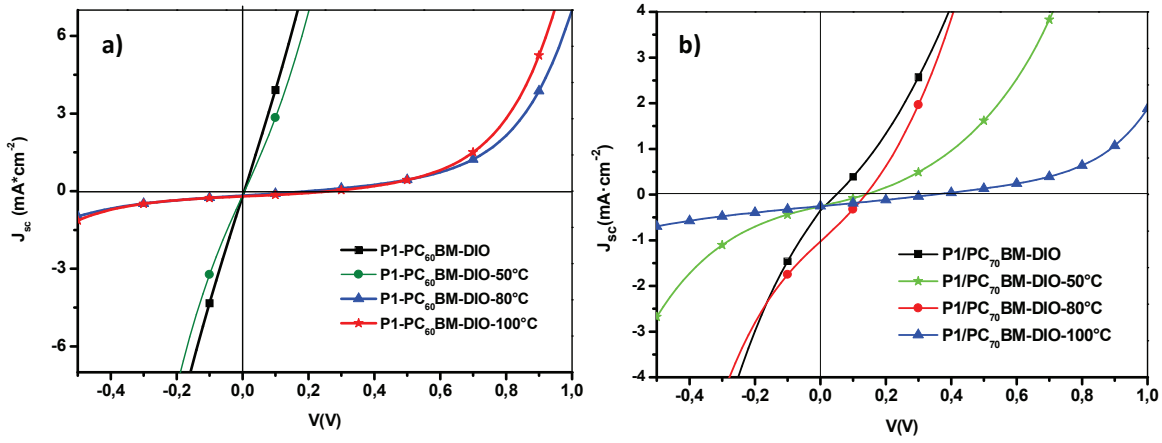

Figure 5.12: J-V characteristics under simulated solar illumination (AM 1.5, 100 mW·cm^{-2}) of solar cells based on: a) P1:$PC_{60}BM$ (1:4 – DIO 2.5% weight ratio) and b) P1:$PC_{70}BM$ (1:4 – DIO 2.5% weight ratio) made on ITO glass covered by a spin-coated layer of PEDOT:PSS starting from a solution of 10 mg·mL^{-1} polymer concentration in the ortho-dichlorobenzene.

System	Efficiency (%)	V_{oc} (V)	FF	J_{sc} ($mA \cdot cm^{-2}$)
P1-C_{60}/Al 80°C	0.00489	0.09932	0.2653	-0.05195
P1-C_{60}/Al 100°C	**0.01459**	**0.26718**	**0.30016**	**-0.05094**
P1-C_{70}/Al	0.003	0.049	0.243	-0.311
P1-C_{70}/A l 50°C	0.008	0.139	0.268	-0.229
P1-C_{70}/Al 80°C	**0.021**	**0.349**	**0.260**	**-0.226**
P1-C_{70}/Al 100°C	**0.015**	**0.158**	**0.273**	**-0.388**

Table 5.1: Photovoltaic characteristics for devices fabricated from blends of P1 at 1:3 ratio under simulated solar illumination (AM 1.5, 100mW·cm^{-2}).

The PCE values of P1/PC_{60}BM blends started to be measurable after annealing at 80°C degrees and further increased after annealing at 100°C. All cell parameters slightly improved (see Table 5.1) probably as a result of an improved percolation in the blend, diminished electron trapping and charge recombination. AFM images, presented in Figure 5.13, clearly show that annealing at 100°C induces an important morphology change.

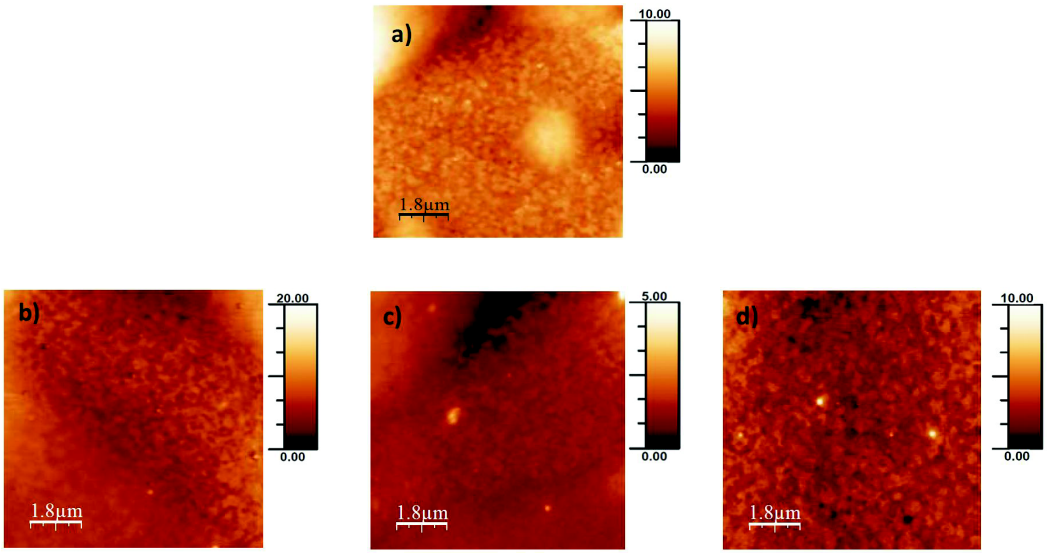

Figure 5.13: AFM images (3 µm x 3 µm) of the films surface morphology (non-contact tapping mode) of the P/PC_{60}BM (1:4) ortho-dichlorobenzene, deposed by spin-coating on PEDOT:PSS a) not annealed and annealed at b) 50°C, c) 80°C and d) 100°C.

For the PC_{70}BM the positive effect of the annealing was visible till the 80°C. Upon further increase of the annealing temperature a worsening of the photovoltaic properties can be noticed. A big change on the morphology could be also observed at 100°C (see Figure 5.14).

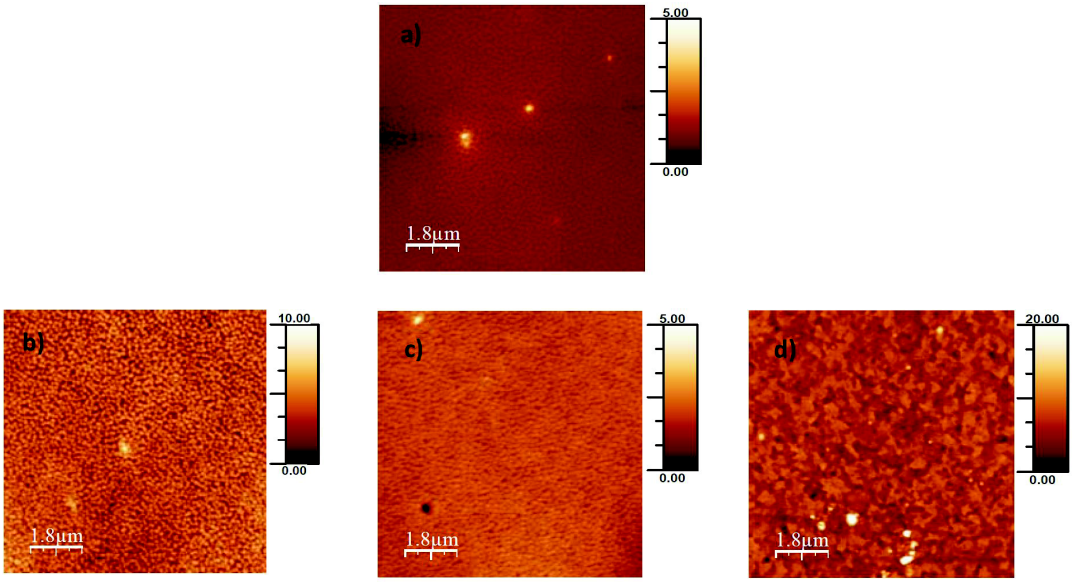

Figure 5.14: AFM images (3 µm x 3 µm) of the films surface morphology (non-contact tapping mode) of the P1/$PC_{70}BM$ (1:4) ortho-dichlorobenzene, deposed by spin-coating on PEDOT:PSS a) not annealed and annealed at b) 50°C, c) 80°C and d) 100°C.

P1/ $PC_{70}BM$ blend was also preliminary tested at the INES. Figure 5.15 shows its J-V characteristics. The fabrication process, detailed in the *Experimental Part*, was carried out in a glove box and differently from the previous set of experiments a configuration glass/ ITO/PEDOT:PSS/**P1**:$PC_{70}BM$/Ca/Al was used. The choice of the $PC_{70}BM$ with **P1** was made following the literature reports [15], which demonstrate better performances of active layers with $PC_{70}BM$ than with $PC_{60}BM$. Six solar cells characterized by the same fabrication conditions were measured, yielding reproducible *J-V* characteristics.

Problems related to films deposition were not more observed (as for previous tests carried out in our laboratory), maybe due to an optimized spin-coating step, and a better *J-V* answer for a weight ratio polymer:$PC_{70}BM$ (1:4) was measured: a V_{oc} of 0.31 V, J_{sc} of -1.46 mA·cm^{-2}, a FF of 0.29 and finally a PCE of 0.13%.

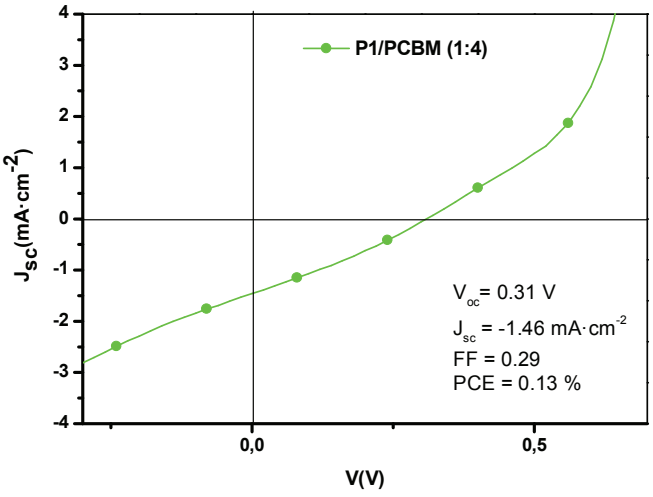

Figure 5.15: J-V characteristics under simulated solar illumination (AM 1.5, 100 mW·cm^{-2}) of solar cells based on P1:$PC_{70}BM$ (1:4) made on ITO glass covered by a spin-coated layer of PEDOT:PSS starting from a solution of 10 mg·mL^{-1} polymer concentration in the orthodichlorobenzene.

No annealing step was carried out on the device substrate because the drying of the cell at 70°C, before the deposition of electrodes, did not bring any change in the morphology of the film and consequently had no effect on the *J-V* parameters.

P2/PCBM blends did not show any measurable photovoltaic effect in preliminary tests. Further optimization test could not be carried out due to the lack of this compound which was prepared in small amounts.

P5, in bulk – heterojunction configuration with PCBM at (1:4) weight ratio and without the adding of additives, yielded a measurable but very weak photovoltaic effect (see Figure 5.16 and Table 5.2).

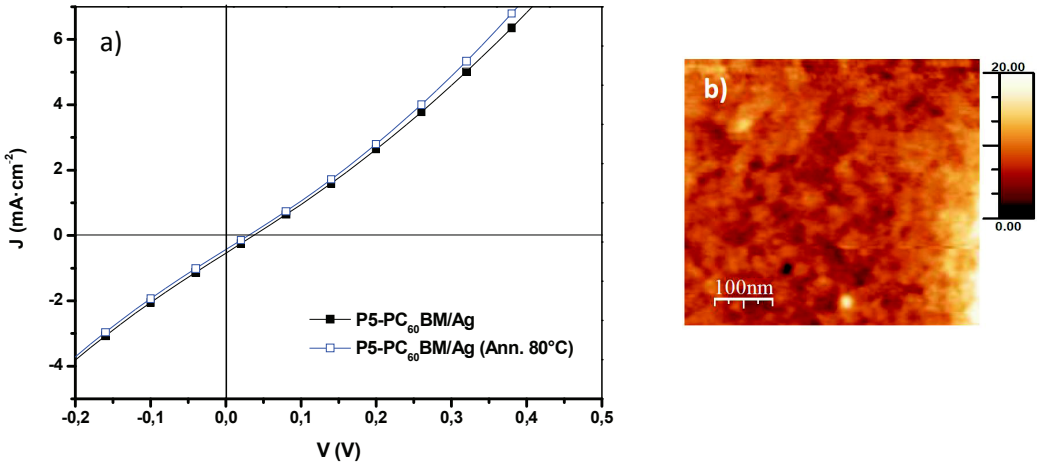

Figure 5.16: a) J-V characteristics under simulated solar illumination (AM 1.5, 100 mW·cm^{-2}) of solar cells P5:PCBM (1:4) made on ITO glass covered by a spin-coated layer of PEDOT:PSS starting from a solution of 10 mg·mL^{-1} polymer concentration in the ortho-dichlorobenzene. b) AFM image (3 µm x 3 µm) of the film surface morphology (non-contact tapping mode) of the P5/PC_{70}BM (1:4) ortho-dichlorobenzene, deposed by spin-coating on PEDOT:PSS.

System	Efficiency (%)	V_{oc} (V)	FF	J_{sc} (mA·cm^{-2})
P5-C_{60}/Ag	0.00447	0.03711	0.24954	-0.48303
P5-C_{60}/Ag 80°C	0.00256	0.22247	0.22247	-0.38545

Table 5.2: Photovoltaic characteristics for devices fabricated from blends of P5:PC_{60}BM at 1:4 ratio under simulated solar illumination (AM 1.5, 100 mW·cm^{-2}).

As in the case of for **P1**, a set of measurements was also carried out for a bulk-heterojunction of P5/PC_{70}BM at (1:4) weight ratio in the INES Laboratory. Compared to **P1** (see Figure 5.15) any relevant answer was measured (see Figure 5.17). Also for this polymer the thermal annealing did not significantly increase the performance of the device.

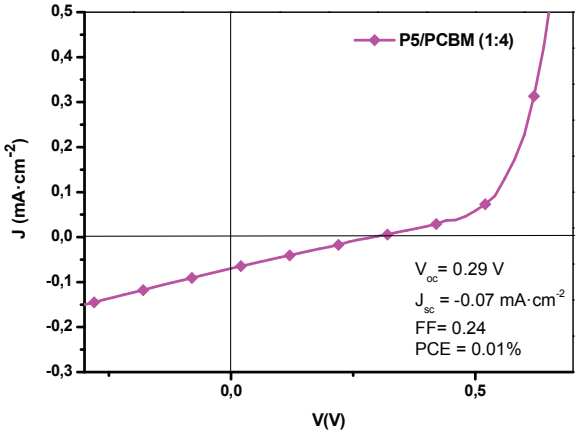

Figure 5.17: J-V characteristics under simulated solar illumination (AM 1.5, 100 mW·cm^{-2}) of solar cells P5:PCBM (1:4) made on ITO glass covered by a spin-coated layer of PEDOT:PSS starting from a solution of 10 mg·mL^{-1} polymer concentration in the ortho-dichlorobenzene.

It could be finally deduced that thiophene spacers in **P1**, characterized by long dodecyl chains, play an important role in the structuration of the polymer phase, changing, as the morphological properties of the polymer/PCBM blends and by consequence improving its electrical transport properties (compare Figure 5.14 and 5.15).

5.7.5 BDT derivatives

Blends of copolymers containing dialkoxybenzodithiophene donor units (**P3** and **P4**) with PCBM were prepared from *o*-dichlorobenzene solutions (5 mg·mL^{-1}). The polymer to PCBM ratio was 1:2. The preparation conditions were established on the bases of already tested procedure developed at the University of Laval. In preliminary tests only **P4** showed a measurable photovoltaic effect. Surprisingly no positive results were obtained for **P3** - the polymer which yielded a PCE of 1.63% in devices fabricated during my stay in the group of Professor Mario Leclerc. Considering the configuration glass/ ITO/PEDOT:PSS/P3 (or **P4**) :PCBM/Ag, films obtained by spin coating from solution of **P3** and **P4** are characterized by a more homogeneous profile than the poly(carbazole) blends. Both **P3** and **P4** where used without additives and the applied thermal annealing process did not result in any significant improvement.

Figure 5.18 a) shows a representative J-V characteristic obtained for the cell with P4/PCBM active layer. In Figure 5.18 b) the blend morphology is presented. The photovoltaic effect is very weak yielding a PCE value of 0.02%.

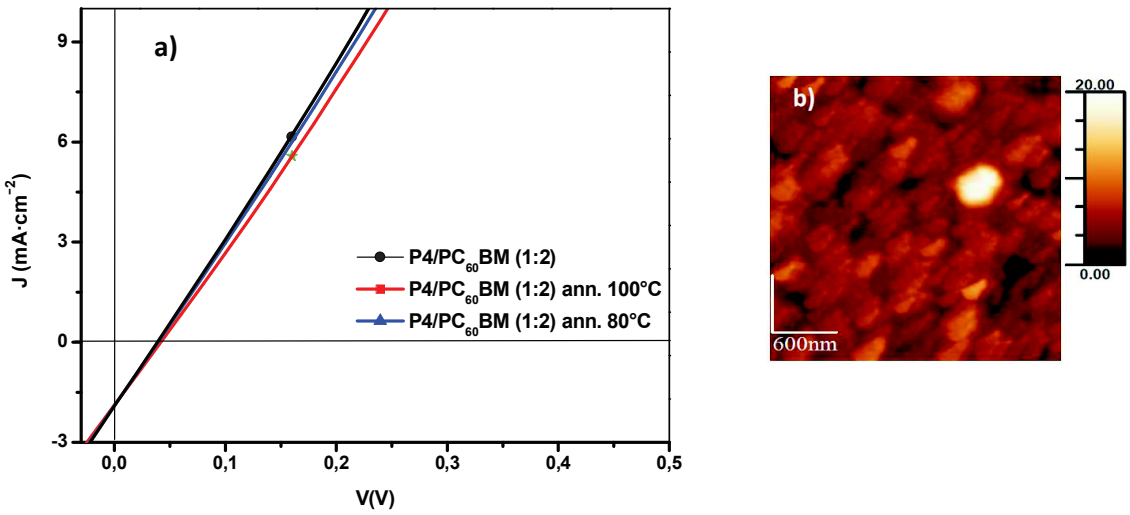

Figure 5.18: a) J-V characteristics under simulated solar illumination (AM 1.5, 100 mW·cm^{-2}) and post-annealing of solar cells P4:PCBM (1:2) made on ITO glass covered by a spin-coated layer of PEDOT:PSS starting from a solution of 10 mg·mL^{-1} polymer concentration in the orthodichlorobenzene. b) AFM image (3 µm x 3 µm) of the film surface morphology (non-contact tapping mode) of the P4/PC$_{70}$BM (1:4) ortho-dichlorobenzene, deposed by spin-coating on PEDOT:PSS.

Further attempts to improve the performace of blends based on **P3** led to the following configuration glass/ITO/PEDOT:PSS/P3:PCBM(1:2)/Ca/Al. In these conditions a measurable photovoltaic effect was registered, yielding the following cell parameters: a V_{oc} of 0.36 V, J_{sc} of -1.57 mA·cm^{-2}, FF of 0.35 and a PCE of 0.20 % (see Figure 5.19).

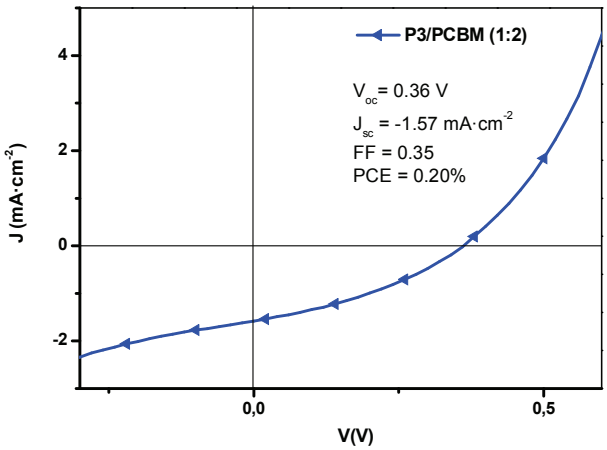

Figure 5.19: J-V characteristics under simulated solar illumination (AM 1.5, 100 mW·cm^{-2}) of solar cells P3:PCBM (1:2) made on ITO glass covered by a spin-coated layer of PEDOT:PSS starting from a solution of 5 mg·mL^{-1} polymer concentration in the ortho-dichlorobenzene.

Large difference in the PCE values obtained for the same polymer (**P3**), using different processing conditions and different configurations, underlines the necessity of precise elaboration of the fabrication procedure in each individual case.

5.7.6 Bithiophene derivatives

P7 belonging to the bisthiophene family of the polymers studied was only preliminary tested. Its choice was stimulated by the literature report indicating that a similar polymer gave an encouraging PCE of about 4%.[16] **P7** was only preliminary tested at the INES Laboratory and the configuration used was the following: ITO/PEDOT:PSS/P7:PCBM(1:1.5)/Ca/Al. Encouraging results were obtained with a V_{oc} of 0.69, J_{sc} of 2.39 mA·cm^{-2}, a FF of 0.35 and finally a PCE of 0.57% (see figure 5.20).

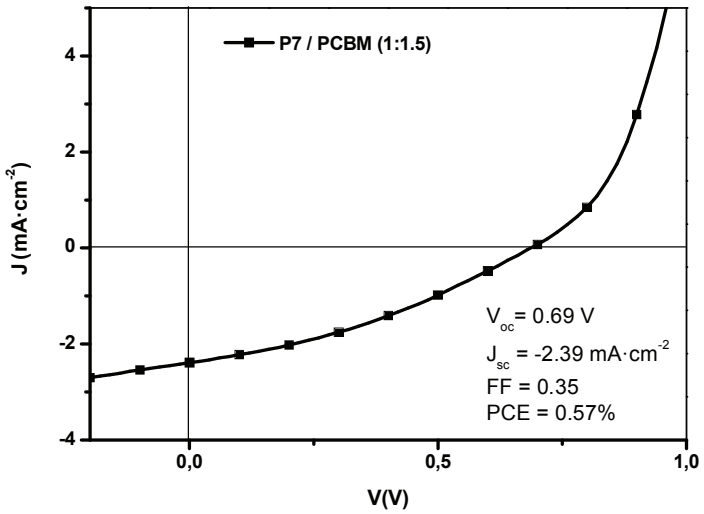

Figure 5.20: J-V characteristics under simulated solar illumination (AM 1.5, 100 mW·cm^{-2}) of solar cells P7:PCBM (1:1.5) made on ITO glass covered by a spin-coated layer of PEDOT:PSS starting from a solution of 8 mg·mL^{-1} polymer concentration in the ortho-dichlorobenzene

5.7.7 IPCE measurements

In collaboration with the INES laboratory I have also performed Incident Photon to Current Efficiency (IPCE) measurements for **P1**, **P3**, **P5** and **P7** (see Figure 5.20).

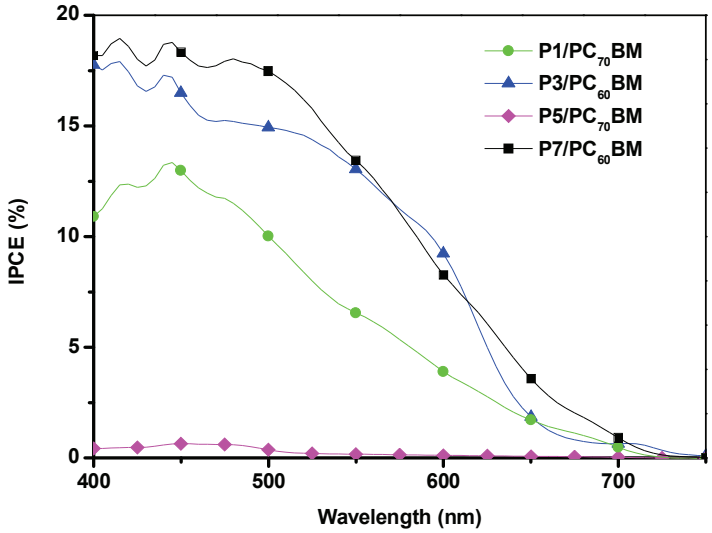

Figure 5.20: IPCE spectra of P1/PC_{60}BM, P3/PCBM, P5/PC_{70}BM and P7/PC_{60}BM.

First, considering the carbazole derivatives **P1** and **P5** is interesting to underline the effect of thiophene spacers passing from **P5** to **P1**. Thiophene allows an important increase of the IPCE for **P1**, reaching 11%. Nevertheless, **P1** tends to absorb mostly around 450 nm and, therefore, only a small fraction of the solar light in the blue part and in the near-UV part of the spectrum is absorbed. It should be underlined that for carbazole derivatives PC_{70}BM rather than PC_{60}BM was used. The first one should allow broad solar spectrum absorption and, its presence, could explain the slow decrease of the slope of the curve.

Passing than to **P3**, according with its lower band gap as compared to **P1**, one can observe not only an increase of IPCE to around 16%, but in addition high IPCE values are recorded for the blue part of the UV-*Vis*-NIR spectrum. A similar, but even more intensive and broader IPCE spectrum was recorded for **P7**.

The behavior of IPCE curve is in agreement with results obtained from *J-V* measurements and the effect of the *push-pull* units on the bandgap of polymers could be discussed. Firstly, all four IPCE spectra show two vibronic structures around 400-450 nm which could be attributed to TPD unit. Then, comparing the spectra slope, after 450 nm, is interesting to observe that the BTD unit in **P3** exhibits broader solar spectrum absorption then the carbazole unit in **P1** and **P5**. Finally, in agreement with *J-V* results, the IPCE of **P7** is the highest one, around 17%. In addition, for this last polymer **P7**, even if it possible to affirm that the bithiophene unit acts an absorption role mostly around 500 nm, according with the band gap value of 2.26 eV, the **P7** spectra could reach wavelength higher than 650 nm. As a consequence to better take advantage of this characteristic the use of the PC_{70}BM acceptor material rather than the PC_{60}BM could be suggested.

5.8 Conclusion

Different polymers were preliminarily tested in different experimental conditions.

First, a complete study on the poly(3,6)carbazole family in BHJ configuration with PCBM allowed to compare two different low band gap copolymers: the 3,6-PCDTBT and 3,6-PCDOTBT. Performances were still very low reaching the best result, with a PCE of about 0.35% for the PCDTBT polymer. We tend to rationalize that, probably, for these polymers the low polymerization degree is one of the principal limiting factor. In addition to this, the steric effect, due to the octyl chains on the 3,6-PCDOTBT, affects the conjugation of the polymer backbone. 3,6-Hole carriers mobilities were measured for PCDTBT polymer demonstrating that mobilities, in poly(3,6) carbazoles are lower than the mobility measured for poly(2,7) carbazole – the best performing polymer of the whole group.

The second two groups of compounds studied were polymers containing thienopyrrolodione acceptor units and 2,7-carbazole or dialkoxybenzothiophene donor units. Of all this polymers **P3** showed the highest PCE values, however detailed studies show that the device performance is very sensitive to the fabrication conditions which must be strictly reproduced in each case, otherwise low PCE values are obtained.

[1] D. Veldman, O. Ipek, S. C. J. Meskers, J. Sweelssen, M. M. Koetse, S. C. Veenstra, J. M. Kroon, S. S. Van Bavel, J. Loos, and R. A. J. Janssen, "Compositional and electric field dependence of the dissociation of charge transfer excitons in alternating polyfluorene copolymer/fullerene blends," *Journal of the American Chemical Society*, vol. 130, no. 24, pp. 7721–7735, 2008.

[2] N. Moliton, "How to model the behaviour of organic photovoltaic cells," *Polymer International*, vol. 55, no. September 2005, pp. 583–600, 2006.

[3] N. Blouin, A. Michaud, D. Gendron, S. Wakim, E. Blair, R. Neagu-Plesu, M. Belletête, G. Durocher, Y. Tao, and M. Leclerc, "Toward a rational design of poly(2,7-carbazole) derivatives for solar cells," *Journal of the American Chemical Society*, vol. 130, no. 2, pp. 732–742, 2008.

[4] J.-M. Verilhac, G. LeBlevennec, D. Djurado, F. Rieutord, M. Chouiki, J.-P. Travers, and A. Pron, "Effect of macromolecular parameters and processing conditions on supramolecular organisation, morphology and electrical transport properties in thin layers of regioregular poly(3-hexylthiophene)," *Synthetic Metals*, vol. 156, no. 11–13, pp. 815–823, 2006.

[5] C. Ottone, P. Berrouard, G. Louarn, S. Beaupré, D. Gendron, M. Zagorska and P. Rannou, A. Najari, S. Sadki, M. Leclerc, A. Pron, "Donor-acceptor alternating copolymers containing thienopyrroledione electron accepting units: Preparation, redox behaviour, and application to photovoltaic cells," *Polymer Chemistry*, vol. 156, p. 2355, 2012.

[6] A. Najari, P. Berrouard, C. Ottone, M. Boivin, Y. Zou, D. Gendron, W. Caron, P. Legros, C. N. Allen, S. Sadki, and M. Leclerc, "High Open-Circuit VoltageSolar Cells Based on New Thieno[3,4-c]pyrrole-4,6-dioneand 2,7-Carbazole Copolymers," *Macromolecules*, vol. 45, no. 4, pp. 1833–1838, 2012.

[7] W. Ma, C. Yang, X. Gong, K. Lee, and A. J. Heeger, "Thermally Stable, Efficient Polymer Solar Cells with Nanoscale Control of the Interpenetrating Network Morphology," *Advanced Functional Materials*, vol. 15, no. 10, pp. 1617–1622, 2005.

[8] S. Wakim, S. Beaupré, N. Blouin, B.-R. Aich, S. Rodman, R. Gaudiana, Y. Tao, and M. Leclerc, "Highly efficient organic solar cells based on a poly(2,7-carbazole) derivative," *Journal of Materials Chemistry*, vol. 19, no. 30, p. 5351, 2009.

[9] N. Blouin, A. Michaud, and M. Leclerc, "A Low-Bandgap Poly(2,7-Carbazole) Derivative for Use in High-Performance Solar Cells," *Advanced Materials*, vol. 19, no. 17, pp. 2295–2300, 2007.

[10] A. Wagenpfahl, D. Rauh, M. Binder, C. Deibel, and V. Dyakonov, "S-shaped current-voltage characteristics of organic solar devices," *Physical Review B*, vol. 82, no. 11, p. 9, 2010.

[11] M. C. Scharber, D. Mühlbacher, M. Koppe, P. Denk, C. Waldauf, A. J. Heeger, and C. J. Brabec, "Design Rules for Donors in Bulk-Heterojunction Solar Cells—Towards 10% Energy-Conversion Efficiency," *Advanced Materials*, vol. 18, no. 6, pp. 789–794, 2006.

[12] G. Li, V. Shrotriya, J. Huang, Y. Yao, T. Moriarty, K. Emery, and Y. Yang, "High-efficiency solution processable polymer photovoltaic cells by self-organization of polymer blends," *Nature Materials*, vol. 4, no. 11, pp. 864–868, Oct. 2005.

[13] S. Cho, J. H. Seo, S. H. Park, S. Beaupré, M. Leclerc, and A. J. Heeger, "A thermally stable semiconducting polymer," *Advanced materials*, vol. 22, no. 11, pp. 1253–1257, 2010.

[14] M. Aryal, K. Trivedi, and W. W. Hu, "Nano-confinement induced chain alignment in ordered P3HT nanostructures defined by nanoimprint lithography," *American Chemical Society nano*, vol. 3, no. 10, pp. 3085–3090, 2009.

[15] F. B. Kooistra, V. D. Mihailetchi, L. M. Popescu, D. Kronholm, P. W. M. Blom, and J. C. Hummelen, "New C_{84} Derivative and Its Application in a Bulk Heterojunction Solar Cell," *Chemistry of Materials*, vol. 18, no. 13, pp. 3068–3073, 2006.

[16] Y. Zou, A. Najari, P. Berrouard, and S. Beaupre, "A Thieno [3 , 4-c] pyrrole-4 , 6-dione-Based Copolymer for Efficient Solar Cells," *Journal of the American Chemical Society*, vol. 132, no. 15, pp. 5330–5331, 2010.

[17] S. Cowan, A. Roy, and A. Heeger, "Recombination in polymer-fullerene bulk heterojunction solar cells," *Physical Review B*, vol. 82, no. 24, pp. 1–10, 2010.

General Conclusion

In this work the attention was focused on the synthesis of new low-band gap polymers and on the adopted chemical strategy aims on developing the so called *push-pull* copolymers: formed by a donor (*push*) and an acceptor (*pull*) electron unit in the polymer backbone. Starting from the chemical synthesis of each monomeric unit with the respective copolymerization, a complete physico-chemical study was carried out on synthesized materials. The synthesis of particularly designed copolymers allowed a detailed study by EPR spectroscopy concerning inter and intra molecular charge transfer in the polymer backbone and from the polymer to acceptor material (as PCBM or nanocrystals). Problems related to test of materials and device fabrications were also broached.

The state of the art of the most known accepting and donating units motivate the choice of the starting moieties later used for the synthesis of the target polymers. The most known *push* and *pull* units were presented, focusing the attention respectively on benzothiadiazole and diketopyrroledione units and on carbazole and benzodithiophene units. Properties of the accepting units were also analyzed, focusing the attention on fullerene derivatives and nanocrystals.

In the second chapter by selecting acceptor (benzothiadiazole or thienopyrrolodione derivatives) and donor (3,6-carbazole, 2,7-carbazole, dialkoxybenzodithiophene) units of different donor-acceptor (DA) strength, it is possible to prepare copolymers with tunable physical properties which, mostly, seem very promising for photovoltaic applications. Moreover, several C-C coupling methods can be efficiently used for the preparation of these tailor-made copolymers, such as Stille, Suzuki and direct coupling.

With the exception of **P1** all other polymers, synthesized in the frame of this research, show moderate M_n and require fractioning to reduce their polydispersity indices. Improvement is therefore needed in establishing such conditions of the polycondensation which lead to low PDI values without the necessity of *post*-polycondensation fractioning.

In the third chapter a detailed physico-chemical characterization was carried out to investigate the potential of materials for photovoltaic application: complementary spectroscopic, electrochemical, diffraction and thermal techniques enabled us to precisely determine properties which could be crucial for the application of materials in the photovoltaic field. Electrochemical and spectro-electrochemical investigations clearly showed that the redox properties of all synthesized polymers make them suitable candidates for applications as donor components of the BHJ layers with PCBM as the acceptor component. The positions of the HOMO and LUMO levels derived from these studies turned out to be in a very good agreement with the ones obtained by DFT calculations. Moreover the developed vibrational model enabled us to precisely attribute all Raman and IR modes of the synthesized (co)polymers. Although all synthesized polymers show appropriate redox properties for BHJ applications **P2**, **P3** and **P4** seem superior in this respect because of better matching of their UV-*Vis*-NIR spectra with solar spectrum.

Thanks to a detailed EPR under illumination and EPR tracing experiments, we have succeeded in characterizing the various electronic transfers in particularly designed *push-pull* copolymers blended with two types of electron acceptor materials: PCBM and $CuInS_2$ nanocrystals. It was possible to evidence intra-molecular electronic transfers, the so called *push-pull* effect, in three studied polymers, by attributing a specific EPR fingerprint (EPR tracing) to each *push* and *pull* species present in polymer backbone. Then, we have addressed the problem of electronic transfer between polymers (donors) and PCMB or nanocrystals (acceptors). It was demonstrated for all considered (co)polymers that an evident charge transfer appears from the conjugated macromolecule to PCBM. On the other hand for polymers blended with NCs only a very weak signal, ascribed to the charge transfer, appears. In this case, knowing that the NCs EPR signal could not be detected, the demonstration of the phenomenon is given by the fingerprint of the polymer appearing only under illumination.

DFT calculations of the spin density of the radical cation for **P2** and **P3** are in agreement with the EPR signals. For the future research, a similar study with an illumination at 600 nm, fitting better with the maximum of the absorption band of the studied polymers should give complementary information.

Finally, the presented (co)polymers were preliminarily tested in different experimental conditions. First, a complete study on the poly(3,6)carbazole family in BHJ configuration with PCBM allowed to compare two different low band gap copolymers: the 3,6-PCDTBT and 3,6-PCDOTBT. Performances were still very low reaching the best result, with a PCE of about 0.35% for the PCDTBT polymer. We tend to rationalize that, probably, for these polymers the low polymerization degree is one of the principal limiting factor. In addition to this, the steric effect, due to the octyl chains on the 3,6-PCDOTBT, affects the conjugation of the polymer backbone. 3,6-Hole carriers mobilities were measured for PCDTBT polymer demonstrating that mobilities, in poly(3,6 carbazoles) are lower than the mobility measured for poly(2,7-carbazole) – the best performing polymer of the whole group.

The second two groups of compounds studied were polymers containing thienopyrrolodione acceptor units and 2,7-carbazole or dialkoxybenzothiophene donor units. Of all this polymers **P3** showed the highest PCE values, however detailed studies show that the device performance is very sensitive to the fabrication conditions which must be strictly reproduced in each case, otherwise low PCE values are obtained.

Further electrical studies will also be done, such as SCLC experiments for the remaining polymers, to measure the mobility of charges within the material and to get a better understanding of the system.

To conclude, as a last optimization technique, taking into account the unavailability of an air-free environment and the impossibility to depose interstitial layers (LiF, Ca…) between the active layer and the electrodes, inversed solar cells could be tested where the systems are known to be environmentally more stable. This includes the development of ZnO and TiO_x layers from sol-gel processes.

In addition, the research and development of new *push-pull* units could open others promising route on chemical engineering dressed to organic photovoltaic materials.

Experimental Part

This part dealt with the presentation of characterization instruments used during this project and the protocols' synthesis of products. It is important to underline that a part of the work was carried out in the "Laboratory of Electroactive and Photoactive polymers" at the Laval University (Canada), where different instrumentation from the SPrAM/INAC laboratory were used for the materials characterization.

a) Instrumentations

UV-*Vis* absorption spectroscopy

Absorption spectra in solution and at the solid state were recorded using a Bio-Tek Instruments UVIKON XS spectrophotomer, Varian Cary 500 or Hewlett Packard HP8452A.

Photoluminescence spectroscopy

The photoluminescence spectra were measured with a spectrofluorimeter Hitachi F-4500.

Electrochemistry

Cyclic voltammetry investigations were performed on either an Autolab potentiostat PGSTAT302, interfaced to a PC computer, or on a Solartron 1287 potentiostat. The studied polymers were deposited onto a platinum working electrode. The experiments were carried out in 0.1 M solution of NBu_4BF_4 in acetonitrile either in a glove box or under constant argon flow. An Ag wire was used as a pseudo-reference electrode and its potential was calibrated at each experiment using Fc^+/Fc couple. Pt (area of 0.785 mm^2) sheet served as a counter electrode.

Nuclear Magnetic Resonance (NMR)

^1H and ^{13}C NMR spectra were recorded using a Varian AS400 or 300 and a 200MHz Bruker Spectrometer.

Atomic Force Microscopy (AFM)

AFM images were recorded with Nanosurf Mobile S instrument in non-contact *tapping*® mode or in contact mode.

X rays diffraction

X-ray diffractogram were recorded using a Siemens D5000 X-ray diffractometer with a $CuK_{\alpha 1}$ radiation source (λ = 1.540598 Å). The operation power was 40 kV, 30 mA and the collimator was 0.8 mm in diameter.

Thermogravimetric characterization

Thermogravimetric analysis (TGA) measurements were carried out with a Mettler Toledo TGA SDTA 851e apparatus at a heating rate of 20 $K \cdot min^{-1}$ under a nitrogen atmosphere. The temperature of degradation (T_d) corresponds to a 5% weight loss.

Differential scanning calorimetry (DSC)

Differential scanning calorimetry (DSC) experiments were performed on a Mettler Toledo DSC823e instrument, calibrated with ultrapure indium. Glass transition temperatures (T_g) were measured at a scanning rate of 20 $K \cdot min^{-1}$, under a nitrogen flow.

UV-*Vis*-NIR spectroelectrochemistry

For the UV-*Vis*-NIR spectroelectrochemical studies, **P1** was deposited onto an ITO electrode. Ag/0.1 M $AgNO_3$ served as a reference electrode and a Pt sheet as a counter electrode. As in the case of cyclic voltammetry, the experiments were carried out in 0.1 M NBu_4BF_4/acetonitrile electrolyte.

Raman spectroelectrochemistry

For Raman spectroelectrochemistry a thin layer of **P1** was deposited onto a platinum electrode. The reference and counter electrodes as well as the electrolyte were the same as in the case of UV-*Vis*-NIR spectroelectrochemistry investigations. The UV-*Vis*-NIR spectra were recorded on a Varian Cary 5000 spectrometer whereas the Raman spectra were obtained using a FT Raman Bruker RFS 100 spectrometer with the near-IR excitation line (1064 nm). UV- *Vis* spectra were recorded using a Bio-Tek Instruments UVIKON XS spectrometer.

Fourier Transform Infrared Spectroscopy

FT-IR spectra were recorded using a FT-IR Bruker Vertex 70 spectrometer.

Elementary Analysis and mass Spectrometry

A Microanalyzer Flash EA1112 CHNS/O Thermo Electron was used for the Elementary Analysis.

For the mass spectrometry analysis was used a LC/MS-TOF Agilent 6210 using ESI electrospray ionization. Products were previously solubilized at a concentration of 0.1 $mg \cdot mL^{-1}$ in HPLC quality solvent and filtered using a PTFE filter of 0.45 um.

Analytical Size-Exclusion Chromatography (SEC)

Analytical Size-Exclusion Chromatography (SEC) fractionation and characterizations on a Chemstation 1260 (Agilent Technologies) equipped with a 300x7.5 mm PLgel Mixed-D 5 µm/104 Å column (Varian), a diode array UV-Vis detector (DAD) and a fraction collector.

Analytical size exclusion chromatography (SEC) characterizations of the fractions of the four *push-pull* low band gap alternated copolymers **P1-P4** obtained after their initial purifications by soxhlet extraction and of the molecular weight-calibrated and low molar weight dispersity value's P1 and P6-F1/F9 sub-fractions were performed on a Chemstation 1260 (Agilent Technologies) equipped with a 300x7.5 mm PL gel Mixed-D 5 µm/104 Å column (Varian), a diode array UV-*Vis* detector (DAD) and a fraction collector.

The molecular weight-calibrated and low molecular weight dispersity value's sub-fractions **P1** and **P6**-F1/F9 sub-fractions were obtained by the SEC fractionation of the soluble fraction in chloroform of the copolymer **P1**. In a single analytical SEC fractionation cycle, up to 9 fractions of an equal 0.25 mL volume were collected with the fraction collector. Five consecutive analytical SEC fractionation cycles were then performed resulting in a cumulated volume of ca. 1.25 mL per sub-fraction. Typically ca. 1.0 $mg \cdot g^{-1}$ HPLC-grade of amylene-stabilized $CHCl_3$ (Acros, 99.8%) stock solutions of the fractions of **P1-P4** after their initial purifications by soxhlet extraction were analyzed. The obtained 1.25 mL $CHCl_3$ solutions of the **P1** and **P6**-F1/F9 sub-fractions were either concentrated or diluted in order to facilitate their analytical SEC characterizations. The column temperature and the flow rate were fixed to 313 K and 1 $mL \cdot min^{-1}$, respectively. The calibration curve was built using 13 polystyrene (PS) narrow standards.

Two runs of 20 µL injection of appropriately diluted or concentrated HPLC-grade of amylene-stabilized $CHCl_3$ (Acros, 99.8%) solutions were typically analyzed for each sample with an UV-*Vis* detection at 375 nm. Macromolecular parameters deduced from the analytical SEC characterizations of the fractions of *push-pull* low band gap alternated copolymers **P1-P4** obtained after their initial purification by soxhlet extractions and of the molecular weight-calibrated and low molar weight dispersity index value's **P1**-F1/F9 sub-fractions are finally obtained.

Electron Paramagnetic Resonance

The EPR experiments were made using an X-band (3cm, 9.7 GHz) ER 200D SRC Bruker spectrometer with 100 kHz field ac modulation for phase-lock detection. The sample is located in a Bruker ER 41040R Optical transmission Resonator (unloaded quality factor Q = 7000) and illuminated at 473,3 nm with a CW output power of 22,1 mW by a laser module Oxxius 473L-20-COL-PP-LAS-01186.

Materials and Film Preparation

The procedure for sample preparation is the following. Considering a concentration of polymer of 5 mg/mL in *o*-dichlorobenzene, different solutions were prepared: two solutions were made with reference polymers **P1** and **P3** and other two solutions are prepared blending **P1** and **P3** with [6,6]-phenyl-C61-butyric acid methyl ester ([60]PCBM) at 1:3 (polymer **P1** or P3/PCBM) ratio and with $CuInS_2$ nanocrystals at 1:3 (polymer **P1** or P3/PCBM) ratios respectively. Finally the **P2** polymer is blended with [6,6]-phenyl-C61-butyric acid methyl ester ([60]PCBM) in *o*-dichlorobenzene (ODCB) at 1:3 ratio. After the dissolution of the active layer materials, the solution is drop casted on a flexible substrate of PET/ITO. Films were finally annealed at 110°C for 3 hours and introduced, once cut, on the EPR tube.

b) Chemicals

All starting organic compounds were purchased from Sigma-Aldrich, Acros, Alfa Aesar, or TCI America and used without further purification.

N-Bromosuccinimide (NBS) was purchased from Aldrich, recrystallized from water and dried prior to use. Catalysts were bought from Strem Chemicals. *n*-butyllithium (n-BuLi) was dosed with 4-bisphenylmethanol. The reaction solvents were distilled prior to use (THF from sodium/benzophenone, acetonitrile from CaH_2), the other solvents were usually ACS grade, coming from Sigma-Aldrich, Fluka, Acros or Carlo Erba without further purification. In Suzuki and Stille polymerization, solvents were purged before using. Reactions were carried out under argon (Ar). The thin layer chromatography (CCM) was realized on aluminum substrates covered by a silica Merck 60 F_{254} gel. The chromatographic columns were realized under positive pressure on silica Merck Geduran Si 60 (0.063-0.2 mm) gel with given solvents. Solvents were evaporated under reduced pressure at temperature inferior to 45°C. Products were dried under vacuum.

c) Synthesis protocols

4,7-Bis(thiophene-2-yl)benzo-2,1,3-thiadiazole (3a)

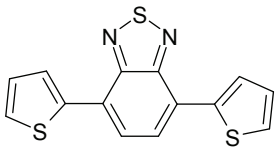

In a solution of 4,7-dibromobenzene-2,1,3-thiadiazole (1 g, 3.40 mmol) and thien-2-yl -boronic (1.65 g, 12.93 mmol) in THF, an aqueous solution of Na_2CO_3 [2 M] (1.62 g, 15.31 mmol) and of $Pd(PPh_3)_4$ (0.39 g, 0.34 mmol) was added. The mixture was refluxed for 27 h under Ar. 26 mL of THF were added. The organic layer was washed with a saturated solution of NaCl (3 x 50 mL) dried with Na_2SO_4 and filtered. The solvent was removed by rotary evaporation to afford the crude product which was subsequently purified by column chromatography (eluent: hexane/CH_2Cl_2 (1:1)). A red solid powder was obtained (0.58 g, 57% yield): ^{1}H NMR (200 MHz, $CDCl_3$, ppm): δ 8.12 (dd, *J* = 1.0 ; 3.7 Hz, 2H), 7.87 (s, 2H), 7,46 (dd, *J* = 1.0 ; 5.1 Hz. 2H); 7.22 (dd, *J* = 3.7 ; 5.1 Hz, 2H); ^{13}C NMR (100 MHz, $CDCl_3$, 100 MHz): δ 152.6; 139.3; 128.0; 127.5; 126.8; 125.9; 125.7; LSIMS m/z (rel. intensity) 301.1 ([M-H$^+$], 100), 302.1 ([M-H$^+$], 19), 303.1 ([M-H$^+$], 16).

4,7-Bis(5-bromothiophene-2-yl)benzo-2,1,3-thiadiazole (4a)

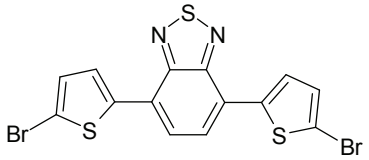

The 4,7-bis(thiophene-2-yl)benzo-2,1,3-thiadiazole (0.50 g, 1.67 mmol) is solubilized in (20 mL) of $CHCl_3$ under Ar atmosphere. The solution was cooled at 0° C and N-bromosuccinimide (0.67 g, 3.77 mmol) was added in the dark. The mixture was warmed up at room temperature and it was stirred overnight. After the evaporation of the solvent, the product was solubilized in THF and precipitated in water; the product was filtered, washed with ethanol and hexane. A red solid powder was obtained (0.69 g, 90% yield): ^{1}H NMR (200 MHz, $CDCl_3$, ppm): δ 7.81 (d, *J* = 4.0 Hz, 2H), 7.79 (s, 2H), 7.16 (d, *J* = 4.0 Hz, 2H); ^{13}C NMR (100 MHz, $CDCl_3$, ppm): δ 152.6, 139.3; 128.0; 127.5; 126.8; 125.9; 125.7; LSIMS m/z (rel. intensity) 455.9 ([M$^{+\cdot}$], 17); 456.9 ([M-H$^+$], 55); 457.9 (([M$^{+\cdot}$], 45); 458.8 ([M-H$^+$], 100); 459.9 ([M-H$^+$], 44); 460.8 ([M-H$^+$], 60); 461.9 ([M$^{+\cdot}$], 15); 462.9 ([M-H$^+$], 10).

4,7-Bis(4-octylthiophene-2-yl)benzo-2,1,3-thiadiazole (3b)

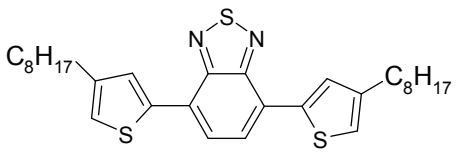

The 2-(4,4,5,5-tetramethyl-[1,3,2]-dioxaborolano-2-yl)-4-octylthiophene (0.49 g, 1.51 mmol) and the 4,7-

Bis(thiophene-2-yl)benzo-2,1,3-thiadiazole (0.13 g, 0.43 mmol))were solubilized in THF (10 mL). An aqueus solution of Na_2CO_3 [2 M] (1.0 mL, 1.90 mmol) and $Pd(PPh_3)_4$ (0.06 g, 0.05 mmol) were added. The mixture was stirred at reflux during two days, under Ar atmosphere. 50 mL of THF were added. The organic phase was washed with a saturated solution of NaCl (4 x 50 mL), dried over Na_2SO_4, filtered and evaporated. The residue was purified by column chromatographic (eluent: hexane/CH_2Cl_2 1:1). The final product is purple solid (0.46 g, 55 % yield): ^{1}H NMR (200 MHz, $CDCl_3$, ppm): δ 7.98 (s, 2H), 7.83 (s, 2H), 7.04 (s, 2H), 2.69 (t, *J* = 7,6 Hz, 4H), 1.71 (m, 4H), 1.34 (m, 20H), 0.88 (t, *J* = 6.6 Hz, 6H); ^{13}C NMR (100 MHz, $CDCl_3$, ppm): δ 152.6 ; 144.3; 139.0; 129.0; 126.0; 125.5; 121.5; 31.9; 30.6; 30.5; 29.4; 29.4; 29.3; 22.7; 14.1 ; LSIMS m/z (rel. intensity) 524.2 ([$M^{+\cdot}$], 100); 525.3 ([M-H^+], 70); 526,3 ([M-H^+], 43).

4,7-Bis(5-bromo-4-octylthiophen-2-yl)benzo-2,1,3-thiadiazole (4b)

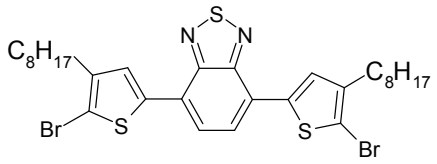

The 4,7-Bis(4-octylthiophene-2-yl)benzo-2,1,3-thiadiazole (0.11 g, 0.21 mmol) is solubilized in CH_2Cl_2 (10 mL). The solution was cooled at 0° C and N-bromosuccinimide (0.75 g, 0.42 mmol) in CH_2Cl_2 (11 mL)) was added dropwise in the dark and under Ar atmosphere. The mixture was kept during 1 h at 0°C and then it was warmed up at room temperature and stirred overnight. Et_2O (40 mL) was added. The solution was washed with a saturated solution of NaCl (3 x 80 mL), dried over Na_2SO_4, filtered and evaporated. A red solid power was obtained (0,13 g, 85% yield) : ^{1}H NMR (200 MHz, $CDCl_3$, ppm): δ 7.73 (s, 2H), 7.66 (s, 2H), 2.62 (t, *J* = 7.6 Hz, 4H), 1,66 (m, 4H), 1,43-1,21 (m, 20H), 0,89 (t, *J* = 6.6 Hz, 6H); ^{13}C NMR (100 MHz, $CDCl_3$, ppm): δ 151.9; 142.9; 138.3; 127.9; 124.9; 124.4; 111.5; 31.9; 29.7; 29.6; 29.4; 29.3; 22.7; 14.1(Note: some overlapping peaks); LSIMS m/z (rel. intensity.) 680.3 ([$M^{+\cdot}$], 47), 681.3 ([$M^{+\cdot}$], 28), 682.3 ([$M^{+\cdot}$], 100), 683.3([$M^{+\cdot}$],46), 684.2 ([$M^{+\cdot}$], 66), 685.3 ([$M^{+\cdot}$], 25); HRMS (ESI) m/z calculated for $C_{30}H_{39}N_2Br_2S_3$ 681.0642 found 681.0649.

3,6-Dibromocarbazole (6)

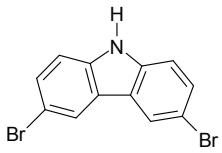

The carbazole (0.50 g, 3.0 mmol) was solved in CH_2Cl_2 (105 mL). SiO_2 silica gel (10 g) previously dried at 120°C was added to the solution. The *N*-bromosuccinimide (NBS) (1.07 g, 6.0 mmol) was then added slowly. The reaction mixture was stirred overnight under argon at room temperature and in dark conditions, then filtered. The silica was washed with CH_2Cl_2 (3 x 15 mL). The solution was washed with a saturated solution of NaCl (3 x 15 mL), dried with Na_2SO_4, filtered and evaporated. A brown solid product was obtained (0.78 g, 80% yield): ^{1}H NMR (200 MHz, Acetone-d_6, ppm): δ 10.66 (bs, 1H), 8.37 (dd, *J* = 0.8, 1.7 Hz, 2H), 7.55 (dd, *J* = 1.7, 8.6 Hz, 2H), 7.50 (dd, *J* = 0.8, 8.6 Hz, 2H); ^{13}C NMR (100 MHz, Acetone-d_6, ppm): δ 141.0, 130.8, 125.8, 125.1, 114.8, 113.4; LSIMS *m/z* (rel. intensity) 326 ([M-H^+], 53), 324 ([M-H^+], 100), 322 ([M-H^+], 60).

N-(Ethylhexanoate)-3,6-dibromocarbazole (7)

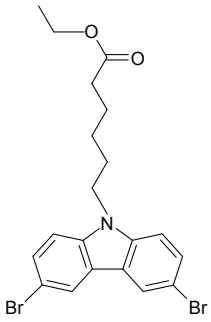

Le 3,6-dibromocarbazole (5.63 g, 17.31 mmol) was dissolved in DMF (35 mL). NaH (1.80 g, 75.00 mmol) was slowly added and the solution was stirred during 30 minutes under Ar at room temperature. The ethyl-6-bromohexanoate (5.1 mL, 28.56 mmol) was added dropwise. The mixture was stirred and refluxed during two days under Ar and in dark conditions. The DMF was evaporated and the crude product was dissolved in a mixture of THF (35 mL) / Et_2O (30 mL), washed with saturated solutions of NH_4Cl (3 x 40 mL), $NaHCO_3$ (40 mL), NaCl (50 mL) and with water (2 x 40 mL). The organic phase was dried with Na_2SO_4, filtered and evaporated. The crude product was purified through silica chromatographic column (eluent: hexane/AcOEt 4:1). The afforded product was a yellow/brown oil (4.51 g, 80% yield): ^{1}H NMR (200 MHz, $CDCl_3$, ppm): δ 8.16 (d, *J* = 1.9 Hz, 2H), 7.56 (dd, *J* = 1.9, 8.9 Hz, 2H), 7.28 (d, *J* = 8.6 Hz, 2H), 4,25 (t, *J* = 7.0 Hz, 2H), 4.12 (m, 2H), 2.29 (t, *J* = 7.3 Hz, 2H), 1.88 (m, 2H), 1.68 (m, 2H), 1.42 (m, 2H), 1.26 (t, *J* = 7.0 Hz, 3H); ^{13}C NMR (100 MHz, $CDCl_3$, ppm): δ 173.4, 139.2, 129.0, 123.4, 123.2, 111.9, 110.3, 60.3, 43.0, 33.9, 28.5, 26.6, 24.5, 14.2 ; LSIMS *m/z* (rel. intensity) 470.0 ([M-H$^+$], 51), 469.0 ([M$^{+\cdot}$], 35), 468.0 ([M-H$^+$], 100), 467.0 ([M$^{+\cdot}$], 48), 466.0 ([M-H$^+$], 53), 465.0 ([M$^{+\cdot}$], 23); HRMS (ESI) *m/z* calculd for $C_{20}H_{21}NO_2Br_2Na$ 487.9836 found 487.9811.

N-(Ethylhexanoate)-3,6-bis(5',5'-tetramethyl-[1',3',2']dioxaborolan-2'-yl)carbazole (8)

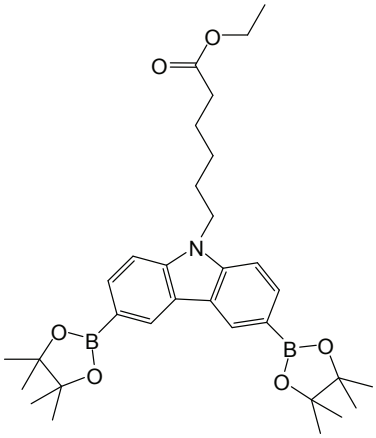

N-(ethylhexanoate)-3,6-dibromocarbazole (0.30 g, 0.64 mmol), bis(pinacolato)diboron (0.56 g, 2.25 mmol), potassium acetate, previously dried (0.38 g, 3.87 mmol) and Pd(dppf)Cl_2 (complexed with CH_2Cl_2 (1 :1)) (0.032 g, 0.039 mmol) were dried during 20 minutes and put in solution under Ar in deoxygenated DMF (10 mL). The mixture was heaten at 60°C during 14 h under Ar, in dark conditions. The solution was filtered, evaporated and purified by chromatographic column (eluent: hexane/AcOEt 1:1), recrystallized in hexane. White crystals were obtained (0.23 g, 75% yield): ^{1}H NMR (200 MHz, $CDCl_3$, ppm): δ 8.67 (s, 2H),

7.91 (d, J = 8.1 Hz, 2H), 7.38 (d, J = 8.1 Hz, 2H), 4.32 (t, J = 6.9 Hz, 2H), 4.09 (m, 2H), 2.23 (t, J = 7.3 Hz, 2H), 1.89 (m, 2H), 1.64 (m, 2H), 1.39 (s, 26H), 1.21 (t, J = 7.2 Hz, 3H); ^{13}C NMR (100 MHz, $CDCl_3$, ppm): δ 173.4; 142.5; 132.0; 128.0; 122.8; 108.0; 83.5; 60.2; 42.8; 34.0; 28.6; 26.6; 24.9; 24.6; 14.2 (Note: some overlapping peaks); LSIMS m/z (rel. intensity) 561.3 ([M-H$^+$], 26), 562.3 ([M-H$^+$], 50), 563.3 ([M-H$^+$], 17), 583.5 ([M-Na$^+$], 43), 584.6 ([M-Na$^+$], 100), 585.5 ([M-Na$^+$], 34) ; HRMS (ESI) m/z calculated for $C_{32}H_{45}NO_6B_2$ 561.3433 found 561. 3447.

4,4'-Dibromo-2-nitrobiphenyl (10)

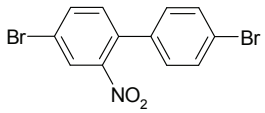

In a solution of 4,4'-dibromobiphenyl (2.00 g, 6.41 mmol) in acid acetic (30 mL), an aqueous solution of HNO_3 at 70% (20 mL) is slowly added. The mixture was stirred, under Ar, up to a total dissolution of the solid. The mixture was cooled to room temperature. A yellow paste was obtained, filtered and recristallized in ethanol. The final product is a yellow solid. (1.94 g, 85% yield): ^{1}H NMR (200 MHz, $CDCl_3$, ppm): δ 8.03 (s, 1H); 7.75 (dd, J = 1.6, 8.2 Hz, 1H); 7.56 (d, J = 8.2 Hz, 2H); 7.31 (s, 1H); 7.16 (d, J = 8.2 Hz, 2H).

2,7-dibromo-9-H-carbazole (11)

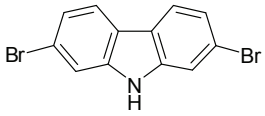

The 4,4'-dibromo-2-nitrobiphenyle (1.20 g, 3.36 mmol) is solubilized in the triethyl phosphite (33 mL). The mixture was stirred at 160°C under Ar for 22 h. Upon cooling the solution to room temperature, the solvent was removed. Crude product was purified by column chromatography (eluent: hexane/CH_2Cl_2 4:1). A white solid product was obtained (0.52 g, 48 % yield): ^{1}H NMR (200 MHz, $CDCl_3$, ppm): δ 8.08 (s, 1H), 7.88 (d, J = 8.3 Hz, 2H), 7.56 (d, J = 1.0 Hz, 2H), 7.36 (d, J = 8.3 Hz, 2H); ^{13}C NMR (100 MHz, $CDCl_3$, ppm): δ 144.4; 123.3; 122.7; 122.5; 119.9; 114.9; HRMS (ESI) m/z (rel. intensity) 322.0 ([M-H$^+$], 51), 323.9 ([M-H$^+$], 100), 325.9 ([M-H$^+$], 45).

2,7-dibromo-N-(2-octyl)carbazole (12)

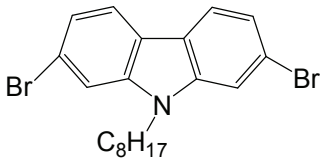

To 2,7-dibromocarbazole (1 g, 3.07 mmol) and anhydrous DMF (8 mL) was added slowly KOH (0.086 g, 0.48 mmol). After 30 minutes 2-octylbromide (0.590 g, 3.07 mmol) was added under argon. The solution was stirred at 70°C for 18 h. The reaction was quenched with water and extracted with dichloromethane. Organic fractions were dried over $MgSO_4$ and the solvent was removed in vacuum. The crude product was purified by column chromatographic (eluant: hexane) to afford a colorless oil, which slowly solidified. (1.15 g, 80% yield) ^{1}H NMR (200 MHz, $CDCl_3$, ppm): δ 7.76 (s, 1H); 7.70 (d, 2H,); 7.54 (dd, 2H); 4.17 (t, 2H);

1.82 (m, 2H); 1.82 (m, 2H); 1.30 (m, 8H); 0.88 (t, 3H). ^{13}C NMR (100 MHz, $CDCl_3$, ppm): δ 143.03; 128.44; 121.81; 117.90; 90.80; 43.25; 31.81; 29.28; 29.15; 28.78; 27.13; 22.64; 14.13. HRMS(ESI): calcd for $[C_{30}H_{23}Br_2N$](M*+H)$^+$: Calc. m/z : 530.9920 found : 530.9906 mp: 59-60°C.

2,7- Bis(4,4,5,5-tetramethyl-1,3,2-dioxaborolan-2-yl)-N-9'-octylcarbazole (14)

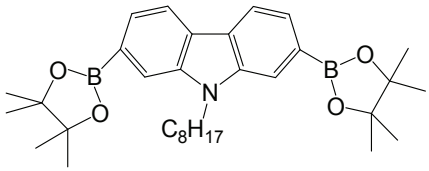

The 2,7-dibromo-N-(2-octyl)carbazole (0.48 g, 1.10 mmol) was solubilized in THF anhydrous (12 mL) and cooled down at -78°C. *n*- BuLi [2.5 M in hexane] (1.91 mL, 2.31 mmol) was added dropwise to the solution. The mixture was stirred at -78°C for 1 h before adding the 2-isopropoxy-4,4,5,5- tetramethyl-1,3,2-dioxaborolane (0.47 g, 2.59 mmol). After one hour of additional stirring at -78°C, the reaction was warmed up at the room temperature overnight. The mixture was pured into water (150 mL) and the organic layer was extracted four times with diethyl ether (4 x 150 mL). The combined organic layer was dried with $MgSO_4$ and the solvent was removed by rotary evaporation to afford the crude product. After recrystallization in methanol and acetone (10:1) colorless crystals were obtained (0.37 g, 60% yield). ^{1}H NMR (200 MHz, $CDCl_3$, ppm): δ 8.61 (br, 2H); 8.41 (t, 2H); 8.09 (d, 2H); 4.50 (m, 2H); 2.33 (m, 2H); 1.61 (m, 2H); 1.33 (s, H) 1.22 (br, 6H); 1.19 (br, 6H); 1.17 (br, 16H); 0.87 (t, *J* = 7.8 Hz, 6H) ^{13}C NMR (100MHz, C_6D_6 , ppm): δ 142.81; 139.42; 127.59; 126.94; 125.77; 125.77; 125.44; 121.06; 118.66; 116.26; 116.22; 90.80; 43.25; 31.81; 29.28; 29.15; 28.78; 27.13; 22.64; 14.13.

9-Heptadecane p-toluenesulfonate (29)

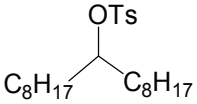

In a bottom flask a solution of p-toluenesulfonyl chloride (12.39 g, 65.21 mmol) in CH_2Cl_2 (51.1 mL) was added to a cold solution (0-5°C) of heptadecan-9-ol (13.38 g, 52.6 mmol), of $Me_3N{\cdot}HCl$ (13.26 g, 31.15 mmol) in CH_2Cl_2 (51.1 mL). The mixture was stirred at 0-5°C for 90 minutes and, subsequently, precipitated in water (100 mL). The organic layer was extracted with CH_2Cl_2 (3 x 150 mL) and dried over Na_2SO_4. The crude product was obtained after the solvent removal and purified by column chromatographic (eluent: 90% hexane, 10% ethyl acetate) to afford a colourless oil which tends to crystallize. (12.03 g, 89% yield): ^{1}H NMR (200 MHz, $CDCl_3$, ppm): δ 7.79 (d, *J* = 8.2 Hz, 2 H); 7.32 (d, *J* = 8.1 Hz, 2H); 4.53 (m, 1 H); 2.44 (s, 3H); 1.55 (m, 4 H); 1.22 (m, 24 H); 0.88 (t, *J* = 7.1 Hz, 6H). ^{13}C NMR (100 MHz, $CDCl_3$, ppm): δ 142.0; 123.3; 122.6; 122.5; 119.9; 114.9; 84.81; 34.25; 31.98; 29.59; 29.43; 29.30; 24.82; 22.79; 21.74; 14.25.(Some overlapping peak). HRMS (ESI):calcd for $C_{24}H_{46}NO_3S$; (M*+NH_4^+) : Calc. m/z : 428.3198 found : 428.3205 mp: 32°C.

N-9'-Heptadecanyl-2,7-dibromocarbazole (30)

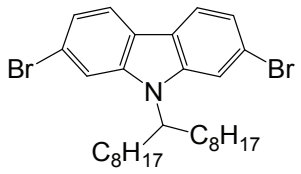

To a solution of 2,7-dibromo-9-H-carbazole (7.50 g, 23.08 mmol) in DMSO (56 mL), a potassium hydroxyde powder (6.47 g, 115.38 mmol) was added. After a complete dissolution of the 2,7-dibromo-9-H-carbazole, a solution of 9-Heptadecane p-toluenesulfonate (14.02 g, 34.62 mmol) in DMSO (37 mL) was added dropwise to the mixture during 120-150 min. The solution was stirred overnight and precipitated in 400 mL of cold water. The resulting mixture was extracted three times with hexane (3 x 300 mL). The combined organic layer was washed twice with 200 mL of H_2O, twice with 100 mL of brine, and the organic layer was dried over $MgSO_4$. The solvent was removed by rotary evaporation to afford the crude product, finally purified by column chromatography (eluent: 100% hexane). A colourless product was obtained (10.90 g, 86.7% yield). ^{1}H NMR (200 MHz, $CDCl_3$, ppm): δ 7.90 (br 2H); 7.70 (br, 1H); 7.54 (br, 1H); 7.33 (br, 2H); 4.42 (br, 2H); 2.19 (br, 2H); 1.14 (br, 22H); 0.97 (br, 2H); 0.83 (t, J = 6.3 Hz, 6H). ^{13}C NMR (100MHz, $CDCl_3$, ppm): δ 143.03; 139.56; 122.44; 121.61; 119.90; 119.13; 112.29; 57.09; 57.07; 33.61; 31.87; 29.42; 29.40; 29.26; 26.86; 22.74; 14.21. HRMS(ESI): calcd for [$C_{29}H_{41}Br_2N$](M*+H)$^+$: Calc. m/z : 61.1606 found : 561.1611 mp: 59-60°C.

2,7- Bis(4,4,5,5-tetramethyl-1,3,2-dioxaborolan-2-yl)-N-9'-heptadecanylcarbazole (32)

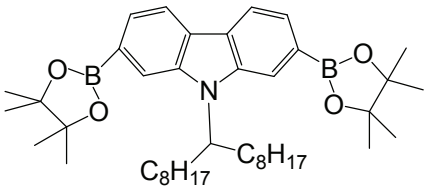

The N-9'-Heptadecanyl-2,7-dibromocarbazole (6.5 g, 11.96 mmol) was solubilized in THF anhydrous (120 mL) and cooled down at -78°C. *n*- BuLi [2.5 M in hexane] (9.81 mL, 24.52 mmol) was added dropwise to the solution. The mixture was stirred at -78°C for 1 h before adding the 2-isopropoxy-4,4,5,5- tetramethyl-1,3,2-dioxaborolane (4.04 g, 26.55 mmol). After one hour of additional stirring at -78°C, the reaction was warmed up at the room temperature overnight. The mixture was precipited in water (150 mL) and the organic layer was extracted four times with diethyl ether (4 x 150 mL). The combined organic layer was dried with $MgSO_4$ and the solvent was removed by rotary evaporation to afford the crude product. After recrystallization in methanol and acetone (10:1) colorless crystals were obtained (4.57 g, 60 % yield). ^{1}H NMR (200 MHz, $CDCl_3$, ppm): δ 8.61 (br, 2H); 8.41 (t, J = 8.1 Hz, 2H); 8.19 (d, J = 7.8 Hz, 1H); 8.14 (t, J= 8.1 Hz, 2H); 8.09 (d, J = 7.7 Hz, 1H); 4.50 (m, 1H); 2.33 (m, 2H); 1.61 (m, 2H); 1.22 (br, 4H); 1.19 (d, J = 7.7 Hz, 1H); 4.50 (m, 1H); 2.33 (m, 2H); 1.61 (m, 2H); 1.22 (br, 4H); 1.19 (br, 12H); 1.17 (br, 12H); 1.03 (br, 20H); 0.87 (t, J = 7.8 Hz, 6H) ^{13}C NMR (100MHz, C_6D_6 , ppm): δ 142.81; 139.42; 127.59; 126.94; 125.77; 125.77; 125.44; 121.06; 118.66; 116.26; 116.22; 83.81; 83.71; 56.82; 34.20; 32.18; 29.78; 29.62; 29.60; 27.10; 25.09; 23.03; 14.39. HRMS(ESI): calcd for [$C_{41}H_{65}B_2NO_4$](M*+H)$^+$: Calc. m/z : 657.5099 found : 657.5105 mp : 59-60 °C.

5-methyl-4H-thieno[3,4-c]pyrrole-4,6(5H)-dione (15a)

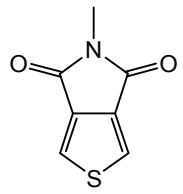

A solution of thiophene-3,4-dicarboxylic acid (5 g, 29.00 mmol) in acetic anhydride (420 mL) was stirred at 75°C for 2 hours. The solvent was removed and to the crude product was added dioxane (102 mL), DMAP (10 g, 87.00 mmol) and *n*-methylamine 2M in ethanol (1.68 g, 2.22 mL, 24.90 mmol). The solution was stirred at 55°C for 20 hours. Acetic anhydride (135.2 mL) was added and the reaction mixture was stirred for 4 hours at 80°C. Then the reaction was quenched with water (500 mL) and was extracted with dichloromethane (4x80 mL). The combined organic layers was dried with $MgSO_4$ and evaporated to dryness to obtain a dark powder. The crude product was purified by chromatographic column using dichloromethane/ethyl acetate (95%/5%) as eluent to afford the title product as a white solid. Recrystallization in isopropanol gives white crystals (1.95 g, yield: 40% yield). ^{1}H NMR (200 MHz, $CDCl_3$, ppm): δ 7.84 (s, 2H); 3.20 (s, 3H). ^{13}C NMR (100MHz, $CDCl_3$, ppm): δ 163.0, 139.85, 125.85, 24.63. HRMS(ESI): calcd for $[C_7H_5N_1O_2S_1](M^*+H)^+$: Calc. m/z : 167.0041 found : 167.0037 mp: 154°C .

Synthesis of 1,3-dibromo-5-methyl - 4H -thieno[3,4-c]pyrrole-4, 6(5H)-dione (16a)

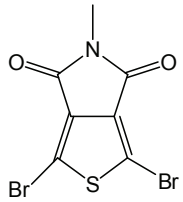

To a solution of 5-methyl-4H-thieno[3,4-c]pyrrole-4,6(5H)-dione (4 g, 23.87 mmol) in a mixture of trifluoroacetic acid (61.72 mL) and sulfuric acid (21.60 mL) was added N-bromosuccinimide (12.75 g, 71.62 mmol). The solution was stirred 1 hour in the dark at room temperature. Then the solution was poured into 20 mL of cold water. The precipitate was filtered and washed with water, acetone and methanol. The solid obtained was filtered on silica pad with chloroform as eluent to give the pure product as a yellow solid (6.72 g, 86% yield). ^{1}H NMR (200 MHz, $CDCl_3$, ppm): δ 3.12 (s, 3H). ^{13}C NMR (100 MHz, $CDCl_3$): δ 160.67; 135.01; 113.35; 24.94. HRMS (ESI): calcd for $[C_7H_3Br_2N_1O_2S_1](M^*+ H)^+$: Calc. m/z : 332.8251 found : 332.8258 mp: 227°C.

Synthesis of 3-dodecylthiophene

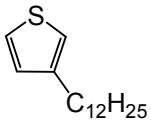

The commercial product, 3-bromothiophene (7.24 g, 44.3 mmol) was added slowly to a solution of $Ni(dppp)Cl_2$ (289 mg, 0.53 mmol, 0.012 equiv) in 40 mL dry ethyl ether in an air-free flask. To the reaction mixture was then added *n*-$C_{12}H_{25}MgBr$ solution (1.0 M in ether; 44.4 mL, 44.4 mmol) dropwise at room temperature. After addition, the brown solution was stirred at 60 ºC overnight. Upon cooling to room

temperature, 200 mL of H_2O was added to the reaction, and the resulting mixture was extracted three times with 200 mL of diethyl ether. The combined organic layer was washed twice with 200 mL of H_2O, twice with 100 mL of brine, and the organic layer was dried over $MgSO_4$. After filtration, the solvent was removed by rotary evaporation to afford a brown oil that was purified by chromatographic column on silica gel with hexane as eluent. A colorless oil was obtained as pure product (7.57 g, 68% yield). ^{1}H NMR (200 MHz, $CDCl_3$, ppm): δ 7.26 (dd, 1H), 6.97 (d, 2H), 6.94 (d, 2H), 2.65 (t, 2H), 1.65 (m, 2H), 1.32 (m, 18H), 0.92 (t, 3H). ^{13}C NMR (100 MHz, $CDCl_3$, ppm): δ 143.46, 128.50, 125.22, 119.95, 32.14, 30.79, 30.51, 29.92, 29.89, 29.86, 29.84, 29.70, 29.58, 22.92, 14.35. (Some overlapping peaks).

Synthesis of 2-bromo-3-dodecylthiophene

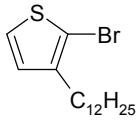

NBS (4.14 g, 23.4 mmol) was added to a solution of 3-dodecylthiophene (5 g, 19.8 mmol) in chloroform (15 mL) and glacial acetic acid (15 mL), and the reaction mixture was stirred in the dark at room temperature for 2h. Then the reaction mixture was diluted with 50 mL of H_2O and extracted three times with 100 mL of chloroform. The combined organic layer was washed twice with 100 mL of aqueous KOH solution (10 wt%), and twice with 100 mL of brine, and dried over $MgSO_4$. After purification by column chromatography, the product was obtained as a colorless oil (4.91 g, 74% yield). ^{1}H NMR (200 MHz, $CDCl_3$, ppm): δ 7.16 (d, 1H), 6.77 (d, 1H), 2.54 (t, 2H), 1.55 (m, 2H), 1.27 (m, 18H), 0.87 (t, 3H). ^{13}C NMR (100 MHz, $CDCl_3$, ppm): δ 142.18, 128.44, 125.32, 108.99, 32.15, 29.96, 29.90, 29.87, 29.80, 29.64, 29.60, 29.58, 29.45, 22.93, 14.36 (Note: some peaks in ^{13}C NMR spectrum overlap).

Synthesis of 2-(trimethylstannyl)-3-dodecylthiophene (17c)

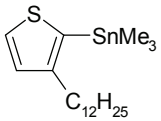

An *n*-butyllithium solution (2.5 M in hexane; 7.23 mL, 18.07 mmol) was added dropwise to a solution of 2-bromo-3-decylthiophene (5 g, 15.06 mmol) in THF (30 ml) at -78 ºC. After addition, the reaction mixture was stirred at -78 ºC for 30 min. and then warmed to room temperature for 1h. Then the mixture was cooled to -78 ºC, and a trimethylstannyl chloride solution (1.0 M in THF, 18.07 mL, 18.07 mmol) was added in one portion. Next, the cold bath was removed and the mixture was stirred at room temperature for 1h. The reaction mixture was then quenched by adding 100 mL of H_2O, followed by three times extraction with 50 mL of ethyl acetate. The combined organic layer was next washed twice with 100 mL of brine and dried over $MgSO_4$. After filtration, the solvent was removed by evaporation to afford a yellow oil as the crude product (80% purity by ^{1}H NMR), which can be used for the next step without further purification (5.17 g, 83% yield). Note that the crude product contains about 10% 3-dodecylthiophene. ^{1}H NMR (200 MHz, $CDCl_3$, ppm): δ 7.51 (d, 1H), 7.08 (d, 1H), 2.61 (t, 2H), 1.60 (m, 2H), 1.28 (m, 18H), 0.89 (t, 3H), 0.36 (s, 9H).

Synthesis of 1,3-bis(3-dodecyl-2-thienyl)-5-methyl-4H-thieno[3,4-c]pyrrole-4 ,6(5H)-dione (18a-c)

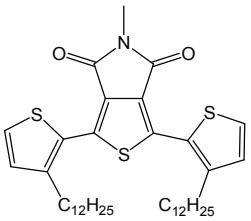

The 1,3-dibromo-5-methyl-4H-thieno[3,4-c]pyrrole-4, 6(5H)-dione (2.10 g, 4.96 mmol) was dissolved into dry toluene (200 mL). 2-(trimethylstannyl)-3-dodecylthiophene (15.00 mmol, 4.76 mL), and bis(triphenylphosphine) palladium(II) dichloride (210 mg, 6%) were added to the reaction mixture. The solution was refluxed for 24 h then cooled and poured into water. The mixture was extracted twice with dichloromethane. The organic phases were combined, washed with brine, and dried over anhydrous magnesium sulphate. The solvent was removed under reduce pressure and the crude product was purified by column chromatography using dichloromethane:hexane as the eluent (ratio 1:1) to afford the product as a green powder (1.29 g, 40 % yield). ^{1}H NMR (200 MHz, $CDCl_3$, ppm): δ 7.41 (d, 2H); 7.02 (d, 2H); 3.12 (s, 3H); 2.77 (m, 4H); 1.65 (m, 4H); 1.24 (m, 36H); 0.87 (t, 6H). ^{13}C NMR (100 MHz, d_8-THF, ppm): δ 162.59; 144.56; 137.40; 130.79; 130.11; 127.86; 125.11; 32.14; 30.76; 29.91; 29.89; 29.86; 29.85; 29.82; 29.73; 29.67; 29.57; 22.91;14.35 .One peak is missing due to the deuterated solvent. HRMS (ESI):calcd for $[C_{39}H_{57}N_1O_2S_3](M^{*+}H)^+$: Calc. m/z : 667.3551 found : 667.3555 mp: 70°C.

Synthesis of 1,3-bis(5-bromo-3-dodecyl-2-thienyl)-5-methyl-4H-thieno[3,4-c]pyrrole-4,6(5H)-dione (19a-c)

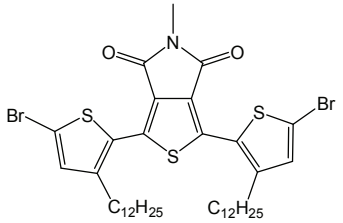

1,3-bis(3-dodecyl-2-thienyl)-5-methyl-4H-thieno[3,4-c]pyrrole-4,6(5H)-dione (4) (0.690 g, 1.02 mmol) was dissolved in a mixture of chloroform (14.83 mL) and trifluoroacetic acid (14.83 mL) (1:1). The solution was kept in the dark. N-bromosuccinimide (0.395 g, 2.22 mmol) was added and the solution was stirred at 55°C overnight. The solution was quenched with water. The solid obtained was purified by column chromatography using dichloromethane:hexane as the eluent (ratio 1:1) (0.33 g, 40% yield). ^{1}H NMR (200 MHz, $CDCl_3$, ppm): δ 6.98 (s, 2H); 3.12 (s, 3 H); 2.71 (m, 4H); 1.56 (m, 4H); 1.24 (m, 36 H) 0.86 (t, 6H). ^{13}C NMR (100 MHz, $CDCl_3$, ppm): δ 162.37; 145.22; 135.83; 132.86; 130.98; 126.47; 32.16; 30.57; 29.97; 29.91; 29.90; 29.89; 29.80; 29.66; 29.63; 29.60; 24.63; 22.93; 14.36.(Some overlapping peaks). HRMS (ESI): calcd for $[C_{39}H_{55}Br_2N_1O_2S_3](M^{*+}H)^+$: Calc. m/z : 823.1761 found: 823.1749 mp: 63°C.

Synthesis of 3-ethyl 4-methyl 2-aminothiophene-3,4-dicarboxylate (20)

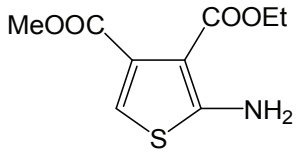

To a solution of methyl 2-oxopropanoate (32.50 g, 318.4 mmol), ethyl cyanoacetate (32.75 g, 289.5 mmol), sulphur (11.20 g, 43.66 mmol) and 150 mL of N,N-dimethylformamide in one-neck 1L-flask was added dropwise a solution of triethylamine (75 mL) and N,N-dimethylformamide (150 mL) during a period of two hours at room temperature. After the addition, temperature was raised to 50°C overnight. The solution was cooled at room temperature and 1L of water was added. The product crystallized after 48 hours into the mixture and was then filtered to obtain long white needles (39.00 g, 58% yield). ^{1}H NMR (200 MHz, acetone d_6, ppm): δ 6.99 (broad peak), 6.69 (s, 1 H), 4.20 (q, 2H, *J* = 7.0 Hz), 3.76(s, 3H), 1.28 (t, 3H, *J* = 7.3 Hz). ^{13}C NMR (100 MHz, acetone d_6, ppm): δ 165.9, 165.1, 164.7, 133.6, 111.4, 104.3, 60.3, 52.1, 14.6. HRMS (ESI): calcd for $[C_9H_{11}O_4S](M^*+H)^+$: Calc. m/z : 230.0482 found : 230.0484 mp: 105°C.

Synthesis of 3-ethyl 4-methyl 2-iodothiophene-3,4-dicarboxylate (21)

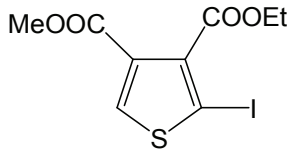

3-ethyl/4-methyl/2-aminothiophene-3,4-dicarboxylate (15 g, 65.4 mmol) in 2M HCl_{aq} (365 mL) was stirred at room temperature for 20 minutes. The solution was cooled to 0 °C and $NaNO_2$ (8.73 g, 88.1 mmol) was added to the solution. The mixture was allowed to react for 30 minutes. Then KI (27.14 g, 163.5 mmol) was added in small portions. The solution was allowed to react for 45 minutes, then the mixture was extracted with diethyl ether (10 x 75 mL), washed with sodium bisulfite (5 x 100 mL of saturated solution) and water (3 x 100 mL). The combined organic layer was dried with Na_2SO_4 and evaporated to dryness. The crude product was chromatographed over silica gel using methylene chloride as eluent to give an orange oil (11.5 g, 52% yield).^{1}H NMR (200 MHz, $CDCl_3$, ppm): δ 8.09 (s, 1H), 4.42 (q, 2H, *J* = 7.1 Hz), 3.85(s, 3H), 1.40(t, 3 H, *J* = 7.1 Hz).^{13}C NMR (100MHz, $CDCl_3$, ppm): δ 164.5, 161.0, 140.6, 138.3, 133.9, 77.2, 62.1, 52.4, 14.2. HRMS (ESI):calcd for $[C_9H_{10}IO_4S](M^*+H)^+$: Calc. m/z : 340.9342 found : 340.9339

Synthesis of 2-iodothiophene-3,4-dicarboxylate (22)

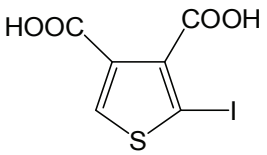

To a solution of 3-ethyl/4-methyl/2-iodothiophene-3,4-dicarboxylate (10 g, 29.40 mmol) in 500 mL of HCl [2M], was stirred at reflux in a one-neck flask for 24 hours. The solution was extracted with diethyl ether (10 x 150 mL). The combined organic layers was dried with Na_2SO_4 and evaporated to dryness to obtain a white solid (7.51 g, 86% yield).^{1}H NMR (200 MHz, acetone d_6, ppm): δ 9.69 (broad peak), 8.42 (s, 1H). ^{13}C NMR (100MHz, $CDCl_3$, ppm): δ 165.5, 162.0, 142.1, 140.3, 134.0, 79.0. HRMS (ESI): calcd for

$[C_6H_3INaO_4S](M^*+ Na)^+$: Calc. m/z : 320.8689 found : 320.8695 mp: 174°C (uncorrected).

Synthesis of 1-iodo-5-methyl-4H-thieno[3,4-c]pyrrole-4,6(5H)-dione (23)

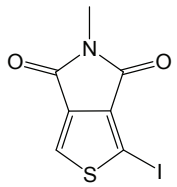

A solution of 3-ethyl-4-methyl/2-iodothiophene-3,4-dicarboxylate (8) (5 g, 16.60 mmol) in acetic anhydride (231 mL) was stirred at 75°C for 2 hours. The solvent was removed and to the crude product was added dioxane (58.56 mL), DMAP (3 g, 6.08 mmol) and *n*-methylamine 2M in ethanol (1.68 g, 2.22 mL, 24.90 mmol). The solution was stirred at 55°C for 20 hours. Acetic anhydride (77 mL) was added and the reaction mixture was stirred for 4 hours at 80°C. Then the reaction was quenched with water (500 mL) and was extracted with dichloromethane (4x80 mL). The combined organic layers was dried with $MgSO_4$ and evaporated to dryness to obtain a dark powder. The crude product was purified by column chromatography using dichloromethane/ethyl acetate (95%/5%) as eluent to afford the title product as a white solid. Recrystallization in isopropanol gives white crystals (3.80 g, 76% yield).^{1}H NMR (200 MHz, $CDCl_3$, ppm): δ 7.84 (s, 1H), 3.13 (s, 3 H), ^{13}C NMR (100MHz, $CDCl_3$, ppm): δ 162.6; 162.1; 137.0; 133.7; 132.7; 126.6, 25.03. HRMS (ESI): calcd for $[C_7H_4I_1N_1O_2S_1](M^*+H)^+$: Calc. m/z : 292.9007 found : 292.9014, mp: 95°C.

Synthesis of 5,5'-di-methyl-4H,4'H-1,1'-bithieno[3,4-c]pyrrole-4,4',6,6'(5H,5'H)-tetraone (24)

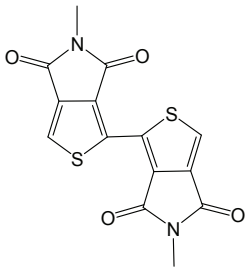

To a solution of 1-iodo-5-methyl-4H-thieno[3,4-c]pyrrole-4,6(5H)-dione (0.380 g, 1.29 mmol) in dry N,N-dimethylformamide (12.60 mL) was added copper(0) powder (0.327 g , 5.15 mmol). The solution was heated at 140°C for 24 hours. The mixture was cooled down and filtered on cellite. The solvent was removed to give a yellow powder (0.34 g, 79% yield).^{1}H NMR (200 MHz, $CDCl_3$, ppm): δ 7.89 (s, 2H), 3.64 (s, 6H).^{13}C NMR (100 MHz, $CDCl_3$, ppm): δ 162.53; 162.1; 137.0; 133.7; 131.27; 126.6; 25.03. HRMS (ESI): calcd for $[C_{14}H_8N_2O_4S_2](M^*+ H)^+$: Calc. m/z : 331.9925 found : 331.9920, mp degradation at 310°C.

Synthesis of 3,3'-dibromo-5,5'-dimethyl-4H,4'H-1,1'-bithieno[3,4-c]pyrrole-4,4',6,6'(5H,5'H)-tetraone (25)

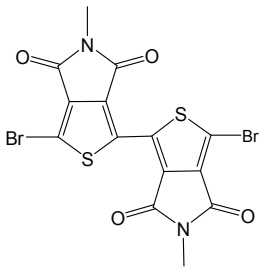

To a solution of 5,5'-dimethyl-4H,4'H-1,1'-bithieno[3,4-c]pyrrole-4,4',6,6'(5H,5'H)-tetraone (0.75 g, 1.42 mmol) in a mixture of trifluoroacetic acid (8 mL) and sulfuric acid (2 mL) was added N-bromosuccinimide (1.01 g, 5.69 mmol). The solution was stirred 1 hour in the dark at room temperature. Then the solution was poured into 20 mL of cold water. The precipitate was filtered and washed with water, acetone and methanol. The solid obtained was filtered on silica pad with chloroform as eluent to give the pure product as a yellow solid (0.50 g, 71% yield).^{1}H NMR (200 MHz, $CDCl_3$, ppm): δ 3.64 (s, 6H). ^{13}C NMR (100 MHz, $CDCl_3$, ppm): δ 162.53; 162.1; 137.0; 133.7; 131.27; 126.6; 25.19. HRMS (ESI): calcd for $[C_{14}H_8N_2Br_2O_4S_2](M^*+H)^+$: H)$^+$: Calc. m/z : 687.0380 found : 687.0393 mp: degradation at 325°C.

Synthesis of 3,3'- bis(3-dodecyl-2-thienyl) -5,5'-dimethyl- 4H,4'H-1,1'-bithieno[3,4-c]pyrrole-4,4',6,6'(5H,5'H)-tetraone (26)

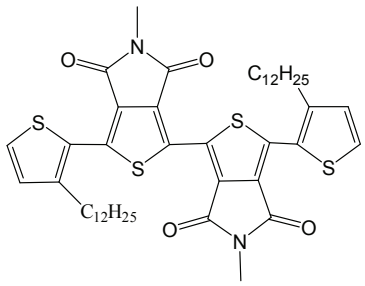

The 3,3'-dibromo-5,5'-dimethyl-4H,4'H-1,1'-bithieno[3,4-c]pyrrole-4,4',6,6'(5H,5'H)-tetraone (0.100 g, 0.20 mmol) was dissolved into dry toluene (4.87 mL). 2-(trimethylstannyl)-3-dodecylthiophene (0.209 gr, 0.51 mmol), and bis(triphenylphosphine) palladium(II) dichloride (7 mg, 6%) were added to the reaction mixture. The solution was refluxed for 24 h then cooled and poured into water. The mixture was extracted twice with dichloromethane. The organic phases were combined, washed with brine, and dried over anhydrous magnesium sulphate. The solvent was removed under reduce pressure and the crude product was purified by column chromatography using dichloromethane:hexanes as the eluent (ratio 1:1) to afford the product as a yellow solid (0.10 g, 63 % yield). ^{1}H NMR (200 MHz, $CDCl_3$, ppm): δ 7.41 (d, 2H); 7.02 (d, 2H); 3.12 (s, 6H); 2.77 (m, 4H); 1.65 (m, 4H); 1.24 (m, 36H); 0.87 (m, 6H). ^{13}C NMR(100 MHz, $CDCl_3$, ppm): δ 162.6; 162.0; 137.40; 132.7; 130.90; 130.11; 127.86; 126.6; 125.11; 38.9,; 32.14; 30.76; 29.91; 29.89; 29.86; 29.85; 29.82; 29.73; 29.67; 29.57; 22.91; 14.35. Some overlapping peaks. HRMS (ESI): calcd for $[C_{46}H_6N_2O_4S_4](M^*+H)^+$: Calc. m/z : 832.3436 found : 832.3441, mp degradation [uncorrected].

Synthesis of 3,3-bis(5-bromo-3-dodecyl-2-thienyl)-5,5'-dimethyl-4H,4'H-1,1'-bithieno[3,4-c]pyrrole-4,4',6,6'(5H, 5'H) -tetraone (27)

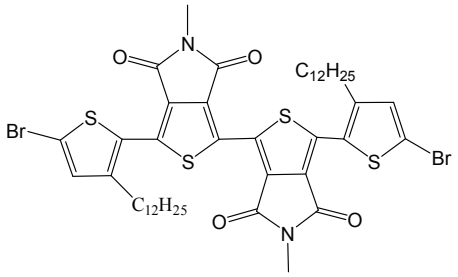

3,3'-bis(3-dodecyl-2-thienyl)-5,5'-dimethyl-4H,4H'-1,1'-bithieno[3,4-c]pyrrole-4,4',6,6'(5H,5H')-tetraone (0.500 g, 0.590 mmol) was dissolved in a mixture of chloroform (8.56 mL) and trifluoroacetic acid (8.56 mL) (1:1). The solution was kept in the dark. N-bromosuccinimide (0.231 g, 1.29 mmol) was added and the solution was stirred at 55°C overnight. The solution was quenched with water. An orange solid was obtained (0.30 g, yield: 50%). ^{1}H NMR (200 MHz, $CDCl_3$, ppm): δ 6.98 (s, 2H); 3.12 (s, 6H); 2.71 (m, 4H); 1.56 (m, 4H); 1.24 (m, 36 H) 0.86 (m, 6H). ^{13}C NMR (100 MHz, $CDCl_3$, ppm): δ 162.6; 162.0; 137.40; 132.7; 130.90; 130.11; 127.86; 126.6; 125.11; 38.9, 32.14; 30.76; 29.91; 29.89; 29.86; 29.85; 29.82; 29.73; 29.67; 29.57; 22.91; 14.35. Some overlapping peaks. HRMS (ESI): calcd for $[C_{46}H_{58}Br_2N_2O_4S_4](M^*+H)^+$: Calc. m/z : 988.1646 found : 988.1658, mp: 175 °C.

Thiophene-3-carbonyl Chloride (34)

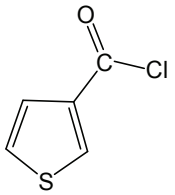

Thiophene-3-carboxylic acid (38.4 g, 0.3 mol) and 60 mL of methylene chloride were put into a 250 mL flask. The mixture was cooled by ice-water bath, and then oxalyl chloride (76.2 g, 0.6 mol) was added in one portion. The reactant was stirred overnight at ambient temperature, and a clear solution was obtained. After removing the solvent and unreacted oxalyl chloride by rotary evaporation, **(34)** was obtained as colorless solid. It was dissolved into 100 mL of methylene chloride and used for the next step.

N,N-Diethylthiophene-3-carboxamide (35)

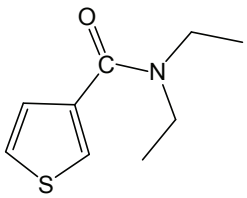

In a 500 mL flask in ice-water bath, 62.5 mL of diethylamine (43.8 g, 0.6 mol) and 100 mL of methylene chloride were mixed, and the solution of thiophene-3-carbonyl chloride was added into the flask slowly. After all of the solution was added, the ice bath was removed, and the reactant was stirred at ambient temperature for 30 min. Then, the reactant was washed by water several times, and the organic layer was

dried over anhydrous $MgSO_4$. After removing solvent, the crude product was purified by distillation under vacuum, a pale yellow oil was obtained (41.6 g, 95% yield). ^{1}H NMR (200 MHz, $CDCl_3$, ppm): δ 7.48 (S, 1H), 7.32 (d, 1H), 7.20 (d, 1H), 3.41 (m, 4H), 1.19 (t, 6H).

4,8-Dihydrobenzo[1,2-b:4,5-b′]dithiophen-4,8-dione (36)

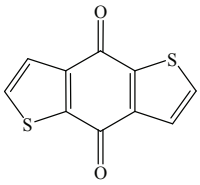

N,N-Diethylthiophene-3-carboxamide (36.6 g, 0.2 mol) was put into a well-dried flask with 200 mL of THF under an inert atmosphere. The solution was cooled down by an ice-water bath, and 70 mL of *n*-butyllithium (0.2 mol, 2.9 mol·L^{-1}) was added into the flask dropwise within 30 min. Then, the reactant was stirred at ambient temperature for 30 min. The reactant was poured into 500 g of ice water and stirred for several hours. The mixture was filtrated, and the yellow precipitate was washed by 200 mL of water, 50 mL of methanol, and 50 mL of hexane successively. A yellow powder was obtained (34.94 g, 78% yield). ^{1}H NMR (200 MHz, $CDCl_3$, ppm): δ 7.75 (d, 2 H), 7.95 (d, 2 H).

4,8-di(2-ethylhexyloxyl)benzo[1,2-b:3,4-b']dithiophene (37)

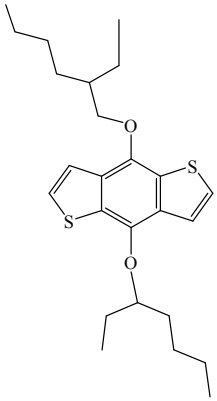

The 4,8-Dihydrobenzo[1,2-b:4,5-b′]dithiophen-4,8-dione (4.4 g, 20 mmol), zinc powder (2.86 g, 44 mmol), and 60 mL of water were put into a 250 mL flask; then 12 g of NaOH was added into the mixture. The mixture was well stirred and heated to reflux for 1 h. During the reaction, the color of the mixture changed from yellow to red and then to orange. Then, 2-ethylhexyl bromide (15 g, 60 mmol) and a catalytic amount of tetrabutylammonium bromide were added into the flask. After being refluxed for 2 h, the color of the reactant should be yellow or orange; if the color of the reactant was red or deep red, an excess amount of zinc powder (1.3 g, 20 mmol) should be added. Then, the reactant was refluxed for 6 h. The reactant was poured into cold water and extracted by 200 mL of diethyl ether two times. The ether layer was dried over anhydrous $MgSO_4$. After removing solvent, the crude product was purified by recrystallization from ethyl alcohol two times. A colorless crystal (6.87 g, yield 83%) was obtained. ^{1}H NMR (200 MHz, $CDCl_3$, ppm): δ 7.66 (d, 2H), 7.47 (d, 2H), 4.26 (d, 4H), 1.87(tt, 2H), 1.53 (m, 4H),1.37-1.27 (m, 32H), 0.88 (t, 6H). Elemental analysis: Calcd for $C_{50}H_{78}O_2S_2$: C, 73.06; H, 9.74. Found: C, 72.89; H, 9.70.

2,6-Dibromo-4,8-di(2-ethylhexyloxyl)benzo[1,2-b:3,4-b']dithiophene (38)

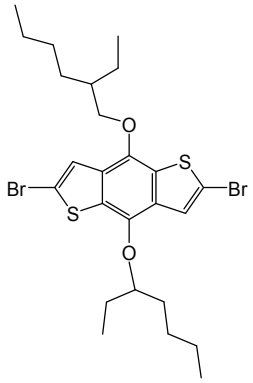

4,8-di(2-ethylhexyloxyl)benzo[1,2-b:3,4-b']dithiophene (5.58 g, 10 mmol) was dissolved into 100 mL of methylene chloride in a 250 mL flask. Bromine (3.2 g, 20 mmol) was dissolved into 60 mL of methylene chloride in a funnel and slowly dropped into the flask under an ice-water bath, and then the reactant was stirred for 4-6 h at ambient temperature. When color of bromine was diminished, all volatile substances were removed under vacuum. The residue was recrystallized by hexane one time. A white solid (5.10 g, yield 89%) was obtained. ^{1}H NMR (200 MHz, $CDCl_3$, ppm): δ 7.43 (s, 2H), 4.17 (t, 4H), 1.83 (tt, 2H), 1.54 (m, 4H), 1.36-1.27 (m, 32H), 0.89 (t, 6H). Elemental analysis: Calcd for $C_{50}H_{76}Br_2O_2S_2$: C, 56.98; H, 7.31. Found: C, 56.78; H, 7.39.

2,6-Bis(trimethyltin)-4,8-di(2-ethylhexyloxyl)benzo[1,2-b:3,4-b']dithiophene (39)

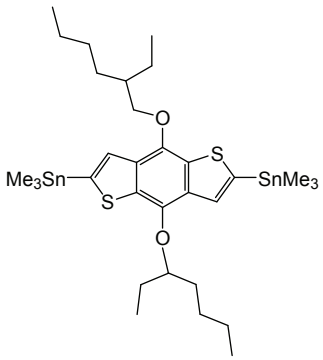

2,6-Dibromo-4,8-di(2-ethylhexyloxyl)benzo[1,2-b:3,4-b']dithiophene (4.30 g, 6 mmol) and 100 mL of THF were added into a flask under an inert atmosphere. The solution was cooled down to -78°C by a liquid nitrogen-acetone bath, and 4.55 mL of *n*-butyllithium (13.2 mmol, 2.9 M in *n*-hexane) was added dropwise. After being stirred at -78°C for 1 h, a great deal of white solid precipitate appeared in the flask. Then, 14 mmol of trimethyltin chloride (14 mL, 1 M in *n*-hexane) was added in one portion, and the reactant turned to clear rapidly. The cooling bath was removed, and the reactant was stirred at ambient temperature for 2 h. Then, it was poured into 200 mL of cool water and extracted by ether three times. The organic layer was washed by water two times and then dried by anhydrous $MgSO_4$. After removing solvent under vacuum, the residue was recrystallized by ethyl alcohol two times. Colorless needle crystals (3.26 g, 76% yield) were

obtained. ^{1}H NMR (200 MHz, $CDCl_3$, ppm): δ 7.63 (s, 2H), 4.17 (t, 4H), 1.86 (tt, 2H), 1.54 (m, 4H), 1.35-1.27 (m, 32H), 0.87 (t, 6H). ^{13}C NMR (100 MHz, $CDCl_3$, ppm): δ 143.131, 140.488, 134.046, 133.009, 129.105, 128.042, 73.618, 31.958, 30.576, 29.736, 29.697, 29.537, 29.402, 26.157, 22.724, 14.154. Some overlapping peaks. Elemental analysis: Calculated for $C_{40}H_{94}O_2S_2Sn_2$: C, 54.31; H, 7.98. Found: C, 54.13; H, 7.78.

Synthesis of 3-tetradecylthiophene

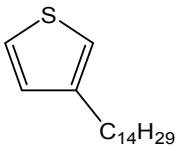

The commercial product, 3-bromothiophene (29.52 g, 145.47 mmol) was added slowly to a solution of $Ni(dppp)Cl_2$ (314 mg, 0.58 mmol, 0.012 equiv) in 40 mL dry ethyl ether in an air-free flask. To the reaction mixture was then added n-$C_{14}H_{25}MgBr$ solution (1.0 M in THF; 145 mL, 145 mmol) dropwise at room temperature. After addition, the brown solution was stirred at 60 ºC overnight. Upon cooling to room temperature, 200 mL of H_2O was added to the reaction, and the resulting mixture was extracted three times with 200 mL of diethyl ether. The combined organic layer was washed twice with 200 mL of H_2O, twice with 100 mL of brine, and the organic layer was dried over $MgSO_4$. After filtration, the solvent was removed by rotary evaporation to afford a brown oil that was purified by column chromatography on silica gel with hexane as eluent. A colorless oil was obtained as pure product (25 g, 68% yield).^{1}H NMR (200 MHz, $CDCl_3$, ppm): δ 7.26 (dd, 1H), 6.97 (d, 2H), 6.94 (d, 2H), 2.65 (t, 2H), 1.65 (m, 2H), 1.32 (m, 19H), 0.92 (t, 3H). ^{13}C NMR ($CDCl_3$, 100 MHz, ppm): δ 143.46, 128.50, 125.22, 119.95, 32.14, 30.79, 30.51, 29.92, 29.89, 29.86, 29.84, 29.70, 29.58, 22.92, 14.35. (Some overlapping peaks).

Synthesis of 2-bromo-3-tetradecylthiophene (40)

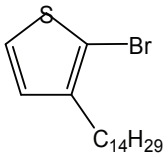

NBS (2.21 g, 10.53 mmol) was added to a solution of 3-tetradecylthiophene (2.96 g, 10.53 mmol) in chloroform (13 mL) and glacial acetic acid (13 mL), and the reaction mixture was stirred in the dark at room temperature for 2h. Then the reaction mixture was diluted with 50 mL of H_2O and extracted three times with 100 mL of chloroform. The combined organic layer was washed twice with 100 mL of aqueous KOH solution (10 wt%), and twice with 100 mL of brine, and dried over $MgSO_4$. After purification by chromatography, the product was obtained as a colorless oil (2.66 g, 74% yield).). ^{1}H NMR (200 MHz, $CDCl_3$, ppm): δ 7.56 (d, J = 5.0 Hz, 1H), 7.13 (d, J = 5.0 Hz, 1H), 2.66 (t, J = 7.5 Hz, 2H), 1.62 (m, 2H), 1.32 (m, 22H), 0.92 (t, J = 7.0 Hz, 3H). ^{13}C NMR (125 MHz, $CDCl_3$, ppm): δ 151.07, 131.48, 130.72, 129.56, 32.80, 32.41, 32.17, 29.93, 29.92, 29.89, 29.88, 29.82, 29.80, 29.61, 22.93, 14.37. (Note: some peaks in ^{13}C NMR spectrum overlap).

Synthesis of 2-(trimethylstannyl)-3-tetradecylthiophene (41)

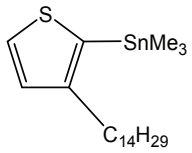

An *n*-butyllithium solution (2.5 M in hexane; 2.85 mL, 7.13 mmol) was added dropwise to a solution of 2-bromo-3-tetradecylthiophene (1 g, 5.94 mmol) in THF (7 ml) at -78 ºC. After addition, the reaction mixture was stirred at -78 ºC for 30 min. and then warmed to room temperature for 1h. Then the mixture was cooled to -78 ºC, and a trimethylstannyl chloride solution (1.0 M in THF, 7.13 mL, 7.13 mmol) was added in one portion. Next, the cold bath was removed and the mixture was stirred at room temperature for 1h. The reaction mixture was then quenched by adding 100 mL of H_2O, followed by extraction three times with 50 mL of ethyl acetate. The combined organic layer was next washed twice with 100 mL of brine and dried over $MgSO_4$. After filtration, the solvent was removed by evaporation to afford a yellow oil as the crude product (80% purity by ^{1}H NMR), which can be used for the next step without further purification (1.33 g, 50% yield). ^{1}H NMR (200 MHz, $CDCl_3$, ppm): δ 7.56 (d, J = 5.0 Hz, 1H), 7.13 (d, J = 5.0 Hz, 1H), 2.66 (t, J = 7.5 Hz, 2H), 1.62 (m, 2H), 1.32 (m, 22H), 0.92 (t, J = 7.0 Hz, 3H), 0.39 (s, 9H). ^{13}C NMR (100 MHz, $CDCl_3$, ppm): δ 151.07, 131.48, 130.72, 129.56, 32.80, 32.41, 32.17, 29.93, 29.92, 29.89, 29.88, 29.82,29.80, 29.61, 22.93, 14.37, -7.75 (Note: some peaks in ^{13}C NMR spectrum overlap).

Synthesis of 4,4'-tetradecyl-5,5'-bis(trimethylstannyl)-2,2'-bithiophene (42)

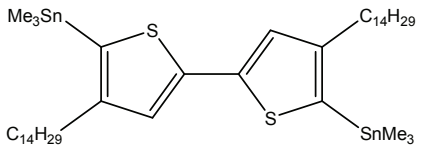

N,N,N', N'-tetramethylethylenediamine (0.30 mL,5.69 mmol) was added to a stirred solution of *n*-butyllithium (2.5 M in hexane; 0.71 mL, 17.72 mmol) in 30 mL ether. After stirring at room temperature for 15 min, the solution was added dropwise to a 41 (1 g, 5.11 mmol) solution in 18 mL ether at room temperature. After this addition, the reaction mixture was refluxed for 1 h and then cooled to -78 ºC. At -78 ºC, $CuCl_2$ (0.81 g, 6.34 mmol) was added in one portion. The reaction mixture was then warmed to room temperature andstirred at room temperature overnight. After acidification with 12 N HCl solution and dilution with 80 mL of H_2O, the mixture was extracted three times with 80 mL of dichloromethane. The combined organic layer was next washed twice with 200 mL of brine and dried over $MgSO_4$. The organic solution was filtered, and the solvent was then removed by rotary evaporation to yield a brown residue, which was purified by column chromatography over silica gel with hexane as eluent. The product (>95% purity by ^{1}H NMR) was further purified by recrystallization from hexane to remove a contaminating isomer, finally affording a yellowish solid as the desired product (2.88 g, 54% yield). ^{1}H NMR (200 MHz, $CDCl_3$, ppm): δ 7.13 (s, 2H), 2.56 (t, J = 7.5 Hz, 4H), 1.60 (m, 4H), 1.28 (m, 44H), 0.90 (t, J = 7.0 Hz, 6H), 0.40 (s, 18H). ^{13}C NMR (100 MHz, $CDCl_3$, ppm): δ 151.80, 142.90, 131.10, 126.17, 33.10, 32.24, 32.20, 32.16, 30.01, 29.93, 29.92, 29.90, 29.84, 29.82, 29.80, 29.60, 22.93, 14.37.(Note: some peaks in ^{13}C NMR spectrum

overlap).

6,6'-dibromoisoindigo (45)

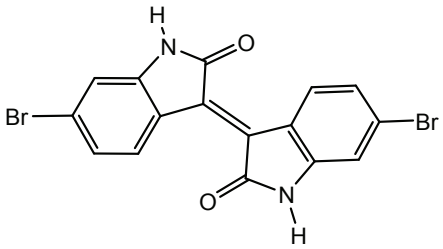

To a suspension of 6-bromooxindole (500 mg, 2.36 mmol) and 6-bromoisatin (533 mg, 2.36 mmol) in AcOH (15 mL), conc. HCl solution (0.1 mL) was added and heated under reflux for 24. The mixture was allowed to cool and filtered. The solid material was washed with water, EtOH and AcOEt. After drying under vacuum, it yielded brown 6,6'-dibromoisoindigo (0.72 g, 92%). The product was used without further purification.

6,6'-dibromo-di(2-tetradecyl)isoindigo (46a)

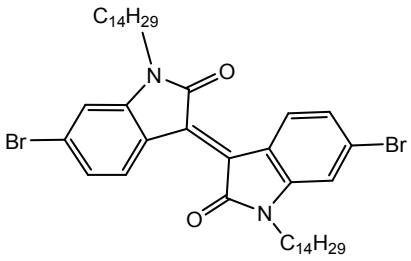

To a suspension of 6,6'-dibromoisoindigo (300 mg g, 0.714 mmol) and potassium carbonate (985 mg, 7.14 mmol) in dimethylformaldehyde (DMF) (15 mL), 1-bromo-tetradecane (519 g, 1.88 mmol) was injected through a septum under nitrogen. The mixture was stirred for 15 h at 100°C and then poured into water (100 mL). The organic phase was extracted by CH_2Cl_2, washed with brine and dried over $MgSO_4$. After removal of the solvent under reduced pressure, the deep-red solids were purified by silica chromatography, eluting with (CH_2Cl_2: Hexane = 1:1) to give 6,6'-dibromo-N,N'-(2-tetradecyl)-isoindigo (0.34 g, 75%) ^{1}H NMR (200 MHz, $CDCl_3$, ppm): δ 9.00 (d, J = 8.7 Hz, 2H), 7.13(dd, J_1 = 8.7 Hz, J_2 = 1.5 Hz, 2H), 6.81 (d, J = 1.5 Hz, 2H), 3.60-3.48 (m, 4H), 1.90-1.72(m, 4H), 1.43-1.20 (m, 44H), 0.95-0.82 (m, 6H). ^{13}C NMR (200 MHz, $CDCl_3$, ppm): δ 170.5, 168.1, 147.0, 146.2, 135.4, 134.0, 133.3, 132.6, 131.2, 130.9, 126.8, 125.2,123.5, 122.7, 120.5, 113.7,111.6, 33.10, 32.24, 32.20, 32.16, 30.01, 29.93, 29.92, 29.90, 29.84, 29.82, 29.80, 29.60, 22.93, 14.37. (Note: some peaks in ^{13}C NMR spectrum overlap).

2-Bromo-(5-octyl)thiophene (48)

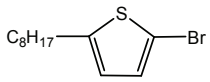

NBS (5.66 g, 31.83 mmol) was added to a solution of 5-octyl-thiophene (5 g, 25.46 mmol) in chloroform (26 mL) and glacial acetic acid (26 mL), and the reaction mixture was stirred in the dark at room temperature for 2h. Then the reaction mixture was diluted with 50 mL of H_2O and extracted three times with 100 mL of chloroform. The combined organic layer was washed twice with 100 mL of aqueous KOH solution (10 wt %), and twice with 100 mL of brine, and dried over $MgSO_4$. After purification by chromatography, the product was obtained as colorless oil (5.16 g, 75% yield). ^{1}H NMR (200 MHz, $CDCl_3$, ppm): δ 7.56 (d, J = 5.0 Hz, 1H), 7.13 (d, J = 5.0 Hz, 1H), 2.66 (t, J = 7.5 Hz, 2H), 1.62 (m, 4H), 1.32 (m, 8H), 0.92 (t, J = 7.0 Hz, 3H). ^{13}C NMR (100 MHz, $CDCl_3$, ppm): δ 151.07, 131.48, 130.72, 129.56, 32.80, 32.41, 30.3, 29.93, 23.2, 22.93, 14.37.

6,6'-dibromo-di (5-octylthiophene)isoindigo (46b)

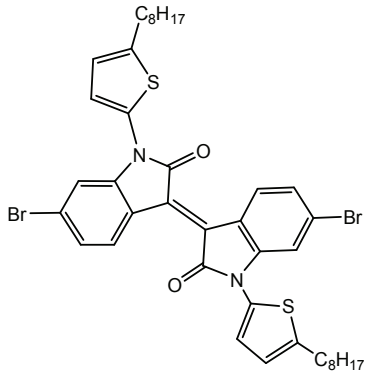

The 6,6'-dibromoisoindigo (0.480 g, 1.14 mmol) was solubilized in 30 mL of DMF and Cu_2O (0.363 g, 4.56 mmol) and 2-Bromo-(5-octyl)thiophene (0.934 g, 3,42 mmol) were added to the mixture. The reaction mixture was stirred and refluxed for three days, cooled down, poured into water (100 mL). The precipitate was filtered off and treated with boiling ethyl acetate (5x 70 mL). Combined hot ethyl acetate solutions were filters from insoluble matter, solvent evaporated and the residue was recrystallized from 1-propanol to give (0.28 g, 32% yield). ^{1}C NMR (200 MHz, $CDCl_3$, ppm): δ 170.5, 168.1, 151.07, 149.7, 147.0, 146.2, 135.4, 134.0, 133.3, 132.6, 131.48, 141.7, 130.72, 129.96, 131.2, 130.9, 129.56, 126.8, 125.2,123.5, 122.7, 120.5, 113.7,111.6, 42.8, 41.8, 32.8, 32.41, 31.9, 30.3, 29.93, 29.7, 29.5, 23.2, 22.93, 22.7,14.4, 14.1. (Some peak peaks in ^{13}C NMR spectrum overlap).

Polymers

Synthesis of P1

2,7-(bis(4,4,5,5-tetramethyl-1,3,2-dioxaborolan-2-yl)-N-9-heptadecanylcarbazole) (0.158 g, 0.24 mmol), 4,7-Bis(5-bromothiophene-2-yl)benzo-2,1,3-thiadiazole (0.199 g, 0.24 mmol), $Pd_2(dba)_3$ (2 mol %) and 2-dicyclohexylphosphino-2',6'-dimethoxybiphenyl (SPhos) (5 mol %) were putted in a flask. The system was purged three times by vacuum/argon cycling. The solids were dissolved in 15 mL degassed toluene and K_2CO_3 [2M] was added. The temperature was increased to 110°C and the reaction was stirred for 3 days. As end-capping agents were added bromobenzene (0.01 mL, 0.10 mmol) and, after an additional hour, phenyl boronic acid (6.0 mg, 0.05 mmol). After an additional hour, the mixture was cooled to room temperature and poured in cold methanol and water H_2O (5:1). The precipitate was filtered. Soxhlet extractions were carried out with acetone and with n-hexane to remove the catalyst residues and low molecular weight materials. The polymer was then additionally extracted with chloroform. The solvent was reduced to about 30 mL and the mixture was poured into cold methanol. The polymer was collected by filtration. The polymer was further purified to remove metal traces (m = 190 mg, 82%). ^1H NMR (200 MHz, $CDCl_3$, ppm): δ 8.09(br, 2H); 7.61-7.15 (br, 6H), 4.56 (br, 1H), 3.80 (br, 3H); 2.71 (br, 4H); 2.26 (br, 4H),1.32-1.22 (br, 60H), 0.85 (br, 12H). T_d = 425°C. Calc. for $C_{68}H_{96}N_2O_2S_3$: C 76.35%, H 9.05%, N 2.62%, S 8.99%. Measured: C 76.42 %, H 9.06%, N 2.50 %, S 8.02%.

Synthesis of P2

2,7-(bis(4,4,5,5-tetramethyl-1,3,2-dioxaborolan-2-yl)-N-9-heptadecanylcarbazole) (0.106 g, 0.61 mmol), 3,3-bis(5-bromo-3-dodecyl-2-thienyl)-5,5'-dimethyl-4H,4'H-1,1'-bithieno[3,4-c]pyrrole-4,4',6,6'(5H, 5'H) - tetraone (0.16 g, 0.61 mmol), $Pd_2(dba)_3$ (2 mol %) and 2-dicyclohexylphosphino-2′,6′-dimethoxybiphenyl (5 mol %)were put in a flask. The system was purged three times by vacuum/argon cycling. The solids were dissolved in 15 mL degassed toluene and K2CO3 [2 M] was added. The temperature was increased to 110°C and the reaction was stirred for 3 days. As end-capping agents were added bromobenzene (0.01 mL, 0.10 mmol) and, after an additional hour, phenyl boronic acid (6.0 mg, 0.05 mmol). After an additional hour, the mixture was cooled to room temperature and poured in cold methanol and water H_2O (5:1). The precipitate was filtered. Soxhlet extractions were carried out with acetone and with n-hexane to remove the catalyst residues and low molecular weight materials. The polymer was then additionally extracted with chloroform. The solvent was reduced to about 30 mL and the mixture was poured into cold methanol. The polymer was collected by filtration. The polymer was further purified to remove metal traces (m = 0.078 g, 32%). 1H NMR (200 MHz, $CDCl_3$, ppm): δ 8.09 (br, 2H), 7.61-7.15 (br, 6H); 4.12 (br, 1H); 3.80 (br, 6H),1.85 (br, 4H), 1.53 (br, 4H),1.50-1.35 (br, 60 H), 0.87 (br, 12H). Td = 365°C.

Synthesis of P3

2,6-Bis(trimethyltin)-4,8-di(2-ethylhexyloxyl)benzo[1,2-b:3,4-b']dithiophene (0.152 g, 0.19 mmol), 4,7-Bis(5-bromothiophene-2-yl)benzo-2,1,3-thiadiazole (0.19 g, 0.19 mmol), $Pd_2(dba)_3$ (2 mol %) and triphenylarsine ($AsPh_3$) (8 mol %) were put in a dry bottom flask. The system was then purged three times by vacuum/argon cycling. The solids were dissolved in 5 mL of anhydrous and degassed toluene. The temperature was increased to 110°C. After 2 hours of polymerization, bromobenzene (0.01 mL, 0.10 mmol) was added as end-capping agent. After an additional hour of reaction, trimethyl(phenyl)stannane (0.05 mL, 0.28 mmol) was added to complete the end-capping procedure. After an additional hour, the mixture was

cooled to room temperature and poured in cold methanol and water H_2O (5:1). The precipitate was filtered Soxhlet extractions were carried out with acetone and with n-hexane to remove the catalyst residues and low molecular weight materials. The polymer was then additionally extracted with chloroform. The solvent was reduced to about 30 mL and the mixture was poured into cold methanol. The polymer was collected by filtration. The polymer was further purified to remove metal traces. (m = 0.136 g, 40%). ^{1}H NMR (200 MHz, $CDCl_3$, ppm): δ 8.10-7.61(br, 4H); 4.12 (br, 2H); 3.80 (br, 3H); 1.85 (br, 4H); 1.53 (br, 4H); 1.50-1.53(br, 80H); 0.87 (br, 18H). T_d = 320°C. Calc. for $C_{65}H_{91}NO_4S_5$: C 69.96%, H 8.35%, N 1.27%, S 14.59%. Measured: C 68.80%, H 8.14%, N 1.30%, S 13.99%.

Synthesis of P4

2,6-Bis(trimethylstannyl)-4,8-bis(2-ethylhexyloxyl)benzo[1,2-b:4,5-b']dithiophene (0.130 g, 0.17 mmol), 3,3-bis(5-bromo-3-dodecyl-2-thienyl)-5,5'-dimethyl-4H,4'H-1,1'-bithieno[3,4-c]pyrrole-4,4',6,6'(5H, 5'H) - tetraone (0.14 g, 0.16 mmol), $Pd_2(dba)_3$ (2 mol %) and triphenylarsine ($AsPh_3$) (8 mol %) were put in a dry bottom flask. The system was then purged three times by vacuum/argon cycling. The solids were dissolved in 5 mL of anhydrous and degassed toluene. The temperature was increased to 110°C. After 2 hours of polymerization, bromobenzene (0.01 mL, 0.10 mmol) was added as an end-capping agent. After an additional hour of reaction, trimethyl(phenyl)stannane (0.05 mL, 0.28 mmol) was added to complete the end-capping procedure. After an additional hour, the mixture was cooled to room temperature and poured in cold methanol and water H_2O (5:1). The precipitate was filtered. Soxhlet extractions were carried out with acetone and with n-hexane to remove the catalyst residues and low molecular weight materials. The polymer was then additionally extracted with chloroform. The solvent was reduced to about 30 mL and the mixture was poured into cold methanol. The polymer was collected by filtration. The polymer was further purified to remove metal traces. (m = 0.15 g yield of 55%). ^{1}H NMR (200 MHz, $CDCl_3$, ppm): δ 8.10-7.61 (br, 4H); 4.12 (br, 2H); 3.80 (br, 3H); 1.85 (br, 4H); 1.53 (br, 4H); 1.50-2.35 (br, 80H), 0.87 (br, 18H). T_d = 315°C.

Synthesis of P5

2,7-(bis(4,4,5,5-tetramethyl-1,3,2-dioxaborolan-2-yl)-N-9-heptadecanylcarbazole) (0.158 g, 0.24 mmol), 1,3-dibromo-5-methyl - 4H -thieno[3,4-c]pyrrole-4, 6(5H)-dione (0.199 g, 0.24 mmol), $(Pd_2dba)_3$ (2 mol %) and 2-dicyclohexylphosphino-2',6'-dimethoxybiphenyl (SPhos) (5 mol %) were putted in a flask. The system was purged three times by vacuum/argon cycling. The solids were dissolved in 15 mL degassed toluene and K_2CO_3 [2M] was added. The temperature was increased to 110°C and the reaction was stirred for 3 days. As end-capping agents were added bromobenzene (0.01 mL, 0.10 mmol) and, after an additional hour, phenyl boronic acid (6.0 mg, 0.05 mmol). After an additional hour, the mixture was cooled to room temperature and poured in cold methanol and water H_2O (5:1). The precipitate was filtered. Soxhlet extractions were carried out with acetone and with n-hexane to remove the catalyst residues and low molecular weight materials. The polymer was then additionally extracted with chloroform. The solvent was reduced to about 30 mL and the mixture was poured into cold methanol. The polymer was collected by filtration. The polymer was further purified to remove metal traces (m = 190 mg, 82%).^{1}H NMR (200 MHz, $CDCl_3$, ppm): δ 8.09 (br, 2H); 7.61-7.15 (br, 2H), 4.56 (br, 1H), 3.80 (br, 1H); 2.71 (br, 4H); 2.26 (br, 4H), 0.85 (br, 12H). T_d = 425 °C. Calc. for $C_{36}H_{46}N_2O_2S$: C 75.75%, H 8.12%, N 4.91%, S 5.62%.

Synthesis of P6

Poly[N-9'-heptadecanyl-2,7-carbazole-alt-1,3-dithiophene-5-hexyldecylthieno [3,4-c] pyrrole-4,6-dione was synthesized as follow: 2,7-(bis(4,4,5,5-tetramethyl-1,3,2-dioxaborolan-2-yl)-N-9-heptadecanylcarbazole) (0.135 g, 0.2 mmol), 1,3-dibromo-5-di(thien-2'-yl)-5-hexyldecyl [3,4-c]pyrrole-4,6-

dione (0.199g, 0.2 mmol), $Pd_2(dba)_3$ (2 mol %) and 2-dicyclohexylphosphino-2',6'-dimethoxybiphenyl (SPhos) (5 mol %) were added in a flask. The system was purged three times by vacuum/argon cycling. The solids were dissolved in 15 mL. Degassed toluene and K_2CO_3 [2 M] was added. The temperature was increased to 110°C and the reaction was stirred for 4 days. An end-capping agent was added (bromobenzene (0.01 mL, 0.10 mmol), followed by phenyl boronic acid (6.0 mg, 0.05mmol) one hour later. The mixture was cooled to room temperature and poured into 500 mL of mixture of methanol: H_2O (10:1). The precipitate was filtered through 0.45 μm nylon filter and washed on Soxhlet with acetone followed by hexanes in order to removed catalyst residues and low molecular weight material. Polymers were then extracted with chloroform. The solvent was reduced to about 10 mL and the mixture was poured into cold methanol. The Polymer was recovered by filtration and further purification was done to remove all metals impurities. (70 mg, yield = 37%). ^{1}H NMR (200 MHz, $CDCl_3$, ppm): δ 8.09 （br, 2H, 7.59-7.14 (br, 8H), 4.66 (br, 1H), 3.59 (br, 1H), 2.47-1.95 (br, 8H), 1.55 (br, 16H), 1.26-1.14 (br, 20H), 0.87-0.78 (br, 12H).

Synthesis of P7

1,3-dibromo-5-methyl - 4H -thieno[3,4-c]pyrrole-4, 6(5H)-dione (74.7 mg,0.140 mmol), 4,4'-ditetradecyl-5,5'-bis(trimethylstannyl)-2,2'-bithiophene(100.0 mg, 0.140 mmol), [$Pd_2(dba)_3$] (2.6 mg, 2 mol %), and P(o-tolyl)$_3$ (6.8 mg, 16%) were put in a 15 mL round bottom flask thenpurged with N_2. Chlorobenzene (5 mL) was added and the mixturewas stirred at 130°C for 48 h. Then bromobenzene was added to the reaction and after 1 hour, trimethylphenyltin was also added as a capping agent. After an additional hour of reaction, the whole mixture was cooled to room temperature and poured in 500 mL of cold methanol. The crude polymer was collected, dissolved in hot $CHCl_3$, filtered through a 0.5-μm poly(tetrafluoroethylene) (PTFE) filter, and precipitated in MeOH. The solid was washed with acetone, hexane, and $CHCl_3$ in a Soxhlet apparatus. The $CHCl_3$ solution was concentrated and then added dropwise into MeOH. Finally, the polymer was collected and dried under vacuum (Yield of 77%). ^{1}H NMR (200 MHz, $CDCl_3$, pmm): δ 7.17 (s, 2H), 3.80 (br, 3H), 1.88 (br, 1H), 1.66–1.73 (m, 4H), 1.27–1.49 (m, 48H), 0.86–0.95 (m, 12H).

a) Fabrication of photovoltaic devices and testing

Fabrication and characterization of devices were carried out first at the INES (Institut National Energie Solaire), then at the "Laboratoire des Polymères Electroactifs and Photoactifs" at the Laval UniversiTy (Canada) and finally to the CEA/INAC/SPrAM/LEMOH Laboratory. For this reason experimental conditions varied in each set of tests. In addition to this, in the following paragraph, only information about the fabrication of devices, done in Canada and Chambéry, were provided. Last prelimary tests carried out to the CEA of Grenoble are described in the *Chapter 5*, because we were directly involved in each step of the fabrication.

General procedure for the solar cells production to INES – Institut National de l'Energie Solaire (Chambéry)

Photovoltaic cells for 3,6-carbazole derivatives were realized thanks to the collaboration with Doctors Séverine Bailly and Rémi de Bettignies. Cells were realized following the "sandwich" structure glass/ITO/PEDOT:PSS/active layer/LiF/Al for carbazole derivative and glass/ITO/PEDOT:PSS/active layer/Ca/Al TPD derivatives.

The substrates are characterized by 4.25 cm^2 of surface area which are covered by an ITO layer (substrate thickness of 180 nm). By spin-coating a PEDOT: PSS film of about 50 nm was deposited and dried under vacuum. The active layer was spin-coated in a glove box. A thin (1 nm) layer of LiF and a layer of aluminum were deposited by evaporation under vacuum. Two pixels of active area corresponding to 0.28 cm^2 on each cell were obtained. Contacts were realized with Cr/Au.

The J-V characteristics (I(V)) were recorded under nitrogen atmosphere in a glove box, using a Keithley® SMU 2400 instrument, under light AM 1.5, characterized by 100 $mW.cm^{-2}$ of power.

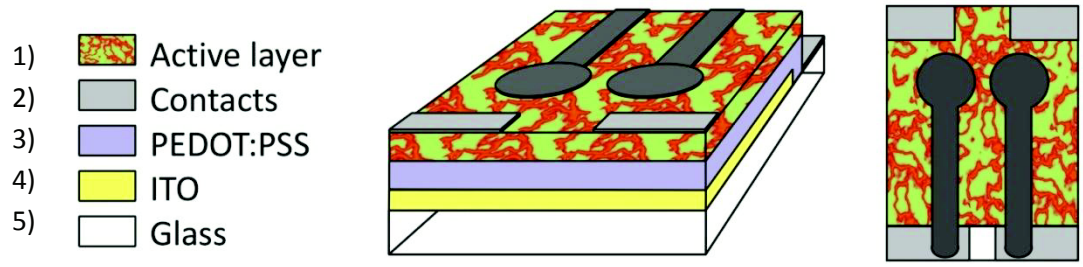

Figure 1: Scheme of solar cell (integral and top view): 1) glass, 2) ITO, 3) contacts, 4) PEDOT:PSS, 5) active layer, 6) LiF/Al.

"Laboratoire des Polymères Electroactifs and Photoactifs" at the Laval Universiy (Canada)

The organic photovoltaic cells were made in collaboration with the Doctor Ahmed El Najari who guides me during fabrication steps od device. Devices were made following the configuration of

glass/ITO/PEDOT:PSS/Polymer:[60]PCBM/Aluminum. Substrates were prepared on commercial (ITO)-coated glass substrate (25 x 25 mm^2) with a sheet resistance of ≤10 Ohms/sq (Thin Film Devices Inc, USA). Each substrate was patterned using photolithography techniques before ITO was etched using warm hydrochloric acid for 20 min. Prior to use, the substrates were cleaned with detergent and deionized water.

Then, they were ultrasonicated in deionized water and in isopropanol. ITO substrates were spin-coated (2000 rpm, 60 s) with a thin film (50 nm) of (PEDOT: PSS, Baytron P, H. C. 12 Starck) and dried at 120°C for one hour. A blend of [6,6]-phenyl C61-butyric acid methyl ester ([60]PCBM) (Nano-C, USA) and polymer was solubilized overnight, filtered through a 0.45 µm poly(tetrafluoroethylene) (PTFE) filter and spin-coated . The devices were completed by deposition of a 100 nm Al layer. This layer was thermally evaporated at a pressure of 3.10^{-5} Torr at room temperature. The thicknesses of films were recorded by a profilometer (Dektak IIa).

Current density versus potential curves (*J–V* characteristics) were measured with a Keithley 2400 Digital Source Meter under a collimated beam. Illumination of the cells was done through the ITO side using light from 150 W Oriel Instruments Solar Simulator and xenon lamp with AM1.5G filter (No. 81094) to provide an intensity of 100 mW. cm^{-2} which was calibrated with a photodiode OSI-optoelectronics UV-013D. All fabrications and characterizations were performed in an ambient environment without a protective atmosphere.

CEA Grenoble INAC/SPrAM/LEMOH) Laboratory - Materials

UV ozone treatment of substrates was carried out in a UV Ozone System (PSD company) followed by film deposition with a spin coater (Spin15). Electrode evaporation was done in both joule heated oven evaporator (VAS company) and electron gun evaporator (PLASSYS company). Device J-V characterisation was done in a controlled atmosphere under simulated AM 1.5G irradiation (100 $mW.cm^{-2}$) using a Xenon lamp based solar simulator (Class AAA from Oriel Inc) and Keithley 2400 voltage source driven with home-made software. The thickness, roughness and morphology of the films were analyzed and measured using an XP2 Ambios Technology profilometer and Nanosurf MobileS AFM.

Annexes

A.1) Cyclic Voltammetry (CV)

Cyclic voltammetry is a very versatile electrochemical technique which allows probing the mechanisms of redox and transport properties of a system in solution. This is accomplished with a three electrode arrangement whereby the potential relative to some *reference* electrode is scanned at a *working* electrode while the resulting current flowing through a counter electrode is monitored in a quiescent solution. The technique is suited for a quick search of redox couples present in a system; once located, a couple may be characterized by more careful analysis of the cyclic voltammogram. Usually the potential is scanned back and forth linearly with time between two extreme values – the switching potentials using triangular potential waveform (Figure 1 a). When the potential of the working electrode is more positive than that of a redox couple present in the solution, the corresponding species may be oxidized (*i.e.* electrons going from the solution to the electrode) and produce an *anodic* current. Similarly, on the return scan, as the working electrode potential becomes more negative than the reduction potential of a redox couple, reduction (*i.e.* electrons flowing away from the electrode) may occur to cause a *cathodic* current. The magnitude of the observed *faradaic* current can provide information on the overall rate of the many processes occurring at the working electrode surface. As is the case for any multi–step process, the overall rate is determined by the slowest step. For an redox reaction induced at a working electrode, the rate determining step may be any one of the following individual step depending on the system: rate of *mass transport* of the electro-active species, rate of adsorption or de-sorption at the electrode surface, rate of the electron transfer between the electro-active species and the electrode, or rates of the individual chemical reactions which are part of the overall reaction scheme. A typical voltammogram is shown in Figure 1.b.

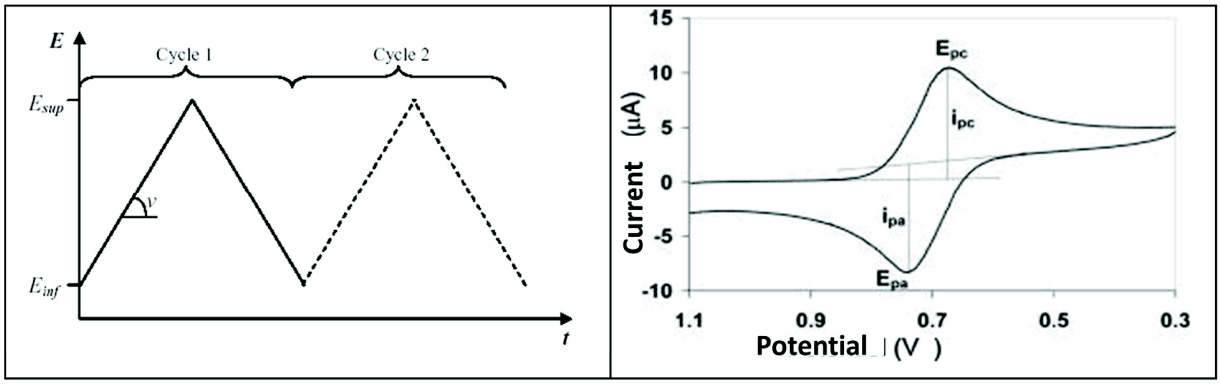

Figure 1: (a) Image of a typical signal imposed at the electrode during the cyclic voltammetry measurement. (b) Behavior of the corresponding i = f(E) curve.

The scan shown starts at a slightly negative potential, up to some positive switching value, at which the scan is reversed back to the starting potential. The current is first observed to peak at E_{pa} (with value i_{pa}) indicating that an oxidation is taking place and then drops due to depletion of the reducing species from the diffusion layer. During the return scan the processes are reversed (reduction is now occurring) and a peak current is observed at E_{pc} (corresponding value, i_{pc}).

Providing that the charge–transfer reaction is reversible, that there is no surface interaction between the electrode and the reagents, and that the redox products are stable (at least in the time frame of the experiment), the ratio of the reverse and the forward current $i_{pr}/i_{pf} = 1.0$ (in Figure 1b $i_{pa} = i_{pf}$ and $i_{pc} = i_{pr}$). In addition, for such a system it can be shown that:

- the corresponding peak potentials E_{pa} and E_{pc} are independent of scan rate and concentration,

- the formal potential for a reversible couple $E^{0'}$ is centered between E_{pa} and E_{pc}:

$$E^{0\prime} = \frac{(E_{pa} + E_{pc})}{2}$$

- the separation between peaks is given by $\Delta E_p = E_{pa} - E_{pc} = {}^{59}/_{n}\ mV$ (for a n electron transfer reaction) at all scan rates (however, the measured value for a reversible process is generally higher due to uncompensated solution resistance and non-linear diffusion. Larger values of ΔE_p, which increase with increasing scan rate, are characteristic of slow electron transfer kinetics).

To distinguish between reversible (diffusion-controlled) and irreversible (charge-transfer controlled) kinetics of electrode process **potential scan-rate** is used as diagnostic tool – the rate of reagent transport is proportional to square root of scan-rate. Thus in one experimental set a shift in reversibility might be executed and analysis of ΔEp *vs.* $v^{1/2}$ gives information on reversibility and applicability of further calculations. The electrochemical processes are occurring at the interface of two different phases, the electrode and the electro-active species in solution. In other words, the processes under studies are

heterogeneous in nature. For the electron transfer to occur, the molecules in solution have to approach the electrode. In a cyclic voltammetry experiment, the solution is kept unstirred; in this situation, mass transport can occur only by diffusion due to concentration gradients created around the electrode surface. The magnitude of the observed signal will be very much a function of these diffusional properties of the system. Intuitively, the current intensity (*i.e.* the flow of electrons) is expected to depend on the surface area of the working electrode and the concentration of the electro-active species. Also, one can expect the voltage scanning rate to affect the concentration profile around the electrode which itself directly affects the rate of charge transport, and for this matter the diffusion coefficient appears explicitly. The expression of the peak current (A) for the forward sweep in a reversible system at 298 K is given by the Randles–Sevcik equation:

$$i_{pf} = (2.69 \cdot 10^5) \cdot n^{\frac{3}{2}} \cdot AD^{\frac{1}{2}} \cdot v^{\frac{1}{2}} \cdot C^*$$

where n is the number of electron equivalent exchanged during the redox process, A (cm^2) the active area of the working electrode, D ($cm^2 \cdot s^{-1}$) and C^* ($mol \cdot cm^{-3}$) the diffusion coefficient and the bulk concentration of the electroactive species; v is the voltage scan rate ($V \cdot s^{-1}$). In the present experiment, the dependence of *ipf on* scan rate and concentration will be examined.

Irreversible and Quasi-reversible Systems

For irreversible processes (those with sluggish electron exchange), the individual peaks are reduced in size and widely separated. Totally irreversible systems are characterized by a shift of the peak potential with the scan rate:

$$E_p = E^0 - \left(\frac{RT}{\alpha \cdot n_a \cdot F}\right) \cdot \left[0.78 - ln\left(\frac{k^0}{D^{\frac{1}{2}}}\right) + ln\left(\frac{\alpha \cdot n_a \cdot F \cdot v}{RT}\right)^{\frac{1}{2}}\right]$$

where α is the transfer coefficient and n_a is the number of electrons involved in the charge-transfer step. Thus, E_p occurs at potentials higher than E^0, with the overpotential related to k^0 (standard rate constant) and α. Independent of the value k^0, such peak displacement can be compensated by an appropriate change of the scan rate. The peak potential and the half-peak potential (at 25°C) will differ by $48/\alpha \cdot n$ mV. Hence, the voltammogram becomes more drawn-out as $\alpha \cdot n$ decreases.

The peak current, given by:

$$i_p = (2.99 \cdot 10^5) \cdot n \cdot (\alpha \cdot n_a)^{\frac{1}{2}} \cdot ACD^{\frac{1}{2}} \cdot v\frac{1}{2}$$

is still proportional to the bulk concentration, but will be lower in height (depending upon the value of α). Assuming $\alpha = 0.5$, the ratio of the reversible-to-irreversible current peaks is 1.27 (*i.e.* the peak current for the irreversible process is about 80% of the peak for a reversible one). For quasi-reversible systems (with $10^{-1} > k^0 > 10^{-5}$ $cm \cdot s^{-1}$) the current is controlled by both the charge transfer and mass transport. The

shape of the cyclic voltammogram is a function of the ratio $k^0/\left(\frac{\pi \cdot v \cdot n \cdot FD}{RT}\right)^{\frac{1}{2}}$.

As the ratio increases, the process approaches the reversible case. For small values of it, the system exhibits an irreversible behavior. Overall, the voltammograms of a quasi-reversible system are more drawn out and exhibit a larger separation in peak potentials compared to a reversible system. Cyclic voltammetry allows the determination of the oxidation and reduction potential and subsequently the HOMO and LUMO levels of the conjugated polymers. Thanks to this technique is also possible studying the electronic transfer reversibility and speed.[1]

A.2) Air stability studies

In addition electrochemical stability is another problem for organic solar cells. Especially under light illumination and by simultaneous exposure to oxygen or water vapor, a rapid photooxidation/degradation occurs. Normally, protection from air and humidity is necessary to achieve long device lifetimes.[2] Normally stability concerns the entire device, consisting of active layers and contacts. Here, it was possible to make some considerations comparing electrochemical results with photoluminescence spectra in *o*-dichlobenzene solution for the polymer P3 and P4. Their spectra were compared with the commercial 2,7-PCDTBT polymer spectrum.

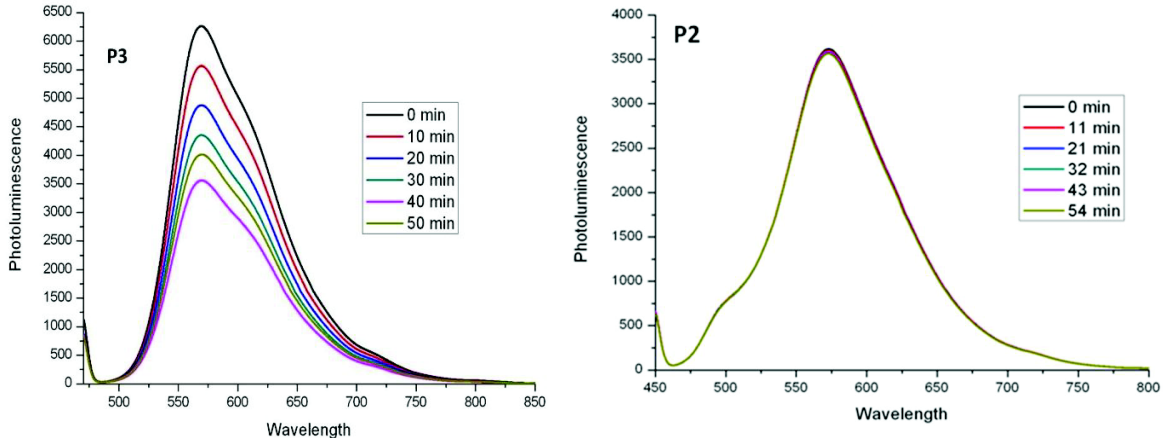

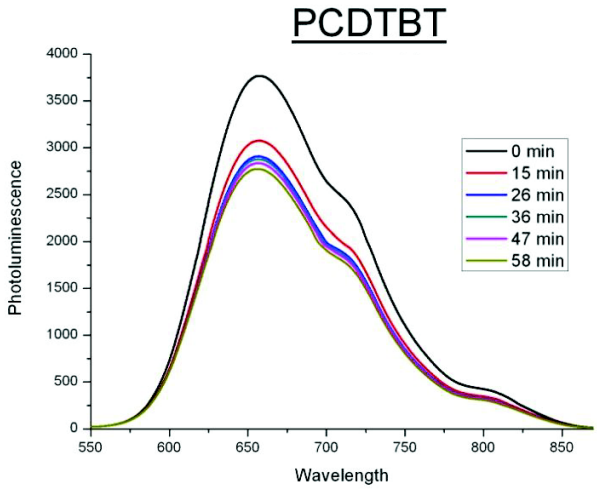

Figure 2: photoluminescence spectra of P3, P4 and commercial 2,7-PCDTBT. Spectra are acquired for solutions of polymer (c = 0.008 mg·mL^{-1}) in o-dichlorbenzene during 1 h, with intervals of about 10 minutes.

Photoluminescence spectra of the **P3** demonstrated an important decrease of the intensity spectra after one hour of solution air exposition; on the other hand the **P2** copolymer didn't seem affected. These results are in agreement with electrochemical data collected in the *Chapter 3 paragraph 3.2.2* where HOMO energy levels, for **P3** and **P2**, were furnished.

P3 polymer was characterized by an HOMO level of -5.04 eV and **P2** by an HOMO level of -5.42 eV. Knowing that an open air stable polymer should be characterized by HOMO level lower than -5.27 eV, which represents the oxidation threshold of the air, consequently **P3** is instable and **P4** is stable to open air conditions.

Comparing the spectra of previous polymers with the one of the commercial PCDTBT which assumes an intermediate behavior, it is possible affirming that the benzodiatiazole unit characterizing the PCDTBT polymer is less stable than the thienopyrroledione one. Then, going back to **P1** polymer is possible to assume that the unit mostly affecting the stability of the polymer is the benzodithiophene one.

A.3 Isoindigo units

In the final part of the work, the interest was moved versus others potential electron accepting units belonging to the isoindigo family. Here, we present the synthesis of two new isoindigos (ID) derivatives: the 6,6'-dibromo-di(tetradecyl)isoindigo **(46a)** and the 6,6'-dibromo-di (5-octylthiophene)isoindigo **(46b)**. The first one was considered as a kind of reference unit and the second one was tested to increase planarity of chains and to try to develop a donor-acceptor effect on neat moiety.

Synthesis of the electron accepting unit: the 6,6'-dibromo-di(tetradecyl)isoindigo (46a) and the 6,6'-dibromo-di (5-octylthiophene)isoindigo (46b)

The synthesis of the repetitive units, **(46a)** and **(46b)**, was carried out in two steps, starting from the

commercially available 6-bromooxindole, **(43)**, and 6-bromoisatin, (**44**). Subsequently tetradecyl chains or a 2,5-bromo-octylthiophene, **(48)**, substituent were branched to both isoindigo nitrogens.
A classical alkylation was carried out to arise **(46a)**. On the other hand, synthesis steps to synthesize the unit **(46b)** were more complex, because it was necessary to link an aromatic group on the nitrogen of the isoindigo molecule without damaging C=O bond. In the literature there were not general approaches to synthesize N-arylated isoindigos: only few indirect examples were explored [3] and, for developing this synthesis, the protocol was based on the direct copper mediated N-arylation of isatins.[4]

The reaction of the (2,5-bromo-octylthiophene) with a bromoisoindigo in the presence of copper (I) oxide in DMF was performed at 120-180°C (see Figure 3), during 36 hours , to arise the final **(50)**.

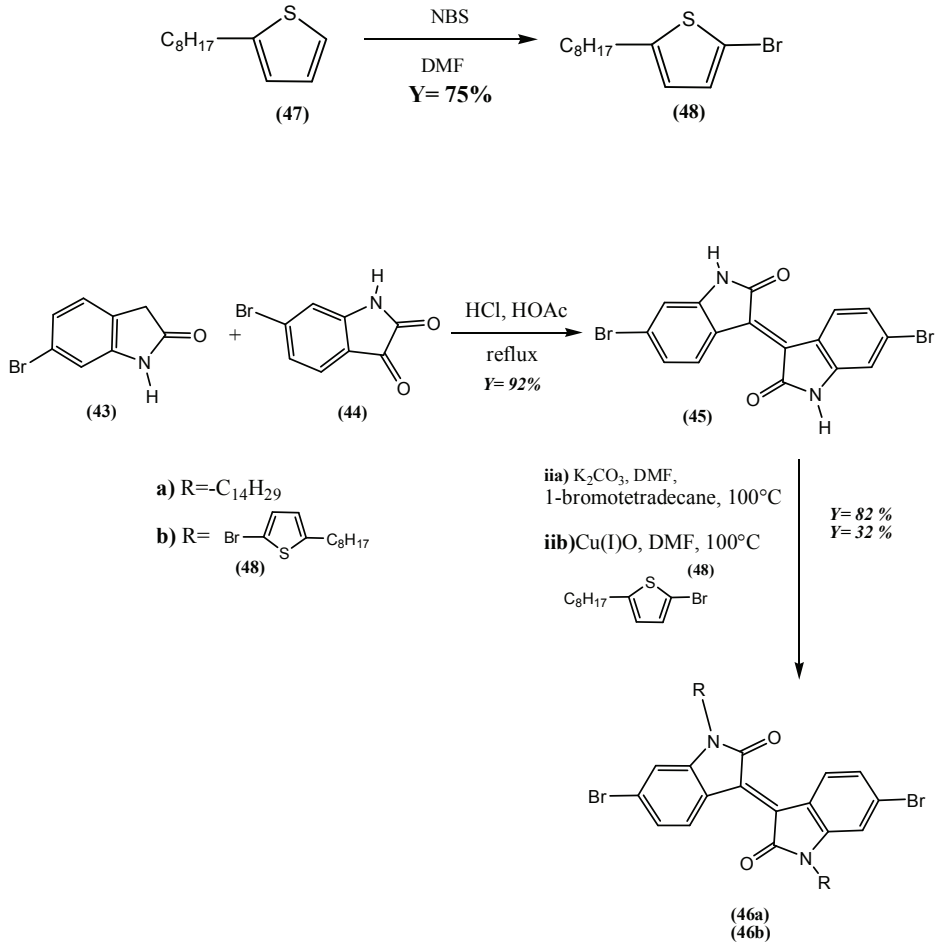

Figure 3: Synthesis steps of isoindigo electron accepting units: the 6,6'-dibromo-di(tetradecyl)isoindigo (46a) and the 6,6'-dibromo-di (5-octylthiophene)isoindigo (46b).

[1] F. Miomandre, S. Sadki, P. Audebert, and R. Méallet-Renault, *Electrochimie, des concepts aux applications*., Dunod, 2005, p. 418.

[2] M. Jørgensen, K. Norrman, S. A. Gevorgyan, T. Tromholt, B. Andreasen, and F. C. Krebs, "Stability of Polymer Solar Cells," *Advanced Materials*, vol. 24, no. 5, p. 580-612, 2011.

[3] A. N. Semyonov, "Design, synthesis and characterization of fluorescent dyes and liquid crystal semiconductors," Kent University, 1996.

[4] G.M. Copola, "N-Arylation of isatins.A direct route to N-arylisation anhydres," *Journal of Heterocyclic Chemistry*, vol. 24 , pp. 1249–1251, 1987.

New donor-acceptor alternating copolymers: preparation, physico-chemical characterization and application to organic photovoltaic cells

Abstract

In this work, the attention was focused on the synthesis of new low-band gap polymers and on the adopted chemical strategy aims on developing the so called *push-pull* copolymers: formed by a donor (*push*) and an acceptor (*pull*) electron unit in the polymer backbone. It was demonstrated that exploited building block approach can lead to copolymers with tunable physical properties. By selecting acceptor (benzothiadiazole or thienopyrrolodione derivatives) and donor (3,6-carbazole, 2,7-carbazole, dialkoxybenzodithiophene) units of different DA strength, it is possible to prepare copolymers through several C-C coupling methods. Detailed physico-chemical studies using complementary spectroscopic, electrochemical, diffraction and thermal techniques enabled the determination of synthesized *push-pull* copolymers properties, which are crucial for their photovoltaic application.
Detailed studies on EPR under illumination and EPR tracing allowed the characterization of various electronic transfers in the presented and particularly designed *push-pull* copolymers, blended with two types of electron acceptor materials: PCBM and $CuInS_2$ nanocrystals. DFT calculations supported the experimental results. Preliminary tests on synthesized copolymers were carried out taking into account all limiting factors concerning the device fabrication.

Key words : *push-pull* copolymers, benzothiadiazole, thienopyrroledione, electronic transfer, organic solar cells, EPR

Nouveaux copolymères donneur-accepteur: préparation, caractérisation physico-chimique et application aux cellules photovoltaïques organiques

Résumé

Ce travail de thèse concerne l'élaboration de nouveaux copolymères à faible bande interdite de type *« push-pull »,* constitués par une unité donneuse d'électrons (*push*) et une unité acceptrice d'électrons (*pull*) en modulant les relations structures-propriétés par stratégie de synthèse. Des copolymères constitués par des unités acceptrices d'électrons (dérivées du benzothiadiazole ou du thienopyrrolodione) et donneuses d'électrons (3,6-carbazole, 2,7-carbazole, dialkoxybezodithiophène) ont été obtenus par différentes méthodes de couplage carbone carbone (C-C). Des études physico-chimiques par des techniques de spectroscopie (UV-visible), d'électrochimie (voltampérométrie cyclique), de diffraction de rayon X et d'analyses thermogravimétriques ont été utilisées pour élucider les propriétés fondamentales des copolymères pour des applications dans le domaine du photovoltaïque organique. Des études de RPE sous éclairement couplées avec de la simulation théorique ont permis l'étude des différents transferts électroniques dans les copolymères push-pull en mélange avec deux types de matériaux accepteurs d'électrons (le PCBM et les nanocristaux de $CuInS_2$). Des calculs de DFT ont mis en évidence une bonne corrélation avec les résultats expérimentaux. Des tests préliminaires en hétérojonctions volumiques sur les (co)polymères ont étés réalisés mettant en évidence les facteurs clés limitant les performances des dispositifs de photovoltaïques organiques.

Mots Clé : copolymères *push-pull*, benzothiadiazole, thienopyrroledione, transfert électronique, cellules solaires organiques, RPE

Donor-acceptor alternating copolymers based on benzodithiazole (BTD) electron accepting units and carbazole (CB) electron donating units: 3,6-carbazoles vs 2,7-carbazoles

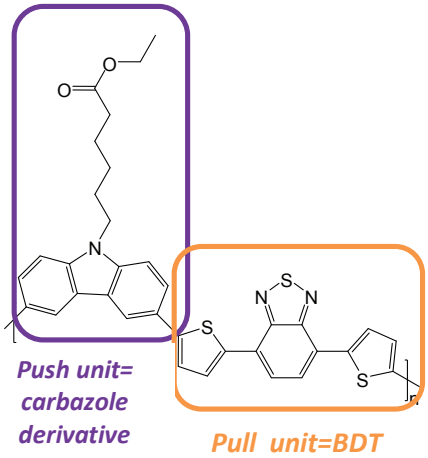

3,6-PCDTBT

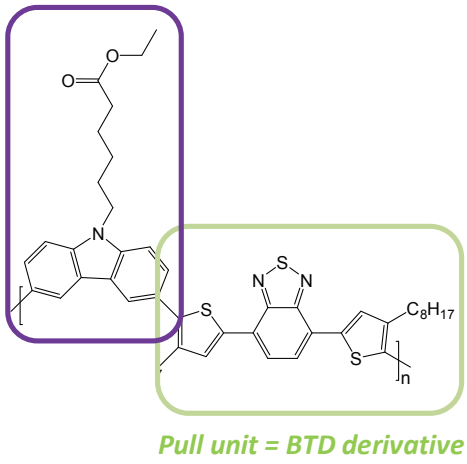

3,6-PCDOTBT

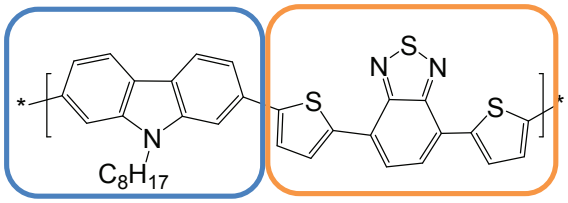

3,6-PoCDTBT

Donor-acceptor alternating copolymers containing a new electron accepting unit: the thienopyrrolodione moiety

- **Carbazole derivatives**

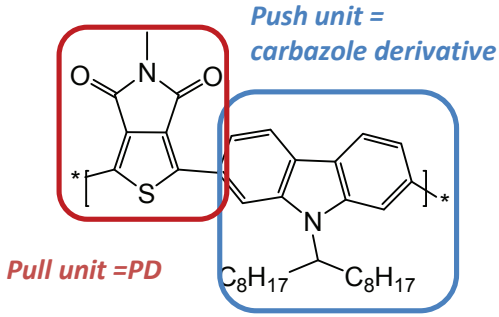

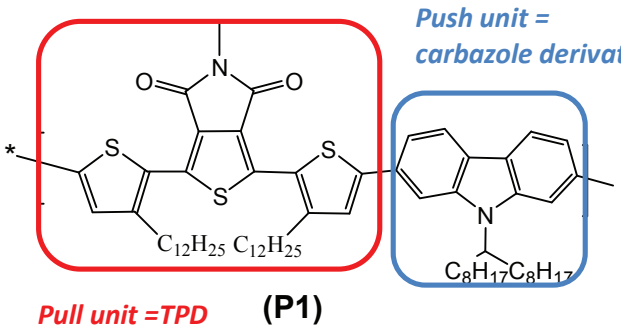

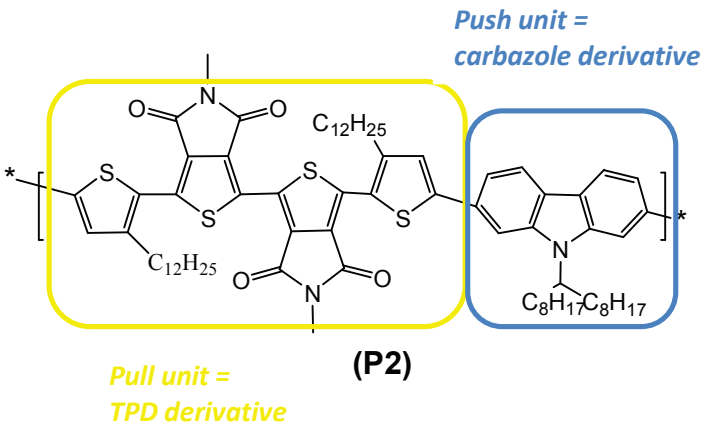

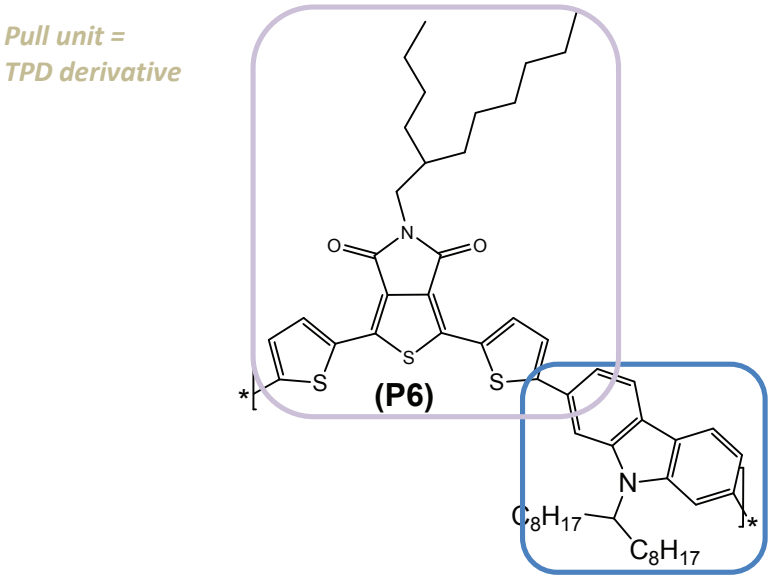

- **Benzodithiphene derivatives**

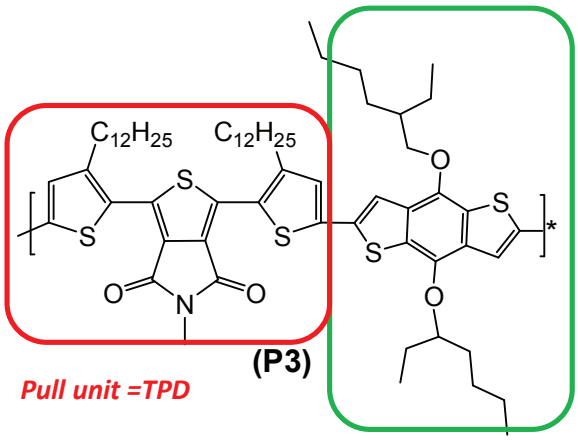

(P3)

Pull unit =TPD

Push unit = BTD

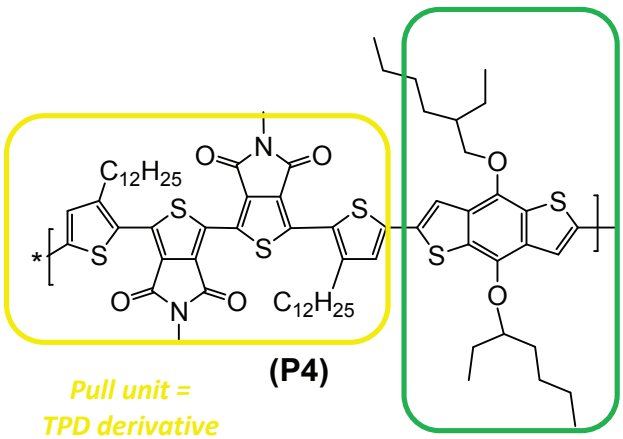

(P4)

Pull unit = TPD derivative

Push unit = BTD

- **Benzodithiphene derivatives**

Pull unit = PD

Push unit = bithiophene

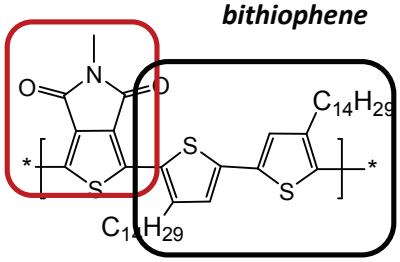

(P7)